THE FORMATION OF PHARMACEUTICAL CO-CRYSTALS BY SPRAY DRYING

B. MEHTA

PHD

2016

The Formation of Pharmaceutical Co-crystals by Spray Drying

An Investigation into the Chemical and Physical Factors Affecting the Production of Pharmaceutical Co-crystals by Fast Evaporation and Spray Drying

Bhanvi MEHTA

Submitted for the Degree of

Doctor of Philosophy

School of Life Sciences

University of Bradford

2016

Abstract

Bhanvi Mehta

The Formation of Pharmaceutical Co-crystals by Spray Drying

An Investigation into the Chemical and Physical Factors Affecting the Production of Pharmaceutical Co-crystals by Fast Evaporation and Spray Drying

Keywords: Spray drying, rotavap, cocrystal, solubility, caffeine, carbamazepine, theophylline.

Crystal engineering study using spray dryer was performed for scale-up and rapid, continuous crystallisation of co-crystals from solution. The study emphasise on developing co-crystals of two structurally similar compounds, caffeine (CAF) and theophylline (THEO) with various di-carboxylic acids. The incongruently soluble pair of CAF and THEO with di-carboxylic acids acquires large solubility difference which is important to consider for its utility in product development. Based on previous assumption that maleic acid (MAL) elevates CAF's solubility; solubility of the two similar compounds was tested in various dicarboxylic acids. Other solubility enhancement strategies such as introduction of surfactant and binary solvents were also scrutinised. A kinetically similar bench-scale technique, rotary evaporator (rotavap) was investigated as a pre-screening tool for the production of co-crystals via spray drying. Furthermore, various process parameters within the spray dryer were optimised to control the kinetic conditions which influence co-crystallisation and quality of the product. Another polymorphic co-crystal pair,

CBZ (carbamazepine) and SAC (saccharin) was examined in various solvents and its degradation was evaluated over a period of few months. In this study, a two-step conversion of CBZ into its degradate was hypothesised. Rotavap delivered a true reflection of co-crystal favoured via spray drying apart from co-crystal pairs depicting polymorphism. Spray dryer offered a unique environment favouring metastable forms of co-crystals irrespective of the starting component stoichiometry; generating CAF:MAL 2:1. However, due to process limitation and solubility constraint, the impurity of CAF in CAF:MAL 2:1 co-crystals could not be abolished.

Dedicated to My Parents

Acknowledgement

I acknowledge the assistance and guidance provided by my supervisors, Prof. Anant Paradkar and Dr. Ian Grimsey; without their knowledge and encouragement, this project would not have been successful. It is a pleasure to thank the lab staff and colleagues for their support and helpful discussions.

I would also like to extend my heartfelt gratitude and appreciation towards my family members for all the support they have given throughout my time at the University.

CONTENTS

LIST OF FIGURES

LIST OF TABLES

Abbreviations

API	:	Active Pharmaceutical Ingredient
ANDA	:	Abbreviated New Drug Applications
ATR	:	Attenuated Total Reflectance
BA	:	Benzoic Acid
BCS	:	Biopharmaceutics Classification System
BET	:	Brunauer-Emmett-Teller
BPD	:	Binary Phase Diagram
CAF	:	Caffeine
CBZ	:	Carbamazepine
CFD	:	Computational Fluid Dynamics
CNC	:	Carbamazepine and Nicotinamide Co-crystal
CSD	:	Cambridge Structural Database
COST	:	"Changing One Separate factor a Time"
CPP	:	Critical Process Parameters
CQA	:	Critical Quality Attributes
CUR	:	Curcumin
DEC	:	Di-electric Constant
DMSO	:	Dimethyl Sulphoxide
DOE	:	Design of Experiment
DPI	:	Dry Powder Inhalers
DSC	:	Differential Scanning Calorimetry
FFED	:	Fractional Factorial Experiment Designs
FID	:	Flame Ionisation Detector
FDA	:	Food and Drug Administration
FTIR	:	Fourier-transform Infrared Spectroscopy

GLU	:	Glutaric Acid
GRAS	:	Generally Recognised As Safe
HPLC	:	High Performance Liquid Chromatography
HT	:	High-throughput
iGC	:	inverse Gas-phase Chromatography
IR	:	Infrared
IND-SAC	:	Indomethacin-Saccharin
KF	:	Karl Fischer
LAG	:	Liquid-Assisted Grinding
MAL	:	Maleic Acid
MO	:	Malonic Acid
MS	:	Mass Spectroscopy
NIC	:	Nicotinamide
NIR	:	Near Infrared
NCT	:	Nicotinamide
NDA	:	New Drug Applications
OX	:	Oxalic Acid
PAT	:	Process Analytical Technology
PCA	:	Paracetamol
PCA	:	Principal Component Analysis
PLS	:	Partial Least Squares
PHL	:	Phloroglucinol
PSD	:	Particle Size Distribution
PSD	:	Phase Solubility Diagram
QbD	:	Quality by Design
RH	:	Relative Humidity
RSD	:	Relative Standard Deviations

SCF	:	Supercritical Fluid
SEA	:	Surface Energy Analyser
SEM	:	Scanning Electron Microscopy
SFCC	:	Solvent-Free Continuous Co-crystallisation
SMPT	:	Solution Mediated Phase Transformation
SSNMR	:	Solid State Nuclear Magnetic Resonance spectroscopy
SU	:	Succinic Acid
SXRD	:	Single X-ray Diffraction
TAR	:	Tartaric Acid
Tg	:	Glass Transition temperature
THEO	:	Theophylline
Tp	:	Particle Temperature
THz-TDS	:	Terahertz Time-Domain-Spectroscopy
TPD	:	Ternary Phase Diagrams
USSC	:	Ultrasound-assisted Solution Co-crystallisation
WLF	:	Willaims-Landel-Ferry
PXRD	:	Powder X-Ray Diffraction

CHAPTER1

INTRODUCTION

Pharmaceutical industries generally focus on the design and development of drug products through important theories, advanced technologies and formulation strategies, to capitalise on compound's perspective as a therapeutic. Conventionally, the solid-state of active pharmaceutical ingredients (APIs) can exist as either amorphous, crystalline, or solvate and hydrate forms with explicit regulatory schemes applied to all (FDA, 2013). These forms can be designed to achieve various physicochemical properties and therefore, influence characteristics such as, bioavailability, solubility, patient acceptance and stability under high relative humidity. Solubilisation approaches including micellar solutions, salt forms, micronisation, co-solvents, often used to improve the dissolution rate of the drug; have shown inadequate improvement in bioavailability due to their specific physicochemical nature. The utilisation of new crystal engineering approaches offer an alternative to the challenges of low aqueous solubility, dissolution rate and bioavailability, whilst preserving the required physical and chemical identity of the product (Yadav *et al*., 2009; Mirza *et al*., 2008; Blagden *et al*., 2007).

Researchers have delved into the design and growth of distinguishable crystalline molecular solids, known as co-crystals as an alternative to salts and solvates. Co-crystals are multi-component assemblies comprised of an API and one or more distinctive co-crystal formers (co-former) which by convention are solid at room temperature. Unlike ionic interactions in other solid-state forms such as salts, association of API with co-former is governed by non-ionic interactions (hydrogen bond or non-covalent interactions) within the same crystal lattice (FDA, 2013).

These co-formers are pharmaceutically acceptable neutral guest compounds, GRAS (Generally Recognised As Safe) which do not modify the pharmacological activity of API but possesses a distinct physicochemical profile (Blagden *et al*., 2008; Scultheiss and Newman, 2009; Sekhon, 2009).

Recently, FDA (Food and Drug Administration) regulation has classified co-crystals as dissociable molecular complexes, "API-excipient" and suggests that it should be treated as a drug product intermediate. The current regulations require supportive information for new drug applications (NDA) and abbreviated new drug applications (ANDAs) of co-crystals stating: a) API and its excipient(s) exist in neutral states, that is, their ΔpK_a (acid dissociation constant) <1 which confirms less than considerable proton transfer; if not, then orthogonal approaches using spectroscopic tools should be examined, and; b) results showing dissociation of an API and its excipient(s) before reaching the site of action (FDA, 2013).

1.1. Co-crystal versus solvates and salts

A pharmaceutical active ingredient can have polymorphs or can crystallise with another molecule to form a co-crystal or a salt, if both the components are solid at room temperature. The crystals formed with one of the components as liquid at room temperature, is designated as a solvate or a hydrate. The multi-component co-crystals and salts may further exist in hydrated or solvate forms and, in addition can have various polymorphs. For example, a new stable salt co-crystal of tiotropium fumarate with fumaric acid (a salt) together with co-former (co-crystal with stoichiometry of 2:1:1) was developed and characterised (Pop, Sieger and Cains, 2009). On the other hand, though solvates have potential to increase dissolution rate, it acquires

toxicological consequences due to the presence of solvent and further loss of solvent over time may account for phase transformations (Yadav *et al*., 2009; Nauha, 2012).

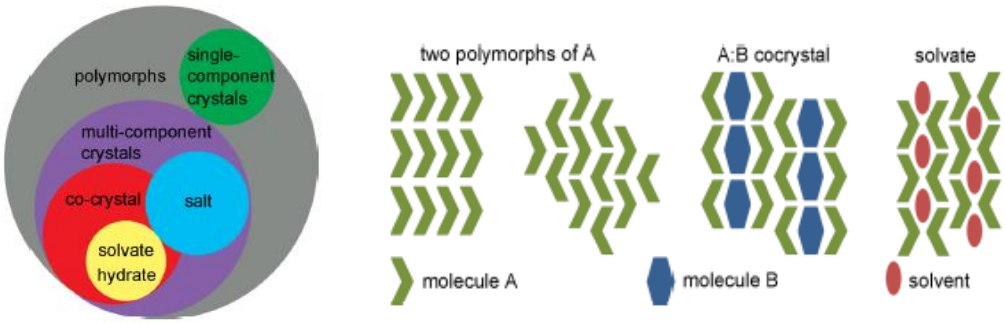

Figure 1.1. *Possible crystal forms attained by an API (Nauha, 2012).*

Pharmaceutical development of the two multi-component structures, salt and co-crystal retain their importance and may sometimes be confused. Though salts are chosen to improve the stability of an API, co-crystals have two intrinsic advantages. First, co-crystals can be formed from acidic, basic and non-ionisable molecules and second is its ability to form co-crystals with numerous potential co-formers (Yadav *et al*., 2009; Sekhon, 2009; Vishweshwar *et al*., 2006).

Salts are formed by transfer of a proton from an acid to a base which is predicted from the pKa values of the two components. Whereas, in a co-crystal no such transfer takes place as it holds the components as neutral entities. Chemistry explains that a pKa difference of at least 2.7 units between the conjugate base and acid is required, i.e. [pKa (base)- pKa (acid) $\geq$ 2.7] to form a stable salt. For example, succinic acid (pKa of 4.2) forms a co-crystal with urea base (pKa of 0.1), whereas a salt formation is favoured with L-lysine base (pKa of 9.5) (Figure 1.2). Most of the base pKa values observed are not high enough to allow proton transfer and hence, form co-crystals. Current studies on co-crystal growth use pKa profiles as a tool to

select co-crystal formers; however, this is not always appropriate (Qiao *et al*., 2011; Blagden *et al*., 2008; Sekhon, 2009).

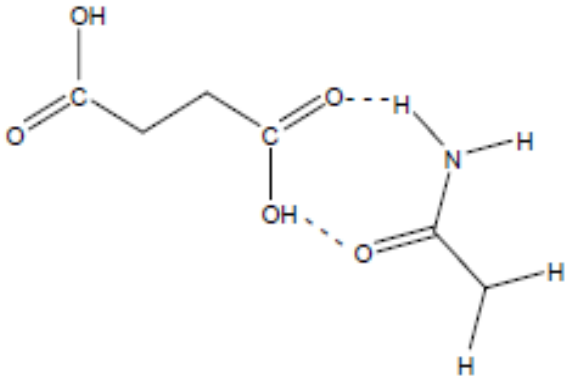

Figure 1.2. *Co-crystal of succinic acid-urea comprising of two hydrogen bonds, i.e. between oxygen atom of urea and hydrogen in succinct acid; second one being, oxygen atom from succinic bonded to hydrogen atom from urea molecule (Sekhon, 2009).*

Moreover, molecular electrostatic potential surface calculations have been used to estimate the degree of transfer between the hydrogen bonded synthons to determine whether a molecular solid is a co-crystal or a salt. Recent studies reported that if the calculated charge on the hydrogen-bond acceptor surpassed a critical value, a salt form was expected, while a value too low did not account for co-crystal formation (Aakeroy, 2010). Further to this, Hammett substituent constant was used as a source model to predict the formation of co-crystals over salts. In an attempt, 90% of the system formed co-crystals from 32 acid/acid combinations of the substituted benzoic acids where co-formers acquire Hammett constants of opposite sign, while the ones with same sign produced only 25%. Therefore, the system was characterised by this direct relation observed between the substituent constants (also denoted by differences in pKa) to forecast the formation of co-crystals (Seaton, 2010; Brittain, 2012).

1.2. Co-crystal design

1.2.1. Physicochemical properties

The investigation of physicochemical properties of a co-crystal is essential to improve the overall stability and development of APIs. Researchers have extensively studied and reviewed these properties, namely, solubility, dissolution, melting point, stability, crystallinity and bioavailability. As stated earlier, it has been assumed that API would retain its intrinsic properties, but there is no recent evidence to sustain the fact. Since, a compound will have its own unique properties pertaining to the situation, there are questions related to the property change with respect to formation of co-crystals (Schultheiss and Newman, 2009; Blagden *et al*., 2007). Some important physicochemical properties are as follows:

Melting point:

It is the temperature at which the solid phase is in equilibrium with the liquid phase and is an important aspect for drug development. The preferred technique for its determination is differential scanning calorimetry (DSC) which gives an additional data on the enthalpy of fusion, for example, to identify complex polymorphic pair (monotropic or enantiotropic) of solids. This physicochemical property is used to characterise compounds and is strongly correlated to their aqueous solubility and vapour pressure. In addition, studies reported that it holds a direct relation with the molecular packing within a co-crystal, which remains indefinable (Blagden *et al*., 2007). Therefore, in a multicomponent system, each component has its own properties that can influence the factors contributing to the melting point and making it difficult to draw conclusions (Schultheiss and Newman, 2009).

Staton and Bak (2008) reported the melting points of 10 co-crystals to an insoluble molecule vanilloid receptor 1 antagonist, (AMG517) where the melting points fell between that of the API and their co-formers. In another survey, 50 co-crystallised samples were analysed and it was deduced that co-crystals alter the melting points of an API which results in a product whose melting point falls either between or lower than the API and co-former. Moreover, high melting points may lead to poor solubility of co-crystals, therefore further extensive studies are required using large number of samples (Schultheiss and Newman, 2009; Qiao *et al*., 2011).

Stability:

There are four different aspects of stability testing: relative humidity stress, thermal stress, chemical stability, and solution stability which depend on the structure and characteristics of the molecule developed. The relative humidity test is used to determine the stability of the solid with respect to atmospheric moisture uptake during processing, storing, handling and packaging. Water sorption and desorption experiments of indomethacin-saccharin co-crystals have shown that relative humidity is not a major concern due to negligible amount of water sorbed (Basavoju *et al*., 2008, Qiao *et al*., 2011). Another study involves the humidity stability of anhydrous caffeine with respect to co-crystals formed with series of dicarboxylic acids. It was observed that co-crystals did not form hydrate but were unstable and underwent polymorphic transformation. The only stable form caffeine/oxalic acid co-crystal displayed better stability than anhydrous caffeine (Blagden *et al*., 2007).

The study on the effect of thermal stress and chemical stability is very limited, but can provide information based on physicochemical stability under accelerated conditions such as 40°C/75% RH and 60°C/75% RH. Other studies discuss DSC

data of non-stoichiometric co-crystals and their conversion after losing the guest molecule. Solution stability is also an important aspect to determine if the co-crystals will dissolve in the GI tract, that is, stays in the solution without getting crystallised (Schultheiss and Newman, 2009).

Further advancement in the field of photo-stability and mechanical-stability has demonstrated improvement in various aspects of both formulation and manufacturing. An increased physicochemical stability and photo-stability was observed in nitrofurantoin, an antibacterial drug used for oral treatment of urinary tract infections; by co-crystallising with 4-hydroxybenzoic acid (Vangala *et al*., 2011). Another study involved two model 1:1 profen-nicotinamide co-crystals (ibuprofen-nicotinamide and flurbiprofen-nicotinamide) prepared by rotary evaporation exhibiting greater tabletting properties than the individual components (Chow *et al*., 2012). A further example of bioactive agent, andrographolide, forms co-crystal with salicylic acid suppressing its chemical transformation into an inactive form (andrographolide sulphate metabolite) (Suresh *et al*., 2013; Smith *et al*., 2011).

Solubility:

Solubility can be increased by both salt and co-crystal in case of a free acid or base, but the two forms are not always distinguished easily. Solubility can either be determined by an observation at a set time point (kinetic solubility) or when it reaches equilibrium over a long period of time (thermodynamic solubility). The equilibrium solubility requires a number of measurements to determine the residence time for the drug in the stomach and intestines. Factors such as, particle size, changes in the drug form, solution media (acidic or basic) and the changing pH of the media can affect the dissolution properties. Therefore, it is recommended that

each observation should be tested at various time points (Schultheiss and Newman, 2009). Recent studies by Good and Rodriguez-Hornedo (2010) reported a time saving method to select and formulate a co-crystal depending on the ratio of concentrations of co-crystal components in the solution at the eutectic point. Further studies explained solubility of co-crystals with acidic, basic, zwitterionic and amphoteric moiety as ionisation constant of the components, product solubility and solution pH (Qiao *et al*., 2011). Modulation of solubility by cocrystallisation in case of extensively studied flavanoid; quercetin with caffeine, caffeine and methanol, and isonicotinamide produced drastic increase in its bioavailability (Smith *et al*., 2011).

Intrinsic Dissolution:

This parameter is independent of formulation effects (for example, particle size) and determines the *in-vivo* performance of APIs as a function of dissolution media properties. APIs belonging to the BCS (Biopharmaceutics Classification System) class II drugs, with high permeability and low solubility are studied for co-crystallisation to enhance their properties. The drug is pressed into a disk and the solution concentration is measured over time and XRPD (X-ray powder diffraction) data is obtained to check for any major form changes. In an experiment, intrinsic dissolution of fluoxetine HCl co-crystals was conducted in water (Figure 1.3). The dissolution rate couldn't be measured accurately due the rapid increase, but a three-fold increase in the dissolution of 2:1 fluoxetine HCl/succinic acid cocrystal was observed compared to the API. Whereas, 1:1 co-crystal of fluoxetine HCl/benzoic acid and 2:1 fluoxetine HCl/fumaric acid were half and same as that of the API respectively. These results may become complicated with co-crystals, therefore, further studies need to recognise various factors to interpret the intrinsic dissolution data correctly (Schultheiss and Newman, 2009; Qiao *et al*., 2011).

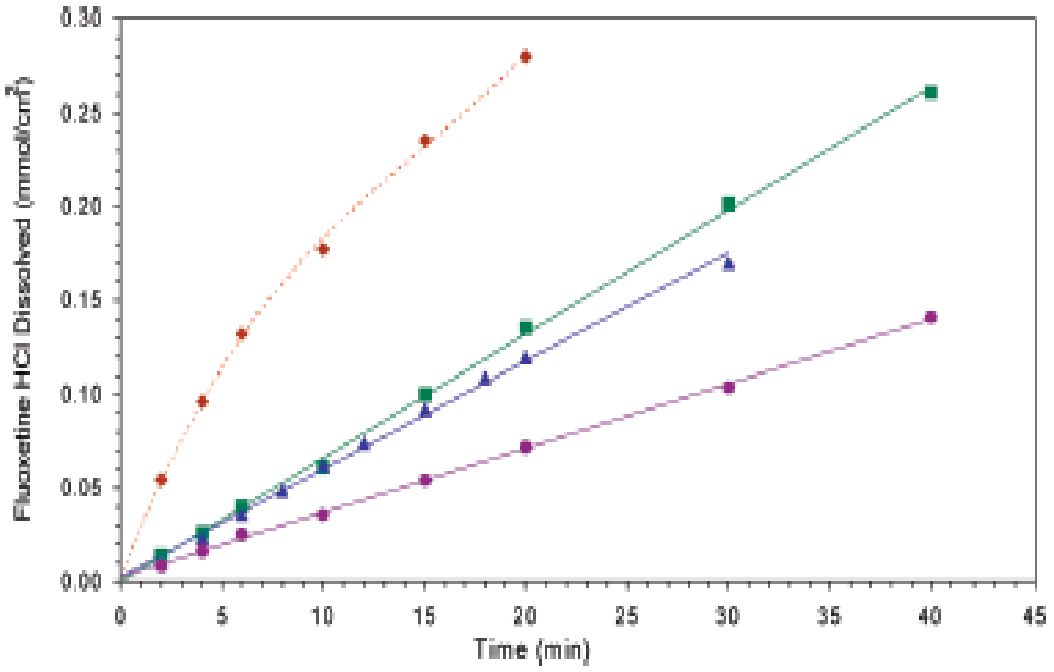

Figure 1.3. *Dissolution profiles of fluoxetine HCl and its co-crystals in water at 100° C: 1) fluoxetine HCl/succinic acid co-crystal (Top ♦); 2) fluoxetine HCl (middle ■); 3) fluoxetine HCl/fumaric acid co-crysta (middle ▲); 4) fluoxetine HCl/benzoic acid co-crystal (bottom ●) (Schultheiss and Newman, 2009).*

Recently, poor aqueous solubility of an API, niclosamide (HNic) was modulated by introducing four new salt co-crystals with sodium and potassium salts, where both the neutral and ionic forms were present in continuance. The new idea of salt co-crystals worked as a reliable method to achieve high intrinsic dissolution rate (Grifasi *et al.*, 2015).

Bioavailability:

Bioavailability is the measurement of absorption of the unchanged administered drug into the systemic circulation and is the ultimate goal for co-crystal investigation. These studies are performed during early development to determine the pharmacokinetics data in animals. The animal bioavailability studies reported on co-crystals so far are very limited. A pharmacokinetic study by McNamara *et al.*, 2006

has shown a three-fold increase in bioavailability using the co-crystal over its API. However, it should be noted that the intrinsic bioavailability study reported the solubility increase of the co-crystal by 18 times due to the conversion into its parent form as revealed by XRD Even though, the co-crystal may have dissociated in the animal studies, it does show an increase in its bioavailability. Another study on indomethacin- sachharin co-crystal has also shown that the increase in bioavailability is significant (Jung *et al*., 2010). There has not been a direct correlation between *in-vitro*/*in-vivo* studies as dissociated co-crystals in *in-vitro* have shown improved bioavailability in animals. Therefore, this area needs to be further explored (Schultheiss and Newman, 2009; Qiao *et al*., 2011).

New strategies have involved supersaturated drug delivery systems such as suspension formulations of co-crystal with its maximum apparent solubility, a surfactant (TPGS, tocopheryl polyethylene glycol succinate) and a precipitation inhibitor (HPC, hydroxyproplycellulose) optimised using *in-vitro* powder dissolution; to successfully improve its bioavailability. It was observed that the danazol:vanillin co-crystal when administered to rats as unformulated traditional neat co-crystal suspension rapidly converted into low-solubility crystal form; depicting low absorption. In addition, the presence of danazol polymorph as suspension with excipient did not produce significant effect on bioavailability. Whereas, co-crystal combination of 1% TPGS surfactant and 2% HPC in *in-vivo* studies resulted in relative bioavailability of 100% suggesting synergy between the excipients (Childs *et al.,* 2013).

1.2.2. Supramolecular chemistry in co-crystal formation

Crystal packing and engineering has now advanced in the preparation or supramolecular synthesis of new solids. The concept of supramolecular chemistry lay particular emphasis upon the idea that the growth of crystalline compound is a manifestation of directed self- assembly of different components. Co-crystal components exist in a specific stoichiometric ratio and are constructed through intermolecular interactions such as hydrogen bonding, p-stacking, and vander Waals forces (Yadav *et al*., 2009; Qiao *et al*., 2011, Khan, 2010; Zukerman- Schpector and Tiekink, 2008). These studies are associated with CSD (Cambridge Structural Database) statistics followed by experimental work to design a new compound after detailed understanding and exploitation of supramolecular synthons. The selection of an appropriate co-former is determined by the detailed knowledge of the functional groups present in the molecule (Shan and Zaworotko, 2008). The most commonly used co-formers that can co-crystallise with APIs include carbohydrates, alcohols, amides, carboxylic acids and amino acids (Figure 1.4). Out of these, carboxylic acid has been extensively studied as a self-complementary hydrogen bond donor and acceptor, amenable to formation of heterosynthons (i.e. bonds between different but complementary functional groups) over homosynthons. The carboxylic acid- amide heterosynthons are more favoured over both carboxylic acid and amide homodimer as in the case of indomethacin-saccharin (IND-SAC) co-crystals (Figure 1.5**)** (Vishweshwar *et. al*., 2006; Qiao *et al*., 2011).

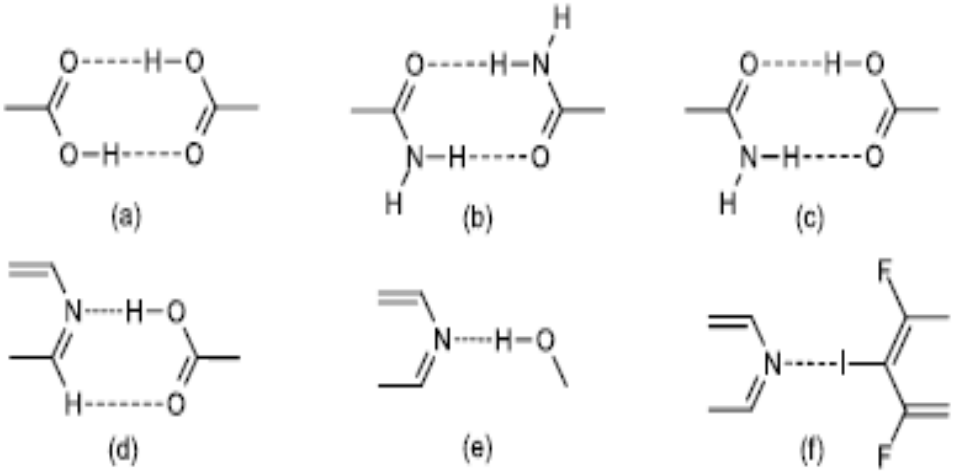

Figure 1.4. *Hydrogen bonding in crystal engineering: (a) acid-acid, (b) amide-amide homosynthons; (c) amide-acid, (d) pyridine-acid, (e) pyridine-hydroxyl and (f) halogen bonding heterosynthons (Nauha, 2012).*

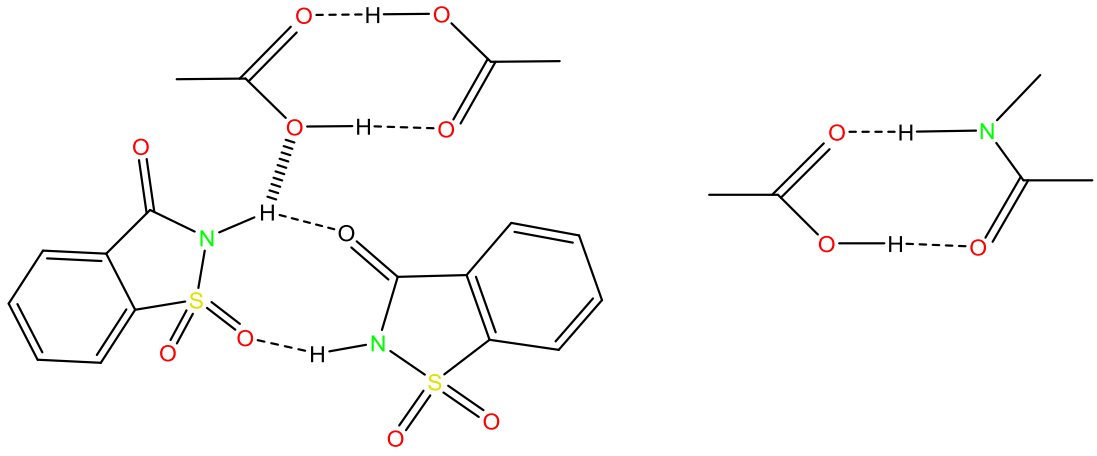

(1) (2)

Figure 1.5. *Indomethacin-saccharin co-crystal structure. (1) acid dimer bonded with weak N-H---O interaction; (2)acid-imide dimer synthon (Qiao et al., 2011).*

However, a conclusion derived in accordance to the empirical rules fall short in the case of IND-SAC co-crystal, where a weak N-H---O bond between indomethacin carboxylic acid synthon interacts with sachharin imide dimer synthon rather than the expected heterodimer between the two synthons (Basavoju *et al.*, 2008).

The designing or packing of the hydrogen bonded synthons in a co-crystal is based upon the structural fit between the components and empirical rules developed by Etter (Etter, 1990; Etter, 1991; Sekhon, 2009). These guidelines use graph set descriptors to propose and classify hydrogen bonding rules as follows:

1) Hydrogen bonding uses all good proton donors and acceptors.

2) Six-membered ring intramolecular hydrogen bonds form in preference to intermolecular hydrogen bonds.

3) The best proton donor and acceptor remaining after intramolecular hydrogen bond formation form intermolecular hydrogen bonds to one another (but all acceptors and donors may not interact with each other) (Etter, 1990; Blagden *et al*., 2008).

Etter *et al.*, 1990 gave rules to explain that detailed work on specific functional groups and the further need for determination of hierarchies of hydrogen bonding. A study based on the hierarchy of hydrogen bond (as per CSD) in a pyridine moiety observed that the strength of carboxylic acid hydroxyl and alcoholic hydroxyl donor groups were comparable, while pyridine-hydroxyl synthon was achieved in the presence of cyano acceptor (Shattock *et al*., 2008; Bis *et al*., 2007). CSD database is a good source to find new useful synthons, but may sometimes be biased towards known repetitive results (Nauha, 2012).

Crystallisation is influenced by other factors such as close packing of molecules, weaker interactions and kinetics. In contrary to Etter's third rule of supramolecular synthon polymorphism, experiments using 4-hydroxybenzoic acid and 2, 3, 5, 6-tetramethylpyrazine produced a polymeric Form I (acid-acid homosynthon) from

acetone and a more stable Form II (acid-pyridine heterosynthon) from acetonitrile-methanol. In addition, Form I transformed into Form II at room temperature which explains for the possible kinetic behaviour (Sreekanth *et al*., 2007; Nauha, 2012).

1.2.3. Computational approaches

Crystallisation can be influenced by various factors such as process parameters, crystallisation medium composition and supersaturation within a process. Screening is a method used to understand and predict the effects of these variables that promote crystal nucleation and growth, in order to identify a robust procedure to develop a desired product (Morissette *et al*., 2004). Procedures involved in pharmaceutical companies can be expensive and time-consuming. Therefore, it demands for simple pre-screening methods to predict crystal structures. Selection of co-crystal former is an important initial step to co-crystal screening. One of the methods anaylsed 131 molecular descriptors such as, size, shape, hydrogen bond donor and acceptor to predict for co-crystals found in CSD (Fabian, 2009). The study found similar shapes and polarity of coformers, but no relation between the size of molecules or the number of hydrogen bond donor and acceptor was observed. Another study used Hansen solubility parameter (Mohammad, Alhalaweh and Velaga, 2011) as a model to postulate that co-crystal formation is enhanced by the miscibility of the two starting compounds. Therefore, these findings could be used as pre-screening step prior to co-crystal development (Nauha, 2012).

1.3. Co-crystal screening

Traditionally, solid forms were synthesised and studied by using different process methods coupled with modern analytical tools of characterisation. Methods

employed for screening such as combination of solvent recrystallisation (Mirza *et al*., 2008), mechanochemistry and thermal analysis are slow and the small fraction of process space can contribute to form diversity. Predictive methods to estimate the crystalline packing arrangement (e.g., hydrates, solvates, co-crystals) and assess their polymeric behaviour has become difficult. Manual screening strategies to explore diversity of a compound discovery cannot be used as a well-established method. Therefore, in order to understand the link between processes that control nucleation and crystal growth, high-throughput (HT) crystallisation systems have been developed. Three steps involved to design these experiments are: design of experiment (DOE), execution and analysis of data, using both hardware and software to track the progress of experiment and store data. These small scale methods help to perform large number of experiments whilst reducing the material demand. In addition, it can create a larger pool to identify functional parameters responsible for forming co-crystal, minimising process modification, risk of form change and evaluate their properties to obtain patent protection (Morissette *et al*., 2004). Further to this, binary and ternary phase diagrams are described below to explain the suitable phases required to for the reproduction of co-crystals.

1.3.1. Scale up of co-crystal hits

The two main issues faced while constructing a solid phase selection strategy for API forming co-crystals are: first, how to implement phase screening in a large space to identify combinations of co-crystals; second, scaling up of the co-crystal hits for pharmacokinetic evaluation. Therefore, ternary phase diagrams (TPD) are constructed to define the equilibria between the solid phase and the chosen solvent. TPD allows the understanding of thermodynamic outcome of co-crystal formation by describing the three phase behaviour of a system [for the components (A and B), co-

crystal (A-B) and given solvent (S)] (Figure 1.6) (Naura, 2012; Blagden *et al*., 2008; Leung *et al*., 2012).

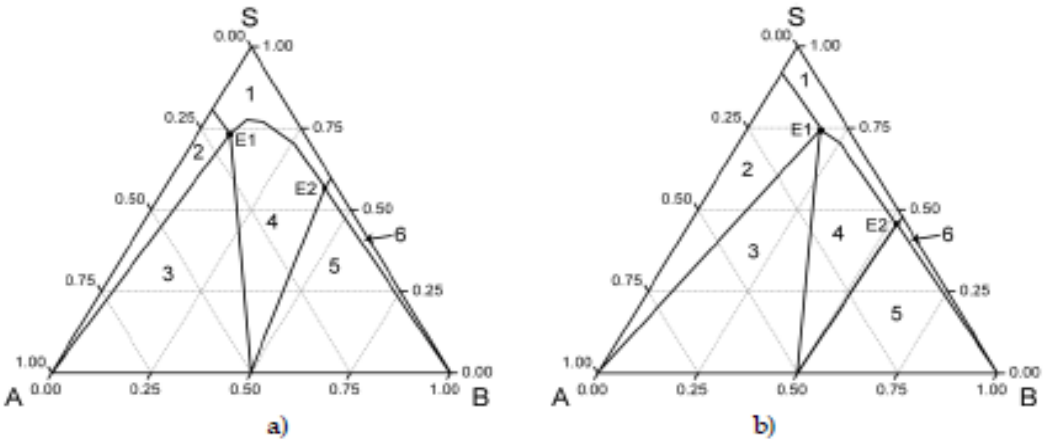

Figure 1.6. *TPD of components A and B forming 1:1 co-crystals in solvent S; a) when solbilities for the two components are quite similar, b) when the solubility of A is far lower than that of B. Measurements in mole fraction (Nauha, 2012).*

Ternary phase diagram is an equilateral triangle with mole or weight fraction of each of the three phases as shown in the figure above. The phase space region within the equilateral triangle depends on the component solubilities, as differences can alter their location and size. This TPD represents six zones for a system with one co-crystal for A and B. Zone 1 has components, A and B dissolved in the solvent and is in a homogenous liquid phase. In zone 2 and 6 there is a solid component A and B, respectively in a liquid phase. Zone 3 has solid component A and 5 has component B, alongside solid co-crystal A-B and a liquid phase. Whereas, zone 4 is the main zone of concern with co-crystal AB and the solvent. The solvent is in equilibrium with A and the co-crystal at point E1, and with B and the co-crystal at point E2. As seen in the figure above, the difference in the system is due to the two types of component dissolution, that is, congruent and incongruent dissolution. Figure 1.6a) shows congruent system, where the components possess similar solubilities, and b) where the second component crystallises as the first one dissolves due to the lower

solubility of A (incongruent system). Therefore, in a congruent system, solution evaporation of equimolar ratio of A and B to the solvent will form 1:1 co-crystal as it goes up the line (Nauha, 2012). Whereas, incongruent mixture in solvent may result in a mixture of co-crystal and single component phase as it either passes through zone 5 (mixed phase) or zone 6 (single phase) (Blagden *et al*., 2008; Nauha, 2012).

A TPD is constructed by measuring the solubility curves of A, B and the co-crystal (x_A, x_B, x_{AB}) thereby explaining the stability of a co-crystal in the solvent (Figure 1.7). The eutectic points E1 and E2 are the points where the solubility curves of the components coincide with the solubility curve of the co-crystal. Straight lines are drawn from these eutectic points to the solid phases A, B and the midpoint on the bottom of the triangle (in case of 1:1 co-crystal). The solubility of the co-crystal with the change in the ratio of the two components is determined by the curve connecting E1 and E2 (Nauha, 2012; Leung *et al*., 2012).

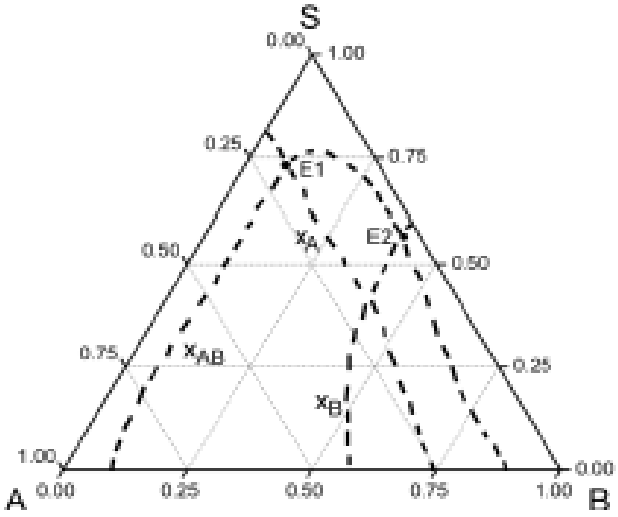

Figure 1.7. *Phase diagram formed by the solubility curves of A, B and the co-crystal in the solvent S, as x_A, x_B and x_{AB} respectively (Nauha, 2012).*

Current work has discovered two new co-crystal forms of compound 1, a GPR119 agonist (API for treatment of type II diabetes) with benzoic acid (BA) and maleic acid (MA) with a new high throughput screening approach. The critical region in the TPD was rapidly mapped and the co-crystals (1-MA and 1-BA) were scaled up by the addition of an anti-solvent. The critical points, E1, E2 and a new third critical point (at the base of the triangle) which did not change with solvent composition, were determined for a binary solvent mixture (Leung *et al*., 2012; Szewczyk *et al*., 2011).

Ternary phase diagrams can be complicated when there is more than one form of co-crystals and is restricted to one solvent at a time. An experiment constructed a reference diagram for a solvent using a calorimetric method to circumvent this issue. The solubility data of A and B, and the slope of the co-crystal curve extracted from the reference diagram were used to estimate the phase diagrams for other solvents (Ainouz *et al*., 2009). Guo *et al*., 2010 attempted to discover co-crystal system (phase diagram) for caffeine and maleic acid which produces two co-crystals with different stoichiometries (1:1 and 2:1). The study failed to determine a single crystal of 2:1 co-crystal through this thermodynamic measurement. However, they could reproduce 1:1 co-crystals from acetone in which the solubilities were quite similar, but still showed an incongruent system. Hence, the observation of new polymorphs of co-crystals or the components implies that the nucleation phase could have been kinetically driven (Blagden *et al*., 2008).

Further study was conducted for the stoichiometrically diverse co-crystal systems of caffeine and maleic acid. It explains that co-crystal zone for 1:1 in the TPD depends on the solubility product of the two components and may disappear if the components acquire different solubilites. However, this does not mean that 1:1 co-

crystals do not occur as it can still be favoured kinetically. The spontaneous crystallisation of 2:1 phase was reported in ethyl acetate solution where the relative solubility was reduced from 40 to 7, compared to that in acetone. This was the first study to investigate the importance of choice of solvent not only on TPD but also as a kinetic screening method of phase nucleation for stoichiometrically diverse co-crystal (Leyssens, 2012).

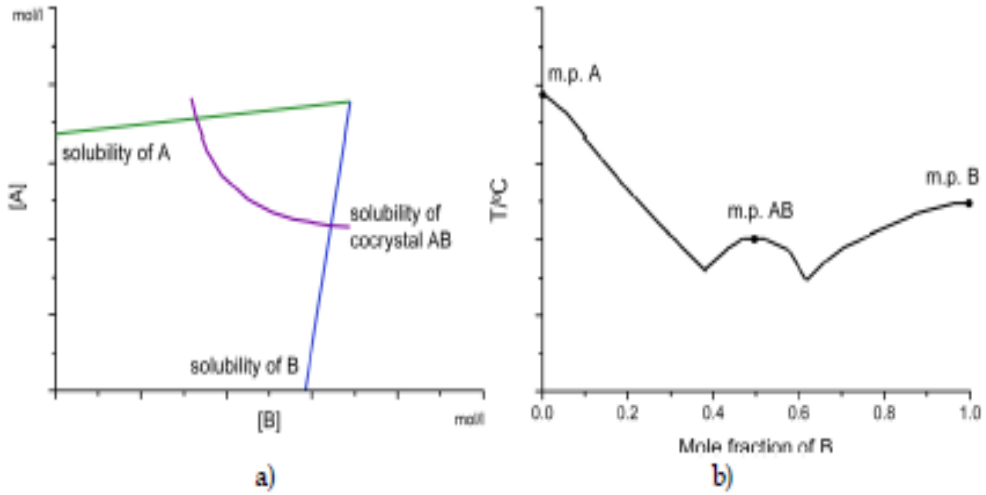

Figure 1.8. *Schematic representation of a) phase solubility diagram, illustrating concentration dependent solubility of A and B, and the solubility of co-crystal AB; b) binary phase diagram (Nauha, 2012).*

In addition to ternary phase diagrams, phase solubility diagram (PSD) and binary phase diagram (BPD) have been used to depict the phase behaviour of the components and co-crystals. PSD represents the solubility curves of A, B and co-crystal AB dependant on the solution concentration of A and B (Figure 1.8a). For example, a decrease in the solubility of (carbamezapine) CBZ and (Nicotinamide) NCT co-crystal was observed with an increase in the concentration of NCT. These findings represent the effect of equilibria between solution concentration and solid phases, and solubility product to induce co-crystal formation (Nehm, 2006). The DSC thermal data of the pure samples and their mixtures are used to construct an

ideal binary phase diagram as shown in Figure 1.8b). It is given by a plot of the melting points of mixture of starting material as a function of the mole fraction of the components. The points for the eutectics between each phase and the number of co-crystalline phases within a system are included. A BPD gives information for solid-state contact between the two components to form co-crystals through a melt interface. However, it cannot be employed for solution crystallisation (Blagden *et al*., 2008; Nauha, 2012).

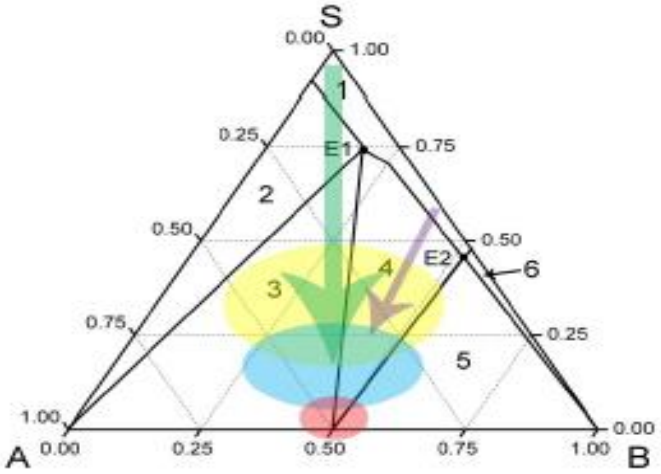

Figure 1.9. *Region of techniques on phase diagram. Green arrow: solution crystallisation from a stoichiometric solution. Purple arrow: reaction crystallisation. Yellow ellipse: slurry crystallisation. Blue ellipse: sonochemical co-crystal formation area. Red ellipse: grinding area (Nauha, 2012).*

Moreover, it is not reasonable to conduct phase diagrams for a screening a large number of coformers. The co-crystal synthesis methods will be discussed further beginning from the solvent crystallisation, solution-mediated transformation, mechano-chemical, and other liquid assisted techniques. Results interpreted in another experiment as η (the ratio of solvent volume to the sample weight) was used to compare techniques such as liquid-assisted grinding and slurry followed by sonication (Friscic *et al.,* 2009). These quantities can be incorporated into the phase

diagram (Figure 1.9) to determine the area of experimentation explored so far (Nauha, 2012).

1.3.2. Solution based crystallisation

The most common technique used for polymorph screening is solution based crystallisation (Zhang *et al*., 2007). This method is of great importance due to the possibility of attaining co-crystals for structure determination by single crystal X-ray diffraction (SXRD). The experiments performed using solution crystallisation begin from zone 1 in the TPD as shown in figure 1.9. In practice, solution crystallisation can be performed by two strategies. First, using evaporation technique which involves co-crystallisation via stoichiometric evaporation of components from various solvents. TPD explains that equimolar components with similar solubilities in a solvent produce 1:1 co-crystal upon evaporation. The use of complex solvent mixtures in case of incongruent dissolution system hinders the formation of solvates and is therefore recommended over congruent systems. However, system with solvent mixtures of varying rate of evaporation lack control and can be hard to handle. Second, use of non-stoichiometric solutions in order to obtain co-crystal stability region as explained by TPDs, using non-congruently saturated solvents. In a study by Childs *et al*., 2008, CBZ added to saturated solutions of 18 coformers attained pure co-crystals (Qiao *et al*., 2011). This is also known as reaction crystallisation which begins with a saturated solution of more soluble component (zone 1) to less soluble component (zone 4) (Nauha, 2012).

Cooling crystallisation is another solution method which has attracted more attention for industrial application. This involves heating and varying the temperature of the crystallisation system by cooling it down. TPD in conjunction with cooling

crystallisation can be used to predict co-crystals, though it can change asymmetrically with temperature. When the solution mixture (zone 4) gets supersaturated with respect to co-crystals upon cooling the thermodynamically expected product is a co-crystal (Qiao *et al*., 2011). But, there might be another kinetic or thermodynamic product at higher temperature that might crystallise out. To overcome this problem, seeding can be utilised in the system (Naura, 2012). An analysis of CBZ/NCT slurry used an in-situ ATR-FTIR (Attenuated total reflectance-Fourier transform infrared spectroscopy) probe to determine the effect of superstauration and kinetic pathway for cooling crystallisation (Gagniere *et al*., 2009).

Supercritical fluid (SCF) technology has been recently applied to the area of pharmaceutical co-crystallisation. It was initially developed to avoid the problems of aggregation and agglomeration observed in case of micronisation, enhancing the drug properties. SCF was discovered as a potential technique to develop indomethacin-saccharin co-crystal by using three steps: solvent power, supercritical anti-solvent technique and fast atomisation of the solution (Padrela, 2009, Sekhon, 2009; Llinas and Goodman, 2008).

Moreover, spray drying has been suggested as an alternative to obtain pure co-crystals from incongruently saturated systems. It is believed that the co-crystals formed via spray drying were mediated by an amorphous phase formation, which is often observed in case of spray drying of pure components. This kinetically controlled route has been suggested to reduce the effects of thermodynamics. The mechanism involved in spray-drying process is not completely understood, therefore further knowledge is required to scale up (Valega and alhalaweh, 2010; Brittain, 2012). Similarly, rotary evaporator (rotavap) has been used as fast solvent

evaporation technique and quick screening tool for new co-crystals forms (Bag *et al.*, 2011).

Pagire *et al.*, (2013) introduced the concept of spherical crystallisation to form CBZ/SAC co-crystals and studied the role of kinetics and thermodynamics in this process favouring its two forms; Form I (stable) and Form II (metastable). This process involves solution of the two components in a good solvent added to a bad solvent, leading to crystallisation and then forming agglomerates with an immiscible bridging liquid added drop-wise to the solution being stirred (Figure 1.10). The degree of supersaturation depending on variables such as solvent selection, solvent proportions, higher stoichiometric ratio of components and, immediate and delayed addition of the bridging solvent acts as a deciding factor favouring one of the two co-crystal forms.

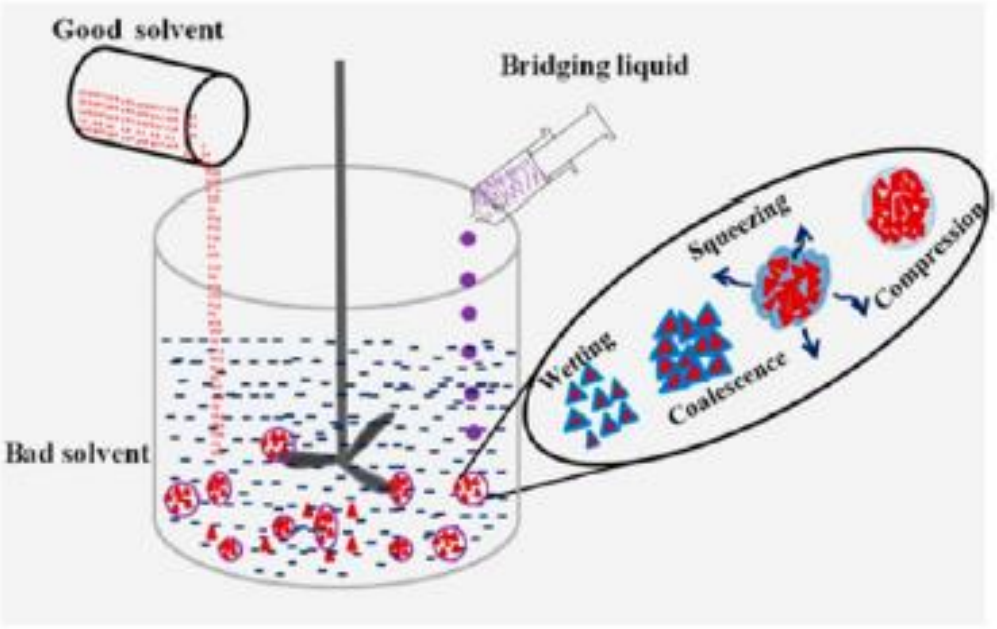

Figure 1.10. *Spherical co-crystallisation process, where bridging solvent leads to agglomeration in stages: coalescence of wetted co-crystals, squeezing of bridging solvent and compression due to agitation (Pagire et al., 2013b).*

For instance, high amount of good solvent favoured Form I; high amounts of saccharin favoured Form II; 2:9 ratio of good to bad solvent favoured Form II, and bridging liquid added 10 minutes after pouring good solvent into bad, resulted in Form II (Pagire *et al*., 2013b).

1.3.3. Solution-mediated transformation

Solution mediated phase transformation (SMPT) is a technique that involves conversion of an API into co-crystal utilising a liquid phase (slurry or suspension equilibration). The mechanism uses minimal amount of solvent required to dissolve the mixture of A and B, represented in the lowest solvent percentage area of TPD (Blagden *et al*., 2008). The solution mediated transformation occurs when the solvent becomes saturated with co-crystal which then crystallises out, dissolving more of A and B until it becomes undersaturated. Some cases might show the emergence of pure A or B alongside co-crystal lying in zone 3 or 5. The main kinetic barrier observed in slurry SMPT is the time taken to attain nucleation of co-crystals (Naura, 2012). SMPT combined with phase diagram was used to detect polymorphs of carbamezapine-isonicotinamide co-crystals. The kinetic barrier helped to identify the formation of a metastable polymorph before it could convert into a more stable one (Horst *et al*., 2008).

An earlier study reported microwave irradiation to illustrate the importance of nanostructures for enabling chemical transformation by sonocrystallisation, forming nano-cocrystals of aminonitropyridines and benzenesulfonic acids (Sekhon, 2009). Sonochemical cocrystal processing method utilises ultrasound to the slurries of co-crystal components. The ultrasound augments the mixing of components, reducing the amount of solvent required. This process assists in dissolution and nucleation of

the co-crystal at a faster rate. Friscic *et al*., 2009 compared two methods, sonochemical and mechano-chemical utilising liquid as a transformation phase, but differing in the amount of solvent and means used to obtain co-crystal. The study deduced the volume of liquid phase in μL mg^{-1} required for the design of co-crystallisation experiment in each case. The observed results favoured the formation of co-crystal when the amount of solvent was lowered, as expected when the solvent is saturated with respect to the reactants. Moreover, mechano-chemical co-crystallisation (i.e. grinding or milling) was chosen over sonochemical due to lower levels of solvent achieved (Naura, 2012).

In the above experiment, thickness of the slurry (lower values of η) was observed to initiate co-crystal formation. The application of ultrasound on the solution affects the nucleation rate due to the presence of cavitation energy. This event of cavitation encourages nucleation at lower supersaturation levels, thereby reducing the induction time and the metastable width. Hence, ultrasound was identified to overcome the challenge of supersaturation in a conventional solution mediated technique, when two components exhibit a distinct variation in their solubilities. Successful studies performed ultrasound assisted solution co-crystallisation (USSC) to produce co-crystals from non-congruent soluble pair of caffeine and maleic acid in methanol. This technique obtained pure 2:1 co-crystals of caffeine-maleic acid which was unsuccessful in the case of slurry sonication and solvent cooling. Further understanding of the nucleation mechanism involved in USSC is still required (Aher *et al*., 2010).

1.3.4. Mechanochemistry

a) Neat or solvent assisted grinding

Over past few years co-crystal preparation via grinding has been a fast and convenient way of screening that involves very little or no solvent. Co-crystals are formed by two different techniques: neat or dry grinding and mechanical liquid-assisted grinding (LAG). Dry grinding consists of mixing of stoichiometric components either manually (using mortar and pestle), or by mechanical means (vibratory mill or ball mill) (Figure 1.11) (Qiao *et al*., 2011; Mirza *et al*., 2008). Co-crystals obtained from solid-state grinding are more consistent compared to that from solution techniques. This may be due to crystallisation conditions, uncontrolled solvent effects and characteristics of hydrogen-bond connectivity. Most of the co-crystals can be developed by both solution and grinding methods, but a few were generated in either of the conditions. Co-crystals developed by solution method has solvent as a stabilising factor for their molecular structure, which may not be feasible while grinding due to the stability of their primary phases. On the other hand, recent technique of adding small amount of solvent during grinding process (liquid-assisted grinding), has an enhanced kinetic effect to facilitate co-crystal formation (Blagden *et al*., 2007). For example, Weyna *et al.*, (2009) discovered 25 new co-crystals via solvent-drop grinding which is green and cost-effective method of production.

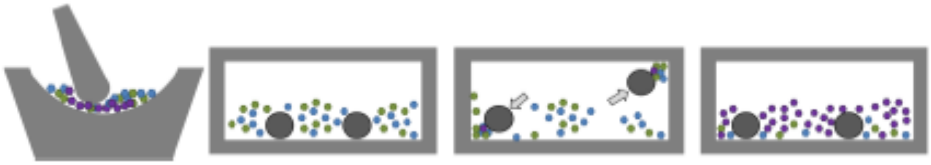

Figure 1.11. *Co-crystals prepared using grinding technique: grinding (mortar and pestle), and ball milling of A and B before, during and after milling. A and B represented by blue and green grow into a purple co-crystal (Nauha, 2012).*

Grinding studies have not completely illustrated its mechanism and have different assumptions. To date mechanisms used to describe neat grinding are molecular diffusion, eutectic formation and amorphous phase acquiring higher energy or mobility for the reactant molecules. This can occur through one of the distinct intermediate bulk phases (a gas, a liquid or an amorphous solid) (Friscic and Jones, 2009). For example, diffusion through gas phase (appropriate vapour pressure) on the surface of the crystals followed by shearing force of grinding, where the reactant molecules develop higher energy with respect to their starting crystalline forms. The mechanism in LAG is supported by solution mediated transformation provided the compounds are soluble in the solvent used. When a solvent in which neither of the components are soluble, kinetic enhancement does not take place and the liquid behave as a diffusion medium. The development in kinetics was justified by additional degrees of orientation and conformational freedom open to the molecules at the various interfaces thereby boosting the chances for molecular collision. Another possibility is the prediction of tiny seeds for co-crystals formed during LAG increasing the rate of co-crystallisation (Trask *et al*., 2004; Qiao *et al*., 2011; Blagden *et al*., 2007).

In addition, the change in the composition of the starting material while grinding seem to control the co-crystal stoichiometry. For example, three of the co-crystals of nicotinamide and five dicarboxylic acids formed in the stoichiometric ratio 1:1 and 2:1, showed reversed stoichiometry upon the addition of excess of nicotinamide. Whereas, two of the co-crystals were more stable as their stoichiometry changed in one direction. Besides the mechanisms explained above, choice of solvent may also control the polymorphic outcome in LAG. It was observed that the nature of solvent

had a profound effect in obtaining two polymorphs of the caffeine co-crystal with glutaric acid (Naura, 2012; Qiao *et al*., 2011).

b) Twin-screw extrusion

Twin-screw extrusion is a viable mechano-chemical method similar to grinding, which produces co-crystals without the use of solvents. The twin screw extruder consists of two parallel screws rotated in different directions to enable mixing and movement of the final product (Figure 1.12). The parameters that influence co-crystal formation are temperature and the extent of mixing. It is an efficient, environmental friendly and scalable process that overcomes the challenges of solution crystallisation, hence avoiding the cumbersome measurements using TPD. This process has been used to demonstrate the continuous solvent-free production of co-crystals such as, caffeine-oxalic acid (Daurio *et al*., 2011) and ibuprofen – nicotinamide (Dhumal *et al*., 2010). Additional work has been performed in monitoring the co-crystal formation using high temperature NIR (near infra-red) probe as a PAT (process analytical technology) tool, in order to envisage the real-time effect of parameters and process understanding as demanded by quality by design (QbD) (Kelly *et al*., 2012).

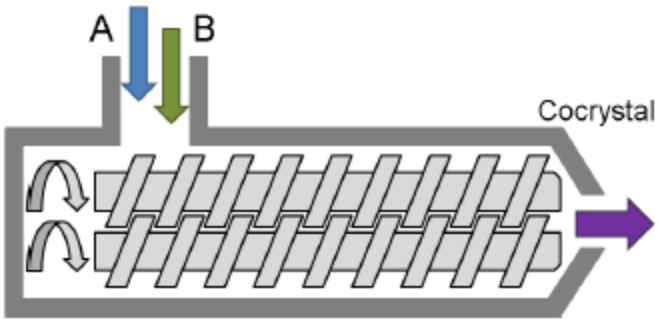

Figure 1.12. *Pictorial representation of a twin screw extruder enhancing co-crystal formation (Nauha, 2012).*

c) Microwave-assisted co-crystals

Microwave-assisted co-crystal is another emerging green technology employed for the synthesis of co-crystals in a short span of time. The study proposed that microwaves enhance the co-crystallisation process by increasing the mobility of the molecule, thereby maintaining the saturation state at the crystal interface. This is explained by the dielectric heating induced by the microwaves which depends on the material properties such as, ability to absorb and convert electromagnetic radiation into heat, and to undergo polarisation within the electromagnetic field (Figure 1.13). Pure 1:1 co-crystals of non-congruent pair of caffeine- maleic acid was developed in the presence of water and methanol. An additional form II of 1:1 caffeine-maleic was observed in methanol. Hence, the results deduce that the factors affecting co-crystal formation via microwave radiation are the dielectric properties and the solubility of the components in the solvent (Pagire *et al*., 2013a).

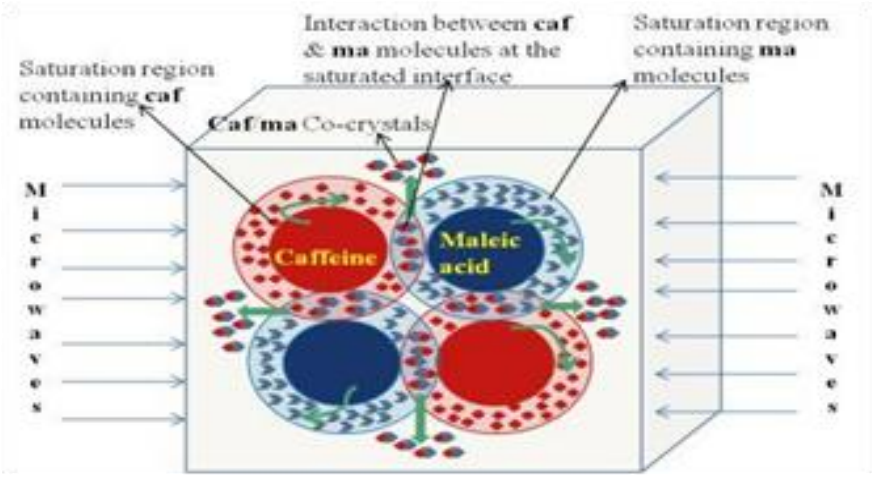

Figure 1.13. *Saturated caffeine/maleic acid 1:1 co-crystals under microwave irradiation (Pagire et al., 2013a).*

1.3.5. Thermal screening

Thermal screening is a good visual technique for early screening of thermally stable and non-volatile compounds. It can either be performed by using a hot-stage thermal microscopy method (also known as Kofler technique) or with a multi-component DSC screening. Hot-stage microscopy has been used historically as a route to access the thermodynamic landscape within the binary phase diagram, in order to visualise the melting profile of a co-crystal system. It utilises the methodology of mixed fusion (or contact), to obtain a zone of mixing by first melting and solidifying one component (high melting point) on the slide, followed by melting the other component (lower melting point) touching the first one, causing simultaneous melting of a portion of first component. This is then viewed and reheated under polarised light to identify the number of phases present and the melt temperatures. The co-crystal production results in two eutectic melting zones on the sides of the zone of mixing, whereas only one eutectic melting zone is observed when no co-crystals are formed (Figure 1.14) (Qiao *et al*., 2011; Nauha, 2012). Further to this, it can be used to observe any polymorphic transition within the individual component and the co-crystals. In a study, the seeds of co-crystals collected from the mixing zone were used to enhance co-crystallisation via solution methods (Blagden *et al*., 2008).

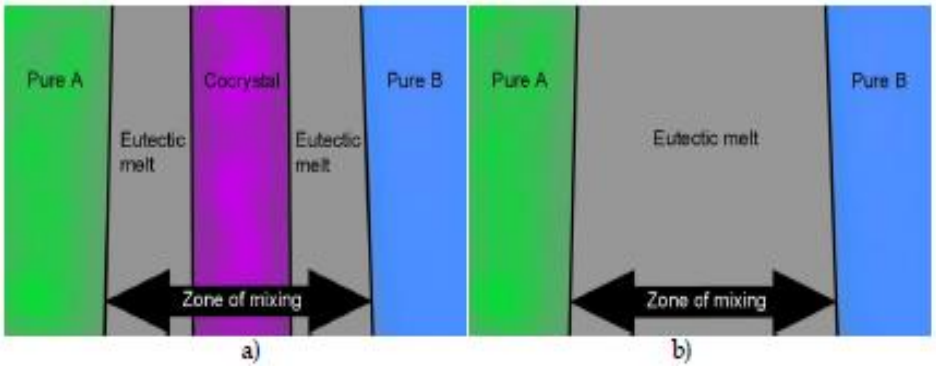

Figure 1.14. *Schematic diagram of mixed fusion method. a) both the eutectics melt leading to zone A, B and co-crystal formed whereas, b) one eutectic melt, hence no co-crystal (Nauha, 2012).*

Thermal screening applying a DSC can be performed on the mixtures of components A and B in different molar ratios, whilst heating. Here, formation of a co-crystal is indicated by the appearance of two consistent endotherms, representing eutectic melting followed by co-crystal melting. The method uses little material and no solvent, however, can be difficult to predict when polymorphs of either of the components exist (Nauha, 2012).

1.4. Co-crystal characterisation

1.4.1. Crystal characterisation

Characterisation of co-crystals involve physicochemical properties determined by various analytical techniques such as, infrared (IR) spectroscopy, single crystal X-ray diffraction (SXRD), powder X-ray diffraction (PXRD), Raman spectroscopy, solid state nuclear magnetic resonance spectroscopy (SSNMR), differential scanning calorimetry (DSC), scanning electron microscopy (SEM), tetrahertz and mass spectroscopy (MS). These techniques help in the structural investigation of crystal formation, that is, checks for crystal purity, any polymorphic transformation or degradation, interaction between the components, mass of the complex and thermal

profile. SXRD is an important technique required to determine the structure of co-crystals at an atomic level, provided a single co-crystal is produced. This condition is hard to achieve in all cases, therefore, PXRD is rather an adopted method to confirm the presence of co-crystals. However, PXRD cannot discriminate co-crystals from other phases that may develop, for example, solvates, hydrates, and polymorphs (Miroshnyk *et al*., 2009; Qiao *et al*., 2011).

To further understand the solid-structure, spectroscopic rules have been developed for distinguishing between salts and co-crystals. Studies engaged in sodium salt formation of different acids and 1:1 co-crystals formed by free acids realised that these systems can be distinguished using IR spectroscopy The energy of carbonyl group in methods involving carboxylic acid, could be used to distinguish co-crystals from salts. When a salt is formed, free acid absorption band found in the frequency range of 1680-1690 cm^{-1} is replaced by anion band at a frequency between 1550-1600 cm^{-1}. Whereas, when a co-crystal is formed, a small shift of absorption band is observed to a higher frequency range of 1700-1730 cm^{-1} (Brittain, 2012). In addition, Raman spectroscopy can be applied to obtain the low frequency vibrational mode and understand the formation of supramolecular synthons. It has many applications in identifying characteristic peaks of co-crystals (Aher *et al*., 2010), and has been further applied as an in-situ observational tool in the high-throughput screening of slurries (Kojima *et al*., 2010).

High-resolution SSNMR is another powerful technique for the characterisation of co-crystals, hard to achieve by SXRD. Various types of NMR chemical shifts can enable element-specific observation of unique nuclei and distinct chemical sites present (Khan *et al*., 2010). A green and automated thermal method, DSC was recently developed for rapid screening of co-crystals (carbamezapine-nicotinamide)

(Lu *et al*., 2008). This technique produces additional thermal data besides melting point, that is, enthalpy of melting. SEM is another important analytical method that produces images by means of a high-energy electron beam generating information on sample's surface topography. Another highly sensitive technique compared to Raman known as terahertz time-domain-spectroscopy (THz-TDS), can identify chiral and racemic hydrogen-bonded co-crystals similar in supramolecular structure. Therefore, integration of different types of spectroscopic methodologies can elucidate better understanding of co-crystalline materials, saving cost and time (Qiao *et al*., 2011).

1.4.2. Particle characterisation

In relation to the effective use of co-crystal as a formulation product post crystal characterisation, other testing tools such as particle size and surface energy analyser can be applied. The particle size of a powder determines its flow and compaction properties (Horiba Scientific, 2014). The shape and size depends on the technique and process parameters involved. The most widely used technique to detect the particle size from submicron to millimeter size is by laser diffraction, which measures the angular scattering of laser beam interacting with dispersed particulate sample. Large spherical particles diffract the light at relatively small angles compared to the smaller particles. The intensity of the angular scattered light is then analysed to obtain the size of particles (Sympatec GmbH, n.d.; Malvern, 2009). The control of particle size distribution is important for reasons such as better dissolution, absorption rates, aerosolisation to penetrate into lungs, suspension and emulsion stability (Horiba Scientific, 2014).

Another technique, surface energy analyser (SEA) involves inverse gas-phase chromatography (iGC) for characterising surface and bulk properties of powder, films, fibres and semi-solids. The principle works by injecting known volumes of gas over the packed solid material in a cylindrical column at a constant flow rate, where it gets absorbed at the surface of the material (Figure 1.15). The FID (flame ionisation detector) measures the time taken by the gas pulse to elute down the column. Different gas phase probe molecules are used to determine wide range of physicochemical information, for example, dispersive and polar surface energy, acid/base interactions, entropy of adsorption, permeability, solubility etc. (Surface Measurement Systems, 2014a).

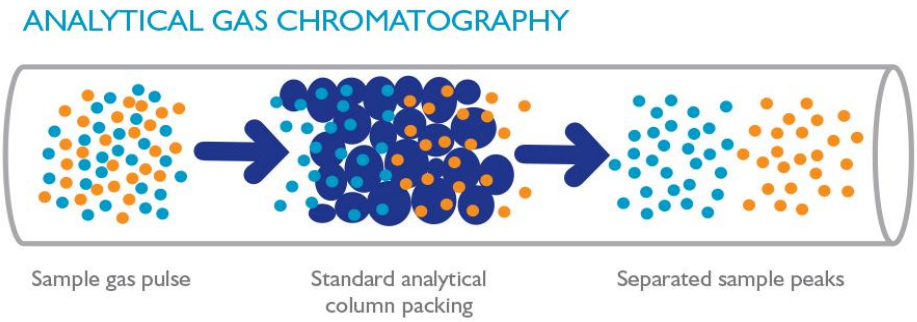

a)

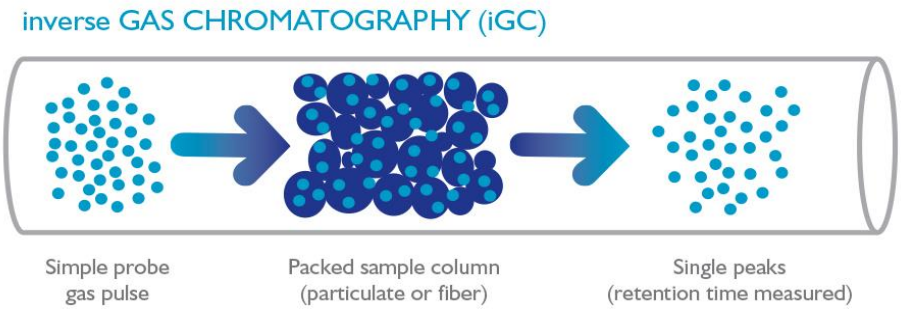

b)

Figure 1.15. *Schematic diagram of: a) conventional gas chromatography (GC); and the reverse, b) iGC followed by SEA (Surface Measurement Systems, 2014b).*

1.5. Challenges in co-crystallisation

New strategies are being examined thoroughly for the development of compounds with suitable physicochemical properties. The complexity of developing molecules is ever increasing with co-crystals that offer more extensive range of co-formers. Introduction of new pharmaceutical engineering processes needs exploration of process variables for discovery of new phases or enhancement in drug's properties. A lot of thermodynamic and kinetic information which is method dependent has been unnoticed. Factors such as type of co-former, the API to co-former ratio, temperature, pressure, technique, solvent, solvent mixtures play an important role in the selection of desired properties (Dafratec, n.d.). Relative solubility of the co-crystal components appear as an important parameter when utilising solution-mediated approaches. For example, highly polar solvent such as acetone shows congruent solubility for curcumin (CUR) and phloroglucinol (PHL); hence producing phase-pure CUR-PHL 1:1 co-crystals. If the solubility of the two components differ a lot; the less soluble component may crystallise out first upon solvent evaporation prior to reaching the co-crystallisation zone (Chow *et al*., 2014).

Co-crystals are known to exhibit enhancement in solubility and hence, dissolution compared to the drug's crystalline and amorphous forms. The crystalline forms have an advantage of being stable compared to the amorphous state. The "spring and parachute" effect for the dissolution of amorphous drug has been related to pharmaceutical co-crystals (Figure 1.16) (Babu and Nangia, 2011).

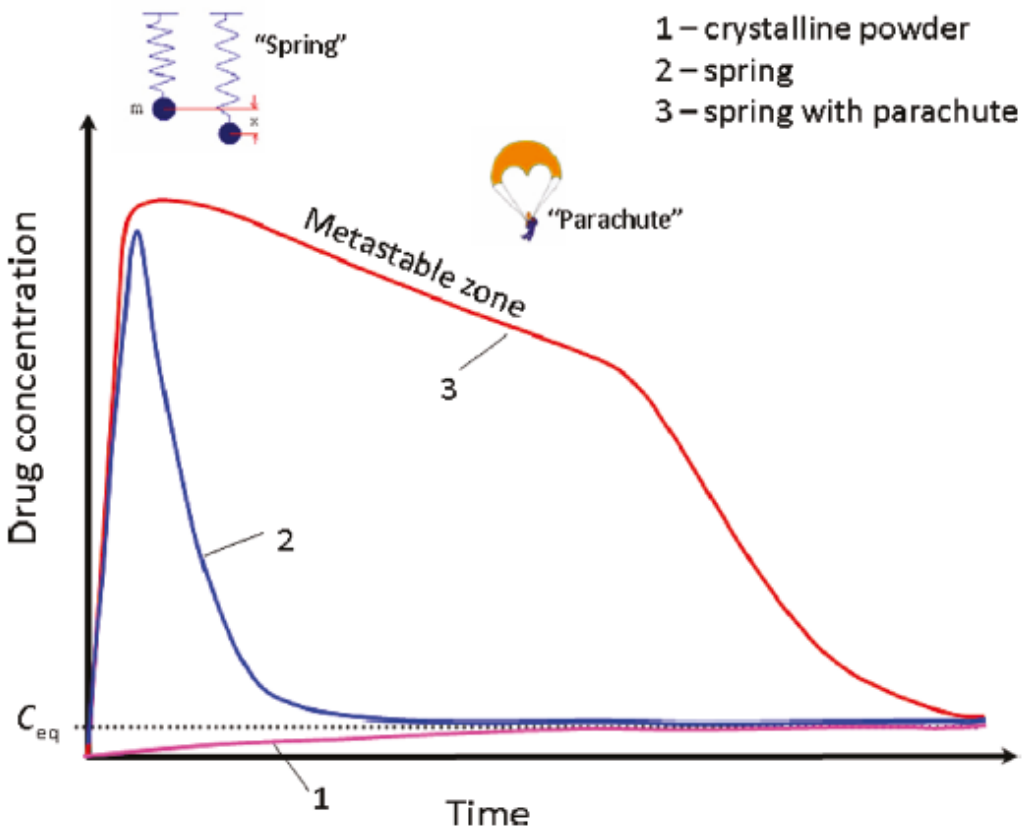

Figure 1.16. *The spring and parachute concept: 1) Low solubility of the crystalline (stable) form; 2) amorphous phase with quick transformation to crystalline form (minutes to hours); 3) Wide metastable zone (hours) maintained by highly soluble forms (Babu and Nangia, 2011).*

The "spring" effect is known to occur due to the quick dissociation of weak hydrogen bonds of co-crystals compared to salts; into amorphous form. The same is observed in case of amorphous drug dispersing from a polymer matrix. The "parachute" phenomenon is maintained over long time-periods due to the transformation of high-energy amorphous form into a metastable form (which possess higher solubility), and then to the stable crystalline form (low solubility) following the Ostwald's Law of Stages (Babu and Nangia, 2011). But, this is may not be a true observation in every co-crystal case. As explained earlier in a study; the conventional aqueous solution of danazol: vanillin co-crystal converted into a low-

soluble crystal form and therefore, it was modified with combination of surfactant and polymer to achieve high absorption levels (Childs, Kandi and Lingireddy, 2013).

1.6. Polymorphism of co-crystals

Polymorphism is an ability of a compound in its solid state, whether it is single or multiple component (co-crystals, salts, hydrates, etc.), to subsist in different crystalline forms bearing same chemical composition (European Medicines Agency, 2014). Polymorphs in solid-state pharamceutics have been an important issue in particular with the development of co-crystals, since they can attain different properties. One of the main properties of concern, that is, solubility can affect drug's bioavailability, efficacy and safety. In addition, polymorph can spontaneously convert from a less stable (metastable) form to a stable form, with the most stable form being least soluble. Therefore, efforts are taken to characterise the most stable form first during the discovery phase, so that it could be used for further testing. A polymorph could be developed in various circumstances such as, change in equipment, manufacturing process, storing conditions etc (Linas and Goodman, 2008; Sekhon, 2009).

Co-crystal provides an opportunity for additional polymorphs with enhanced formulation properties and a rise in patent protection. The growth of the crystals occurs in two steps: first, formation of crystal nuclei; second, growth of these nuclei into a larger single crystal. As explained by Ostwald's rule, the metastable form should exist first. The solution in the metastable state is normally used to produce a single crystal. The width of this metastable region is useful and explains the conditions over which supersaturation can be achieved. Hence, it is used to control

the crystallisation in order to form single crystals over fine precipitates. The figure below shows the time dependant production of polymorphs in various systems, that is, metastable polymorphs observed in a fast process (Linas and Goodman, 2008).

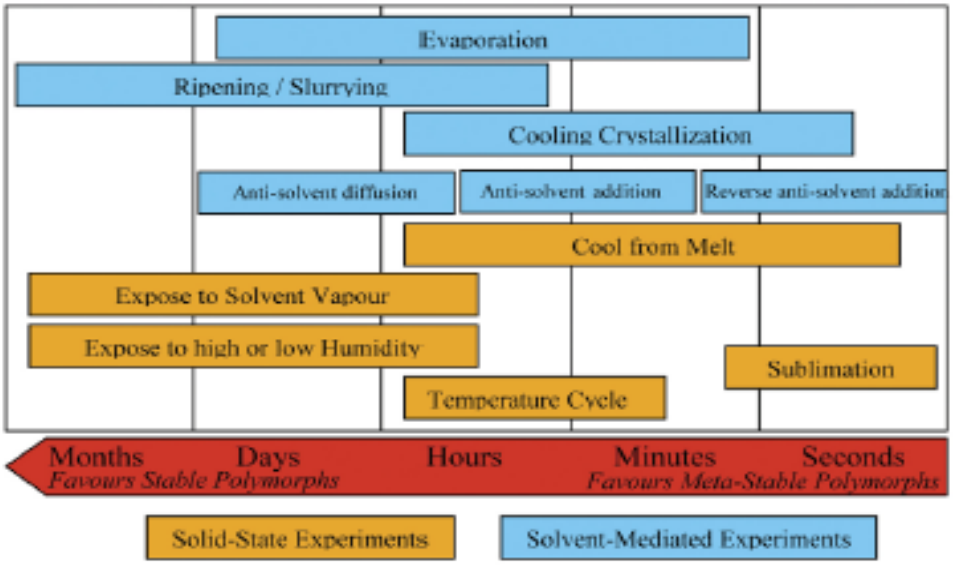

Figure 1.17. *Timescales favouring crystallisation of stable or metastable polymorphs in different techniques (Linas and Goodman, 2008).*

Co-crystal polymorphs of 1:1 caffeine and glutaric acid were observed from solvent evaporation using chloroform. The two forms (Form I and Form II) crystallised simultaneously differing in the torsional angles within the carbons on the methyl group from the acid. On the other hand, both the forms were observed separately in mechanical grinding. Form I was observed with a non-polar solvent, whereas, Form II (stable) was found in a more polar solvent. Form I was unstable under high humid conditions and transformed into Form II in a day. This explains for the stability affected by different polymorphic forms. Further example confirms two polymorphs of 1:1 carbamezapine and saccharin co-crystals. In this case, high-throughput screening was conducted on Form I including 480 experiments using various solvents and their mixtures. In addition, other techniques such as, solvent assisted

grinding and slurry conversion, were performed and characterised using PXRD and Raman spectroscopy. But none seem to produce any additional form of co-crystals. The Form II of the above co-crystal was only found in the case of polymer heteronuclei crystallisation, despite of the deep insight into solution techniques. Unlike the above examples, forms of 1:1 piroxicam and 4-hydroxybenzoic acid cocrystals were distinguished by the tautomeric form present and the hydrogen bond interaction. These were the first discovered forms of co-crystal synthon polymorphism, where one form is present as non-ionised tautomer and other as zwitter-ionic tautomer (Sekhon, 2009; Schultheiss and Newman, 2009).

1.7. Co-crystals as intellectual property

The importance of patents on pharmaceutical co-crystals covers different areas, such as, formulation, method used and the process involved in manufacturing. An invention should qualify three criteria for covering a patent; novelity, utility and non-obviousness. The utility of a co-crystal is not an issue for applications, since there have been many examples illustrating enhanced properties on the therapeutic effects of the API. Furthermore, co-crystals have limited prior art, due to the absence of publications on crystallisation performed with co-former and API. This is an advantage and hence, secures its novelity. The third area of non-obvious is linked to predictability, which is true for co-crystals as crystal engineering and computational analyses are not reliable and therefore, cannot always predict properties and structures. Co-crystals appear to cover a large patent space, even though its predictability is limited. This is accounted due to the fact that there is large number of co-formers, its use as product improvement, chemical structures, and various forms (hydrates, solvates, polymorphs, etc.) discovered (Sekhon, 2009; Schultheiss and Newman, 2009).

Table 1.1. *Examples of co-crystal of pharmaceutical interest.*

API	Co-crystal former	Preparation method	Enhanced property (if known)	Reference(s)
Aceclofenac	Chitosan	Solvent change approach using bio-polymer - Chitosan	Enhanced dissolution	*Mutalik et al., 2008*
Aspirin	4,4'-dipyridil	Slurry conversion		*Walsh et. al., 2003*
Caffeine	Oxalic acid Glutaric acid	Solvent-assisted grinding	Physical stability	*Trask et. al., 2005*
Carbamezapine (CBZ) (Tegretol®)	Saccharin (1:1)	Solution cooling crystallisation ; Solvent drop grinding	Physical stability; favourable dissolution	*Hickey et al., 2007; Wyena et al., 2009*
	Nicotinamide (NIC)	Dihydrate CBZ co-milled with NIC	Stability during storage	*Chieng et al, 2009*
Cytosine	Oxalic acid (4:1) Malonic acid (2:1) Succinic aicd (2:1)	Solvent drop grinding; Solution crystallisation		*Brittain, 2012*
Fluconazole	Maleic, glutaric, fumaric acid	Solvent evaporation		*Brittain, 2012*
Fluoxetine hydrochloride (Prozac®)	Benzoic acid (1:1) Succinic acid (2:1) Fumaric acid (2:1)	Conventional solvent evaporation	Aqueous solubility: Decrease by 50% Two-fold increase in 5 mins Slight increase	*Childs et al., 2004*
Ibuprofen	4,4'-bipyridine Nicotinamide		Higher melting point Racemic form and S-enantiomer	*Walsh et al., 2003; Berry et al., 2008*
Indomethacin	Saccharin	Slow evaporation; Liquid-assisted grinding ; Super-critical fluid	Faster dissolution rate	*Jung et al., 2010; Basavoju et al., 2008; Padrela et al., 2009*
Itraconazole (Sporanox®)	1,4-dicarboxylic acid: L-malic acid	Solvent evaporation	Crystalline, stable form; Improved dissolution rate	*Remenar et al., 2003*
Mefloquine	Several co-formers		Enhanced solubility, dissolution rate; resist conversion into hydrate	*Brittain, 2012*
Norfloxacin	Isonicotinamide Succinic acid Malonic acid Maleic acid	Solvent evaporation	Solubility	*Basavoju et. al., 2006*
Paracetamol	4,4-dipyridyl	Solvent evaporation		*Oswald et. al., 2004*
	Oxalic acid, Theophylline, Naphthalene, Phenazine	Liquid-assisted grinding	Improved mechanical properties/ Enhanced compressibility	*Karki et.al., 2009*
Sulfacetamide (antibiotic for ocular infections)	Isonicotinamide, Caffeine	Liquid-assisted grinding	Reduced solubility for better therapeutic action	*Goud, Khan and Nangia, 2014*

1.8. Techniques

1.8.1. Rotary evaporator (rotavap)

Scientist and engineers continue to execute the removal of solvents using an unavoidable process known as rotary evaporation. Rotary evaporators have been extensively used for single batch and continuous processes. It involves removal of solvents from a solution by heating (Sigma-Aldrich, 2015a). A blanket of vapour persists above a liquid which has a saturation vapour pressure. This pressure increases with temperature until the solution reaches its boiling point; when it becomes similar to the surrounding atmospheric pressure (1 bar) (Monk, 2004, p.188). When assisted with a vacuum, it lowers the surrounding pressure above the solution by getting rid of the vapours and hence, reducing its boiling point. Therefore, it can make evaporation process rapid at lower temperatures under a vacuum. The vacuum levels differ for different solvents in a system. At an optimum vacuum and temperature, the solvent vapours re-condense in the receiving flask with hardly any vapours collecting in the pump. But, if operated at pressures lower than the optimum, the vapours could pass through condenser and condense in the vacuum pump, degrading its performance (Welch vacuum, n.d.).

The figure below shows a rotary evaporator with four major components: hot bath, rotor, condenser, and solvent trap; with an additional vacuum pump which promotes rapid evaporation of solvents with higher boiling points at low pressure conditions (ChemWiki, n.d.).

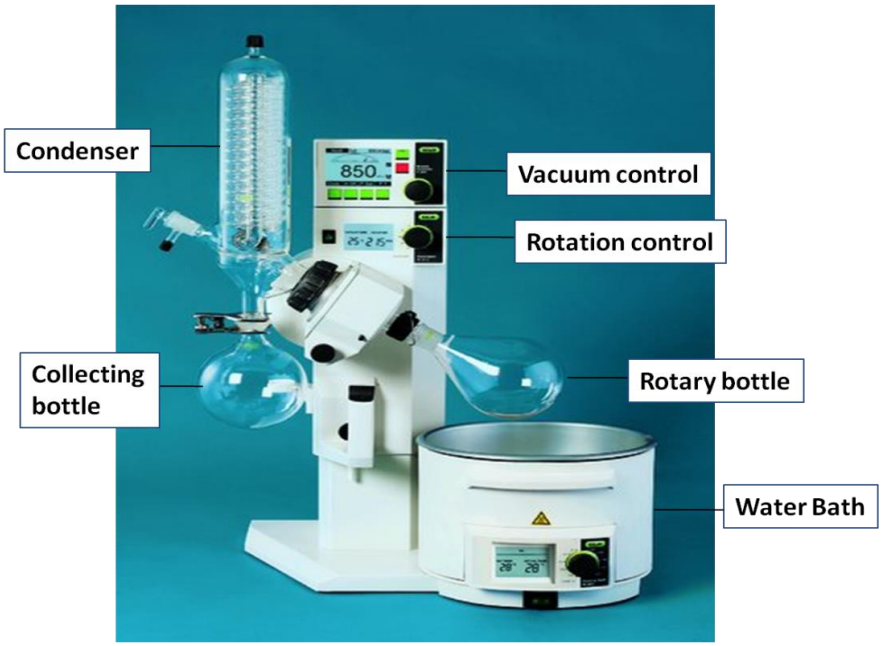

Figure 1.18. *Description of advanced vacuum controlled rotary evaporator (Sigma-Aldrich, 2015b).*

1.8.1.1. Evaporation rate of solvent

This is determined by three different variables: flask rotation speed, bath temperature, and pressure in the flask. The most important variable of concern is the vacuum level as pressure below one atmosphere lowers the boiling point of a solvent. Therefore, the system's functioning could vary depending on the vapour pressure as follows:

1) When pressure is similar to the solvent's vapour pressure at boiling point, the condition set is optimal as most of the solvent condenses out in the condenser without any loss into the pump.
2) When the pressure set is bigger than the solvent's vapour pressure at boiling point, the evaporation slows down.
3) When the pressure is less than solvent's vapour pressure at boiling point, it boils vigorously making the solvent foam and causing considerable loss of the solvent vapours into the pump (Welch vacuum, n.d.).

1.8.1.2. Determining the optimum pressure

The settings for an optimum pressure level for a given solvent are provided by some manufacturers based on various equations such as Reckhard's (equation 1a), where the vapour pressure (P) in mm Hg can be obtained for a given solvent at temperature (T) (Rekhard, 1958).

$$Log\ P = 2.8811 - \frac{[T_A - T]}{[bT]} \qquad \text{(Eq. 1a)}$$

T_A = Boiling point (K) at 1 atmosphere or 760 mm Hg

T = vapour pressure temperature (K) at pressure P (mbar)

b = Reckhard's constant

2.8811 = Adjusting factor for pressure in mm Hg

Table 1.2 represents calculated vapour pressures of solvents at three different temperatures.

Table 1.2 *Reckhard's equation used to measure optimum pressures for solvents at various temperatures (Welch vacuum, n.d).*

Solvent	Constant b	Boiling point at 760 mm Hg (^oC)	Absolute Pressure (mm Hg) for Boiling Point at 25 ^oC	Absolute Pressure (mm Hg) for Boiling Point at 40 ^oC	Absolute Pressure (mm Hg) for Boiling Point at 60 ^oC
Acetone	0.196	56	224	417	N/A
Diethyl ether	0.200	35	517	N/A	N/A
Ethanol	0.159	78	58	131	348
Methanol	0.167	65	119	253	618
Water	0.167	100	24	54	145

Another equation used to illustrate the relationship between boiling point of the liquid and surrounding pressure is the Clausius-Clapeyron's equation. It states that

vapourisation curves of most solvents show a similar relationship between pressure *P*, temperature *T* and enthalpy of vaporisation ΔH_{vap}, where pressure gradually increases with the increase in temperature as shown below,

$$P = Aexp^{(\frac{-\Delta H_{vap}}{RT})} \quad \text{(Eq. 1b)}$$

(University of Waterloo, n.d.)

In this equation, R is a gas constant (8.3145 Jmol-1K-1) and A is an unknown constant. It also calculates the vapour pressure at a different temperature, if enthalpy of vapourisation and vapour pressure is known for a temperature, using the following equation,

$$Ln\frac{P_1}{P_2} = \frac{\Delta H_{vap}}{R}.\frac{1}{T_2} - \frac{1}{T_1} \quad \text{(Eq. 1c)}$$

where, P_1 and P_2 are pressures corresponding to two temperatures, T_1 and T_2 (Turanyl, 2014;University of Waterloo, n.d.). Due to deviation in Clausius-Clapeyron equation at high pressure, a three-parameter, Antoine's equation has been consistently applied to obtain vapour pressure. It involves three "Antoine coefficients", A, B and C which varies depending on substance and is measured over restricted temperatures. The equation is as follows:

$$P = 10^{A-\frac{B}{C+T}} \quad \text{(Eq. 1d)}$$

where, P is the pressure in mmHg and T is temperature utilised in ^{0}C (General chemistry online, 1997-2010).

1.8.1.3. Applications

a) General laboratory use

Rotavap was developed to overcome the problems of overheating and charring caused by conventional distillation systems. With a vacuum system attached, it can help recover solvents at lower pressure and temperatures from temperature sensitive substances. In laboratories; it has been used to obtain clean solvents from used solvents, extraction of essential plant oils, separation of non azeotropic mixtures such as water-acetone, and achieve maximum distillation for low boiling point solvents. New rotavaps have introduced an inert gas supply into the condenser to prevent any conversions during distillation process (IKA, n.d.). However, very low pressure conditions may result into foaming of the solution also referred to 'bumping', which may result into loss of material. Therefore, careful regulation of the vacuum and bath temperature is necessary or a special trap combined with fritted funnel can prevent solid material from passing through (Buchkremer and Brinker, 1990).

b) Co-crystal

A lot of investigation needs to be initiated to understand the role of thermodynamics and kinetics in cocrystallisation. This rising curiosity has led to the use of rotavap as vital technique for screening and manufacturing co-crystals besides narrowing the knowledge gap between other forms of crystalline products. A recent study demonstrated the existence of suspected cocrystal of curcumin (CUR) and phloroglucinol (PHL) employing rotavap. This form wasn't synthesised by other general methods and was only generated under kinetically favourable conditions using fast solvent evaporating process. The most phase pure form was observed with

highly polar solvent such as acetone, aiding congruent solubility for both the components (Chow *et al*., 2014).

Another study utilised rotavap to test formation of paracetamol (PCA) and oxalic acid (OX) 1:1 co-crystal which was only generated by mechanochemical methods. Attempts to form co-crystals using solvent assisted grinding and from solution failed to produce PCA: OX 1:1. Surprisingly, rotavap favoured the formation of PCA: OX from solution mixture of chloroform and methanol. Therefore, the high evaporation rates and supersaturation levels observed in rotavap, seem to play an important role in screening of new co-crystals (Bag, Patni and Reddy, 2011).

1.8.2. Spray drying

Spray drying is a well proven technique for the generation of dry particulates from a solution or suspension by rapid evaporation of the solvent sprayed within a hot gaseous medium (Figure 1.19). It has been applied in pharmaceutical technology to obtain dry particles with distinct properties such as increased aqueous solubility, modified release profiles and enhanced bioavailability. This method was first used to obtain dry homogenous powders of thermolabile plant extracts without undergoing decomposition. The complex fluid dynamics and the drying behaviour of the product within the instrument can alter the drug characteristics which can be controlled by various process parameters, namely inlet temperature, feed rate, feed concentration, aspirator flow rate and atomisation (Sollohub and Cal, 2010).

Pharmaceutical industry has utilised spray drying as an emerging technique with inexhaustible applications explored. Studies involving particle processing techniques apply milling and spray drying as a standard means for particle-size reduction. Spray

drying was considered as an efficient method for particle engineering over milling and lyophilisation due to its ability to control powder characteristics. Numerous viable spray dried forms such as nanosuspensions for dry powder inhalers (DPI), microspheres and microemulsions possess higher dissolution and inhalation properties than mechanically micronised particles. Recently, this well-characterised unit operation has been incorporated into co-crystals (Alhalaweh *et al*., 2013; Sollohub and Cal, 2010; Daggupatti *et al*., 2011).

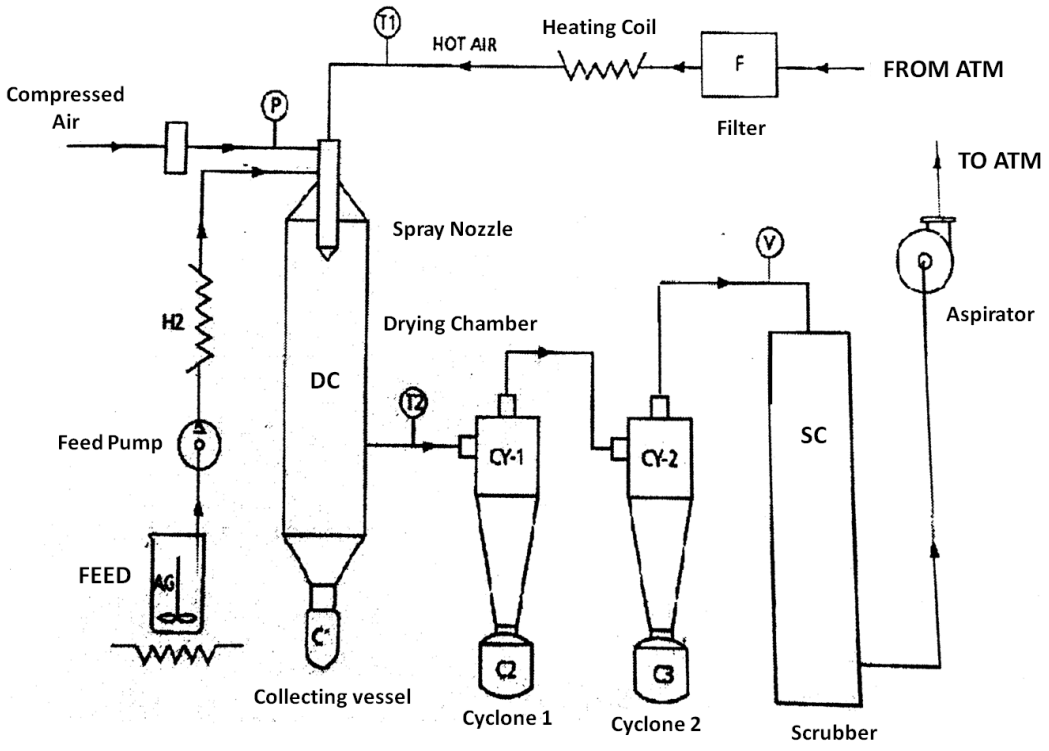

Figure 1.19. *Set up for the LU-228 spray dryer with an open loop (Deshmukh, n.d.).*

1.8.2.1. Application in co-crystals

Most of the conventional screening methods used for developing co-crystals are not suitable for scale-up production. This becomes even difficult in the case of non-stoichiometric systems where careful consideration of the crystallisation factors is required. Methods such as SCF, hot melt extrusion, ultrasound (Aher *et al*., 2010)

and microwave (Pagire *et al*., 2013) have been utilised in order to overcome these challenges. Further need to scale-up and prepare co-crystals from complex systems has involved the use of fast, continuous, 'in-process' crystallisation using spray drying. Current studies using spray drying found that the co-crystals formed in the case of CBZ-GLT (carbamezapine- glutaric acid) and IND-NIC were similar regardless of congruent and incongruent stoichiometric conditions. This study further demonstrates supersaturation in incongruent systems by TPD (as explained in Chapter1, Fig.7), leading to the production of mixed phases. Whereas, formation of pure and uniform co-crystals in case of solvent evaporation of congruent conditions. In contrast, the results obtained by spray drying of incongruent systems do not comply with TPD which could be due to the processing conditions altering the solid-state behaviour and hence, require further understanding (Alhalaweh and Velaga, 2010; Alhalaweh *et al*., 2013).

Another study used liquid assisted grinding to plot phase diagrams for carbamazepine and nicotinamide co-crystal (CNC); to explain the crystallisation pathway involved in producing CNC from incongruently saturating systems. The solution stoichiometry of carbamazepine (CBZ) and nicotinamide (NIC) was varied from 1:1 to 2:1 or 1:2; as agreed with TPD Zone 1(Figure 6). The spray dried product generated was CNC with impurity of either of the two components illustrating the path from Zone 1 to Zone 3 or 5. It is believed that the kinetics involved here is dependent on the solution stoichiometry. Hence, 1:1 solution stoichiometry was used to produce pure CNC co-crystal (Zone 1 to Zone 4) via spray drying. Optimised process parameters were varied and successfully produced co-crystals without any impurity; overcoming batch to batch variation (Patil *et al.*, 2014).

1.8.2.2. Process parameters

Various conditions set up inside a spray dryer have a significant effect on the drying process and the particle formed. On the other hand, these operating conditions may vary depending on the drying characteristics of the drug and the final product required. Therefore, it is essential to optimise the system for the desired output. The main process parameters are as follows:

a) Atomisation

This is the first phase where the liquid feed is reduced into tiny droplets suspended in drying gas that leads to immediate solvent evaporation forming dry particles. The dispersion of these droplets occurs in microseconds within the drying gas, thereby increasing the surface area. This encourages heat transfer from the gas to the droplets resulting in evaporation of solvents in seconds and simultaneous mass transfer back into the system. Therefore, the substance never approaches the inlet temperature, making this process desirable for drying heat sensitive materials. To further explain the droplet-drying kinetics, this quick process first takes place at the droplet surface it surrounds, increasing the solid concentration and further depends on the drying conditions set within the spray dryer (Dobry *et al.*, 2009; Cal and Solohub, 2010; Arpagaus and Schwartzbac, 2008).

Atomisation can be enhanced by different forms of energy integrated into devices (Figure 1.20) such as:

1) Rotary atomisers – These horizontal disc shaped devices are in motion by an electrically driven motor to which the feed is supplied. The centrifugal force generated causes the feed at the centre project towards the brim of the disc forming fine droplets. These discs may be designed with different shaped

grooves to maximise the dispersion properties. Its use is limited because of the deposits formed around the wall of the drying chamber.

2) Pressure nozzle – These are one-fluid hydraulic nozzles where a fluid flows under pressure into a converging channel and out through the orifice of 0.4-4mm in diameter. These nozzles are not appropriate for drying highly viscous feeds.

3) Two-fluid (pneumatic) nozzle – This multi-fluid nozzle operates using a compressed gas which collides with the feed at the tip of the nozzle, resulting in the dispersion of the feed. This nozzle can produce nanoparticles with enhanced absorption and solubility properties of the material. These nozzles have an in-built unblocking needle driven by compressed air in order to overcome in-process clogging of the nozzle.

4) Ultrasonic nozzle – These can be used to atomise high viscosity fluids by applying high electric signal causing vibrations via transducers and further amplified by a nozzle tip. In addition, the droplet size can be controlled by altering the frequency and also produces narrow particle size distribution (Cal and Solohub, 2010).

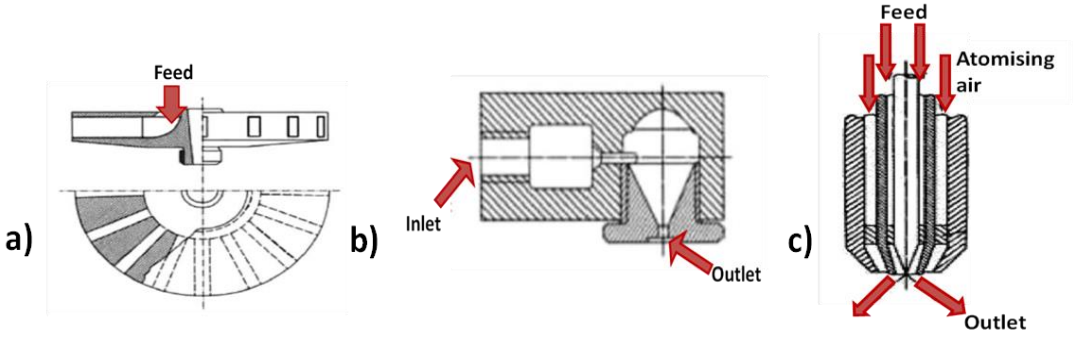

Figure 1.20. *Types of atomisers: a) Rotary atomiser; b) Pressure nozzle; c) Pnuematic nozzle (Cal and Solohub, 2010).*

b) Inlet temperature/ outlet temperature

The feed gets transported by peristaltic pump to the atomisation devices and the heated gas in the drying chamber where evaporation takes place. Each droplet formed inside the chamber is exposed to different local temperature points due to non-laminar gas flow. Factors such as change in atmospheric air humidity, shape of the chamber may also affect the drying conditions. Therefore, in order to accomplish optimal drying conditions and maximum outlet humidity, inlet temperature has to be optimised (Kent and McLeod, 2007; Cal and Solohub, 2010). Moreover, evaporation takes place due to the gradient between the wet surface and not the gas, enabling temperatures not higher than the boiling point of the solvent and hence no thermal load (Buchi, 1997-2002).

The mixing of the spray and the dry gas is an important aspect and influences the properties of the final product. The different modes in which air-droplets contact can be characterised as shown in Table 1.3.

The resulting temperature of the gas carrying dry solid particles after heat and mass exchange inside the chamber is known as the outlet temperature. Thus, this temperature cannot be regulated and is a consequence of the combinative result of parameters such as inlet temperature, atomisation, feed rate and feed concentration. The particles are regarded to possess the same temperature as the outlet before it enters into the separating device or cyclones. Moreover, the difference between inlet and outlet should be as small with high inlet maintained in order to achieve minimum residual moisture in the product (Cal and Solohub, 2010; Buchi, 1997-2002).

Table 1.3. *Three types of construction to distinguish air –droplets contact (Cal and Solohub, 2010).*

Type	Co-current Dryer	Counter-current Dryer	Combined Flow Dryers
Image	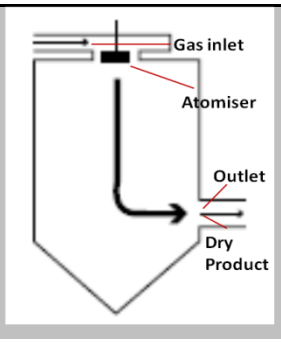	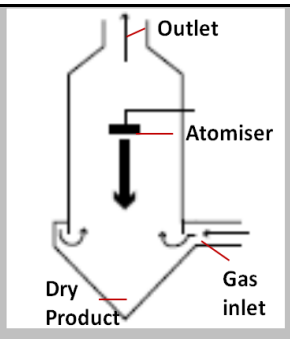	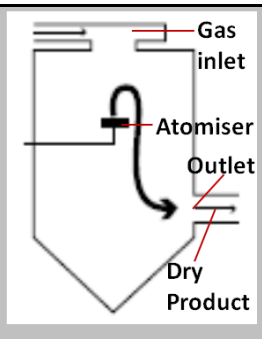
Functioning	Material spray and hot gas flow in the same direction.	Opposite flow. Hot gas upwards and material spray falls downwards.	Product sprayed upwards (counter-current to the drying air) stays in hot zone for a short time. Immediately, pulled down by gravity into cooler zone.
Product	─No exchange of the hot gas with the surrounding. ─Product exposed to sudden evaporation and heated least as drying gas energy is lost in evaporation.	─Air stream lose some heat in its path. ─Droplets hit the coldest gas first and then the hottest. ─No residual moisture. Product extremely hot.	─Fair-size particles obtained in a small chamber.
Drawback	─Droplets may not dry completely before reaching the chamber walls.	─Suitable for thermally stable products. ─Produces porous powders and agglomeration.	─Mixture of the moist and the dried product while descending down. ─Suitable for thermo-stable substances.

c) Other process parameters

The drying gas supply rate is controlled within the system by the aspirator in either suction or injection mode. A system with suction mode undergoes a slight under pressure effect. The speed of gas been sucked can be regulated to change the amount of heated drying gas, affecting the drying performance of the system. The low aspirator speed will decrease the degree of separation in the collecting cyclones and raise the exposure time of the drying gas thereby, reducing the moisture content in the product (Cal and Solohub, 2010; Buchi, 1997-2002).

Another important process control parameter, the solution feed rate, is managed by a peristaltic pump that directs the solution to the nozzle. This parameter has a major influence on the inlet and outlet temperature of the system. A lot more energy is required to evaporate the solvent in case of high feed rates, thereby decreasing the outlet temperature and increasing the difference between the two temperatures. This may also lead to the formation of sticky product on the walls of the chamber. In addition, feed properties such as its viscosity, concentration and the tubes drawing the feed can vary the conditions. Therefore, optimum setting and understanding of the collective effect of the parameters is essential to enhance its efficiency and obtain the desired product (Cal and Solohub, 2010; Buchi 1997-2002).

The product characteristics such as particle size distribution, bulk density, moisture content, morphology, and different forms (granulate, powder and agglomerate) are the dependant variables. These variables can be managed by altering the independent variables, that is, the process parameters to derive the desired quality of the product (Daggupatti *et al*., 2011). For example, a study using gum Arabic (wall material) to form microencapsulated flaxseed oil optimised the spray drying process to obtain the minimum oil on the surface of the dried particles. The inlet temperature condition, solid content and the oil concentration were observed as the critical parameters (Tonon *et.al*., 2011).

1.8.2.3. Process understanding via fundamental models

a)Williams-Landel-Ferry (WLF) kinetics

The product under spray drying conditions may undergo phase transformation from amorphous to crystalline solid depending on the drying kinetics and material physical properties. It was suggested that this transformation was governed by

Willaims-Landel-Ferry (WLF) kinetics. Where, the equation explains that the increase in the difference between the particle temperature (T_p) and the glass transition temperature (T_g), would increase the rate of particle cyrstallisation. Therefore, during spray drying, increase in the inlet temperature may enhance the crystallisation rate as observed in the case of lactose which possess high glass transition temperature (Islam and Langrish 2010; Islam, Langrish and Chiou, 2010). In addition, recent studies on co-crystals also imply its formation driven by kinetic factor (high rate of supersaturation) and glassy state of the material (Alhalaweh and Velaga 2013).

b) Computational fluid dynamics (CFD) models

The process engineering models are based on quality by deisgn (QbD) approach to speed up the development timelines and reduce the amount of API used. These studies employ mass- balance and energy –balance calculations to determine the spray-drying drying space. This involves prediction of ranges of inlet conditions to obtain a continuum of outlet conditions (Dobry *et al*., 2009; Salem, Ahmadlouiedarab and Ghasemzadeh, 2011). A study involved CFD modelling to elaborate drying kinetics inside spray dryer affecting the particle morphology. The figure below shows that in the case of hot and fast drying; the droplet reaches the boiling point of the solvent, creating vapour pressure which keeps the film forming polymer inflated and hence, produces hollow-sphere morphology. Whereas, the particle collapses into "raisin" morphology when under cold and slow drying conditions, as shown in figure 1.21 (Dobry *et al*., 2009).

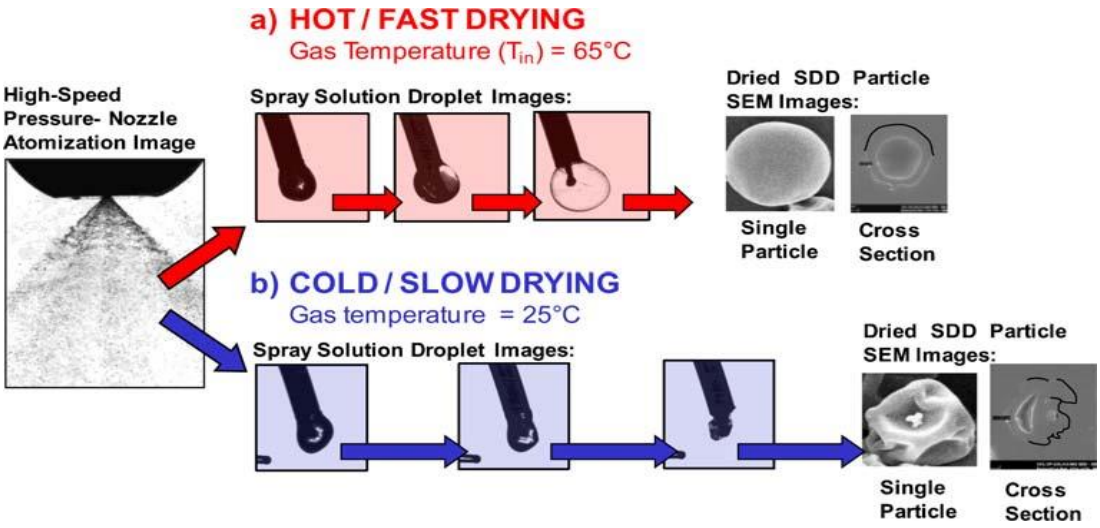

Figure 1.21. *Images of droplets arising from pressure-nozzle atomisation subjected to various drying conditions: a) hot/fast drying conditions and b) cold/ slow drying conditions when a film-forming polymer is used (Dobry et al., 2009).*

c) COST ("Changing One Separate factor a Time") approach and Design of Experiment (DoE)

COST is an instinctive method is used for the screening of the parameters. A study involved this approach to select optimum parameters to coat particles with a plasticiser using spray dryer. The most critical parameters observed from this method were selected and further optimised by a second approach, DoE. The parameters considered for DoE analysis were, inlet temperature, feed rate and atomisation. A three level – three factor factorial design was applied and optimised particles were produced (Bilancetti *et al*., 2010). Another simplistic DoE approach utilising fractional factorial experiment designs (FFED), comprises of a fraction of the complete runs from a full-factorial design. Other statistical tools such as Box Behnken design can also be used to predict the variables involved for attaining specific quality of product (Zhang and Youan, 2010).

d) Multi-variate data analysis

The QbD guidelines lay emphasis on considering critical quality attributes (CQA) and critical process parameters (CPP) to understand the influence of process parameters on the product. CQA involves real-time monitoring of the process using an efficient in-line, online or at line PAT (Process Analytical Technology) tool. A multivariate study exploited NIR (Near infrared) and FTIR (Fourier transform infrared) to compare the amount of residual phenol in spray-dried and freeze-dried insulin formulations combined with DoE. The spectral data obtained was analysed by principal component analysis (PCA) and the projections of PLS (partial least squares). NIR spectra based PLS model was preferred over FTIR, which utilised three components to elucidate the amount of residual phenol/ insulin ratio in both the methods (Maltesen *et al*., 2011).

e) A new distributed parameter model

This model was used to investigate spray drying of a multi-component system, different stages of drying and the optimum conditions for the segregation of the components within the particle. Factors such as feed concentration, solubility of the components and the diffusion coefficients were considered as parameters in this method. The normal two stages of drying explained in earlier studies were: formation of outer solid crust due to the evaporation at the surface of the droplet and diffusion of water vapour through the pores of the solid crust causing mass loss. In this study, the second stage of drying was modified where the droplet is divided into shells of same size with respect to the solute concentrations (Figure 1.22a). The outermost shell or the crust is formed by one or more solutes if their concentrations reach beyond the value of its solubility during the drying process. Moreover, it was

assumed that the solid crust does not diffuse into the wet core, as the solute molecules are bigger compared to water molecules which diffuses during the course of evaporation (Figure 1.22b) (Gac and Gradon, 2013).

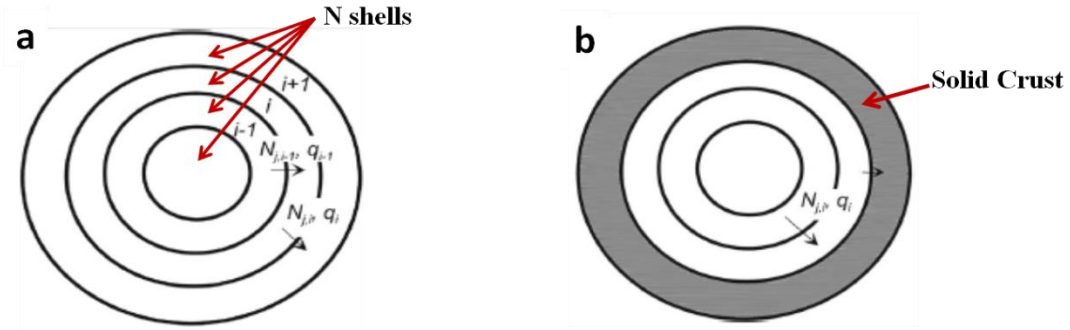

Figure 1.22. *Multi-shell model of a) dried droplet with N number of uniform shells and b) Wet particle with solid crust (Gac and Gradon, 2013).*

This model was used for insoluble nanoparticles (small components) which can diffuse easily through convective mechanism. The degree of segregation was dependant on their solubility in the solution and occurred when the components had different diffusion coefficients. For highly soluble components, small particle was formed and the segregation was negligible. On the other hand, in the case of low soluble components, the outer layer can be distinguished where the component with lower diffusion coefficient is at higher concentration compared to the second component present inside the other portion of the particle. The kinetics of crystallisation and inlet temperature also affects the thickness of the outer layer. Moreover, in a system with solutes of different solubility, a component with higher solubility will have a lower diffusion coefficient, forming higher concentration in the outer layer. In contrast, the concentration of the second component is almost constant in the entire particle space (Gac and Gradon, 2013).

1.9. Aims and objectives

To date, an immense amount of work has been performed on the fundamentals and chemistry supporting the formation of co-crystals; overlooking the challenges that exist in scaling up of these methods. Scalability of conventional methods such as ball-milling, solid-state grinding, LAG is not viable. These mechano-chemical processes require energy that surpasses the supramolecular interactions within the molecules in order to form co-crystals. Therefore, in terms of scalability, these methods lead to homogeneity issues, phase transformation and degradation caused by friction induced within energetic material. On the other hand, solvent based approaches are known to enhance the reaction kinetics by driving the equilibrium to co-crystal formation. Although solution co-crystallisation may be amenable to scalability, limitations such as solubilities of the multiple components and solvate formation, hinder its production on a large scale (Ende, Anderson and Salan, 2014).

One of the studies examined a green solvent-free continuous co-crystallisation approach, (SFCC) by using twin screw extruder for scale-up of carbamazepine (CBZ) and saccharin (SAC) co-crystals. The optimised process parameters required temperatures above the eutectic temperature of the mixture (133^{o}C) to facilitate co-crystallisation. Moreover, the high shear at the mixing zones under elevated temperatures induced additional heat which caused degradation and polymorphic transformation of the material (Joshi, 2012). Thus, additional routes must be adopted in order to overcome these challenges during scale-up. Current work in terms of scale-up has also introduced spray drying as a continuous, one-step and fast evaporating process for producing co-crystals from incongruently soluble pairs; overcoming the issue of contamination and control over stoichiometry (Alhalaweh, and Valega, 2010). However, selection of solvents can be a major obstacle.

Aim

This project aims to investigate the formation of co-crystals using spray drying with the intention of making it a green process i.e. from aqueous media. This research is based on the hypothesis that rotavap could be used as a pre-screening tool and a platform for co-crystallisation amenable to large-scale spray dryer.

Objectives

● To establish solubility for the selected pair and successfully form their aqueous solutions.

● To test co-crystal formation by rotavap as a pre-screening tool.

● To devise a spray drying method for scale-up of co-crystals from aqueous systems.

● To optimise the system by varying different parameters such as the inlet temperature, feed rate, feed concentration, feed temperature and aspirator. Understanding the effect of these variables on the quality of product.

● To successfully employ characterisation techniques such as XRD and DSC to confirm the expected product and its purity.

● To understand the relation between complex formation and high supersaturation levels achieved using these fast evaporation techniques generating co-crystals.

1.9.1. Rationale for selection of model compound

Caffeine (CAF) and maleic acid (MAL) was used as a model system due to their incongruent solubility and diverse stoichiometry. This pair exists in stoichiometric

ratios of 1:1 with two polymorphs, form I and II; and 2:1 (Leyssens *et al*., 2012). Moreover, the solid state properties of anhydrous caffeine revealed the existence of two polymorphs (Trask, Motherwell and Jones, 2005) and a hydrate form which makes it a challenging pair. CAF is a nitrogen containing alkaloid, known as methylxanthine and is represented as a poorly soluble biopharmaceutical classification system (BCS) class II drug (Figure 1.23). Therefore, it is very crucial to obtain a solubility enhancement technique.

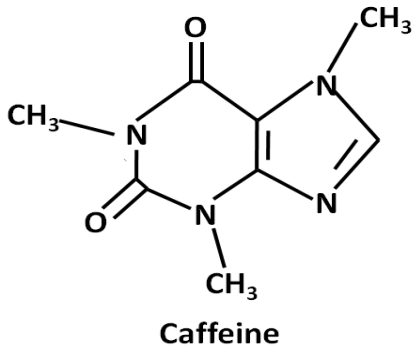

Figure 1.23. *Chemical structure of caffeine.*

Interestingly, Guo *et al*., (2010) observed that the presence of MAL in solvent further increased the solubility of CAF due to complexation. Such compounds can also be referred to as hydrotropes if they aid in solubilisation of a hydrophobic compound in aqueous solution (Kumar, Raja and Jayakumar, 2013). Various studies were involved in its co-crystal formation with di-carboxylic acid (Figure 1.24) in order to increase its physical stability under all RH (relative humidity) conditions (Trask, Motherwell and Jones, 2006).

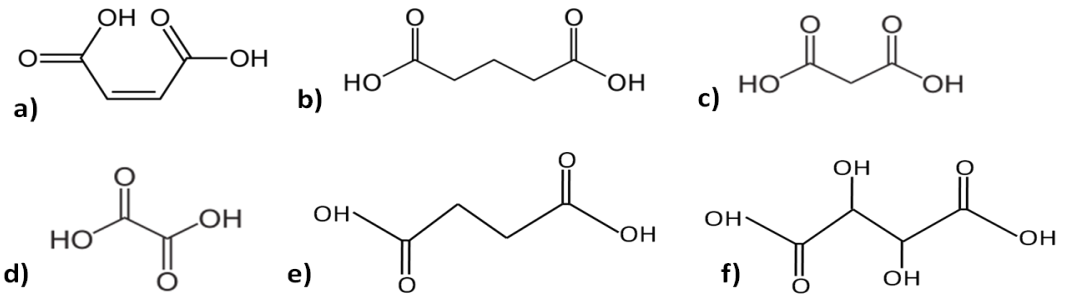

Figure 1.24. *Dicarboxylic acids; a) maleic acid; b) glutaric acid; c) malonic acid; d) oxalic acid; e) succinic acid; f) tartaric acid.*

Therefore, MAL and other dicarboxylic acids such as malonic acid (MO), oxalic acid (OX), glutaric acid (GLU), tartaric acid (TAR) and succinic acid (SUC) were examined for their hydrotropic nature and successful scale-up as co-crystals using spray drying as a green technique.

1.9.2. Overview of thesis structure

Chapter 1 provides an introduction to co-crystals as an alternative to other solid-state forms in medicinal product with enhancement in various properties of the active ingredient. It further explains various techniques utilised in development of these co-crystals and the challenges faced.

Chapter 2 briefly describes the materials and methods utilised in this project.

Chapter 3 scrutinise solubility enhancement of the incongruently soluble pair: CAF and MAL, and co-crystallisation results obtained using rotavap and spray drying. It also observes the effect of process parameters on the quality of product. The limitation faced by the technique and the challenges of the selected pair were discussed.

Chapter 4 examines another chemical analogue of CAF, theophylline (THEO) forming its co-crystals with di-carboxylic acids in aqueous solution and compare results obtained from the two fast evaporating techniques.

Chapter 5 explains the findings for a congruently soluble pair, carbamazepine (CBZ) and saccharin (SAC) when subjected to rotavap and spray drying.

Chapter 6 comprises of general conclusion and proposition for future work, followed by references and appendix

CHAPTER 2

EXPERIMENTAL

2.1. Materials

2.1.1. Chemicals

Caffeine, maleic acid (99%), malonic acid (99%) and oxalic acid (≥99%) were obtained from Sigma Aldrich; glutaric (99%) from Acros; L-(+)-tartaric acid (≥99.7%) from SAFC and succinic acid (≥99%) from Acros were used as supplied. Theophylline was sourced from Kores (India) Ltd; Carbamazepine USP 34 from Jai Radhe Sales (India) and Saccharin (99%) from Sigma Aldrich. Sodium Lauryl Sulphate (SLS) (85%) was purchased from Medical Export Co. Ltd., UK. All compounds were initially characterised by PXRD. Iminostilbene (97%) for stability studies was purchased from Sigma Aldrich. Further details of the above compounds are shown in the table below:

Table 2.1 *List of chemicals used and their physical properties (Chemicalland21, 2013).*

Name	Structure	Properties
Caffeine	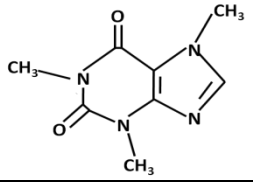	*Formulae*: $C_8H_{10}N_4O_2$ *Molar mass*: 194.19 *M.P.:*235^{o}C *Solubility in water:* Slightly soluble
Maleic acid	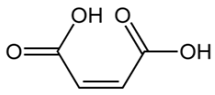	*Formulae:*$C_4H_4O_4$ *Molar mass*: 116.07 *M.P.:*130-2^{o}C *Solubility in water*: Soluble
Malonic acid	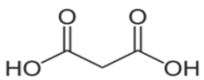	*Formulae*: $C_3H_4O_4$ *Molar mass:*104.06 *M.P.:*135-6^{o}C *Solubility in water:* Miscible
Glutaric acid	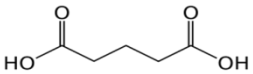	*Formulae:*$C_5H_8O_4$ *Molar mass:*132.12 *M.P.:*95-98^{o}C *Solubility in water:* 430g/L

Oxalic acid	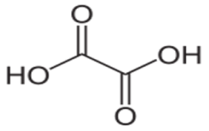	*Formulae:*$C_2H_2O_4$ *Molar mass:*90.03 *M.P.:*102-3^oC *Solubility in water:*1.35g/L
L- Tartaric Acid	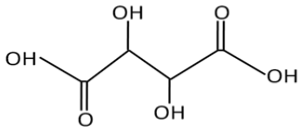	*Formulae*:$C_4H_6O_6$ *Molar mass*: 150.09 *M.P.:*171-4^oC (L or D) *Solubility in water:* Soluble
Succinic Acid	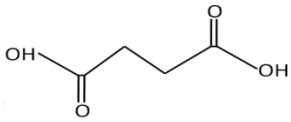	*Formulae:*$C_4H_6O_4$ *Molar mass:*118.09 *M.P.:*187-9^oC *Solubility in water:* Moderately soluble
Theophylline	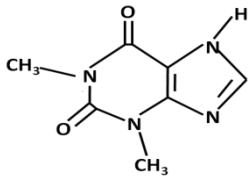	*Formulae:*$C_7H_8N_4O_2$ *Molar mass:*180.16 *M.P.:*270-4^oC *Solubility in water*: Soluble in hot water
Carbamazepine	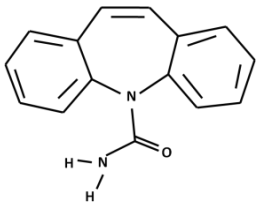	*Formulae:*$C_{15}H_{12}N_2O$ *Molar mass:*236.27 *M.P.:*191-2^oC *Solubility in water*: 17.7mg/L
Saccharin	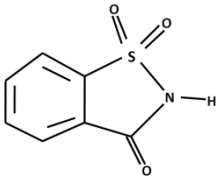	*Formulae:*$C_7H_5NO_3S$ *Molar mass:*183.18 *M.P.:*226-9^oC *Solubility in water:*3.45g/L
SLS		*Formulae:*$NaC_{12}H_{25}SO_4$ *Molar mass:*288.37 *M.P.:*204-7^oC *Solubility in water:*150g/L
Iminostilbene (5H-Dibenz[b,f]azepine)	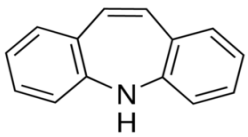	*Formulae:* $C_{14}H_{11}N$ *Molar mass:* 193.25 *M.P.*: 197-9^oC

2.1.2. Solvents used

1. Deionised water was obtained from SG Series Compact water system by Triple Red Limited with purity of 18.2 Mohm/ cm.
2. Some of the selected solvents used were: methanol (99.8%), acetone (99.5%), ethylacetate (99.5%), ethanol (99.8%), chloroform (99%), dimethyl sulphoxide (DMSO) and 1,2-dichloroethane (99.8%).
3. Formic acid (≥ 95%) and acetonitrile (HPLC grade) were used for CBZ: SAC stability studies.
4. Series of alkane probes such as heptane, octane, nonane, decane, undecane with ≥ 99% purity were used for surface energy determination.
5. Karl Fischer reagent, Hydranal®-Composite 5 (methanol free) from Fluka Analytical was used for moisture content determination.

2.2. Methods

This section will give an overview of general methods used and their data described later in relevant chapters. Spray drying, rotavap and some characterisation tools were used in common for all the co-crystallising pairs. Additional methods performed are listed further.

2.2.1. Solubility

a) Aqueous

Prior to aqueous solubility determination, two stock solutions of initial concentration (C_0) 0.1 i.e., 100µg/mL were prepared using caffeine and theophylline. Further six solutions at decreasing concentration (0.02 C_0, 0.04 C_0, 0.06 C_0, 0.08 C_0, 0.1 C_0, and 0.15 C_0) were formed from the above solution and their absorbance value was

recorded using a UV (ultra-violet) spectrometer (Jasco V-730 spectrometer). The absorption maxima for caffeine and theophylline were 272 and 271 nm, respectively. A standard curve of light absorbance versus concentration of solution was created to quantify the concentration of the unknown solution.

An excess amount of weighed caffeine/ theophylline was added to water and 0.04 M co-former solutions. It was then stirred at 500 rpm for 24 hours in closed vials placed inside a jacketed vertical diffusion cell (Copley HDT10) at the desired temperatures. After reaching the suitable equilibrium, stirring was stopped. The solution was then filtered via PTFE filter 0.45 µm within 10 minutes and further diluted to measure its UV absorbance. The excess solid after filtration was dried and its PXRD results observed. The solubility of the compound was determined by exploiting the calibration curve and the average results reported.

b) Organic solvent

Excess amount of caffeine and theophylline were added to selected solvents and stirred at room temperature at 500 rpm for 24 hours to check for their solubility using UV spectrometer. All samples were run in duplicates.

2.2.2. DEC (di-electric constant)

Di-electric constant is also referred to relative permittivity and is defined as the ratio of absolute permittivity of the material ($\boldsymbol{\mathcal{E}}$) compared to permittivity in vacuum ($\boldsymbol{\mathcal{E}_0}$) (Eqtionu 2a). It is denoted by symbol, $\boldsymbol{\mathcal{E}_r}$.

$$\varepsilon_{\boldsymbol{r}} = \frac{\varepsilon}{\varepsilon_{\mathbf{0}}} \qquad \text{(Eq. 2a)}$$

The concept is based on a material made up of atoms with charged particles behaving as dipoles (positive and negative charge ends); when placed between two oppositely charged plates, aligns itself so that the dipole moment opposes the external electric field (E) between the plates normally under vacuum (Figure 2.1). The net reduced electric field is dependent on factors such as temperature, frequency and humidity. For a solvent, its permittivity is measured in terms of its polarity (Maxwell's equations, 2012). This parameter is important for correlating the solubility of ionisable solute in solution or mixture of solutions with varying dielectric properties (Fakhree *et al*., 2010). Earlier studies observed a correlation between the solubility parameter and DEC where solvents had shown association with the solute via H-bonding. It was assumed that a linear correlation exists between DEC and solubility parameter (Gorman and Hall, 1964). DEC is also indicative of thermodynamics of mixing such as Gibbs free energy of mixing in case of binary mixtures where the properties of the two components vary due to factors such as pressure, temperature and composition (UC DavisChemWiki, n.d.; Tripathy and Swain, 1991).

Procedure

Prior to DEC measurements, three-term calibration was performed at the tip of the open-ended co-axial probe using three standards: air, a short circuit, and de-ionised water. The probe (E5071C, Agilent technologies) was then immersed in solvents or mixtures ensuring no bubble formation at the surface. DEC results were processed by Agilent network analysers and software85070E using frequency range from 300 kHz to 2GHz at room temperature.

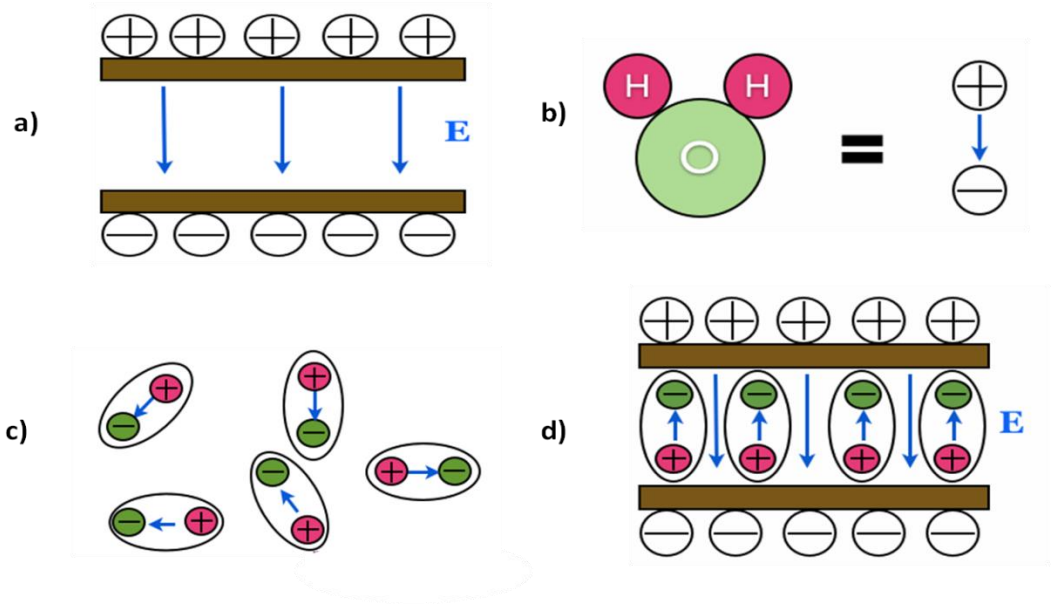

Figure 2.1. *a) Two plates with equal opposite charge and electric field, E under vacuum; b) water molecule as a dipole; c) random course of molecules in absence of the electric field; when water molecules placed between the two plates, d) dipoles arrange according to the charges on the plate and electric field due to dipoles oppose external electric field, E (Maxwell's equations, 2012).*

2.2.3. Preparation of co-crystals via rotavap

Stoichiometric ratios of the API and coformer were dissolved in chosen solvents contained in a round bottom flask. The solvents were evaporated rapidly at optimum vacuum and water bath temperature conditions. The solid product was collected from the flask and dried in the oven at 40^{o}C for 5 hours and then stored in a dessicator. Dried samples were gently triturated into fine powder with pestle and mortar before characterisation.

2.2.4. Preparation of co-crystals by spray-drying

Co-crystals of the selected pairs were prepared by spray drying. Experiments were conducted in a laboratory scale spray dryer LabUltima LU-228 (Figure 2.2), with a 0.7 mm nozzle and main chamber of 1500 mm x 500 mm. A peristaltic pump was used to feed the solution into the main chamber. The aqueous solutions were spray

dried in an open loop configuration with atmospheric air as the drying gas in a co-current manner to the cyclone separators. The organic solutions were evaporated in an inert environment using nitrogen in a closed loop. The experiment was designed varying the main process conditions (Table 2.2): feed rates were between 1- 3 mL/min; aspiration rate between 50 to 70 m^3/h and inlet temperatures varied for water was between 110 and 170^oC. The air flow used was 1.5 bar and the outlet temperature varied depending on the process variables set. The resulting solids were analysed by various characterisation tools. For organic solvents, an inert or closed loop was used with re-circulating nitrogen gas which passes through an oxygen monitoring device, ensuring any leakage of ambient air into the system (Figure 2.3). The inlet temperature utilised for organic solvents varied and was slightly above their boiling point.

Figure 2.2. *LU-228 advanced spray dryer*.

Table 2.2. *Experimental design for spray drying CAF co-crystals with dicarboxylic acids.*

Co-crystal solution	Ratio	Feed Concentration (%)	Inlet Temperature (^oC)	Aspirator (m^3/h)	Feed Rate (mL/min)	Batch No.
CAF:MAL	1:1	6.7% @45^{o}C	110	60	1	1a
		6.7% @45^{o}C	150	60	1	1b
		3.4	110	60	1	1c
		3.4	150	60	1	1d
	2:1	6.7% @45^{o}C	110	60	1	1e
		6.7% @45^{o}C	150	60	1	1f
		3.4	150	60	1	1g
		3.4	150	60	3	1h
		2.5	150	60	3	1i
		1.7	110	60	1	1j
		1.7 @45^{o}C	150	60	1	1k
		1.7	150	40	1	1l
		1.7	150	60	1	1m
		1.7	150	60	3	1n
		1.7	170	60	1	1o
		1	150	60	1	1p
		1	150	60	3	1q
CAF:GLU	1:1	5	150	60	3	2a
		3.4	150	60	3	2b
		1.7	150	60	3	2c
CAF:MO	2:1	3.4	150	60	3	3a
		1.7	150	60	3	3b
CAF:OX	2:1	1.7	150	60	3	4c

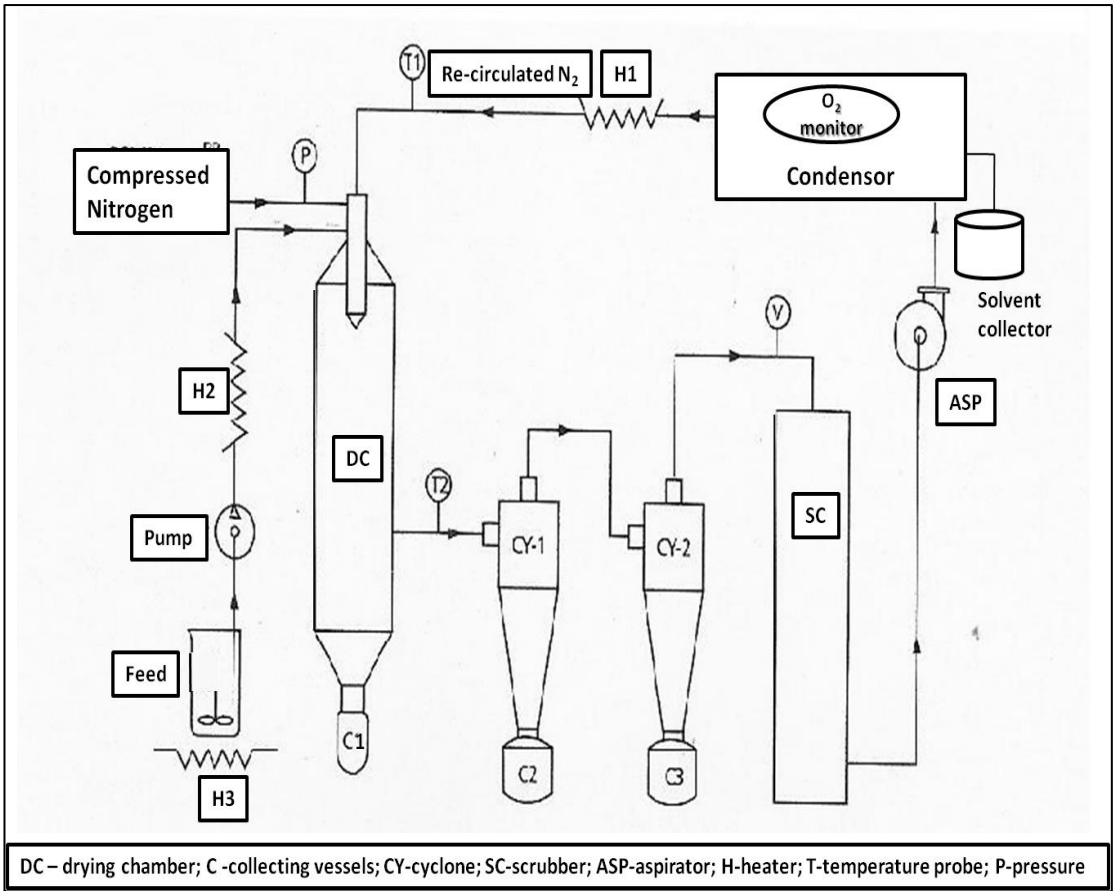

Figure 2.3. *Set-up for the LU-228 spray dryer (inert loop).*

2.3. Characterisation

2.3.1. Powder X-ray Diffraction (PXRD)

The PXRD patterns were observed using a powder diffractiometer, Bruker D8 with CuK alpha radiation ($\lambda = 0.154$nm), and the operating conditions were 40 kV and 40 mA. Data was collected from 5^o to 30^o 2θ with continuous step size of 0.02^o 2θ and stem time of 2s. The data was evaluated using DIFFRAC^{plus} EVA (Version 11.0) software.

2.3.2. Crystal structure data and PXRD patterns

Cambridge structural database (CSD) was used to obtain crystal structure data and PXRD patterns for the APIs and their reported co-crystal forms. Mercury, version 3.0 software was used to visualise the crystal structures. All experimental results were compared to the reference patterns collected from CSD.

2.3.3. Thermal analyses

a) Differential Scanning Calorimetry (DSC)

DSC thermograms were generated using *Q200*0 from TA instruments. Approximately weighed sample (2-4 mg) was enclosed in a sealed aluminium pan and scanned from 25°C to 200°C~300^{o}C (depending on the melting point of the components) at heating rate of 10°C/min under nitrogen atmosphere. The results were analysed using TA Universal analysis software version 4.5A.

2.3.4. Raman spectroscopy

Raman spectra of the samples were obtained using a Raman microscope (Renishaw Plc., UK) with 785 nm stabilized diode excitation. A 100x objective lens was used to focus laser spot at the sample placed on aluminium holder. Spectra were obtained in the region 100cm^{-1} and 1800cm^{-1} with 100% laser power acquiring 10 accumulations. The data was acquired for CBZ: SAC FI and FII using Grams/AI version 9.1 spectroscopic software.

2.3.5. Fourier-Transform Infrared (FTIR) Spectroscopy

Infrared absorption spectra for CBZ: SAC co-crystal was obtained using PerkinElmer Spectrum 100 FT-IR. The samples were scanned from 500 cm^{-1} to 4000

cm^{-1} with an average of 4 scans. The data was acquired using Universal ATR (attenuated total reflectance) accessory.

2.4. Additional methods

2.4.1. Water content by Karl Fischer (KF) titration

Samples prepared by spray drying in aqueous solutions were tested for its moisture content by performing volumetric titration using 701 KF Titrino KF titrator from Metrohm. The system was calibrated with 25 µL of water. Approximately 100 mg of sample was weighed and poured into methanolic solution till the first excess iodine content was detected. The used volume of iodine containing Karl Fisher solution generated moisture content in the samples. Each sample was analysed in duplicate.

2.4.2. Particle Size Distribution (PSD)

The particle size distribution of spray dried material was analysed by laser diffraction (Sympatec GmbH, Helos Disperse) where sample were sieved using 180 µm sieve and placed in a dry powder disperser (RODOS/M). A reference measurement was taken before running each sample for 5sec at 2% optical concentration. The results were obtained at pressures (1 bar and 4 bars) in duplicates using lens, R1 (0.18-0.35µm). The data was collected using HELOS sensor and analysed using Windox5 software.

Microscopic visualisation of particle size

The sieved samples were lightly spread on glass slide and viewed under microscope (Zeiss-AxioCam MRc 5). The images were taken using the software, AxioVision

2.4.3. Scanning Electron Microscopy (SEM)

SEM was used to characterise and visualise morphology of co-crystals. The samples were placed on aluminium stubs (Agar Sceintific, Stansted, UK) with self-adhesive carbon mounts. All samples were gold plated with deposition of 10 mm gold using electric current of 25 mA. Sample images were collected using FEI Quanta 400 scanning electron microscope (Cambridge, UK) under high vacuum and working distance of 10mm at various magnification levels utilising XTM microscope control software V 2.3.

2.4.4. Stability study

The spray dried CBZ: SAC co-crystal samples were placed in a dessicator at room temperature with drying agent (silica gel) to protect the samples from moisture and its degradation examined using HPLC (High performance liquid chromatography).

HPLC

The experiment was performed on a Waters e-2695 system (Aligent Technologies, 1200 series) equipped with a PDA 2998 detector and degasser. The mobile phase was composed of acetonitrile with 0.1% v/v formic acid and water with 0.1% v/v formic acid. A gradient method was used varying organic phase from 2% to 98% in 10 minutes; to 2% in next 2 minutes and constant for further 2 minutes; separating CBZ and its degraded product (iminostilbene). The sample volume was 10 μL injected by autosampler and scanned at 219, 253 and 285 nm using 1.2 mL/min flow rate. A Waters symmetry C18 column with dimensions of 4.6 x 250 mm and particle size of 5 μm was employed. Column temperature was set at 25^{o}C and results observed using Empower 3analysis software.

a) Calibration curve for iminostilbene

Two stock solutions of iminostilbene with initial concentration (C_0) 0.1 i.e., 100µg/mL were prepared in acetonitrile. Further six dilutions: 0.01 C_0, 0.02 C_0, 0.03 C_0, 0.04 C_0, 0.05 C_0, 0.06 C_0were formed. These were then analysed using HPLC method stated above to obtain area under the curve values. The calibration curve of concentration versus area under the curve was constructed to get a linear plot. The linear equation generated from the plot was used to calculate the unknown amount of iminostilbene present in the spray dried CBZ: SAC samples.

b) Sample preparation

Sample solutions of 500 µg/mL concentration were prepared in acetonitrile and filtered through 0.45 µM nylon filter membrane to obtain a clear solution. The unknown amount of iminostilbene was determined under HPLC analysis and results were exracted with the aid of calibration curve.

2.4.5. Surface Energy Analyser (SEA)

Surface Measurement System-iGC 2000, UK Ltd was used to measure the dispersive surface energy of CBZ: SAC co-crystals processed via spray drying using three different feed rates (1mL, 2mL and 3 mL). The samples were weighed and packed into salinised glass columns (2mm ID) with glass wool covering sample at either side of the column. SEA was set at 30^{o}C column temperature and 0% relative humidity. Columns were pre-conditioned with methane for 3 hours to nullify dead volume. BET (Brunauer-Emmett-Teller) values were obtained by passing octane at flow rate of 10 sccm (standard cubic centimetres per minute) to calculate the surface heterogeneity (Table 2.3; Figure 2.4). Series of linear alkane probes (heptane, octane, nonane, decane) were injected to analyse dispersive component of surface energy

(Table 2.4) using Dorris and Gray method. The data was analysed using SMS Cirrus Plus software.

Dorris-Gray method:

Dorris and Gray demonstrated that the adsorption of an ideal gas phase on solid is independent of the n-alkane chain length, and that the surface covered by CH_2 group is the same as cross-sectional area it acquires in bulk liquid with parallel layout of n-alkane series. This method is less dependent on probe input parameters, where the retention of dispersive probes does not rely on injection size (Gamble *et al*., 2012). It is based on the theory that the absorption dispersive free energy of a methylene group can be estimated from the slope of a line of adsorption free energy from series of *n*-alkane probes against the carbon number, *n*. The equation is as follows:

$$\Delta G^{CH2} = -RT.\ln\left(\frac{V_{N,n+1}}{V_{N,n}}\right) \qquad \text{(Eq. 2b)}$$

where ΔG^{CH2} is the dispersive free energy, R is the gas constant, T is the temperature in Kelvin (K), $V_{N,n}$ is the retention volume of the probe with *n* carbon number (Shi, Wang and Jia, 2011).

Table 2.3. *Experimental details for calculating BET values.*

Flow Rate (sccm):	10		
Target Column RH (%):	0	**Target Column Temperature (°C):**	30

ID	Solvent Name	T. F. S. Coverage	Temp. (°C)	Flow (sccm)	Duration (min.)	FID Gain
1	OCTANE	0.0025	30	10	5	10x
2	OCTANE	0.003	30	10	5	10x
3	OCTANE	0.0035	30	10	5	10x
4	OCTANE	0.004	30	10	5	10x
5	OCTANE	0.005	30	10	5	10x
6	OCTANE	0.01	30	10	5	10x
7	OCTANE	0.02	30	10	5	10x
8	OCTANE	0.03	30	10	5	10x
9	OCTANE	0.04	30	10	5	10x
10	OCTANE	0.05	30	10	5	10x
11	OCTANE	0.06	30	10	5	10x
12	OCTANE	0.07	30	10	5	10x
13	OCTANE	0.08	30	10	5	10x
14	OCTANE	0.09	30	10	5	10x
15	OCTANE	0.1	30	10	5	10x
16	OCTANE	0.2	30	10	5	10x
17	OCTANE	0.3	30	10	5	10x
18	OCTANE	0.4	30	10	5	10x
19	OCTANE	0.5	30	10	5	10x

Table 2.4. *Experimental set-up for determining the surface heterogeneity of the samples (each solvent was run 6 times).*

Solvents	***% Coverage***	***Column Temperature (°C)***	***Flow (sccm)***	***Flow time (minutes)***	***FID gain***
Hexane; Heptane; Octane; Nonane	0.015	30	10	5	10x
	0.05	30	10	5	10x
	0.09	30	10	5	10x
	0.16	30	10	5	10x
	0.26	30	10	5	10x
	0.3	30	10	5	10x

a)

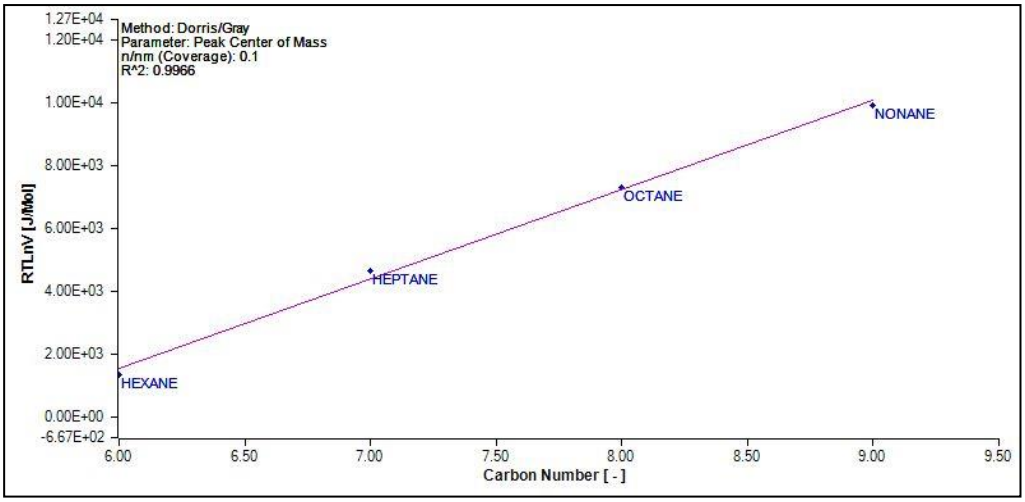

b)

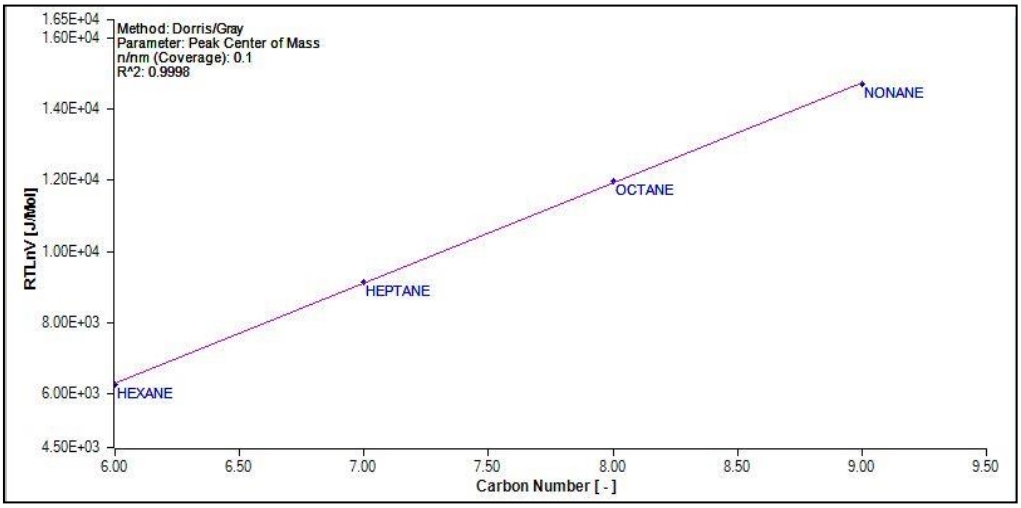

c)

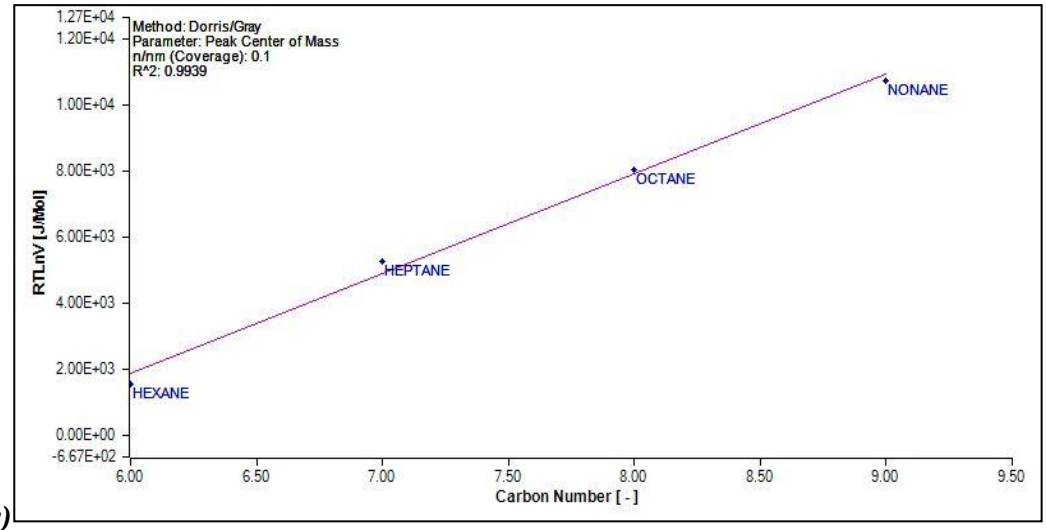

Figure 2.4. *Linear plots of surface heterogeneity of samples processed at feed rates a) 1mL/min; b) 2ml/min and c) 3mL/min.*

2.4.6. CBZ: SAC 1:1 Form I co-crystal (prototype)

Equimolar ratios of CBZ and SAC were weighed and dissolved in 62.5/37.5% v/v ethanol / methanol mixture and heated to 70^{o}C for 1 hour under reflux. The temperature was lowered in increments of 10^{o}C and the precipitated co-crystals were filtered, dried and characterised.

CHAPTER 3

CAFFEINE AND DI-CARBOXYLIC ACIDS COCRYSTAL RESULTS

This chapter explores the application of spray dryer in generating co-crystals of CAF primarily with MAL, an extensively studied pair; and other dicarboxylic acids. CAF's increased solubility in dicarboxylic acid was examined in aqueous solution with an intention of making it a green technique for scale-up of incongruently soluble mixtures. Rotavap has been used as a pre-screening tool to establish if co-crystals could be predicted prior to utilisation of large-scale spray dryer. This study achieves almost phase pure metastable CAF:MAL 2:1 which has been hard to generate via several solution-based methods to date. Various attempts such as process optimisation and solubilisation were made to attain highly pure co-crystals.

3.1. Crystal data

3.1.1. Caffeine

CAF is a nitrogen containing alkaloid, known as methylxanthine and is used as a psychoactive drug, smooth muscle relaxant and an analgesic. The anhydrous solid form of CAF can exist as two forms, the most stable being, β over α which was used during this study. The unit cell belongs to Cc space group with a=43.04 Å, b= 15.07 Å, c= 6.95 Å, $\alpha = 90^{o}$, $\beta = 99.03^{o}$ and $\gamma = 90^{o}$ (CSD Ref: NIWFEE03). The crystal structure and calculated PXRD pattern are shown below:

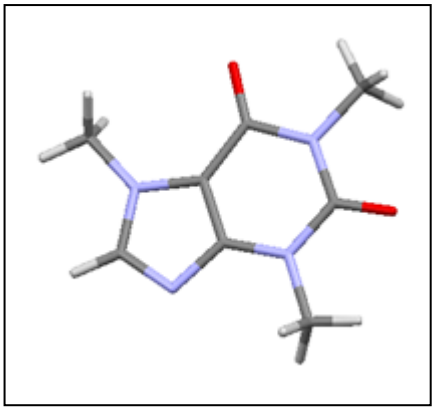

Figure 3.1. *Crystal structure of caffeine (CSD Ref: NIWFEE03).*

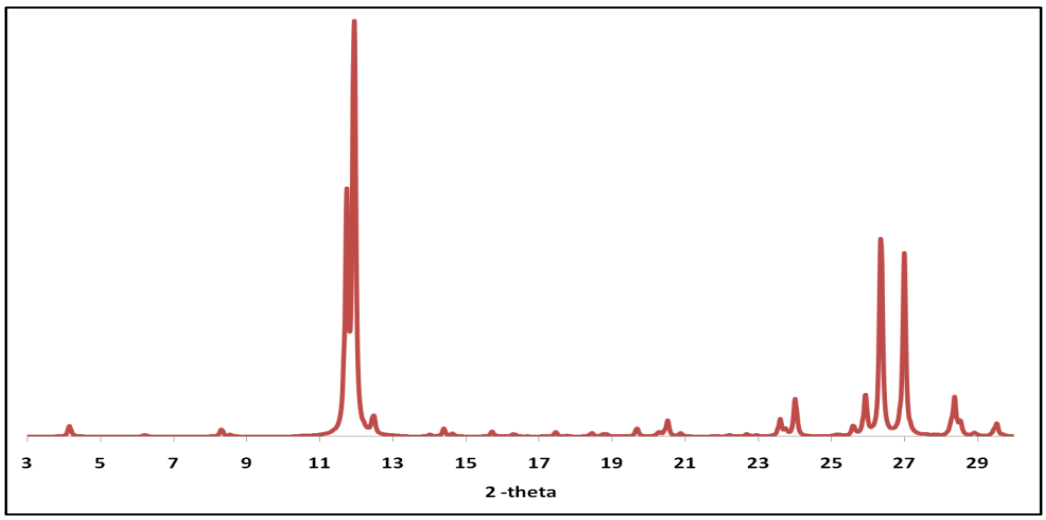

Figure 3.2. *Calculated PXRD pattern for caffeine with a characteristic peak at 12^o 2θ (obtained from CSD).*

3.1.1.1. Caffeine monohydrate

This compound is prone to hydrate formation under high RH conditions. Conversely, this hydrate form can transpose back to β-caffeine at lower RH with 61% RH being the dehydration line. Every mole of this non-stoichiometric hydrate crystalline structure contains 0.8 moles of water (Trask, Motherwell and Jones, 2005). The dimensions of the unit cell are: a = 14.8 (1) Å, b= 16.7 (1) Å, c = 3.97 (3) Å, α= 90^o, β= 97 (5)^o and γ= 90^o with space group P2$_1$/a. The crystal structure and PXRD pattern are shown in the figures below.

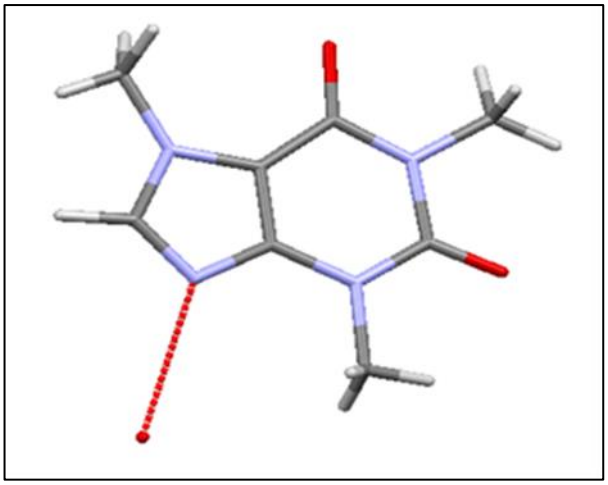

Figure 3.3. *Crystal structure of caffeine monohydrate (CSD Ref: CAFINE).*

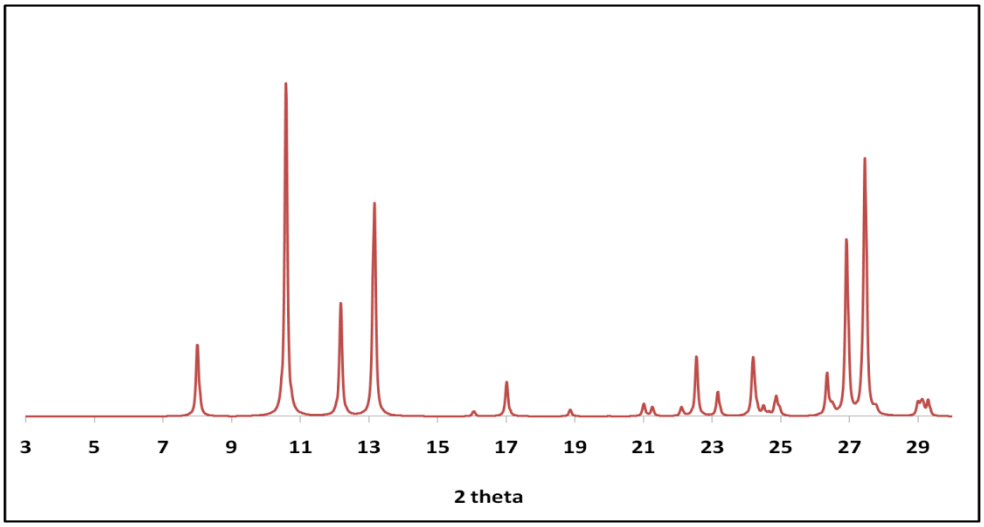

Figure 3.4. *Calculated PXRD pattern for caffeine monohydrate with characteristic peak at 10.5^{o} 2θ (CSD Ref: CAFINE).*

3.1.2. Maleic acid

MAL encloses localised C=O and C-OH groups which act as hydrogen bond donor and acceptor to form intermolecular H-bonding. These two groups have significant difference in their bond lengths i.e. C=O ~ 1.205Å and C-OH ~ 1.311Å. The molecule skeleton holds itself in *cis* conformation and locks into a planar conformation by intramolecular hydrogen bonding (Audet *et al*., 1990). The unit cell shows a *Pc* space group with a = 3.69, b = 7.48, c = 8.59, α = 90^{o}, β = 102.2^{o} and γ =

90^{o} (CSD Ref: MALIAC13). The figures below show the crystal structure and calculated PXRD patterns adopted from CSD.

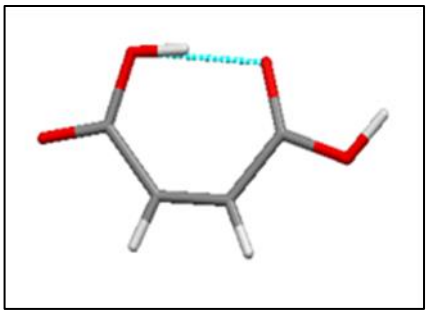

Figure 3.5. *Crystal structure of maleic acid (CSD Ref code: MALIAC13).*

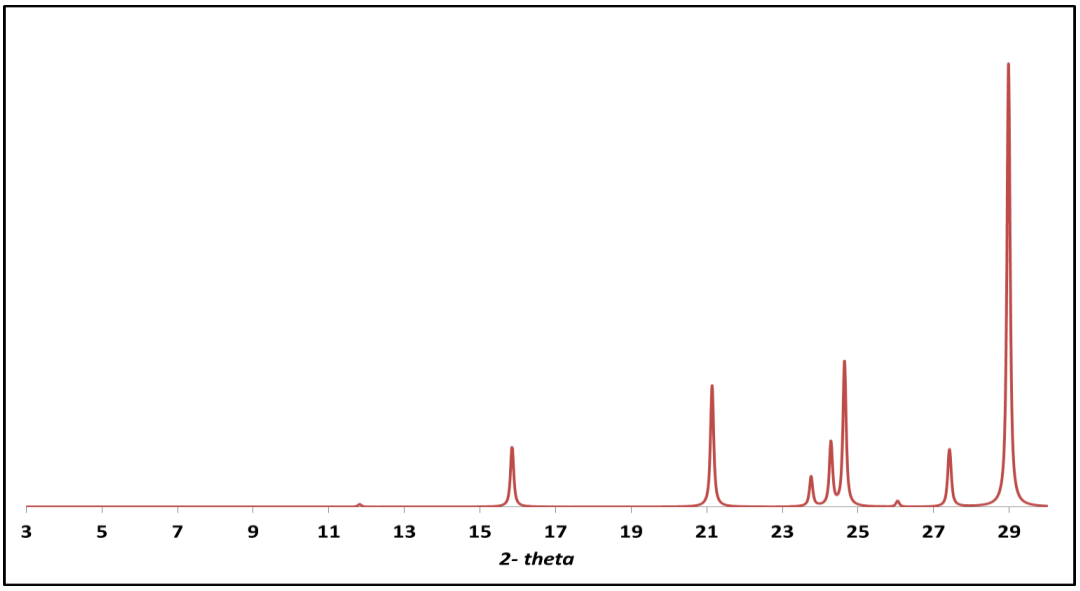

Figure 3.6. *Calculated PXRD pattern for maleic acid (collected from CSD).*

3.1.3. Caffeine maleic acid co-crystals

3.1.3.1. CAF / MAL 1:1 co-crystal, Form I

Caffeine has a pK_a of 3.6 as a result of weakly basic imidazole nitrogen present in the structure. Therefore, the potential salt-complex formation ability is limited to strong acids. The basic imidazole nitrogen and two carbonyl oxygens of CAF act as hydrogen bond acceptors. It exist as a neutral co-crystal with di-carboxylic acids

forming hydrogen bonds between unionised imidazole nitrogen and the carboxylic acid; i.e. an expected $[R_2^2(7)]$ heteromeric synthon with strong O-H----N and weak C-H---O hydrogen bonding (Trask, Motherwell and Jones, 2005).

The *cis* orientated maleic acid of CAF:MAL 1:1 Form I shows an intramolecular $[S_1^1(7)]$ hydrogen-bond motif along with intermolecular heterosynthon $[R_2^2(7)]$ between CAF-MAL dimeric units (Leyssens *et al*., 2012). The crystal structure and calculated PXRD pattern for CAF:MAL 1:1 Form I are given below.

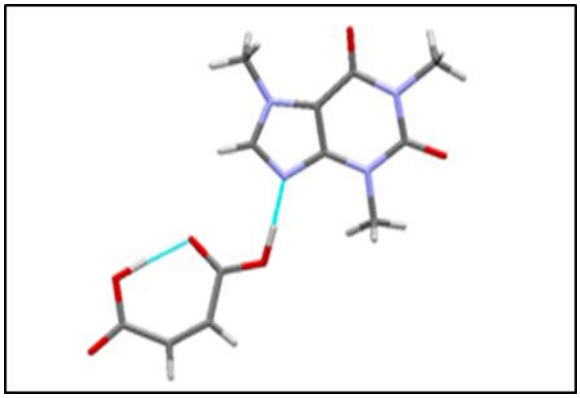

Figure 3.7. *Crystal structure of 1:1 caffeine / maleic acid co-crystal Form I (CSD Ref: GANYEA).*

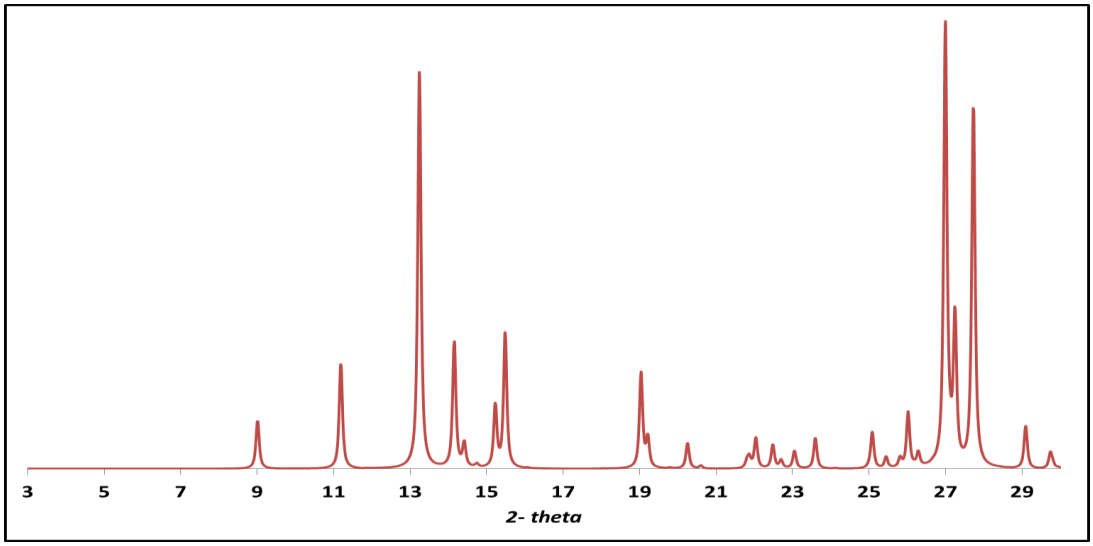

Figure 3.8. *Calculated PXRD pattern for CAF / MAL 1:1 Form I (obtained from CSD).*

3.1.3.2. CAF / MAL 1:1 co-crystal, Form II

The CAF:MAL 1:1 Form II exists as a triclinic crystal with two CAF and two MAL molecules in a unit cell. The intramolecular hydrogen bonding is absent in this polymorph which is mutilated by 80^{o} torsion of O-C-C-C. There is an intermolecular heterosynthon between the CAF-MAL dimer. The two dimmers are further connected by a $[R_2^2(8)]$ homosynthon between two adjacent carboxylic acid groups forming four component strand. Though a strong COOH homosynthon is present, this polymorphic state depicts reduced stability due to the distortion of maleic acid's planar structure which explains its low density. Also, the expand in N---(H)O distance from 2.51 Å to 2.73Å demonstrate a weakly bonded $[R_2^2(7)]$ heterosynthon (Leyssens *et al*., 2012). The crystal data and calculated PXRD pattern for this crystal form are shown in Figure 3.9 and Figure 3.10, respectively.

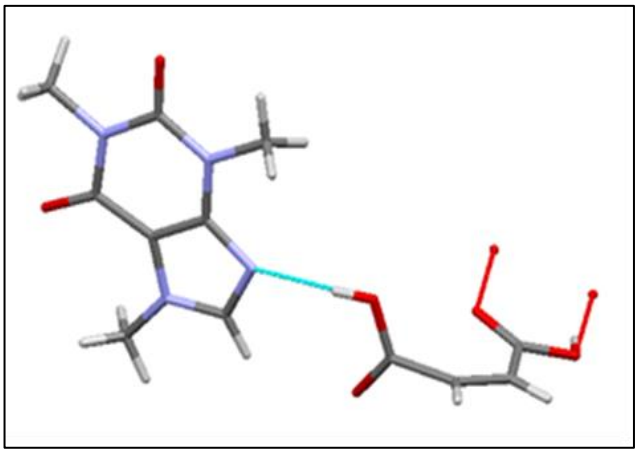

Figure 3.9. *Crystal structure of 1:1 caffeine / maleic acid co-crystal Form II (CSD Refcode: GANYEA01).*

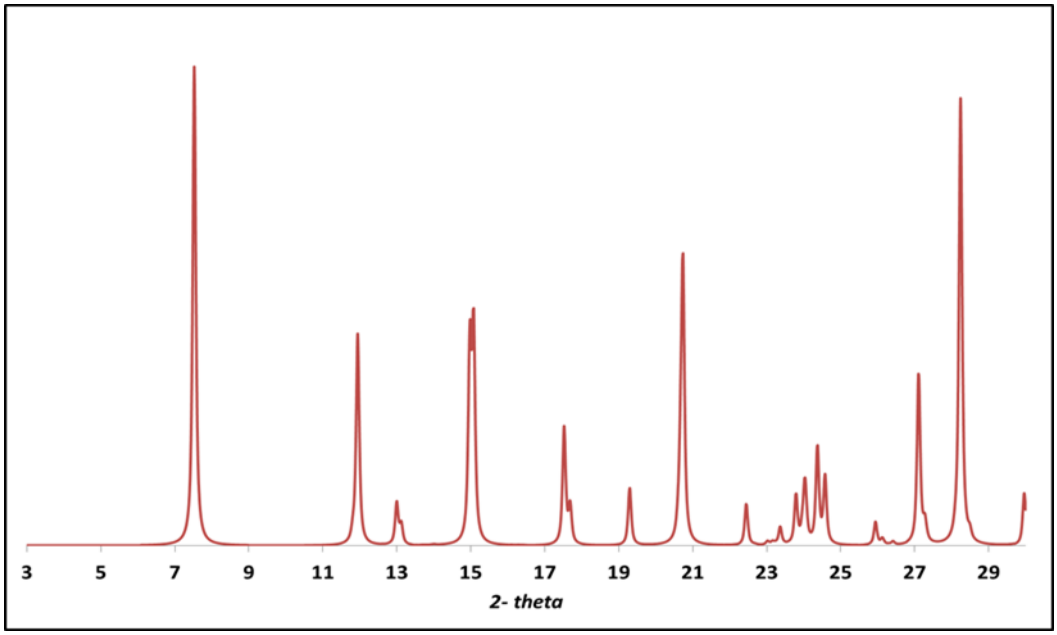

Figure 3.10. *Calculated PXRD pattern for 1:1 caffeine / maleic acid co-crystal Form II with characteristic peaks at 7.52, 11.94, 13, 15 and 17.5^{o} 2θ (collected from CSD).*

3.1.3.3. CAF / MAL 2:1 co-crystal

This crystal form acquires a monoclinic system where each unit cell is composed of two dimeric 2:1 CAF-MAL strand, i.e., 8 CAF molecules. No intramolecular hydrogen bonding is observed as seen in 1:1 Form I. The carboxylic acid groups of mal acid are twisted to give unstable *trans* orientation, forming two intermolecular [$R_2^2(7)$] heterosynthon with CAF. Hence, the deformation of MAL and increase in N---(H)O distance to 2.98Å explains for lower density of 2:1 CAF-MAL (Leyssens *et al.*, 2012). The crystal structure and calculated PXRD pattern for this crystal form are demonstrated in Figure 3.11 and Figure 3.12, respectively.

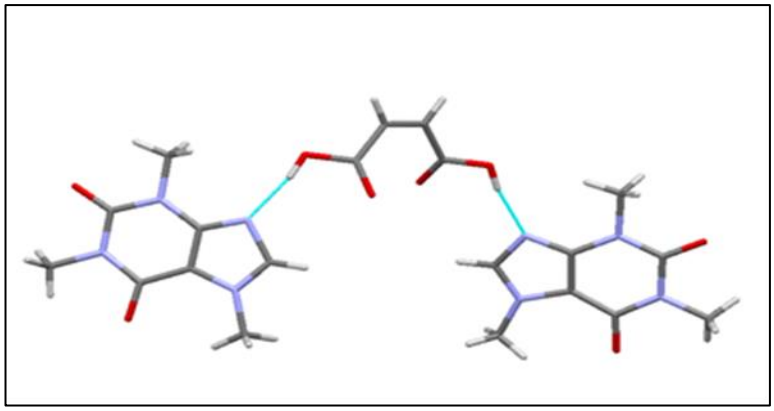

Figure 3.11. *Crystal structure of 2:1 caffeine / maleic acid co-crystal (CSD Ref: GANYIE01).*

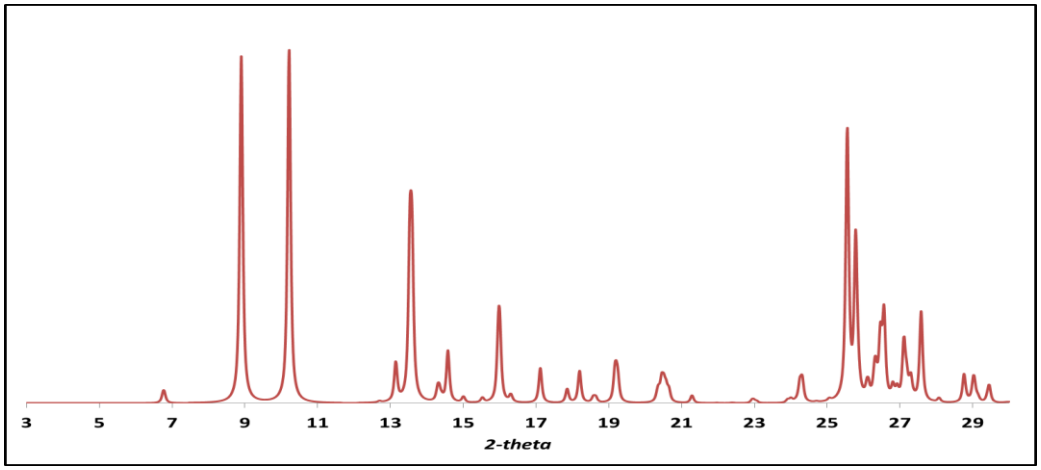

Figure 3.12. *Calculated PXRD pattern for 2:1 caffeine / maleic acid co-crystal with characteristic peaks at 8.9, 10.2, 13.14, 13.5 and 16^{o} 2θ (obtained from CSD).*

3.1.4. Malonic acid

MO is known to exist as five different polymorphs: α, β, γ, δ and ε with the difference in their packing patterns. It can form hydrogen bonding as it holds two proton acceptors and donors. For all the forms, the molecules are arranged in similar inclined zigzag fashion with carboxylate groups forming dimers by $R_2^2(8)$ hydrogen linkage. The triclinic β form is stable at room temperature with two non-equivalent cyclic hydrogen bonded dimers, which at higher temperatures (360 K), transforms into equivalent bonded structure, orthorhombic α form. With the increase in

temperature from 13-371 K, first order two phase transition was observed from γ to β and β to α. No unit cell dimensions were reported for orthorhombic δ form. Unlike β form, the new ε form has alternating carboxylate dimmers along and parallel to the planes down the column (Figure 3.14) (Reddy, Delori and Foxman, 2013). The crystal structure and PXRD pattern of malonic acid are shown in the Figure 3.13 and Figure 3.15, respectively.

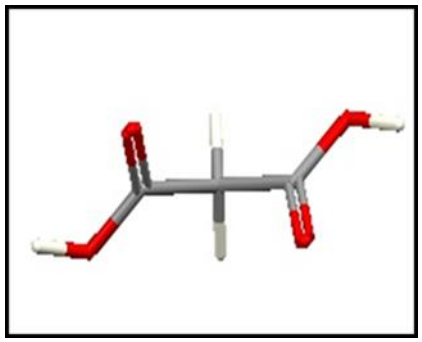

Figure 3.13.*Crystal structure of malonic acid (CSD Ref: MALNAC03)*

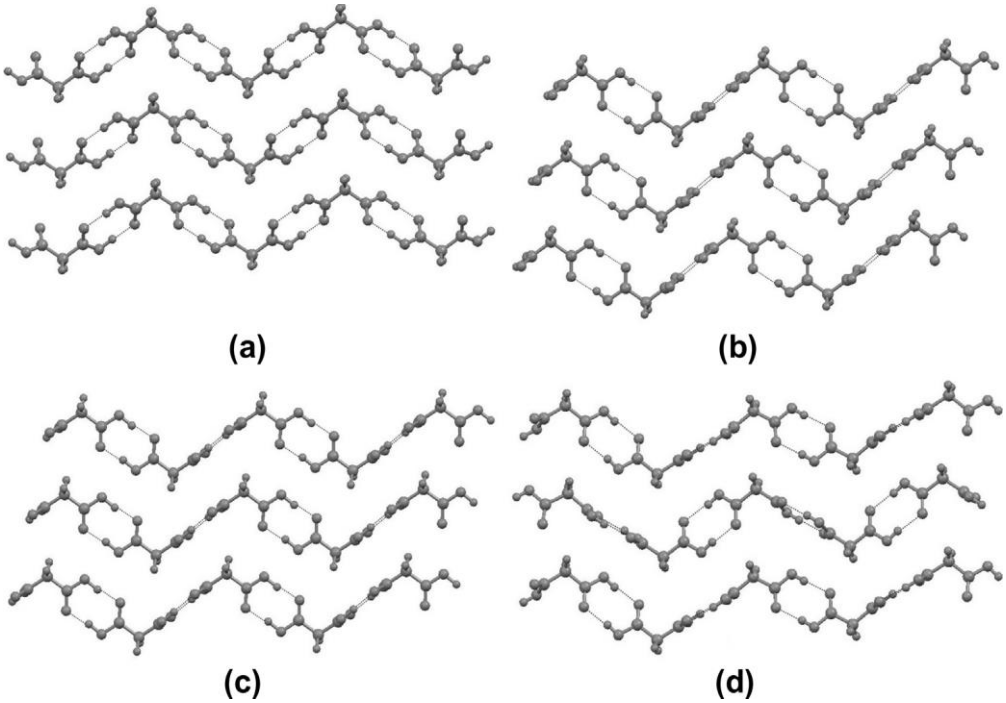

Figure 3.14. *Structural arrangement of malonic acid polymorphs: a) α-form: equivalent cyclic hydrogen bonded dimeric units; b) β-form: non-equivalent cyclic hydrogen bonded units; c) γ-form: H bonding between symmetry dependent molecules within the asymmetric unit; d) ε-form: alternating inclined carboxylate dimers along and parallel to the planes below the column (Reddy, Delori and Foxman, 2013).*

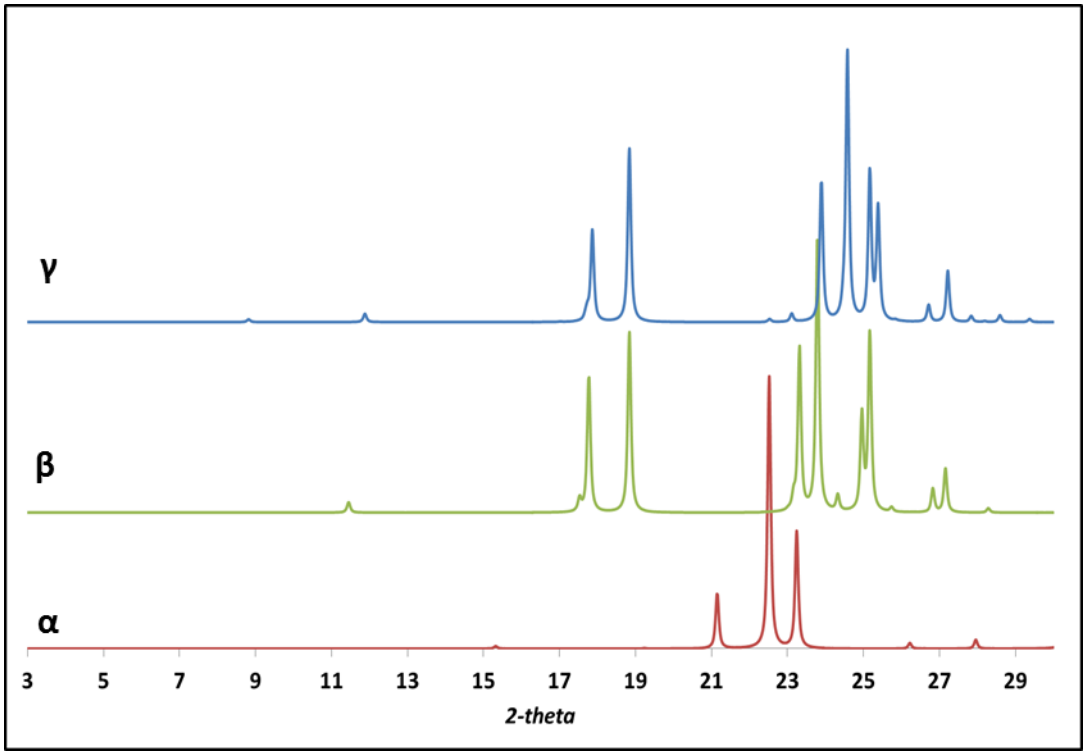

Figure 3.15. *Calculated PXRD pattern for malonic acid (CSD Ref: α-form (MALNAC03), β-form (MALNAC) and γ-form (MALNAC07)).*

3.1.5. Caffeine malonic acid co-crystal

CAF: MO 2:1forms orthorhombic crystal system with space group *Fdd2* and unit cell dimensions: a=30.39 (12) Å, b=31.28 (16) Å, c= 4.67 (2) Å, α=90^{o}, β=90^{o} and γ=90^{o}. The trimeric unit (caffeine-acid-caffeine) is held together by intermolecular hydrogen bonding between two carboxylate groups of each acid molecule with imidazole nitrogens of two caffeine molecules. This trimeric arrangement shows a V-shaped geometry appearing as a "kinked dumbbell" (Figure 3.17) (Trask, Motherwell and Jones, 2005). The crystal structure and PXRD pattern of CAF: MO co-crystal is shown in Figure 3.16 and Figure 3.18, respectively.

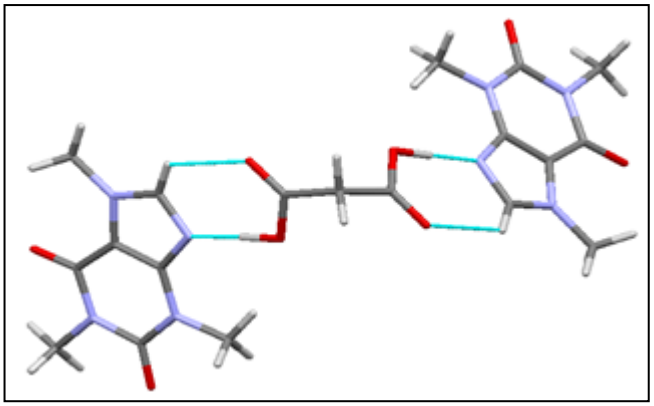

Figure 3.16.*Crystal structure of CAF: MO 2:1 cocrystal (CSD Ref: GANYAW).*

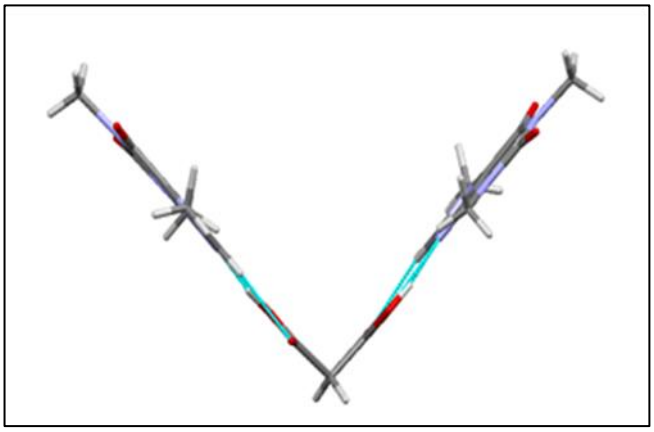

Figure 3.17. *Angled view: V-shaped geometry of trimeric CAF: MO 2:1 co-crystals processed in Mercury 3.5 (CSD Ref: GANYAW).*

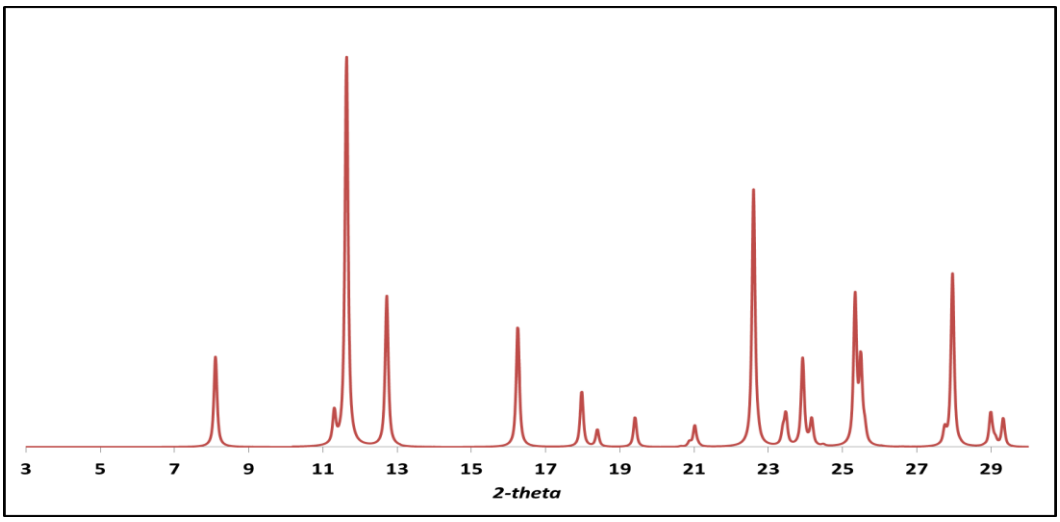

Figure 3.18. *PXRD pattern of CAF:MO 2:1 co-crystal obtained from CSD.*

3.1.6. Oxalic acid

OX molecule has a single carbon-carbon bond length and is planar in structure with carbonyl groups in *trans*-form (Figure 3.19). The structure exists as α (orthorhombic) and β (monoclinic) polymorphs based on their molecular orientation while forming intermolecular hydrogen bonding (Naumov*et al.*, 1996). The PXRD pattern for OX is illustrated in Figure 3.20.

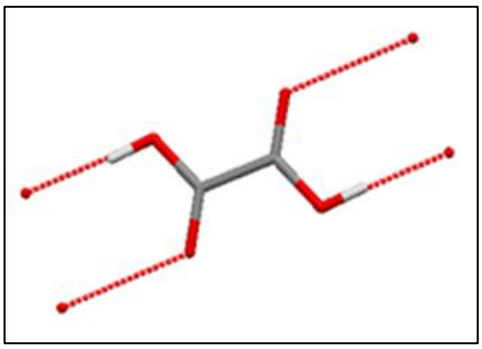

Figure 3.19. *Crystal structure of oxalic acid (CSD Ref: OXALAC11).*

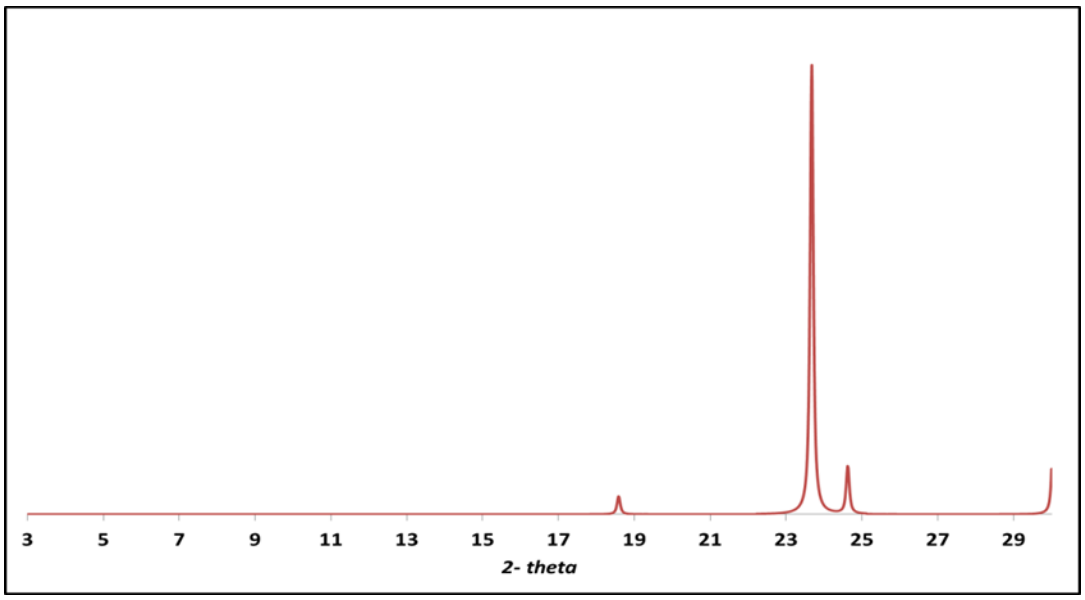

Figure 3.20. *Calculated PXRD pattern for oxalic acid (extracted from CSD).*

3.1.7. Oxalic acid dihydrate

Oxalic acid as α and β arrangement can incorporate water molecules placed asymmetrically between the C=O groups forming dihydrate. The α polymorph is formed by a short linear bond between acid proton and lone pair of water oxygen (II) and long bonds (I, III) formed between acid oxygen lone pair and water proton. Whereas, β polymorph only exists as a deuterated form with bond II bisecting the lone pair orbital on water oxygen (Figure 3.21) (Ebisuzaki and Angel, 1981).

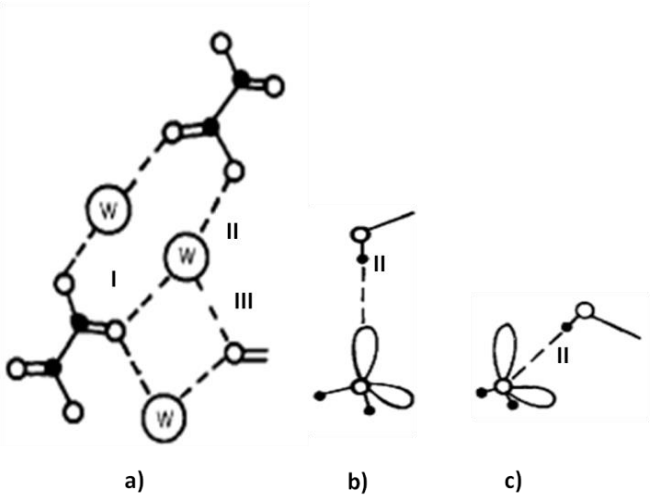

Figure 3.21. *Oxalic acid dihydrate: a) depicts the different bond arrangement between oxalic acid and water (W) molecule: long (I and III) and short (II) hydrogen bonds; b) α polymorph with linear short bond II; c) β deuterated dihydrate polymorph with acid proton dissecting the lone pair orbital on water oxygen (Ebisuzaki and Angel, 1981).*

The crystal structure and PXRD pattern for OX dihydrate is shown in the figures below:

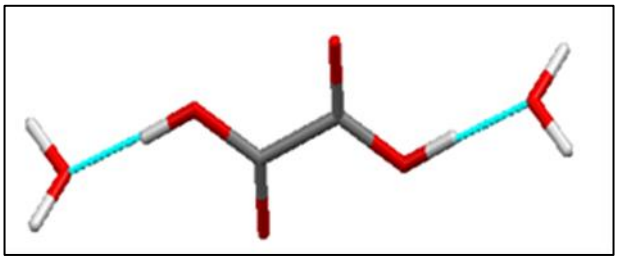

Figure 3.22.*Crystal structure of oxalic acid dihydrate (CSD Ref: OXACDH26).*

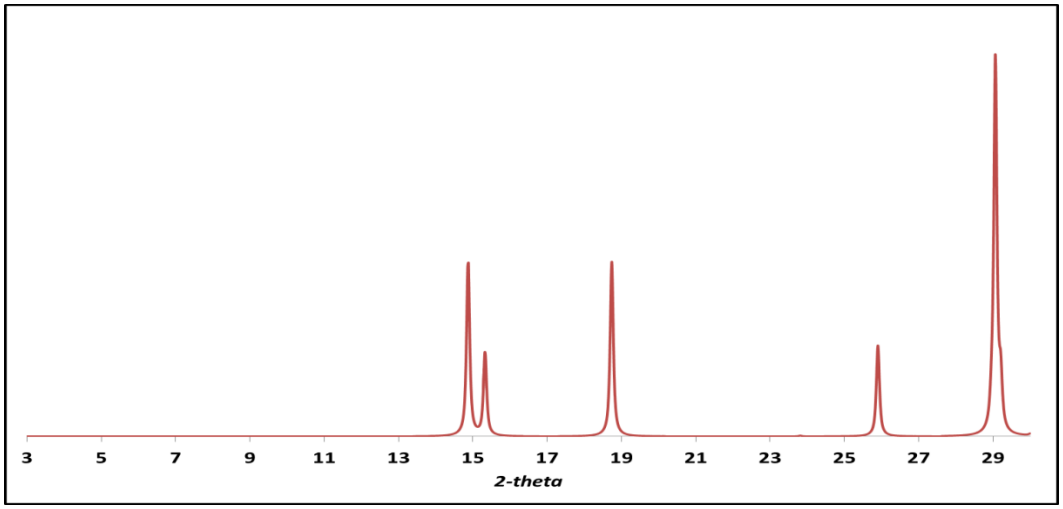

Figure 3.23.*Calculated PXRD pattern for oxalic acid dihydrate (adopted from CSD).*

3.1.8. Caffeine oxalic acid co-crystal

CAF:OX 2:1 co-crystal is a flat trimeric structure forming heterodimeric synthon as observed in CAF:MO but differs in its crystal packing, i.e. "dumbbell-shaped" (Figure 3.25) (Trask, Motherwell and Jones, 2005). The crystal has a space group of $P2_1/c$ and unit cell dimensions: a=4.41 (10) Å, b=14.77 (5) Å, c=15.91 (6) Å, α=90^o, β=96.49^o (10) and γ=90^o (CSD Ref: GANXUP). The crystal structure and PXRD data for CAF:OX co-crystal is displayed in Figure 3.24 and Figure 3.26, respectively.

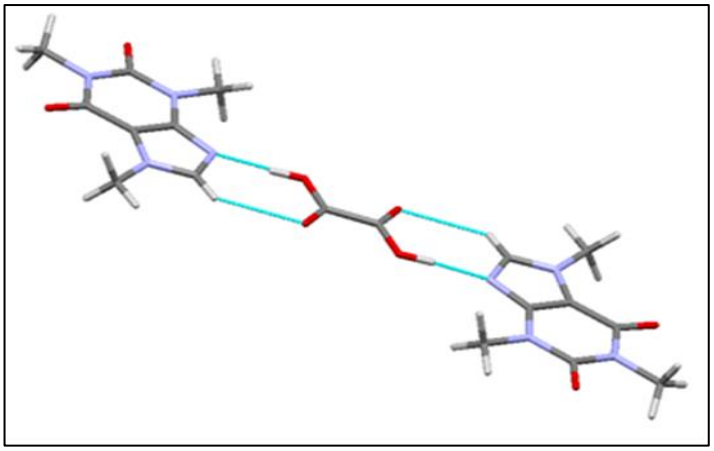

Figure 3.24. *Structural data for bis (caffeine) oxalic acid (obtained from CSD).*

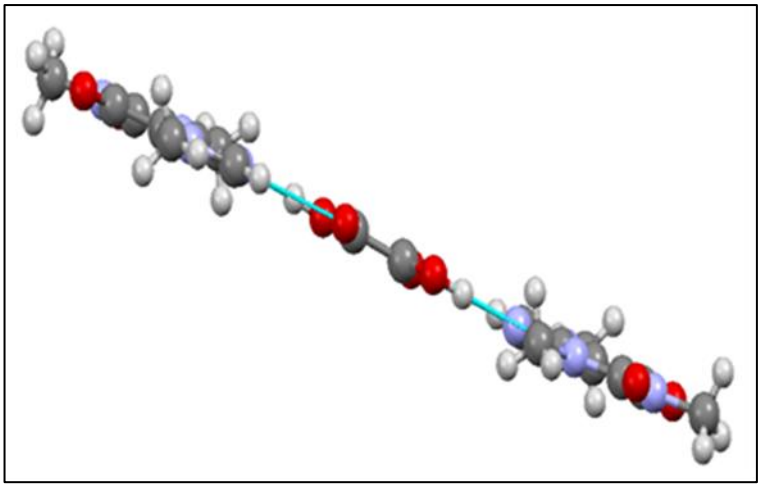

Figure 3.25. *Angled view of CAF:OX 2:1 planar trimeric unit processed using Mercury 3.5 (Trask, Motherwell and Jones, 2005).*

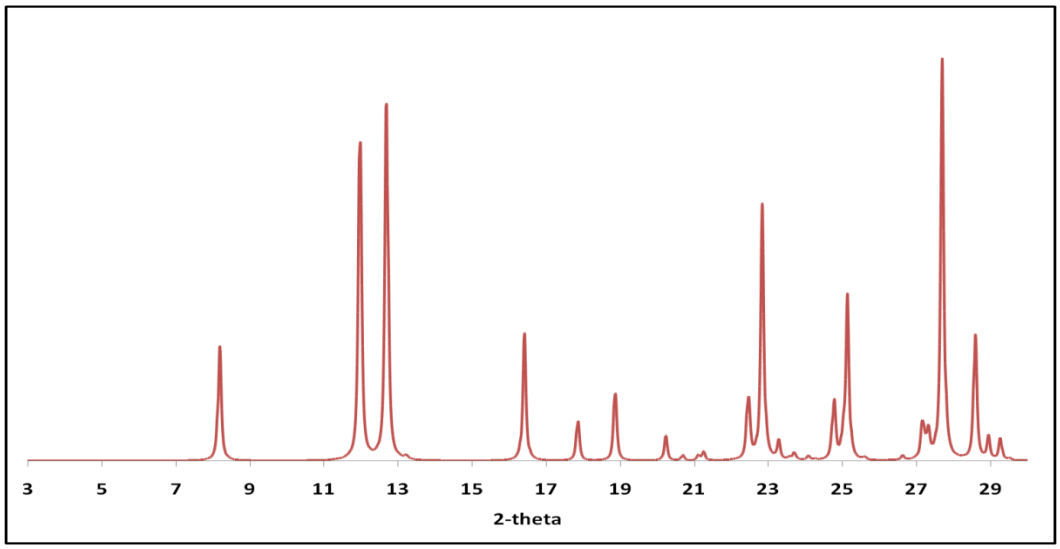

Figure 3.26. *PXRD pattern of CAF:OX 2:1 collected from CSD.*

3.1.9. Glutaric acid

GLU is a dicarboxylic acid with an odd number of carbon atoms and exists as two polymorphs: α and β. The transformation of β to metastable form (α) was favoured at higher temperatures with transition temperature of 63^{o}C and also at relative humidity above 60% (Yueng, Ling and Chan, 2010). The thermodynamically stable form, β has a distinctive space group, *C* 2/c, creating a monoclinic system with β= 145.04^{o}.

The molecules bind to each other by double or "cyclic" hydrogen bonds creating long chains. Each unit cell contains four non-equivalent molecules (Flakus and Miros, 1999). Whereas, α form leads to crystal destruction and reduced unit cell. The crystal structure and PXRD pattern for glutaric acid are depicted in the figures below.

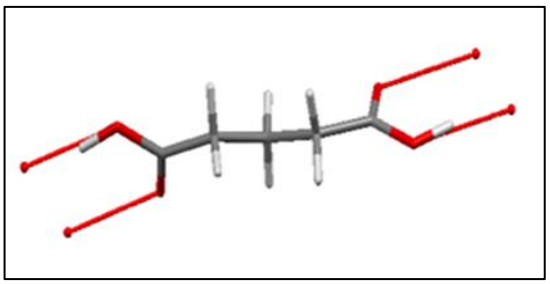

Figure 3.27.*Crystal data for glutaric acid (CSD ref: GLURAC12).*

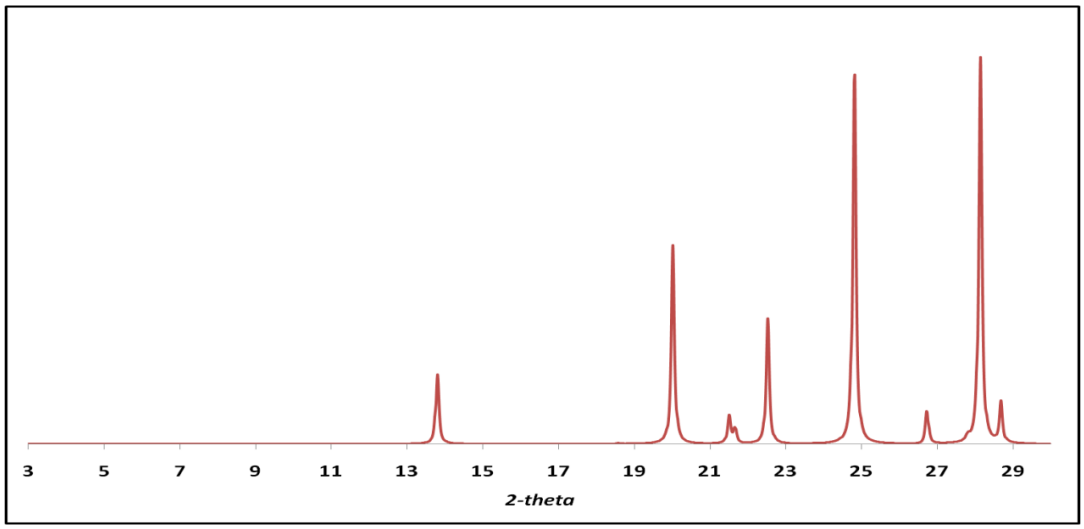

Figure 3.28.*Calculated PXRD pattern for glutaric acid (collected from CSD).*

3.1.10. Caffeine glutaric acid co-crystal

CAF: GLU 1:1 exhibit similar hydrogen bonding similar to CAF: MAL 1:1, where the heteromeric interaction (O-H---N) is only observed with one of the two carboxylic acid group. This indicates that GLU molecule may have a weak second

carboxyl group that did not favour H-bonding to caffeine imidazole nitrogen, producing 1:1 co-crystal. The 1:1 CAF: GLU also shows two polymorphic forms, I and II which are conformational in nature due to different torsion of the aliphatic chain (Trask, Motherwell and Jones, 2005). The crystal structure, crystal arrangement and PXRD pattern of two polymorphic forms of CAF: GLU 1:1 is shown in figures as follows:

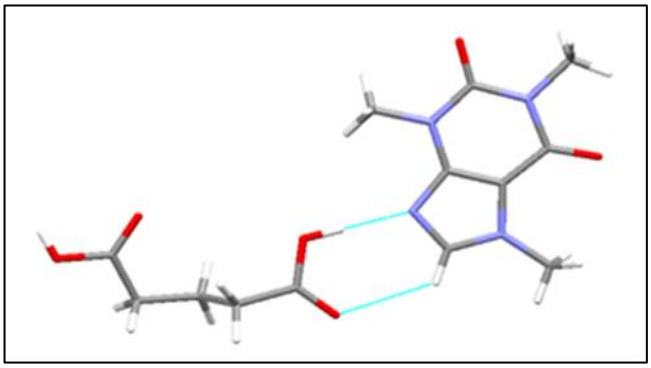

Figure 3.29.*Crystal data for CAF: GLU 1:1 co-crystal (CSD Ref: EXUQUJ).*

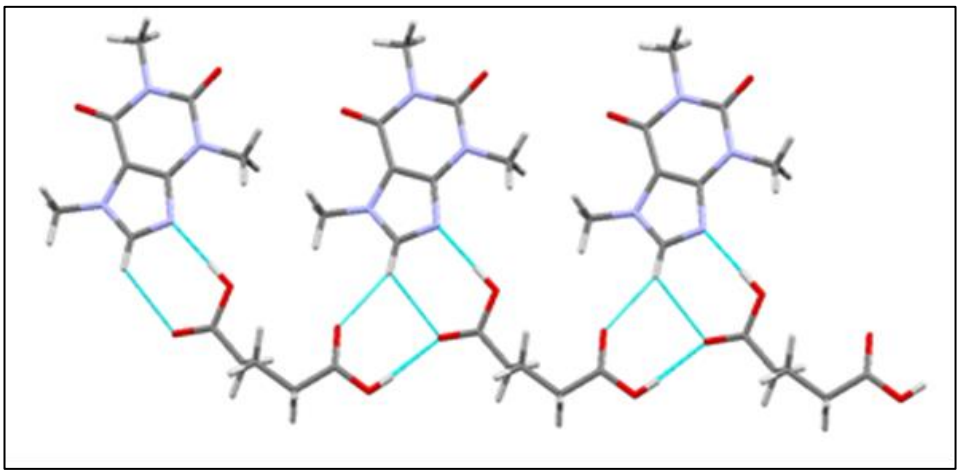

Figure 3.30 *Sheet of CAF: GLU ribbon processed in Mercury 3.5 (Trask, Motherwell and Jones, 2005).*

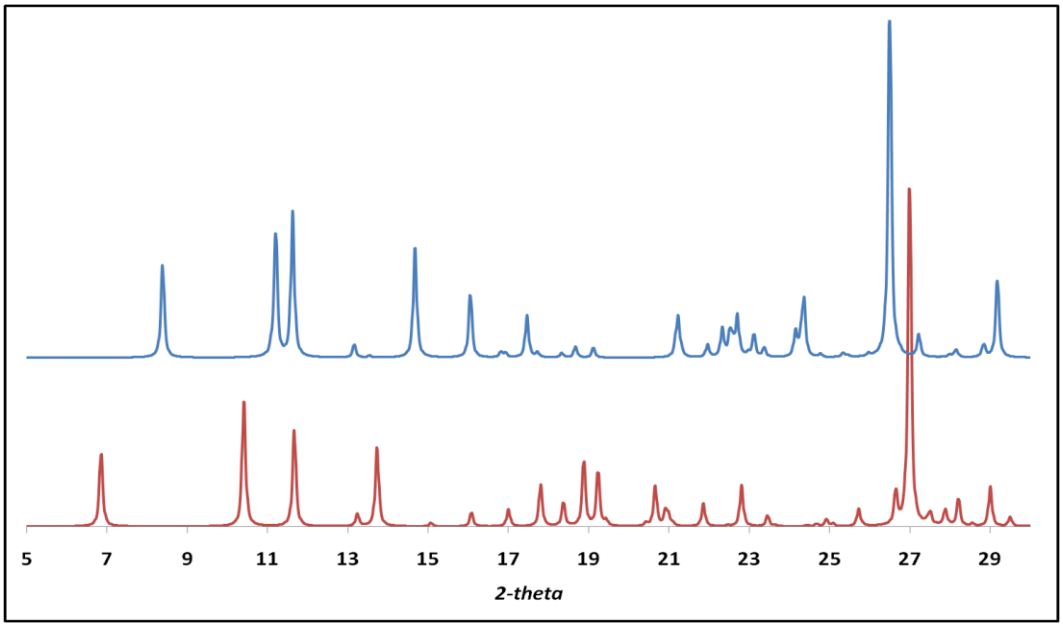

Figure 3.31.*Calculated PXRD patterns for CAF: GLU 1:1 Form I (bottom) and II (top) (extracted from CSD).*

3.1.11. Tartaric acid

TAR is an enantiomer with no heavy atoms and low symmetry. It can exist in three forms: D-, L- and meso- form. The combination of the left and right-handed crystal forms a racemate, i.e. d-(l)-tartaric acid. The d-(l)-tartaric acid is a monoclinic crystal with space group *P-1* and unit cell dimensions: a= 7.73Å, b=5.96Å, c=6.18Å, $\alpha=90^{o}$, $\beta=100.35^{o}$ and $\gamma=90^{o}$ (Stern and Beevers, 1950; Friscic *et al*., 2006). The figure below shows the crystal data for d-(l)-tartaric acid.

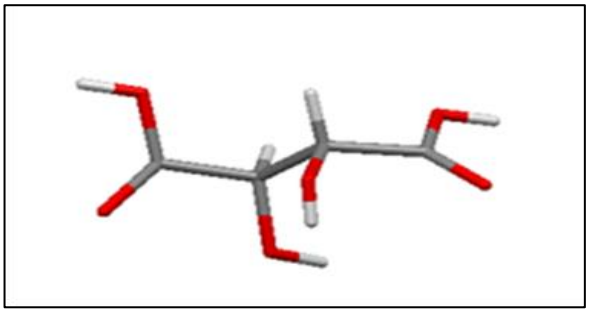

Figure 3.32.*Crystal data for d-(l)-tartaric acid (CSD ref: TARTAL01).*

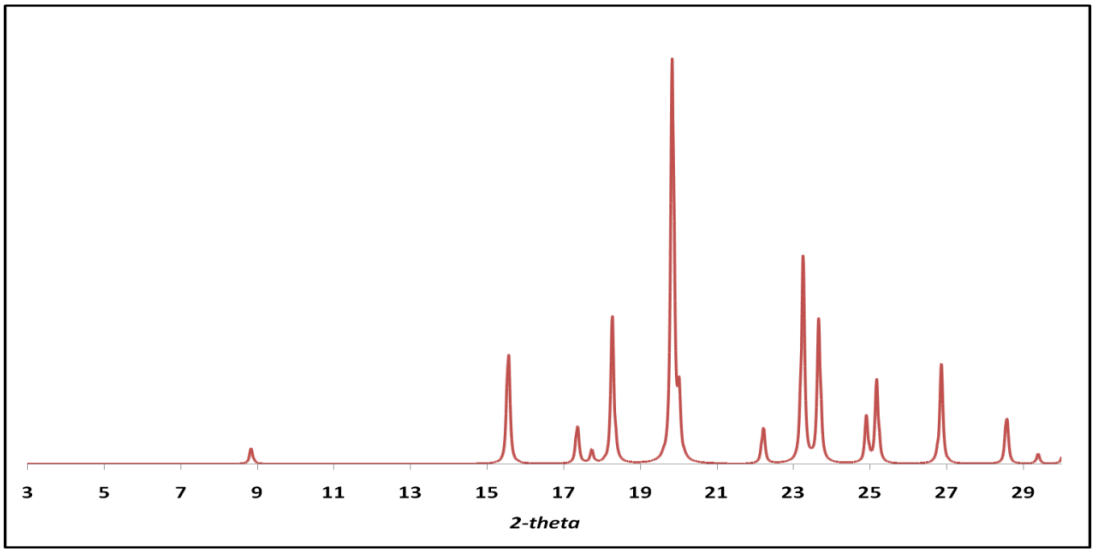

Figure 3.33. *PXRD for d-(l)-tartaric acid obtained from CSD ref: TARTAL01.*

3.1.12. Caffeine tartaric acid co-crystal

CAF and TAR can form 1:1 co-crystals via an intermolecular heterosynthon between the nitrogen of CAF and hydroxyl molecule of TAR (OH----N) as shown in Figure 3.34 (Friscic *et.al*., 2006). The PXRD pattern for CAF:D-TAR is illustrated in Figure 3.35.

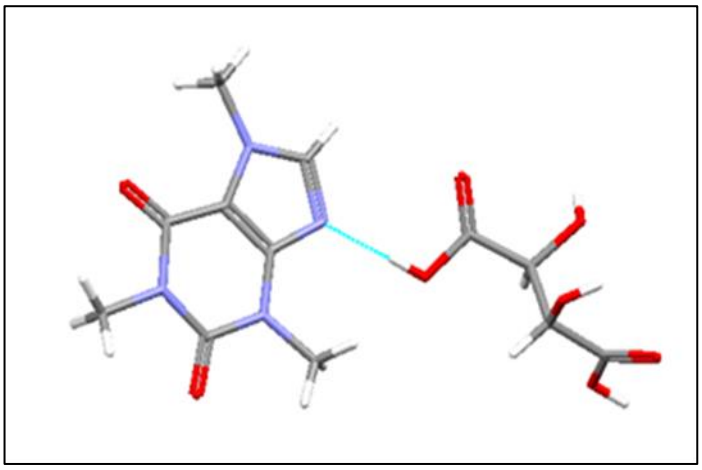

Figure 3.34.*Crystal structure of CAF: D-tartaric acid. (CSD Ref: NEXWUJ).*

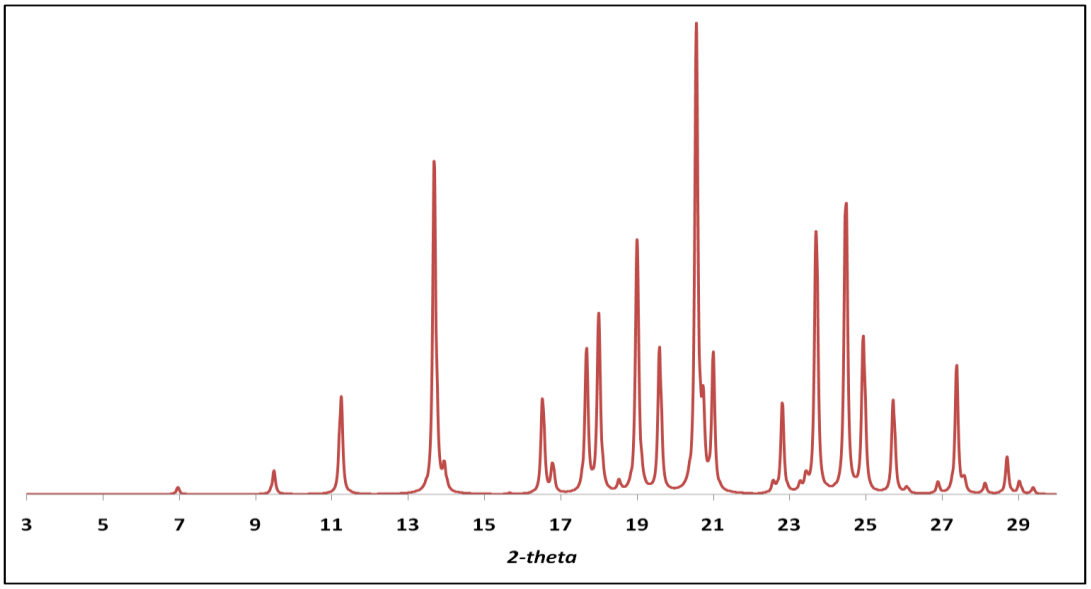

Figure 3.35.*PXRD pattern for 1:1 CAF:D-tartaric acid (CSD Ref: NEXWUJ)*

3.1.13. Succinic acid

It exhibits two polymorphs: a triclinic (α) and monoclinic (β) form with different patterns of H-bonding within the crystal lattice. α form was observed in supersaturated solutions over β polymorph which prevailed in low saturated solutions. Also, factors such as nature of the solvent may also influence this conversion (Yu *et al*., 2012). The PXRD patterns below show characteristic peak at 22^{o} and 27^{o} for α polymorph (Figure 3.37). The crystal structure of SU is shown in Figure 3.36.

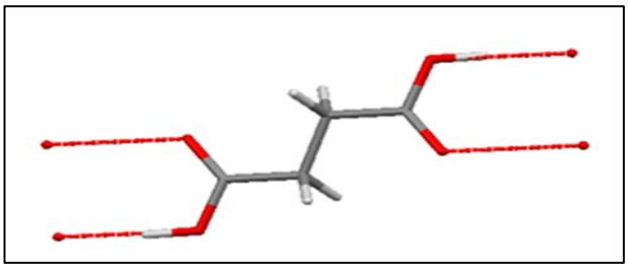

Figure 3.36 *Crystal structure for succinic acid (CSD Ref: SUCACB07).*

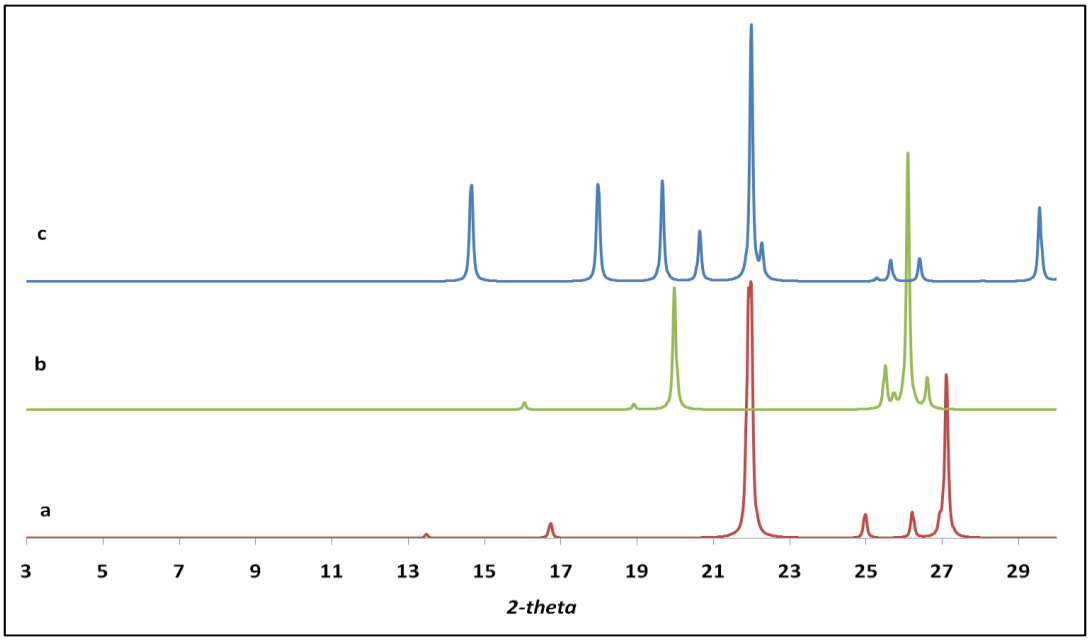

Figure 3.37. *PXRD patterns for SU: a) alpha polymorph; b) beta polymorph c) anhydride form. (CSD Ref: SUCACB06, SUCACB07, and SUCANH).*

3.1.14. Caffeine succinic acid co-crystal

No structural information available for this simple binary co-crystal.

Instead, a study attempted co-crystallisation of CAF and SU by creating host inclusion lattice in the presence of guest molecules such as $CHCl_3$ (chloroform) and $CHBr_3$ (bromoform). The CAF and SU molecules were combined to form a heteromolecular host framework forming a structure depending on the properties of the guest molecule and their bonding ability (i.e. hydrogen and halogen bond). The guest molecules favoured different host frameworks which determined the stoichiometric ratio of CAF and SU. The two frameworks formed were with stoichiometric ratios of 1:1 and 4:1 in presence of CCl_4 (carbon tetrachloride), and $CHCl_3$ as guest molecules, respectively (Friscic *et al*., 2008). The PXRD pattern for CAF: SU: $CHCl_3$ host-guest induced co-crystal is shown in figure below.

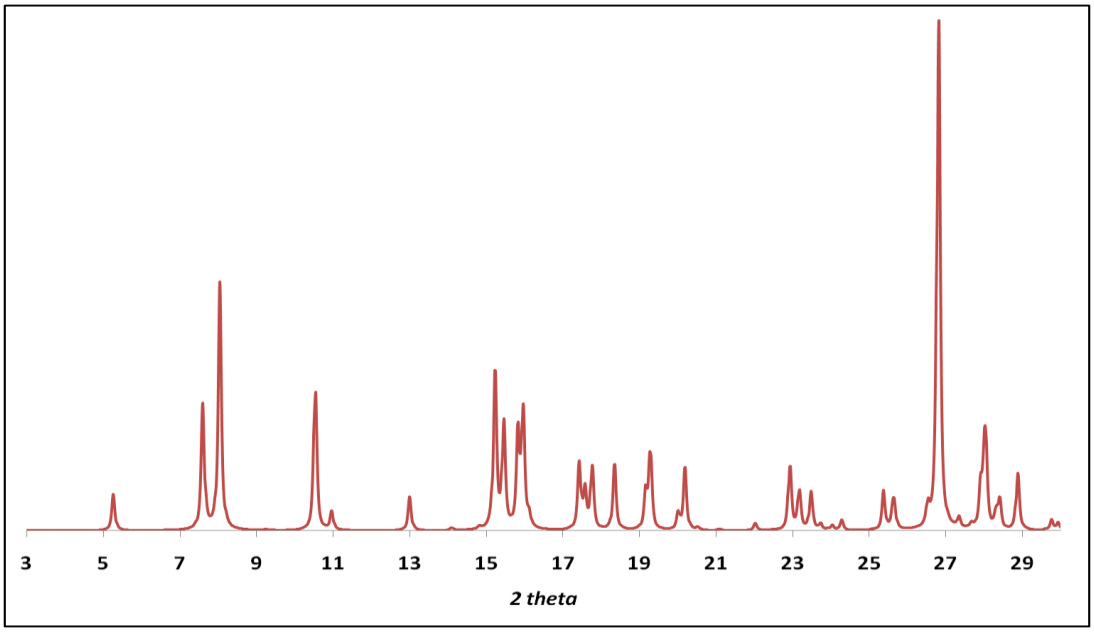

Figure 3.38. *PXRD for CAF:SU: $CHCl_3$ co-crystal (CSD Ref: 2.(CHCl3)2).*

3.2. Solubility

For proficient screening and scale-up of co-crystals, determination of the component's solubility could offer a significant influence in drug development. In this study, we investigated solubility in water, aqueous co-former solutions and selected organic solvents to deduce whether the incongruently soluble co-crystal pairs can be generated by a green approach.

3.2.1. Aqueous solubility

A calibration curve was constructed according to Beer-Lambert Law to determine CAF's solubility in various solutions. The linear equation was obtained as shown in figure below.

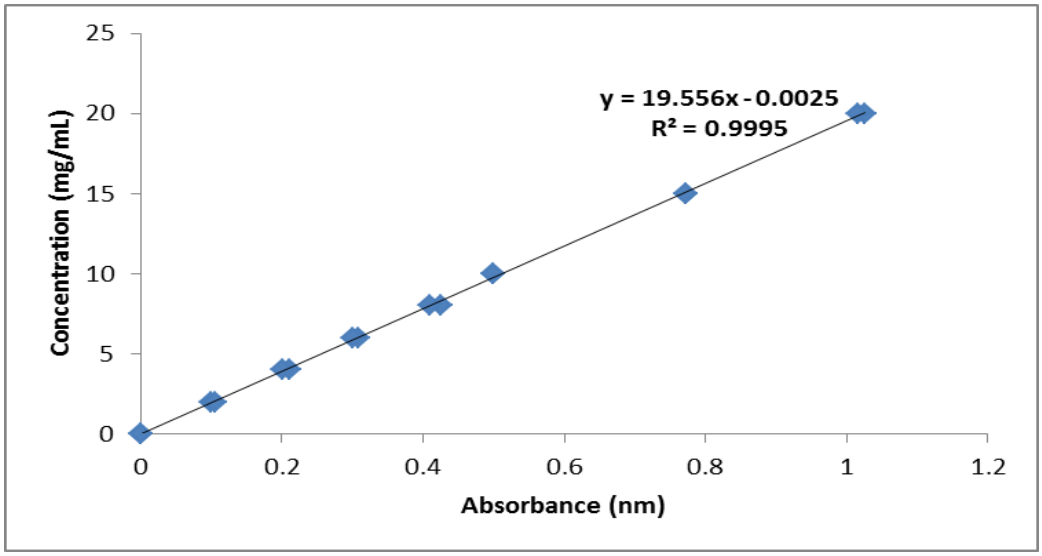

Figure 3.39. *Beer-Lambert calibration curve for CAF concentration against UV absorbance.*

The mole fraction solubilities (x) of caffeine in water (Table 3.1) and 0.04 M di-carboxylic acid solutions were measured from 294 to 323 K as summarised in Table 3.2. The dicarboxylic acid concentration of 0.04M was based on the highest concentration of mal holding CAF in water at room temperature and hence, used for other acids to test for solubility and compare results. It must be noted that succinic acid took several hours to dissolve in water until it gave a clear solution before solubility tests were performed. The solubility measurements in di-carboxylic acid solutions were correlated as a function of temperature (Figure 3.40) from equation 3a (Hu, Wang and Cai, 2009) and a plot of ln x vs 1/T was generated.

$$\ln x = A + B/(T/\mathrm{K}) \qquad \text{(Eq. 3a)}$$

Table 3.1. *Mole fraction solubility of caffeine in water at various temperatures*

.

T/K	*Caffeine solubility (mg/mL)*	*Mole fraction (10^3x)*
294	20.7	1.11±0.11
313	26.4	1.43±0.05
323	63.8	4.99±0.02
333	92.5	7.18±0.05

Table 3.2. *Mole fraction solubility of caffeine in six 0.04 M di-carboxylic acid solutions at 294, 313 and 323 K.*

T/K	***Caffeine (mg/mL)***	***Mole fraction (10^3x)***	***$(x-x^{cal})/x$***
Maleic acid			
294	63.0	3.40±0.06	0.007
313	126.7	6.82±0.17	-0.025
323	132.7	7.14±0.15	0.017
Malonic acid			
294	44.8	2.42±0.06	0.009
313	100.7	5.43±0.08	-0.031
323	102.4	5.52±0.06	0.021
Oxalic acid			
294	32.8	1.77±0.12	0.001
313	71.1	3.84±0.06	-0.004
323	97.8	5.27±0.01	0.003
Glutaric acid			
294	53.8	2.91±0.09	0.000
313	101.0	5.44±0.08	0.001
323	138.7	7.46±0.11	-0.001
Tartaric acid			
294	31.5	1.70±0.04	-0.001
313	51.0	2.76±0.06	0.003
323	66.7	3.60±0.09	-0.002
Succinic acid			
294	37.9	2.05±0.07	0.001
313	94.7	5.11±0.10	-0.001
323	144.5	7.77±0.13	0.001

The relative standard deviations (RSD) and parameters A and B for each di-carboxylic acid solution are listed in Table 3.3 and were calculated from equation 3b (Hu, Wang and Cai, 2009).

$$RSD = \left(\frac{1}{N} \sum_{1}^{n} \left(\frac{x - x^{calc}}{x} \right)^2 \right)^{1/2} \qquad \text{(Eq. 3b)}$$

Where, x^{calc} stands for the calculated values from the linear equation 3a and N is the number of experimental data points.

Figure 3.40. *Experimental mole fraction solubilities of caffeine in di-carboxylic acid solutions and water (markers); calculated solubilities from equation 1 (linear).*

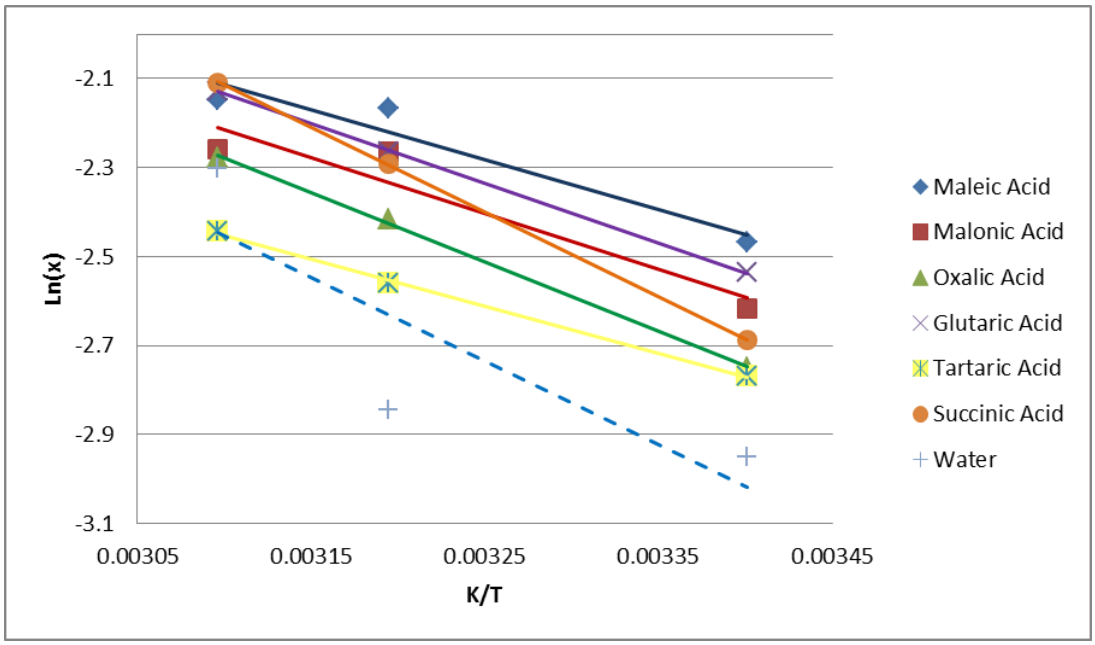

Table 3.3. *A and B values and the root-mean –square deviations of the measured solubilities from the calculated results.*

Acid solution	***A***	***B***	***RSD***
Maleic acid	1.3464	-1116	**0.018**
Malonic acid	1.6633	-1251.4	**0.022**
Oxalic acid	2.5584	-1560	**0.003**
Glutaric acid	2.0107	-1337.1	**0.001**
Tartaric acid	0.8216	-1056.1	**0.002**
Succinic acid	3.7715	-1898.8	**0.001**

An increase in the trend of solubility was observed with temperature in all di-carboxylic acid solutions and water. The solubility of caffeine shows the highest value from 294 to 323 K in maleic acid and the lowest in tartaric acid solution, which was probably due to their structures and interaction with water. The slight difference among the solubilities of CAF in each dicarboxylic acid solution might be unobvious due to the similar polarity. On the other hand, the mole fraction solubility of caffeine in water alone at range of temperatures was used for comparison. A

significant increase in solubility was observed in all di-carboxylic acid solutions except for tartaric acid and the increase was highest at the room temperature (294 K). Dicarboxylic acids can easily solvate in polar solvents due to the presence of hydrophilic groups and may self-associate or form H-bonding to induce solubility of insoluble organic substances. This enhanced solubility explains the hydrotropic nature of dicarboxylic acids which undergoes complexation with CAF (Guo *et al*., 2009; Kumar, Raja and Jayakumar, 2014) via weak interactions. The solubility of CAF decreases in the order: MAL >GLU>MO>SUC> OX > TAR >water.

CAF is assumed to self-polymerise in water and the formation of high order hydrates was thought to increase its solubility (Paruta, Sciarrone and Lordi, 1965). X-ray diffraction analysis was carried on the filtrate from these solutions to ensure any transformation of CAF into its hydrate form. The transition temperature from anhydrous to hydrous form for CAF is 45-55^{o}C (Wikstrom, Kakidas and Taylor, 2008); which was observed in water at 50^{o}C (323 K) and 60^{o}C (333 K). In the presence of di-carboxylic acids, hydrate peaks seem to emerge from MO, OX, GLU and TAR solutions at room temperature. The transformation was observed predominantly in oxalic acid solutions at all temperatures (Appendix I). But the extent of hydration could also be an important factor that needs to be considered.

3.2.2. Organic solvents

The solubility of CAF was further tested in selected organic solvents used in previous studies to investigate co-crystal formation with mal (Leyssens *et al*., 2012; Guo *et al*., 2009). The results obtained at room temperature are shown in Table 3.4.

Table 3.4. *Solubility of caffeine (mg/mL) in organic solvents at room temperature.*

Solvent	*Methanol*	*Acetone*	*Ethyl acetate*
Solubility (mg/mL)	15.6±0.02	16.2±0.06	7.2±0.01

The observations clearly indicate low solubility of CAF in organic solvents than in water. The enhancement in CAF solubility by complexation in aqueous solutions of dicarboxylic acids was considered as a suitable approach to obtain co-crystal phases via a green route.

3.2.3. Di-electric Constant (DEC)

The change in relative permittivity of water in the presence of dicarboxylic acids which successfully produced co-crystals with CAF was determined as a measure of change in its chemical polarity affecting solubility. Firstly, DEC values were obtained for solutions saturated with respect to dicarboxylic acids at various points, starting from 0.04 M till they reach saturation point at room temperature, that is, MAL at 5M, GLU at 3.25 M, OX at 1 M and MO at 13.45 M (Table 3.5). Therefore, the solubility of dicarboxylic acid in water increases in the order: OX<GLU<MAL<MO.

Table 3.5. *DEC values at 0.04M and saturated solutions of dicarboxylic acids in water*.

Acid conc.	**Oxalic acid**	**Glutaric acid**	**Maleic acid**	**Malonic acid**
0.04 M	77.2	77.6	77.2	77.9
Saturated solution	65.2	56.2	48.3	37.8

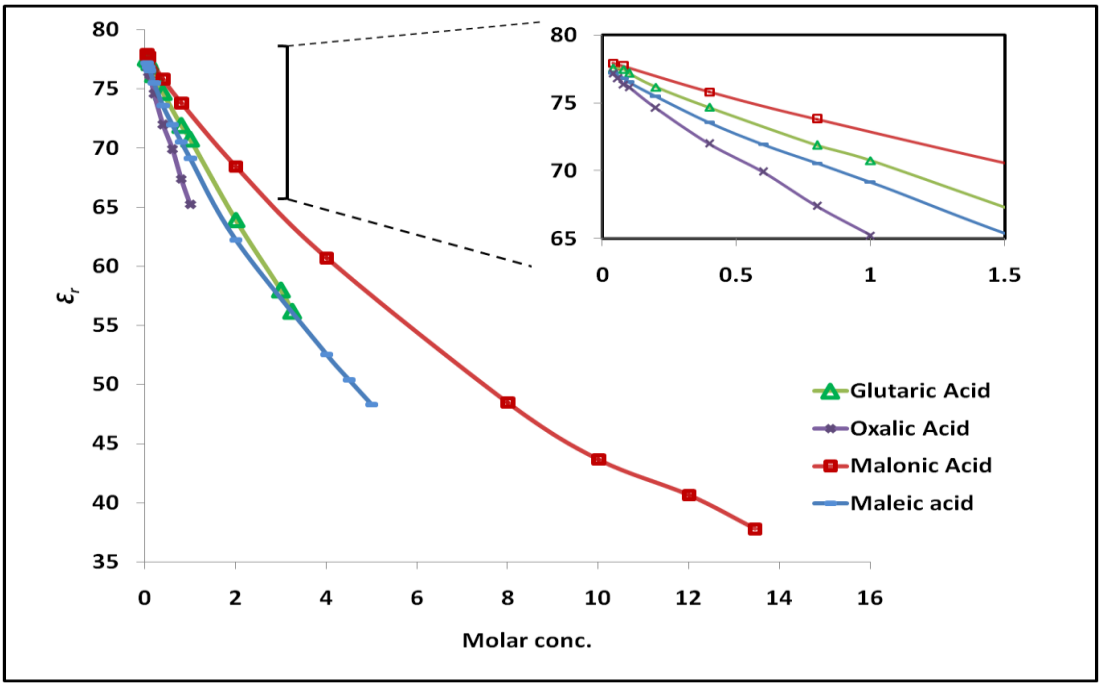

Figure 3.41. *Graphical representation of DEC ($\mathcal{E}_r$) values against the molar concentration of dicarboxylic acids.*

The results explain that at low concentrations i.e., 0.04 M, the relative permittivity is similar for all acids and it progressively decreases till they reach their saturation points. At a particular molar concentration, eg: 1 M, the DEC values were in order: OX<MAL<GLU<MO.

Hildebrand's theory on solubility correlates dielectric constant ($\mathcal{E}_r$) with solubility parameters (δ) attaining a linear relationship expressed by the following equation:

$$\delta = 0.22\ \mathcal{E}_r + 7.5 \qquad \text{(Eq. 3c)}$$

A close linear correlation was observed in solvents with same chemical behaviour or molecular associations. Paruta *et al*., (1962) found the best correlation for solvents that had tendency to associate via H- bonding. That is, solubility parameter vs DEC plots of solvents such as water, methanol, ethanol, ethyl acetate etc. produced a linear trend. Alongside linear correlation, a positive slope was noted for polar solute

in less-polar solvent, whereas, a negative slope was seen when a non-polar solute dissolved in high-polar solvents (Gorman and Hall, 1964). Similarly, a negative slope is illustrated in Figure 3.41 for all dicarboxylic acids due to its association with highly polar solvent, water.

The inter- and intra-molecular H-bonding of a solute such as dicarboxylic acid gets obstructed when dissolved in water as the donor and acceptor molecules on the solute associate via H-bonding. Debye model representation has been used to explain the induced dipole moment (dipole relaxation motion of molecules) in solvents which illustrates their H-bonding potency. Polar liquid such as water undergoes dipole-dipole intermolecular interactions, thereby causing re-orientation of the molecular arrangement. Water has highest polarity with DEC value of 80 at 20^{o}C which is attributed to its hydrogen bonding capacity. Hence, DEC can be used to estimate the polarity of a solution. Other hydrophobic liquids possess a DEC less than 15, due to low dipole moment or collisions (Book: Son, 2014).

Paruta (1964) later examined an increase in solubility of range of solutes with the increase in the concentration of sucrose solution and simultaneous decrease in their DEC values. The decrease in DEC was indicative of solvency attributes of sucrose syrup and reduction in polarity. The association between solute and solvent molecules may transform the linearity of the plot i.e., producing a linear or flat non-linear relationship. The plot above does not show the best linear trend for all the dicarboxylic acids at higher concentrations. The decline in DEC values explains the reduction in polarity of the solution as the dicarboxylic acid concentration increases. The solute with highest solubility (malonic acid) attains the lowest DEC value as it undergoes highest molecular association with water, reducing its dipole moment compared to other acids.

Secondly, DEC values were also collected for 0.04 M dicarboxylic solutions with addition of CAF in increments till it became saturated, as shown in Figure 3.42. The DEC values of saturated acid solutions are provided in Table 3.6

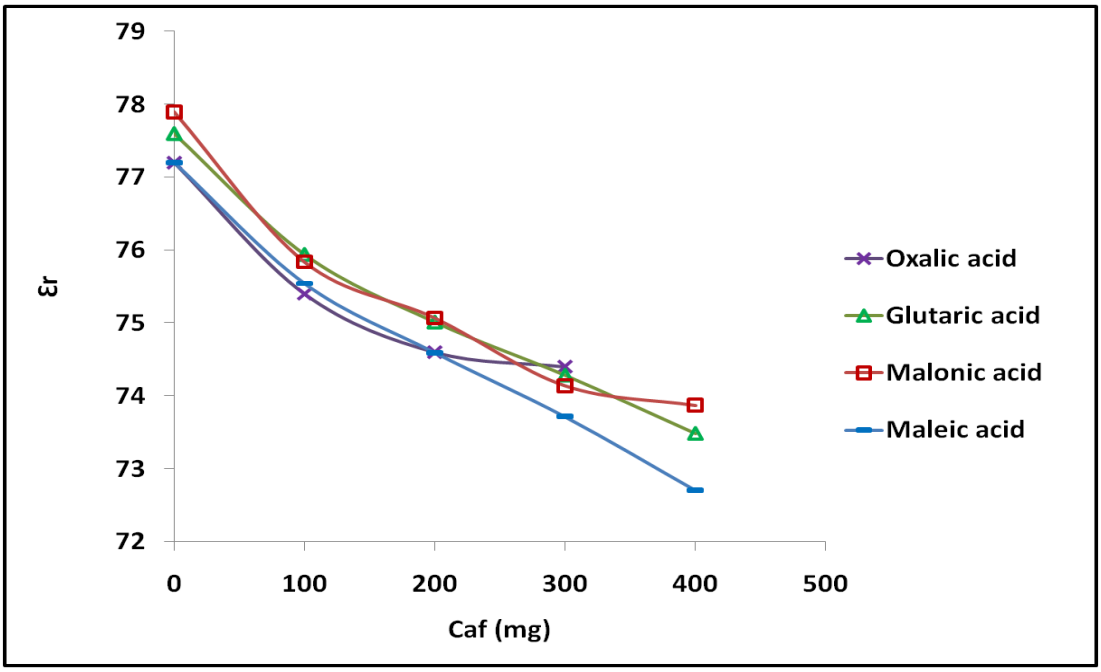

Figure 3.42. *A DEC plot against CAF concentration till the dicarboxylic acid (0.04M) solutions attained saturation point.*

Table 3.6. *DEC values of saturated dicarboxylic acid (0.04M) solutions wrt. CAF.*

CAF Concentration	**DEC**			
	Oxalic acid	*Glutaric acid*	*Maleic acid*	*Malonic acid*
No CAF	77.2	77.6	77.2	77.9
Saturated wrt. CAF	74.4	73.5	72.7	73.9

Apshingekar (2014) observed an increase in trend of CAF solubility with increase in MAL until the CAF to MAL ratio in the mixture was low i.e., CAF solubility decreased at higher mal concentrations. On the other hand, mal solubility was decreased with the increase in CAF concentration. It was suggested that polar compound like mal has potential to form hydrogen bonding with water, therefore, the DEC decreases. Further addition of CAF disrupts the association contributing to a

new dipole moment changing the overall DEC and hence, solubility. In this study, CAF's solubility was examined at lower dicarboxylic acid concentration which agrees with the results of the study above. The DEC value of each dicarboxylic acid is same at 0.04 M concentration as described before, which illustrates that all the solutions exhibit same polarity regardless of the acids present. Further addition of CAF may possibly disrupt the molecular interaction which will vary for each acid solution, reducing its bonding capacity and hence polarity. The oxalic acid solution saturated at lower concentration compared to other solutions. The polarity of the acid solution is in order: OX>MO>GLU>MAL which complies with CAF's solubility reported earlier, i.e OX<MO<GLU<MAL. Therefore, maleic acid solution depicts highest complexation rate with CAF, enhancing its solubility compared to other acids and its H-bonding capacity decreased due to high molecular association producing lowest DEC value.

3.3. Fast evaporating techniques

It must be noted that preliminary tests were performed in order to observe whether all dicarboxylic acid formed co-crystals via spray drying before progressing with the proposed study. The trial test results did not generate co-crystals of CAF with SU and TAR and hence, were not included in this study. As mentioned before, no co-crystal of CAF has been reported with SU (Trask *et al*., 2005; Friscic *et al*., 2008) via grinding or from solution, but, a three component solvate co-crystal was reported with chloroform (Friscic *et al.*, 2008). It was suggested that CAF: SU co-crystal show physical instability and may form weak bonds with solvent molecules. On the other hand, CAF: TAR could not be generated by grinding method (Trask *et al.*,

2005), whereas, CAF:L-TAR and CAF:D-TAR were successfully produced by solvent grinding in nitromethane (Friscic *et al*., 2006). This could be due to the complexity of the chiral compound, TAR.

3.3.1. Rotavap

Rotavap was used as a pre-screening tool to predict the kinetically-driven co-crystals from large-scale spray dryer as it is continuous, fast and easy to operate, and possess similar mechanism of rapid evaporation. To investigate the formation of co-crystals by rotavap technique, stoichiometric ratios of CAF and co-formers were prepared. The solvents for CAF and MAL pair were selected based on solvent approaches by previous studies (Leyssens *et al*., 2012; Guo *et al*., 2010; Pagire *et al*., 2014) (Table 3.8). The solutions were subjected to higher temperatures to solubilise the incongruently soluble starting components, hence, raising the solvent vapour pressure. Reduced pressure conditions were used to enable rapid evaporation. The vapour pressure of the solvent subjected to various temperatures was calculated using Antoine's equation (Chapter 1, Eq. 1d). The parameter values for each solvent are provided for the temperature range used in the experiments as shown in the table below.

Table 3.7. *Antoine's parameters obtained for each solvent to determine their vapour pressure (DDBST GmbH, n.d.).*

Solvent	**Antoine's equation parameters**		
	A	**B**	**C**
Water	8.1	1730.6	233.4
Methanol	8.1	1582.3	239.7
Acetone	7.1	1220.0	230.7
Ethyl acetate	7.3	1369.4	235.5

Table 3.8. *Experiments conducted for the production of CAF and dicarboxylic acid co-crystals via rotavap.*

Solution Mixture	Solvent	Concentration (%)	Bath Temp (^{o}C)	Vapour pressure of solvent (mbar)	Reduced Pressure Applied (mbar)	XRD
CAF:MAL 1:1	*Water*	3.4	70	233	180	*2:1+* ***M††***
	Water	3.4	70	233	65	*2:1 + 1:1††+****M†***
	Methanol	2	50	555	200	*1:1+2:1††+****M†***
	Ethyl acetate	2	80	830	600	*2:1 +* ***M††***
	Acetone	2	70	1585	560	*2:1 +* ***M††***
CAF:MAL 2:1	*Water*	1.7	75	384	123	*2:1 +* ***C††***
	Water	3.4	75	384	123	*2:1 +* ***C††***
	Methanol	2.4	60	844	200	***C****+ 2:1††+ 1:1†*
	Ethyl acetate	2.4	80	830	200	*2:1 +* ***C††***
	Acetone	2.4	70	1585	330	*2:1 +* ***C††***
CAF:OX 2:1	*Water*	2	75	384	123	*2:1**
CAF:MO 2:1	*Water*	3.4	75	384	123	*2:1**
CAF:GLU 1:1	*Water*	5	75	384	123	*1:1* ***FII****
****---phase pure; †--traces; ††---minor; C --- CAF; M---MAL; FII---Form II***						

3.3.1.1. CAF:MAL

Surprisingly, fast evaporation of CAF:MAL 1:1 solution (Figure 3.43) led to the nucleation of major 2:1 co-crystals with impurity of MAL. On the other hand, solutions of 2:1 stoichiometry generated major 2:1 co-crystal (Figure 3.44) with CAF impurity. Also, impurity of 1:1 was observed in water at a very low pressure condition and in methanol solutions. A report analysed phase pure co-crystals via rotavap for congruently soluble components. Selection of solvent was considered important in terms of polarity and solvency for successive nucleation of the components. It is generally assumed that crystallisation pattern follows Ostwald's rule of successive stages where stable form is favoured under slow supersaturation in

contrast to accelerated conditions supporting the metastable form. This was confirmed by the production of curcumin (CUR) and phloroglucinol (PHL) metastable co-crystal via rotavap in a suitable solvent aiding congruent solubility (Chow *et al*., 2012).

So far, it has been really difficult to obtain 2:1 co-crystals of CAF: MAL from solution at 25^{o}C and hence, was claimed to be a metastable form (Guo *et al*., 2010). Due to rapid evaporation, the solution shoots up to point of uncontrolled co-crystallisation, leaving insufficient time for either of the components to nucleate. In this case, three factors may seem to play a significant role, i.e. solubility, rate of evaporation and kinetics favouring metastable form. The rate of evaporation is dependent on the temperature and pressure conditions set as explained in chapter 1.8.1.2. The vapour pressure of water at 70^{o}C and 75^{o}C is 233 and 384 mbar, respectively, and the pressure settings applied was less than these values (Table 3.8). The impurity of 1:1 was observed when the reduced pressure (65 mbar) was set too low than the optimum pressure (233 mbar) causing solvent foaming and hence, disrupting the consistency of rate of loss of solvent and nucleation.

Additional tests were performed in organic solvents to check if we can reproduce CAF:MAL 1:1 co-crystal . Organic solutions containing CAF: MAL 1:1 and 2:1 ratio produced major 2:1 with MAL and CAF impurity, respectively. However, impurity of 1:1 was only observed in methanol from both starting ratios of 1:1 and 2:1. This is a true reflection of earlier report that recognised solvent- driven stoichiometrically diverse CAF: MAL co-crystals, where methanol addition to 2:1 favoured 1:1 co-crystals (Trask *et al*., 2005). Even though, the solubility of CAF in organic solvents was low; presence of MAL increases its solubility due to complexation. Pagire *et al*., (2014) reported CAF solubiltity in 0.4 mM MAL

solutions of organic solvents. Water and methanol were found to be good solvents compared to acetone and ethyl acetate. It was established that methanol favoured almost phase pure 1:1 co-crystal under microwave irradiation. Therefore, methanol plays a convincing role in nucleation of 1:1 co-crystal form but kinetically driven technique may hinder this formation generating mixtures of both 1:1 and 2:1.

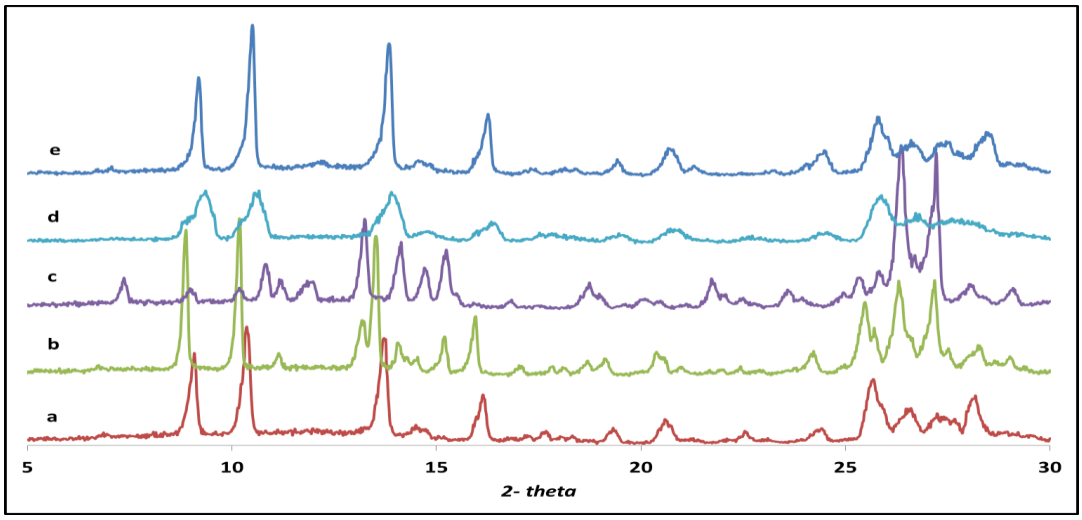

Figure 3.43. *PXRD pattern for CAF:MAL 1:1 solutions under rotavap: a) 3.4% water @ 180Mbar; b) 3.4% water @ 65mbar; c) 2% methanol @ 200mbar; d) 2% ethyl acetate @ 600mbar; e) 2% acetone @560 mbar.*

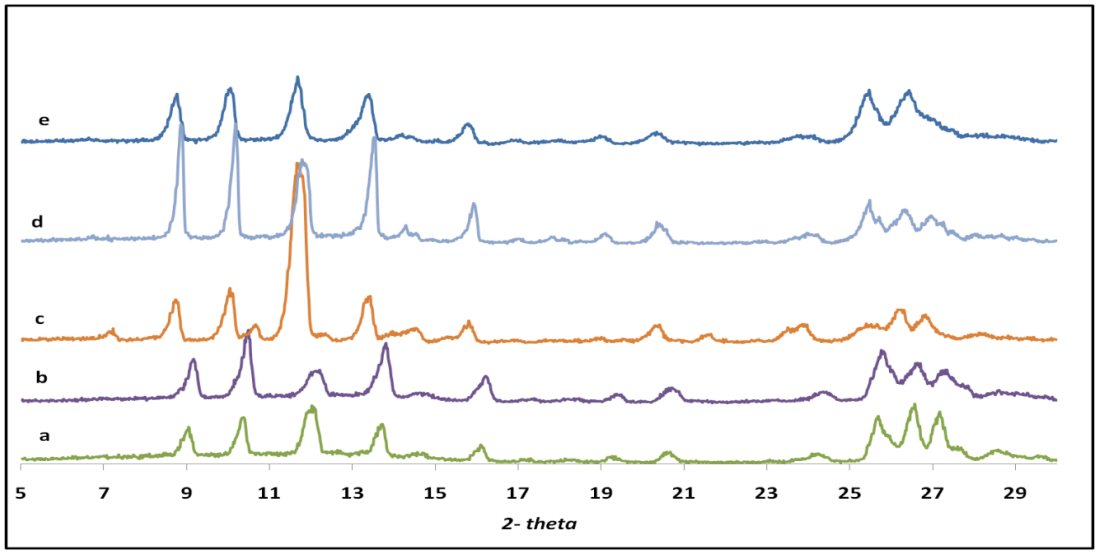

Figure 3.44. *PXRD pattern for CAF:MAL 2:1 solutions under rotavap: a) 1.7% water @ 123 mbar; b) 3.4% water @ 123 mbar; c) 2.4% methanol @ 200 mbar; d) 2.4% ethyl acetate @ 200 mbar; e) 2.4% acetone @ 330 mbar.*

3.3.1.2. CAF and other dicarboxylic acids

Unlike CAF and MAL, the aqueous solutions of CAF and other dicarboxylic acid produced pure co-crystals without any impurity as they only exist in one stoichiometric ratio. Rapid evaporation of CAF and GLU 1:1 solution favoured co-crystal with polymorphic Form II (Figure 3.45). The results assured that spray drying can be used as a green system to design CAF and dicarboxylic acid co-crystals.

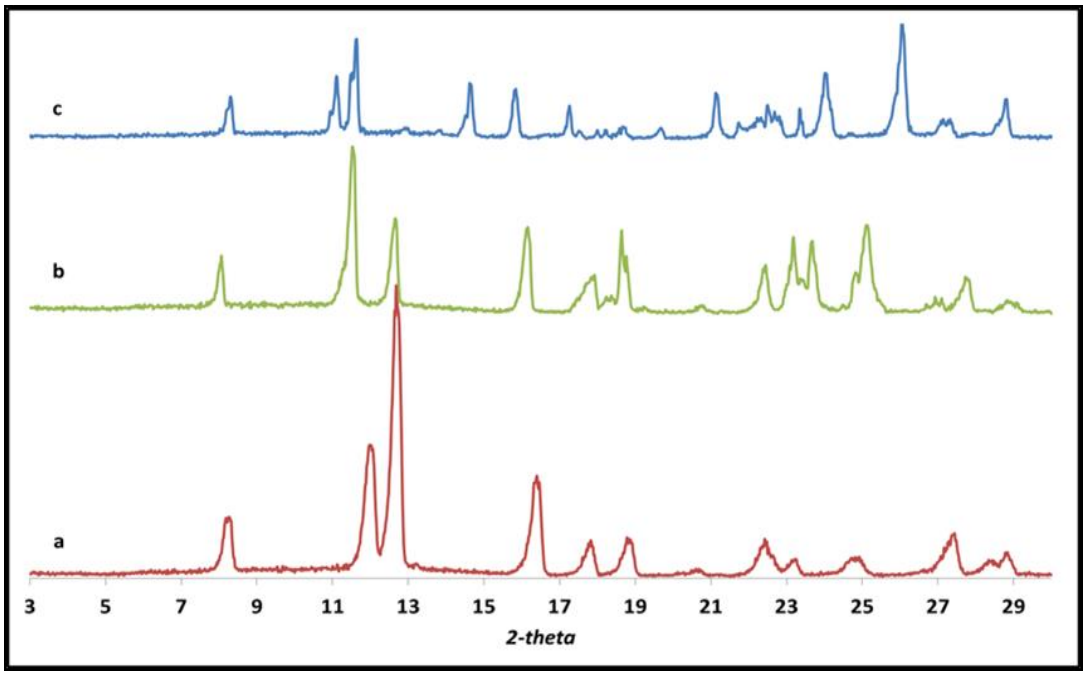

Figure 3.45. *PXRD patterns for co-crystal obtained via rotavap: a) CAF:OX 2:1; b) CAF:MO 2:1; c) CAF:GLU.*

3.3.2. Preparation of phase pure co-crystals via spray drying

This study explores the use of water as a green solvent for the synthesis of co-crystals and scale-up using spray drying. The incongruently soluble pair of CAF and di-carboxylic acids was spray dried as seen in Table 3.9. The stoichiometric ratios of CAF and acid (1:1 or 2:1) were dissolved in water and different strengths of solutions formed were spray dried. The spray drying system was optimised by altering parameters such as inlet temperature, feed concentration, feed temperature,

feed pump rate, atomisation, and aspirator rate.

3.3.2.1. Spray dryer optimisation

The first few test experiments were run with a range of inlet temperature between 110^{o}C to 250^{o}C. For temperatures above 200^{o}C, the product was found sticking to the walls of the chamber. These wall depositions were may be due to van der Waals and electrostatic forces, less crystalline product and other physical properties of the product such as solubility and flowability. Studies on crystallisation upon storage have shown material temperature above their glass transition temperature undergo such changes. Therefore, the degree of crystallinity depends on the operating conditions within the dryer and the feed properties, thereby, altering the drying environment inside the chamber (Chiou and Langrish, 2008).

In addition, improving the capacity of the spray dryer can help overcome the issue of sticky material. That is, by increasing the difference between the inlet and outlet temperature in order to achieve maximum evaporation. The outlet temperature should be maintained in such a way that it is neither too low (not drying the product) nor too high; leaving excess capacity unutilised (Kent and McLeod, 2007). The evaporation process of the water from product uses the heat from the drying air and approaches the wet bulb temperature. As the particle further dries, the temperature increases and remains at or below the outlet air temperature. This rapid evaporation process and high heat transfer coefficients can effectively help drying at moderate temperatures. Furthermore, to avoid stickiness the droplet has to be dry while suspended in the chamber before hitting the walls. Therefore, reducing the feed rate and inlet temperature can maintain outlet temperature required to obtain dry product (Arpagaus and Schwartzbach, 2008).

The optimum temperature for the caffeine and di-carboxylic acid aqueous solution without any sticky material was 110^{o}C-150^{o}C. Therefore, all experiments were run at 150^{o}C to achieve maximum solvent evaporation and dry product. Moreover, hygroscopic material may readsorb the vapours if exposed to cold surfaces in the dryer, for example, non-insulated areas, collecting vessels and, during analysis (Arpagaus and Schwartzbach, 2008). The key process parameters: inlet, outlet temperature and feed rate were maintained, and the others having least process impact were attuned accordingly.

3.3.2.2. CAF and MAL

a) Aqueous system

CAF solution in water was spray dried at high inlet temperature and surprisingly, no hydrate form was generated which could account for fast evaporation and well insulated system. Initial experiments were performed with high concentration CAF and MAL feed solutions (6.7%) heated at 45^{o}C. In theory, heating the feed solution close to the inlet temperature is ideal to increase the heat capacity as less energy is required from heater to evaporate water (Kent and McLeod, 2007). The spray drying results of CAF and MAL 1:1 and 2:1 under incongruent condition were similar with minute impurities (Table 3.9). The co-crystals generated in both the cases were 2:1 alongside unreacted MAL for 1:1 (Figure 3.46) and CAF for 2:1 feed solution in accordance to rotavap results (Figure 3.47).

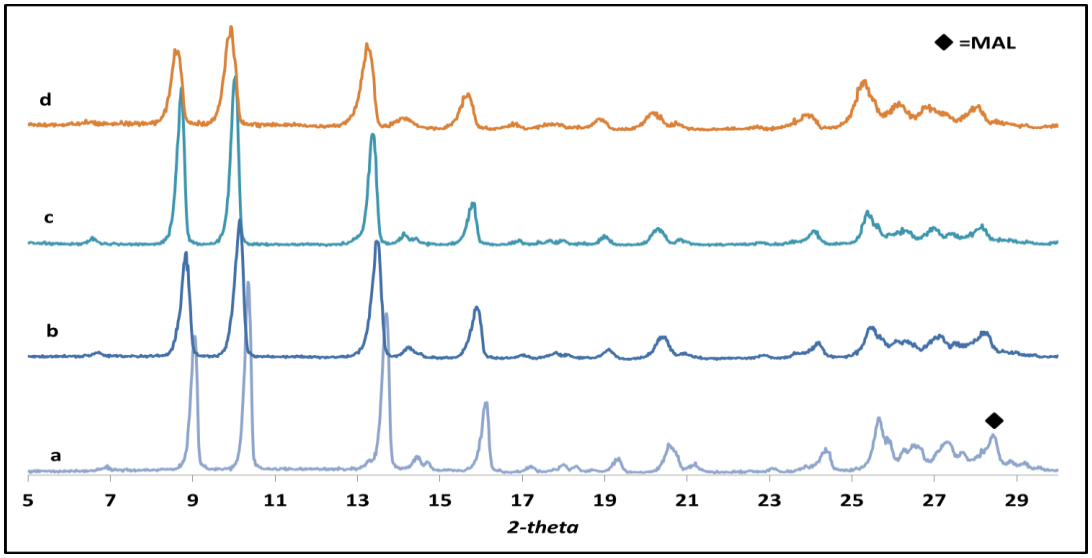

Figure 3.46. *PXRD pattern for spray dried CAF: MAL 1:1:a) 3.4% at 110^{0}C; b) 3.4% at 150^{o}C; c) 6.7% heated at 110^{o}C; d) 6.7% heated at 150^{o}C.*

Table 3.9. *Production of caffeine and di-carboxylic acid co-crystals by spray drying after optimisation of the experimental parameters.*

0.04 M acid solution	Solubility of CAF at 294 K (mg/mL)	Stoichiometric ratios	Batch No.	XRD result
Maleic acid	63.0	1:1	1a	*2:1 + M††*
			1b	*2:1 + M††*
			1c	*2:1 + M††*
			1d	*2:1 + M††*
		2:1	1e	*2:1 + C††*
			1f	*2:1 + C††*
			1g	*2:1 + C††*
			1h	*2:1 + C††*
			1i	*2:1 + C††*
			1j	*2:1 + C††*
			1k	*2:1 + C††*
			1l	*2:1 + C††*
			1m	*2:1***
			1n	*2:1 + C†*
			1o	*2:1 + C††*
			1p	*2:1 + C†*
			1q	*2:1 + C†*
Glutaric acid	53.8	1:1	2a	*1:1 FI*
			2b	*1:1 FI*
			2c	*1:1 FI*
Malonic acid	44.8	2:1	3a	*2:1*
			3b	*2:1*
Oxalic acid	32.8	2:1	4c	*2:1*

*****---Almost Phase Pure;††--- minor; †---traces; C---CAF; M---MAL; FI---Form I***

The existence of the two starting components as impurity was also seen in case of solvent-driven stoichiometrically diverse co-crystal phases (1:1 and 2:1) by grinding. Moreover, the pure forms could not be matured via solution (Trask *et al.*, 2005). Another report constructed ternary phase diagram of the three components: CAF, MAL and solvent to understand what regulates the existence of the two co-crystal forms. MAL was observed to enhance CAF solubility by 4.28% in acetone via complexation as CAF has weak solvation property. Only pure CAF:MAL 1:1 co-crystal was generated from acetone solution, whereas, 2:1 was obtained by grinding with acetone. The phase diagram depicted narrow zones for 1:1 and 2:1 co-crystals. However, addition of acetone to 2:1 led to its conversion into a mixture of 1:1 and CAF; submerging the zones. Therefore, this form was considered metastable and not suitable for production from solution at 25^{o}C (Guo *et al.*, 2010).

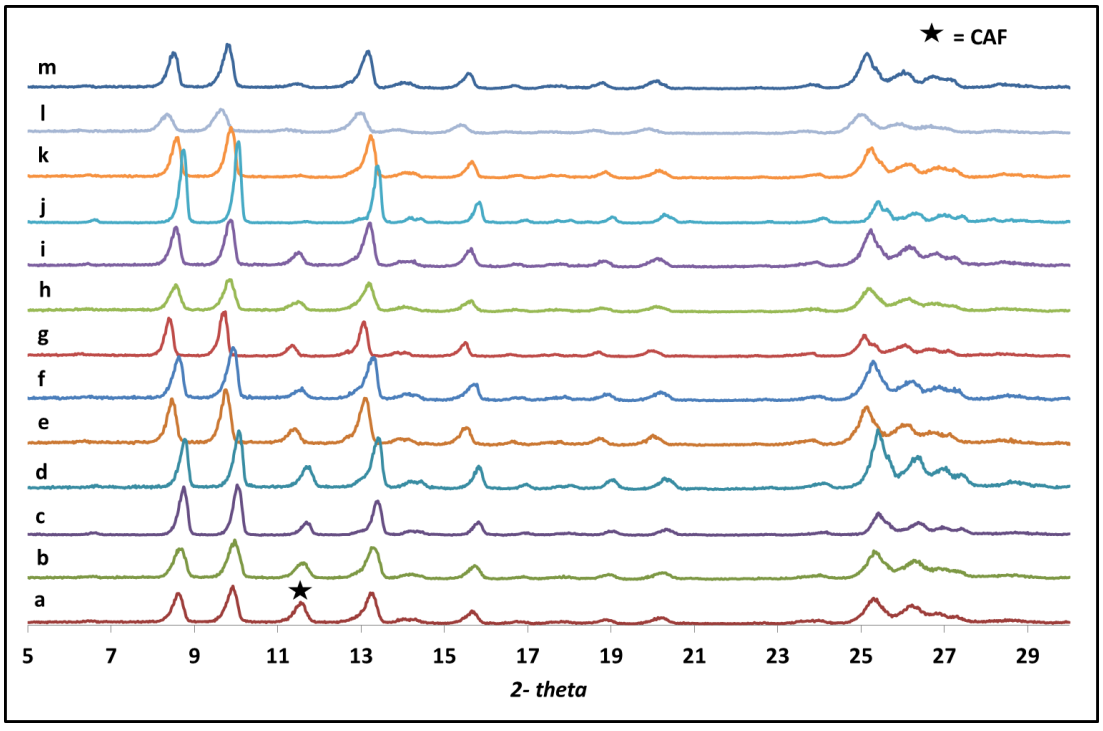

Figure 3.47. *Powder x-ray diffraction pattern (PXRD) for spray dried CAF-MAL 2:1 with CAF impurity - a) 6.7% (heated feed at 45^{o}C), 110^{o}C inlet; b) 6.7% (heated feed), 150^{o}C inlet; c) 3.4% feed, 1mL/min; d) 3.4%, 3mL/min; e)2.5%, 3mL/min; f) 1.7%, 110^{o}C inlet; g)1.7%, 170^{o}C; h) 1.7%, 40m^{3}/hr; i) 1.7% (heated feed) k) 1.7%, 3mL/min; l) 1%, 1mL/min; m) 1% , 3mL/min. Almost phase pure 2:1 CAF:MAL - j) 1.7%, 1mL/min.*

Ultrasound assisted study generated pure 2:1 co-crystals in high molar concentration of MAL i.e. when CAF: MAL ratio taken was 1:3.5 in methanol. It was suggested that cavitation induced by ultrasound caused simultaneous supersaturation of the two components, but higher proportion of MAL was required (Aher *et al*., 2010). Leyssen *et al*., (2012) reproduced CAF:MAL 2:1 from solution and thought that the effect of choice of solvent on phase diagram was neglected previously. It was established that ethyl acetate reduced the relative solubility of MAL versus CAF from 40 to 7 compared to acetone producing two different stoichiometries (1:1 and 2:1) and also obtained a new polymorph of 1:1 i.e., Form II while screening from solution. Therefore, 2:1 metastable form prevailed at kinetically-driven high supersaturation levels breaking the intramolecular bond of MAL during nucleation which favoured strong intermolecular heterosynthons. The unreacted MAL obtained along with 2:1 co-crystal after spray drying 1:1 stoichiometry is self-explanatory. But, the transformation into 2:1 co-crystal in contrast to one's anticipation of 1:1 could be due to kinetically favoured high supersaturation conditions; altering the binding tendency of the two molecules, besides their solubility characteristics (Alhalaweh *et al*., 2013).

Another unanticipated outcome from spray drying 2:1 CAF and MAL solution yielding 2:1 co-crystals and unreacted CAF was not easy to rationalise. Similar results were observed in study utilising microwave irradiation where supersaturation rate was accelerated by stimulating dipole rotation of the molecules and reducing the crystallisation time in slurry. Low solvent concentration, solubility and limited time were thought to restrict the adequate equilibrium condition and kinetics (Pagire *et al*., 2013). Furthermore, two solubility phase diagram for CAF and MAL was created in aqueous slurry and sonicated slurry solutions after establishing increased

solubility of CAF in aqueous solution of MAL. In aqueous slurry, 2:1 co-crystal was successfully produced at higher ratios of CAF: MAL i.e, 75:25. Phase pure zones for 2:1 and 1:1 were depicted in the phase diagram. Ultrasound further augmented the solubility of CAF and MAL, but no difference was observed in the layout of this new phase diagram. On the contrary, no pure 2:1 co-crystals were formulated and 1:1 co-crystal zone shrunk as opposed to one's expectation. This was explained as a result of instability of co-crystal phase in slurry leading to dissociation due to differences in solubility (Apshingekar, 2014).

Even though, MAL further dissolves CAF in water; the highest 2:1 solution concentration attained at room temperature was 3.4%. CAF's concentration in this solution was above its intrinsic solubility, held by weak molecular complexation with MAL. The operating conditions were altered and a low concentration feed solution at room temperature was spray dried in an attempt to avoid impurity. A decrease in the caffeine peak was observed with the decrease in the strength of the solution and subsequent lowering of the feed rate. Due to the operating system limitations and the drying environment requisite for CAF: MAL co-crystal, only one condition successfully generated almost phase pure 2:1 CAF: MAL co-crystals (Figure 3.47, j). At 1.7% concentration, CAF exists freely at its intrinsic solubility, reducing the complexation with MAL in the solution. Secondly, reduced feed rate diminishes the droplet size and the energy required to evaporate the solvent causing immediate evaporation. Thus, signifying that inlet temperature, feed concentration and feed rate were essential to kinetically control spray drying of incongruently saturating systems and yield almost phase pure forms. Moreover, the operating system of spray dryer gives us an opportunity to make fine adjustments and control the kinetic environment which is not valid for rotavap.

Recently, a solvent-free continuous melt extrusion technique successfully reproduced CAF: MAL 1:1 and 2:1 co-crystals on a large-scale by controlling their stoichiometry. This technique surmounts the issue faced by solution based processes such as, solvation, nucleation and solubility. It was observed that 1:1 could be converted into 2:1 by addition of CAF, but the opposite was not feasible by addition of MAL. Nonetheless, the reverse could only be achieved by melt seeding 2:1 with phase pure 1:1 (Kulkarni *et al*., 2015). The reason behind such a disparity in different methods is ambiguous and is believed to occur due to an unknown exchange between kinetics and thermodynamics of the co-crystallisation process. Interestingly, the drying kinetic conditions inside the spray dryer appear to offer a unique environment for the generation of CAF:MAL 2:1 from aqueous solution regardless of the starting components' stoichiometry.

b) Organic solvent

Co-crystallisation experiments were also conducted in organic solvents in an attempt to form 1:1 co-crystals and to investigate reproducibility of rotavap results. Due to very low solubility of CAF in organic solvents only equivalent molar (1:1) solutions were used. These solutions were heated externally before being fed into the system to obtain minimal considerable strength (2-4%) that can retrieve product via spray drying. The PXRD results shown in

Figure 3.48, demonstrate that metastable form 2:1 was favoured which complies with rotavap results. Due to the very low solution concentrations and solubility constraints in organic solvents, no further experiments were performed.

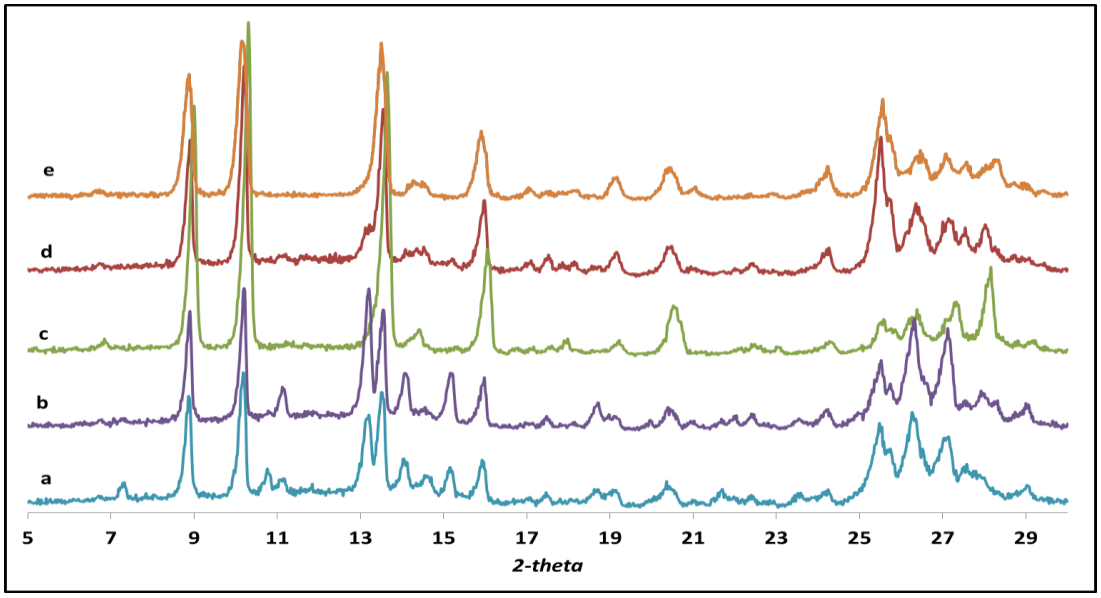

Figure 3.48. *PXRD patterns for CAF and MAL1:1 solution in: a) methanol @ 70°C; b) methanol @ 90°C; c) acetone @ 70°C; d) ethyl acetate @ 80°C ; e) ethyl acetate @ 90°C.*

The co-crystals obtained from acetone and ethyl acetate produced 2:1 co-crystal with impurity of unutilised MAL. Whereas, minor impurity of CAF: MAL 1:1 was noticed in methanolic solutions. A trace of 1:1 form II was observed with characteristic peak at 7.36 at lower temperature condition (70°C). Solvent-grinding in methanol generated 1:1 co-crystal with impurity (Task *et al*., 2005). Leyssens *et al*., (2012) first found 1:1 form II which was stable in ethyl acetate solution for a week before it transformed into form I. Therefore, form I was considered the most stable form. In addition, microwave irradiation generated mixture of both form I and II in methanol, where form II appeared in the mixture at lower methanol concentration of 2-4% (Pagire *et al*., 2013). In contrast, ultrasound assisted co-crystallisation in methanol favoured 2:1 co-crystal under excess MAL conditions (Aher *et al*., 2010). These results indicate that methanol assists selective growth of 1:1 co-crystal; however, high supersaturation conditions can supersede the favoured phase and produce 2:1 as observed in ultrasound and spray drying. It is important to note that other factors such as solvent concentration and temperature in microwave

and spray drying, respectively, can affect crystallisation and produce traces of 1:1 form II.

c) Sodium Lauryl Sulphate (SLS)

In an enthusiastic approach towards procuring phase pure 2:1 co-crystal, an anionic surfactant, SLS was introduced in the aqueous system. FDA approves the use of surfactant to solubilise drug products that are sparingly soluble in water as long as the amount is rationalised (FDA, 1997). In accordance to the regulations, SLS can be safely used as a surfactant in food products such as juices, dry beverages not exceeding 25 parts per million (equivalent to 25 mg/L) (FDA, 2015). Pharmaceutical products contain amounts ranging from 0.004 to 0.6 mg in oral dosage form; 0.01-0.02% in oral liquid dosage forms and 0.1 to 12.7% in lotions, ointments and creams (Smolinske, 1992, p.359). Some of the dissolution methods found on FDA approved database have used SLS ranging from 0.25- 2% in water (FDA, n.d.).

Solubility and DEC:

Prior to spray drying, CAF solubility was determined in aqueous solutions of 1 and 2% SLS as shown in table below.

Table 3.10. *Solubility of CAF in SLS solutions in comparison to water alone.*

Solvent	**Water**	**1% SLS**	**2% SLS**
CAF Solubility (mg/mL)	20.7 ±0.11	20.7 ±0.13	21.2± 0.05

Unfortunately, no significant increase in solubility of CAF was noticed, even though, SLS acts as a powerful solubilising agent. The change in DEC observed for 1% SLS solution was 79.5±0.1 compared to water 80.2±0.02. This insignificant decrease

indicates that the two solutions acquire quite similar polarities. CAF and MAL 2:1 molar concentration (3.4%) was prepared in 1% SLS solution and spray dried in an anticipation that the results can vary by introducing a surfactant. The PXRD pattern (Figure 3.49) shows almost phase pure 2:1 co-crystals with CAF impurity (235^0C). However, DSC thermogram (Figure 3.50) indicates a melt endotherm for 2:1 co-crystal (119^0C) and at 273^0C for SLS, with absence of CAF impurity. This could be due to low amorphous content of CAF as seen in PXRD (non-sharp, low intensity peak), which under thermal exposure gains mobility to form co-crystal. Therefore, addition of surfactant produced almost phase pure results at a higher concentration (3.4%) and higher feed rates (2mL/min); though, the solubility of CAF was almost similar. Thus, indicating that surfactant plays a major role in solubilising and associating poorly water soluble molecules.

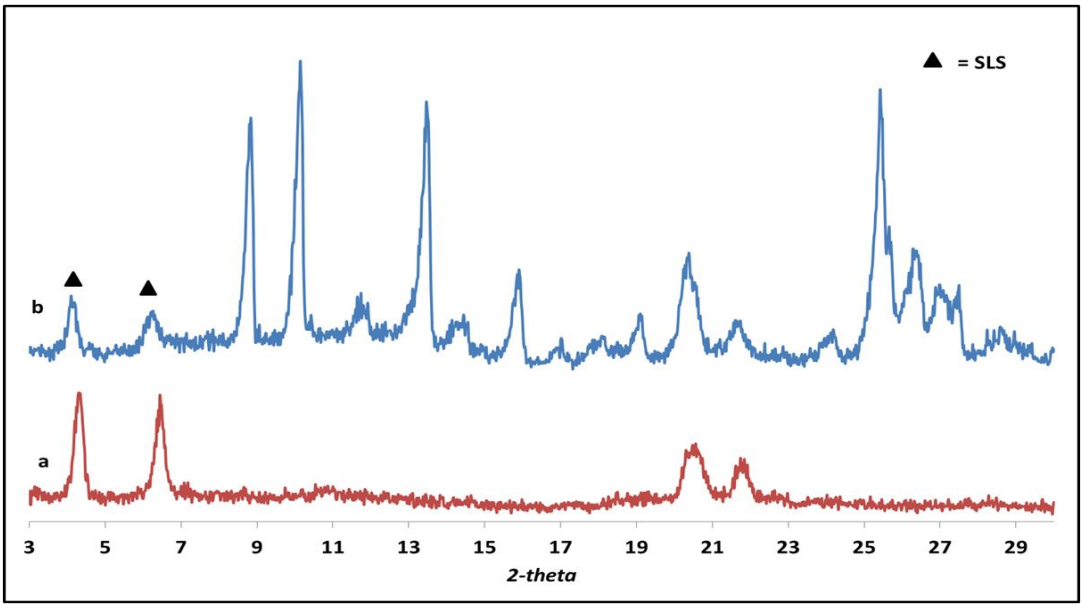

Figure 3.49. *PXRD pattern for: a) SLS with characteristic peaks at 4.28, 6.44; b) almost phase pure CAF:MAL 2:1 from 1% SLS solution.*

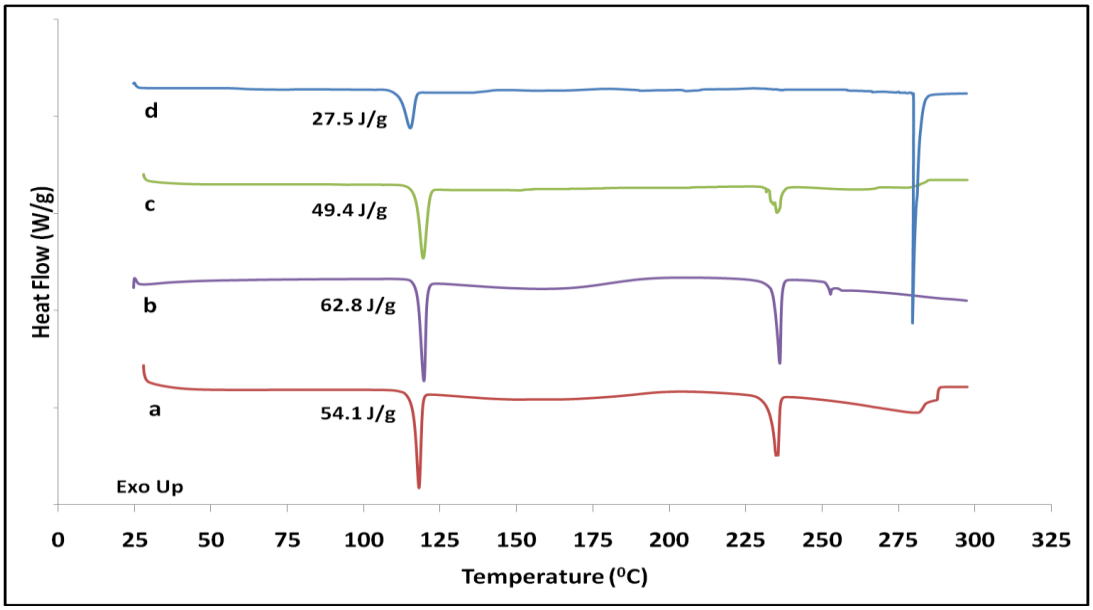

Figure 3.50. *DSC thermogram representing heat flow as a function of temperature for CAF and MAL 2:1 solutions spray dried at: a) 1%, 3mL/min; b) 1.7%, 3mL/min; c) 1.7%, 1mL/min; d) 3.4% in 1% SLS, 2mL/min.*

Surfactants usually undergo micelle formation in solution at a critical micelle concentration (CMC). Below CMC, surfactant forms a thin monolayer at the surface of water, which above CMC associates into colloidal clusters; reducing surface tension. SLS is an anionic surfactant which dissociates at the surface into active anion, $CH_3(CH_2)_{11}OSO_3^-$ and cation, Na^+. The hydrophilic OSO_3^- are oriented facing inside towards the water at the surface, and the lipophilic hydrocarbon alkyl group, $CH_3(CH_2)_{11}$ is directed outside. At CMC, the molecules self-aggregate and form a micelle with lipophilic core and anionic groups on the surface towards hydrophilic water. The micelles undergo constant dissociation and reformation due to kinetic factors such as surfactant concentration. The concentration used in this study was above SLS's CMC value of 0.03% (Rahman *et al.*, 2009). In water, molecules associate via H-bonding or dipole-dipole forces. A molecule in any liquid will experience equal attractive and repulsive forces in all directions, whereas, at surface these are not exhibited at one direction. The asymmetrical forces give rise to surface

tension and therefore, polar solvents possess higher surface tension (Mandavi, Sar and Rathore, 2008).

Surfactant helps to lower the surface tension and hence, solubilise the non-polar molecule trapped inside micelle. However, it has been suggested that presence of other molecules may alter the CMC value. In this case, hydrotropes such as MAL contains charged polar molecules that may interfere with the hydrophilic head group of the micelle. Due to their like charges, i.e. anions, repulsion might take place between ions; changing micelles shape, thereby, affecting the surface packing (Mandavi, Sar and Rathore, 2008). Other factors such as process parameters may also affect the arrangement of micelles holding CAF.

3.3.2.3. Caffeine and other di-carboxylic acids

The above optimised process parameters were successfully used to obtain phase pure co-crystals of caffeine with malonic acid, oxalic acid and glutaric acid (Figure 3.51). In case of glutaric acid, FI of 1:1 co-crystal was kinetically favoured as observed in an earlier study (Alhalaweh and Velaga, 2010). However, these results conflict with those of rotavap where FII of CAF:GLU co-crystals were generated. Trask *et al*., (2005) generated CAF:GLU FI in non-polar solvent, cyclohexane and FII in fairly polar, chloroform via solvent grinding. Whereas, solution growth led to simultaneous precipitation of the two conformational polymorphs. Further analysis of RH stability studies reflected conversion of CAF:GLU FI into FII at high RH conditions before dissociating into components. The incompatibility observed in the CAF: GLU results for the two evaporating methods could be due to the fact that the nucleating components in rotavap are still in contact with the solvent until it all gets vapourised (Figure 3.52). The increased residence time within the flask may lead to inter-

conversion due to association and dissociation of the unstable components whilst drying.

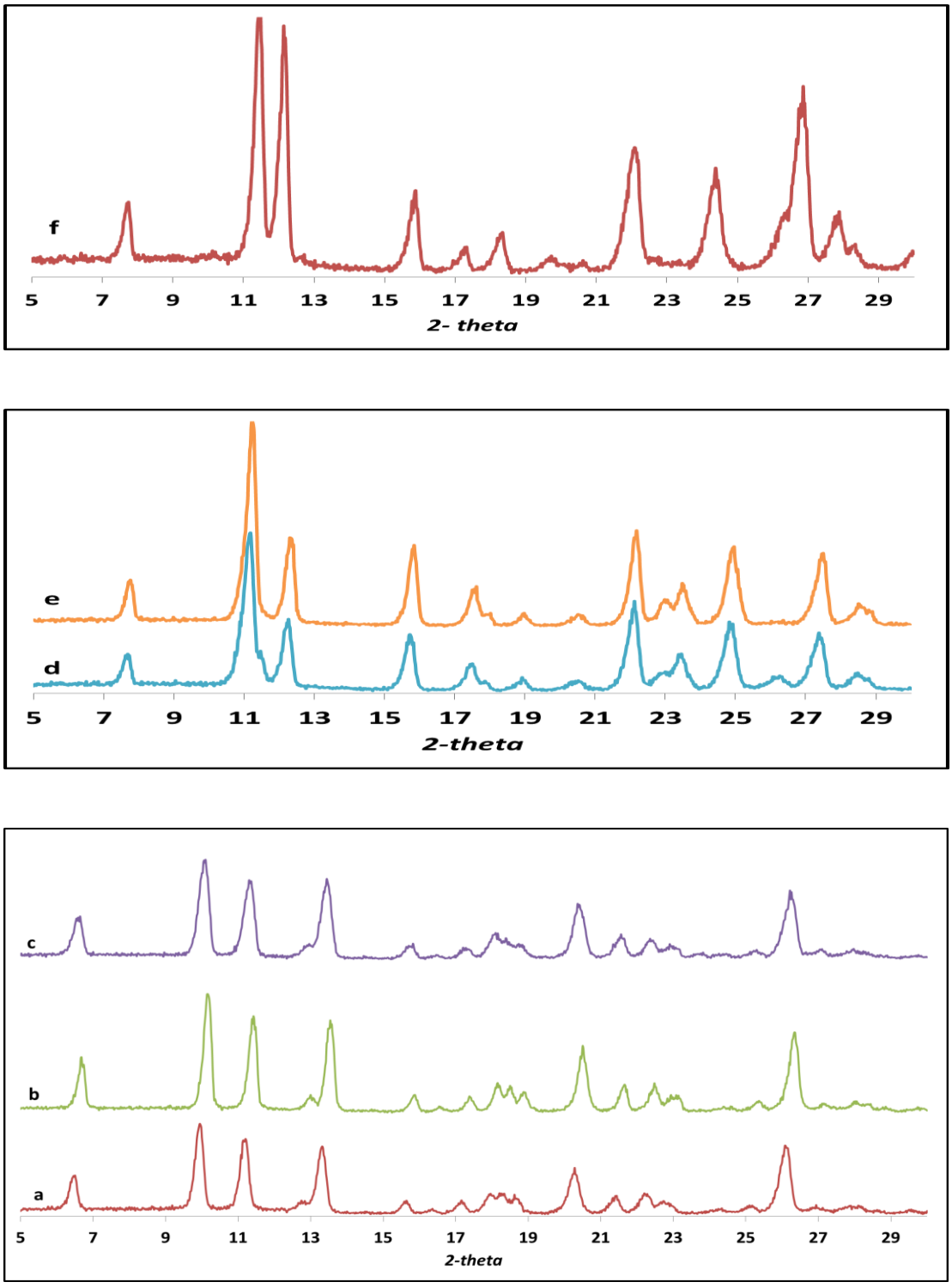

Figure 3.51. *PXRD patterns for caffeine (CAF); glutaric acid (GLU); malonic acid (MO); oxalic acid (OX); a) CAF-GLU 1:1 Form I - 5% feed solution, b) 3.4 % solution, c) 1.7 % solution; d) CAF-MO 2:1 - 3.4 % feed solution, e) 1.7% solution; f) CAF – OX 2:1 - 1.7% feed solution.*

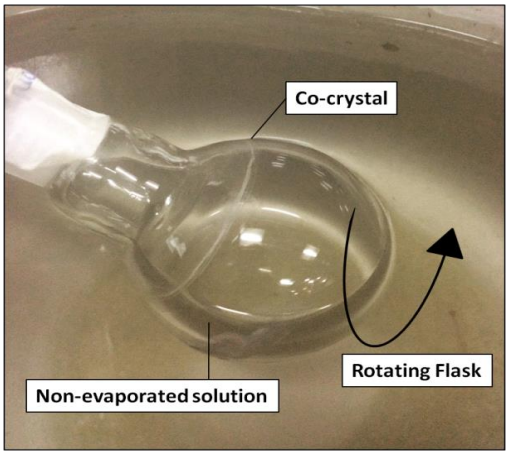

Figure 3.52. *Co-crystal nucleation under rotavap while in contact with the evaporating solution.*

Unlike CAF- MAL, other di-carboxylic acids possess one stoichiometry of co-crystal; 1:1 or 2:1. Furthermore, the solubility of CAF with respect to each dicarboxylic acid decreases in the order of MAL>GLU>MO>OX; which corresponds to the highest feed concentration that can be spray dried (Figure 3.53). It is clearly observed that GLU forms the highest concentration solution with CAF at room temperature due to its 1:1 stoichiometric ratio, where only one caffeine molecule interacts with an acid molecule.

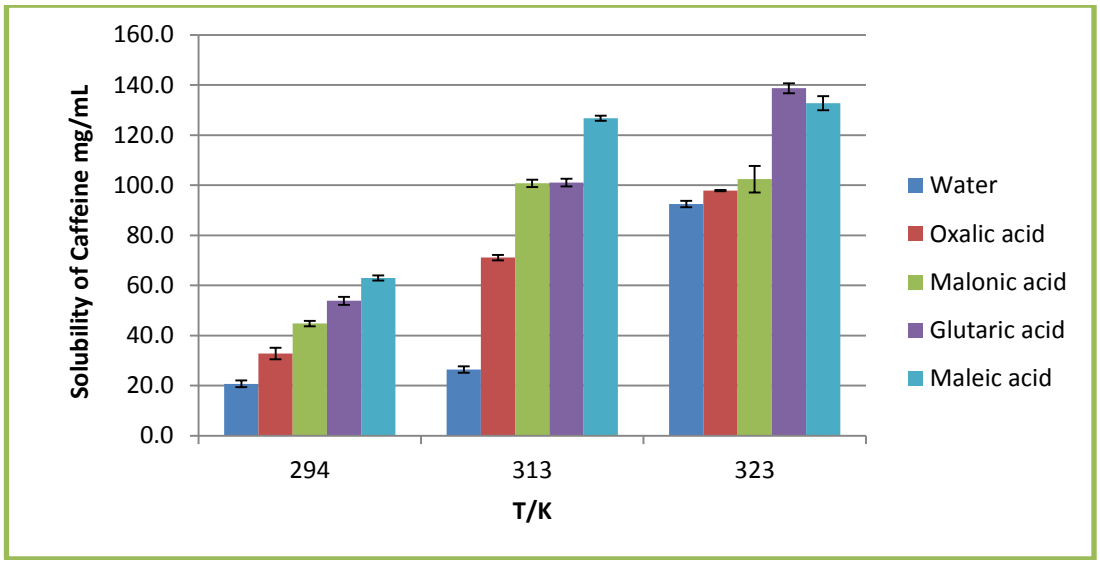

Figure 3.53. *Graphical representation of solubility of caffeine (mg/mL) in di-carboxylic acid solutions and water at temperatures ranging from 294 K (room temperature) to 323 K (50^{o}C).*

The complexity in CAF: MAL co-crystal production compared to other di-carboxylic acids can be due to the following reasons: 1) relative solubility of caffeine in di-carboxylic acid solutions; 2) stoichiometric diversity; 3) chemical structure and complexation/solvation in the solvent. So far, CAF-MAL 2:1 has been formed by solvent drop grinding, slurry co-crystallisation, ultrasound, and hot-melt extrusion. The scale-up of the incongruently soluble co-crystals from solution is a vital issue. It is difficult to suggest the mechanism of instantaneous drying of the liquid, production of a solid form in one step and relate it to their stability zones in the phase diagram. The results restate that spray drying can be used as a green method suitable for the synthesis and scale-up of co-crystals of incongruently soluble compounds. However, this method involves careful control of process conditions to influence the co-crystallisation tendency, especially in case of CAF-MAL pair. Interestingly, surfactant produced almost phase pure CAF: MAL 2:1 without modifying the process conditions which indicates the importance of solubilisation in controlling successful nucleation of the stoichiometrically diverse incongruent pair.

3.4. Product quality

3.4.1. Water content/ Karl Fisher

The quality of the product was determined by investigating the effect of process variables and material property in controlling the residual moisture content. The FDA centre of biologics evaluation and research sets a guideline for the examination of moisture content in dried biological products. The biologics regulation in 21 CFR 610.13 states that freeze dried product with heterogeneous mixture have different ways in which water may be bound due to varying chemical and physical interaction

within the material and hence, should be evaluated and not exceed the set limits. Karl Fischer is an approved methodology which obtains both surface and bound water compared to gravimetric method. The standards set for residual moisture was low from less than 1% to 3%, protecting the stability and activity of the drug over long period of time. The exception to 1% limit is set for products where the stability, purity and potency of the product are established for the entire dating period (FDA, 1990). Moisture content calculated for the spray dried products is as follows:

Table 3.11. *Moisture determination in spray dried samples using Karl Fischer methodology*.

Solution	**Inlet Temperature (^{o}C)**	**Feed Concentration (%)**	**Feed Rate (mL/min)**	**Aspirator (m^3/h)**	**Moisture content (%)**
CAF:MAL 2:1	150	1.7	1	60	0
	150	1.7	2	60	0
	150	1.7	3	60	0.62 ± 0.01
	150	1.7	1	**70**	0.42±0.02
CAF:MAL 2:1 + SLS	150	**3.4**	**2**	60	1.45±0.09
CAF:GLU 1:1	150	**5**	**3**	60	0.33±0.06
CAF:MO 2:1	150	**3.4**	**3**	60	0.39±0.03
CAF:OX 2:1	150	**2**	**3**	60	0.37±0.02

Process parameters such as feed rate, inlet temperature, atomisation, and aspirator rate could affect the moisture content in the final product by varying the size of the droplet, resident time and heat exposure. CAF:MAL products subjected to various process parameters were analysed using Karl Fischer. The above table shows the absence of moisture for samples spray dried at very low feed rates (1-2 mL/min) and optimum aspirator condition. At a higher feed rate of 3mL/min, bigger droplets were exposed to heat; and at high aspiration rate (70 m^3/h), the residence time of particles in the drying chamber was minimised, thereby, raising their water content levels. The percentage water in these samples was less than 1% which is well within FDA

criteria. However, over 1% moisture content was obtained with SLS even at low feed rate (2mL/min), which is indicative of the surfactant's hygroscopic nature. Therefore, presence of surfactant can affect the stability of the product. Also, comparable results were obtained for CAF co-crystals with other di-carboxylic acids at 3 mL/min independent of the feed concentration utilised.

Particle size distribution observed for CAF:MAL spray dried products are shown in Table 3.12. The results do not comply with the expected increasing size one would predict with increasing feed rate. The median particle dimension (X_{50}) observed for feed rates of 1, 2 and 3 mL/min were 12.1, 6.2 and 7.4μm. The distribution curves observed were distorted and deviates from symmetry with the presence of some primary particles at a lower size range (Appendix II). However, SLS samples show a normal distribution with X_{50} of 4.1 μm. The microscopic images of samples depict some very small primary particles alongside big chunks of irregularly shaped particles (**Error! Reference source not found.** and ***Figure 3.55***).

Table 3.12. *Particle size distribution of spray dried CAF:MAL co-crystals.*

.

Conc. (%)	**Inlet Temp (°C)**	**Feed rate (mL/min)**	**Particle size distribution (μm) Method: Lens- R_1 (0.1-35μm) Dispersive pressure: 4bar 40mm/s**			**Particle volume over particle size**
			X_{10}	X_{50}	X_{90}	*VMD (Volume mean diameter in μm)*
1.7	150	1	1.3±0.09	12.1±0.11	27.8±0.05	13.52
1.7	150	2	0.9±0.03	6.2±0.04	19.4±0.17	8.29
1.7	150	3	1.0±0.00	7.4±0.18	26.0±0.11	10.67
3.4 1% SLS	150	2	0.8±0.00	4.1±0.06	9.4±0.29	4.76

a)

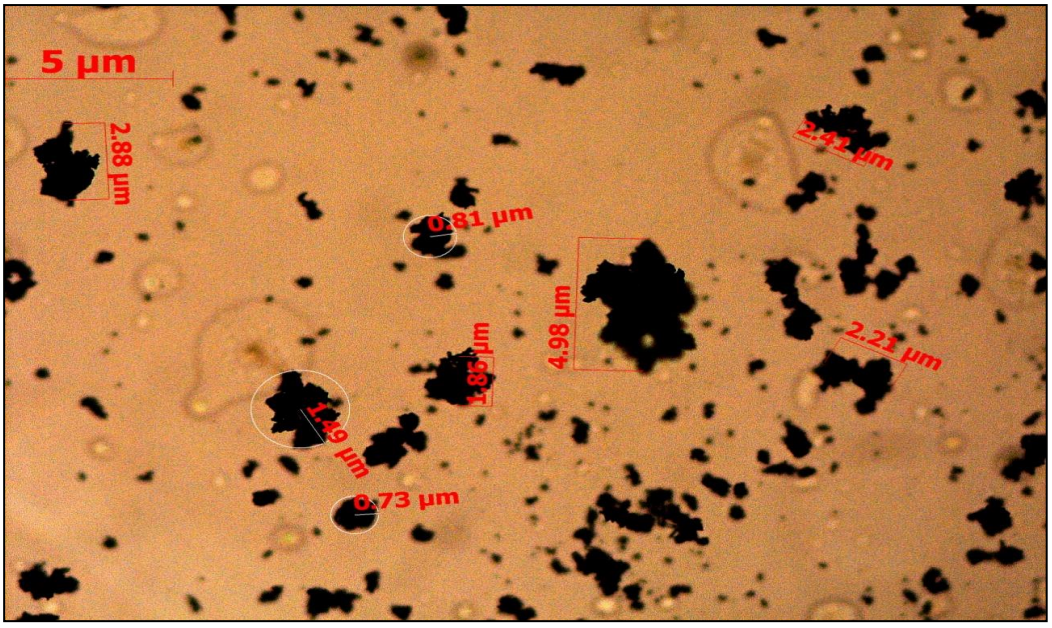

b)

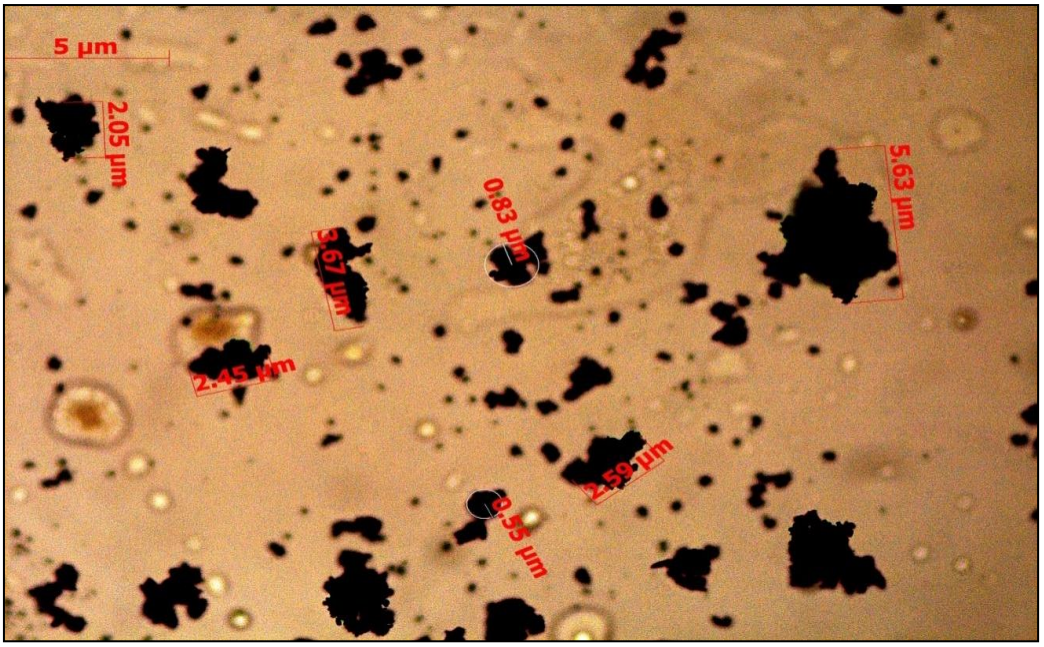

Figure 3.54 *Microscopic image of CAF:MAL samples at a) 1mL/min; b) 2mL/min.*

c)

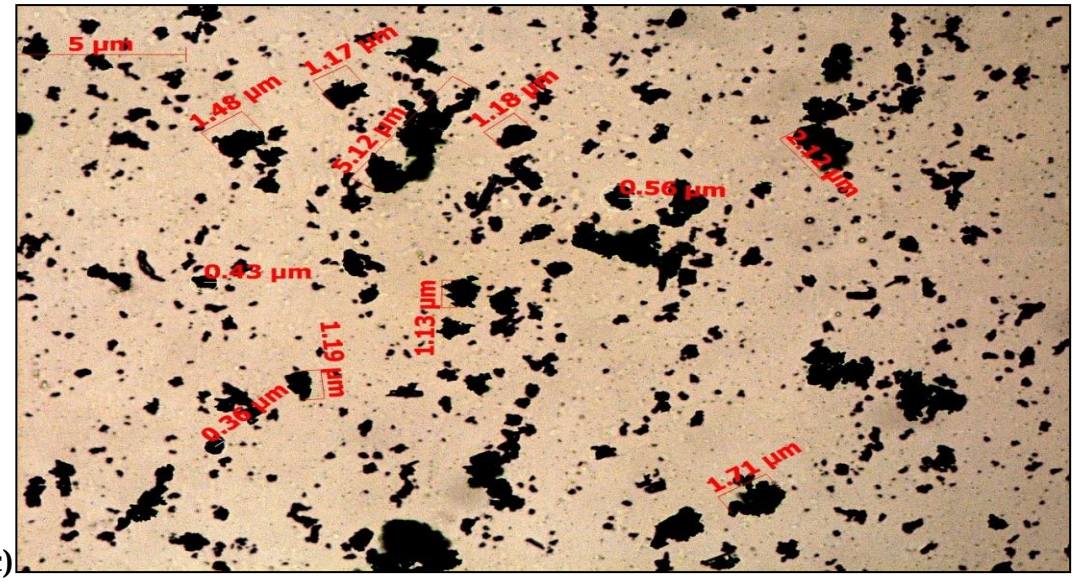

d)

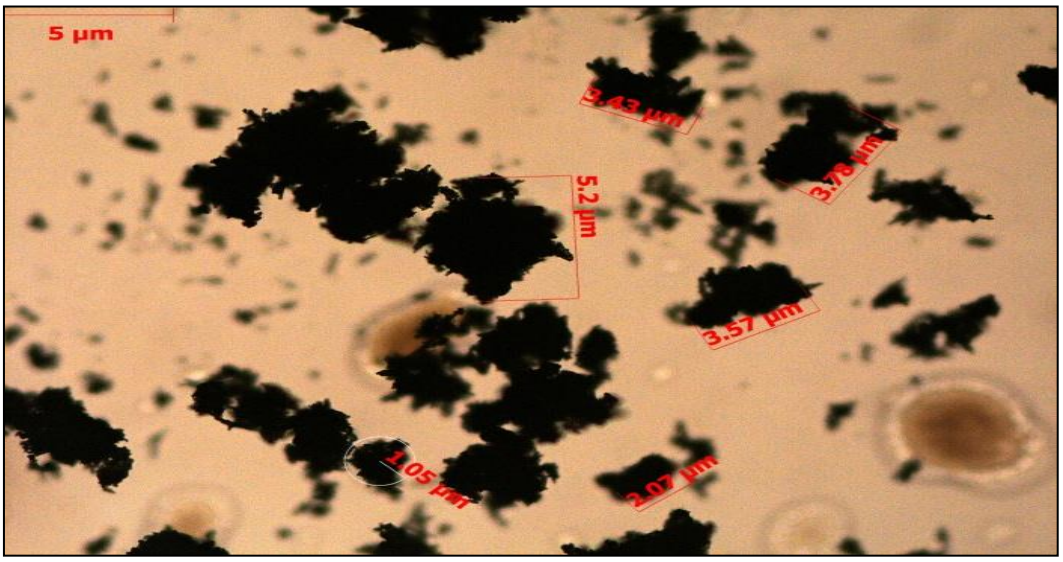

Figure 3.55. *Microscopic image of CAF:MAL samples at c) 3mL/min; d) SLS.*

To further understand the unusual distribution pattern, SEM images for 1 and 3 mL/min samples and SLS were examined (Figure 3.56 and Figure 3.57). The samples produced by low feed rate (1mL/min) show small primary particles clustered together with a strongly bound texture. Whereas, at higher feed rate (3mL/min), the sample emerges as vague needle shaped like CAF clumped together with few indentations.

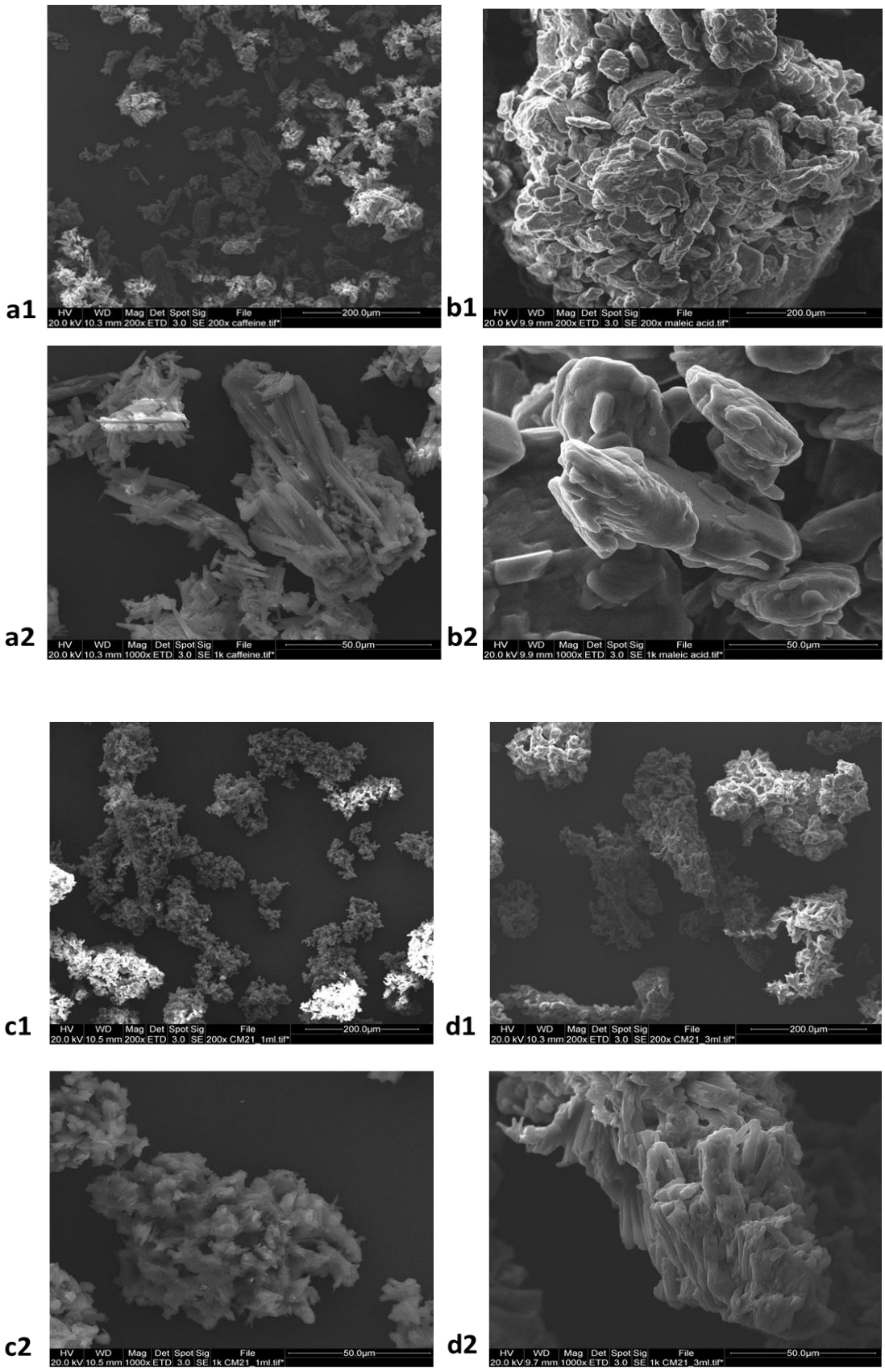

Figure 3.56. *SEM images of CAF: a1) 200x, a2)1000x; MAL: b1) 200x, b2) 1000x; CAF:MAL: 1mL/min c1) 200x, c2) 1000x; CAF:MAL 3mL/min: d1) 200x, d2) 1000x.*

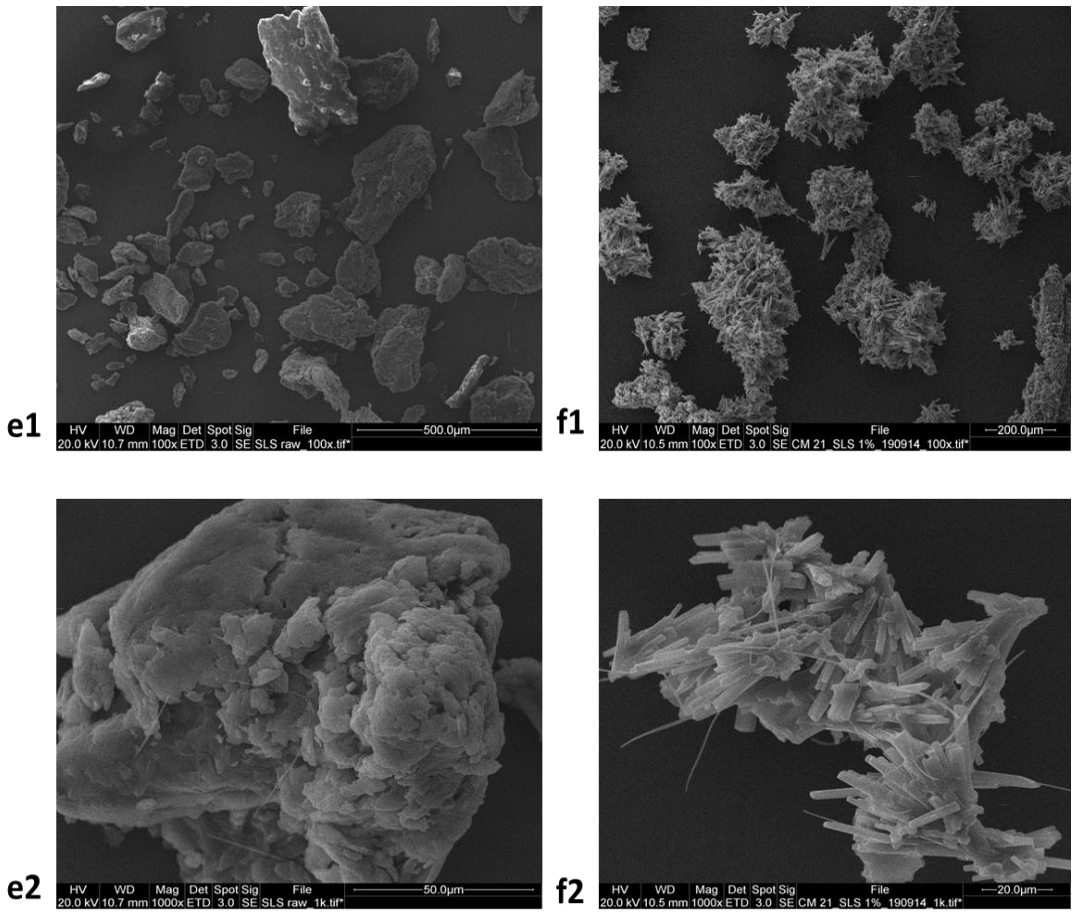

Figure 3.57. *SEM images of SLS: e1) 200x, e2) 1000x; CAF:MAL SLS: f1) 200x, f2) 1000x.*

It appears that the dispersive pressure of 4 bars used while determining particle size breaks the needle shaped structures more easily but not well enough to separate the smaller primary particles. In contrary, the particles developed with SLS are well-defined and much more separated individual needle-shaped structures bound together, which is likely to get broken down into primary particles by the dispersive pressure utilised. However, as the laser diffraction is sensitive to spherical shaped particles, it may not process these rod-like irregular particles properly. Therefore, the data observed wasn't a true reflection of the particle size or VMD for CAF: MAL co-crystals due to their crystal growth morphology.

Summary:

Solubility of CAF in water was significantly improved in the presence of di-carboxylic acids acting as a hydrotrope. However, its solubility in organic solvents was relatively poor than in water. DEC values were obtained to find a correlation between the chemical polarity of the solution and solubility. The values were similar for 0.04 M solutions of dicarboxylic acids utilised, depicting similar polarity. Upon CAF's addition to these solutions, polarity decreased with an increase in CAF's concentration, due to high molecular association with the solvent, reducing its dipole moment. Experiments conducted using rotavap produced 2:1 CAF:MAL co-crystals with minor impurity in all solvents apart from methanol, where 1:1 traces were also observed. Interestingly, CAF:MAL 2:1 was generated from both 1:1 and 2:1 starting ratios of CAF and MAL solution. Pure co-crystals were obtained with OX and MO in water. Whereas, in case of CAF:GLU which exists in two polymorphic forms; Form II was favoured. Spray drying resulted in similar products yielding CAF:MAL 2:1 with either CAF or MAL impurity depending on the starting component's ratio. The process parameters were varied with the intention of reducing CAF impurity while preparing CAF:MAL 2:1 co-crystals from 2:1 solution mixtures. High inlet temperature, low feed rate and low solution concentration were important parameters reducing CAF's impurity. Due to the restriction in parameter range, a surfactant (SLS) was introduced into the solution. Unfortunately, the impurity couldn't be eradicated completely, but almost phase pure co-crystals were formed at higher feed concentrations. However, the hygroscopic nature of SLS resulted in high water content in the samples. Pure CAF co-crystals were obtained with OX, MO and GLU. Metastable CAF:GLU FI was favoured as opposed to rotavap, due to a better evaporating environment being offered.

CHAPTER 4

THEOPHYLLINE AND DI-CARBOXYLIC ACIDS COCRYSTAL RESULTS

This chapter utilises another methylxanthine like CAF, theophylline known as a bronchodilator for treating respiratory disorders such as asthma. It explores similar solubility behaviour in aqueous dicarboxylic acid solutions as observed for CAF. Due to low solubility compared to CAF; solubility in binary solvents was scrutinised. Co-crystals obtained from rotavap in the selected binary solvent were correlated to spray dried results.

4.1. Crystal data

4.1.1. Theophylline

Despite being a chemical analogue to CAF, THEO acquires a good hydrogen bonding complexity due to the absence of one methyl group (Figure 4.1). The presence of hydrogen donor and acceptor makes it both weakly acidic (pK_a 8.6) and basic (pK_a11.5) in nature (Trask, Motherwell and Jones, 2006).THEO can exist as four anhydrous polymorphs and converts into a hydrate form under raised RH conditions. These polymorphs differ in their structural arrangement where FI is stable at higher temperatures and FII is most stable form at room temperature. FIII is regarded as highly metastable form which readily converts into FII. FIV has been recently identified by solvent mediated conversion of FI and FII and is considered as the most thermodynamically stable form with plate-like morphology. FI attains an orthorhombic structure belonging to $Pna2_1$ space group and cannot be produced by

solution method but via solid-state conversion at high temperatures 538-41 K. F IV is monoclinic with two asymmetric molecules and space group of $P2_1/c$ (Khamar *et al*., 2011). The stable FII links THEO molecules into a chain via strong donor (N-H) bonding to basic nitrogen (N) belonging to $Pna2_1$ space group with unit cell dimension: a=24.61 (2) Å, b= 3.83 (4) Å, c= 8.50 (5) Å. The figures below show the crystal structure and PXRD pattern adopted from CSD.

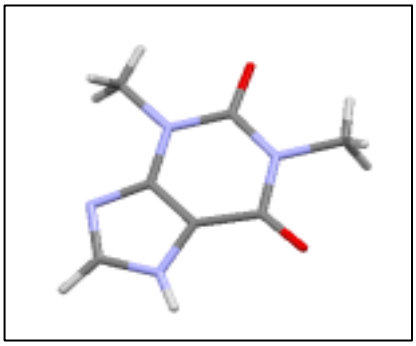

Figure 4.1 *Crystal structure of THEO FII (CSD Ref: BAPLOT01).*

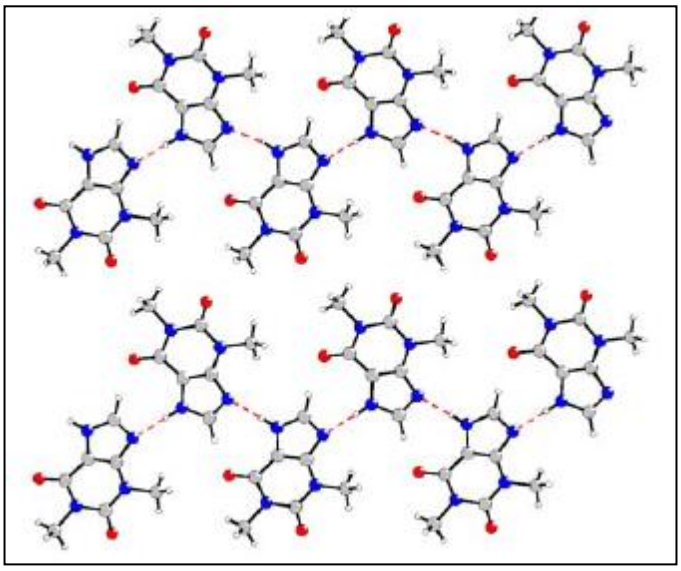

Figure 4.2. *Molecular packing of THEO FII forming H-bonded ribbons (Trask, Motherwell and Jones, 2006).*

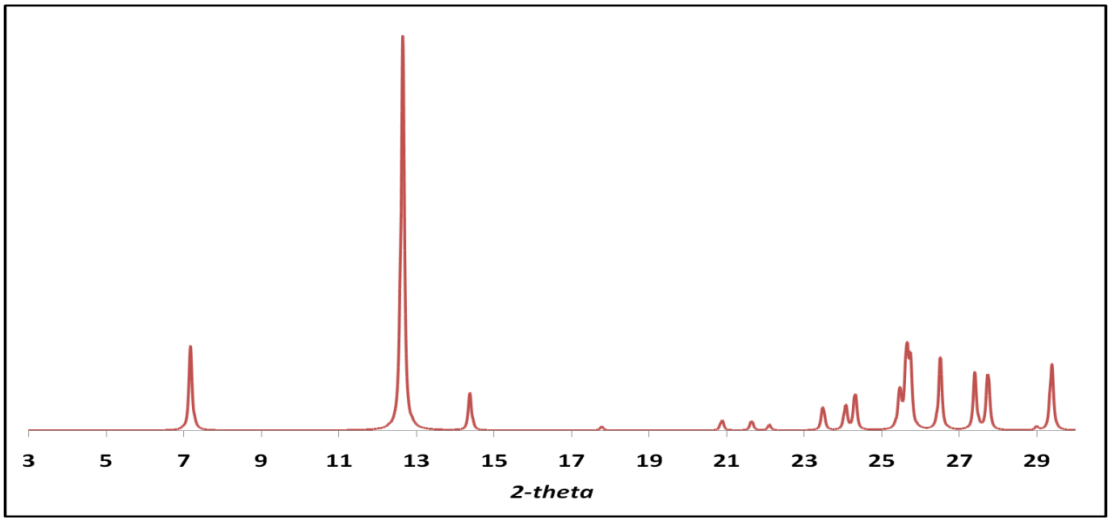

Figure 4.3. *PXRD pattern of THEO anhydrate (obtained from CSD).*

4.1.2. THEO monohydrate

Introduction of a water as a competing hydrogen bond donor readily forms O-H...N hydrogen bond with THEO's basic nitrogen. The N-H donor group builds up a secondary H-bond with the carbonyl oxygen in adjacent THEO (N-H...O) forming a cyclic dimer motif; $R_2^2(10)$ (Figure 4.5). This motif comprises of a hydrogen bonded ring with 10 atoms, of which 2 are H-bond donors and 2 are acceptors (Trask, Motherwell and Jones, 2006). The dimensions of the unit cell are: a= 4.47 (2) Å, b= 15.36 (5) Å; c= 13.12 (5) Å, β= 97.79^o with space group $P2_1/n$. The crystal structure and PXRD pattern are shown below.

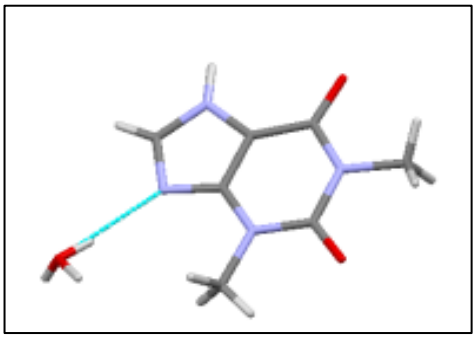

Figure 4.4. *Crystal structure of THEO monohydrate (CSD Ref: THEOPH02).*

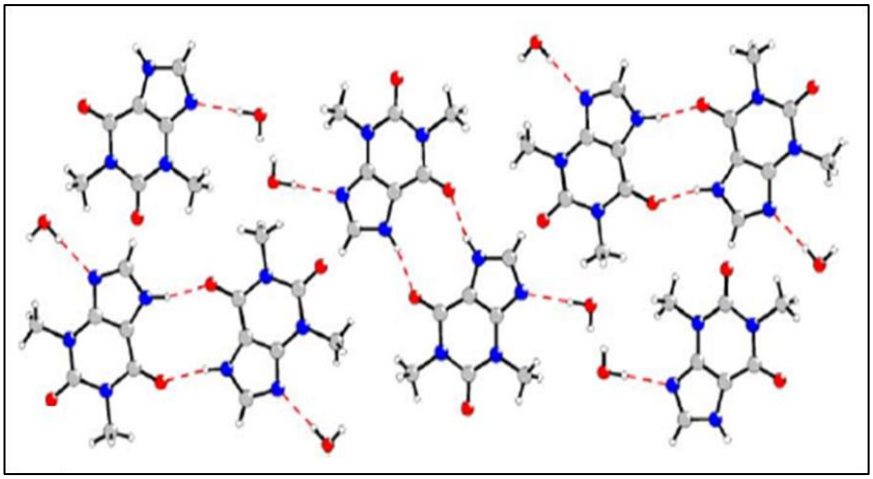

Figure 4.5. *Crystal arrangement of THEO monohydrate forming dimers (Trask, Motherwell and Jones, 2006).*

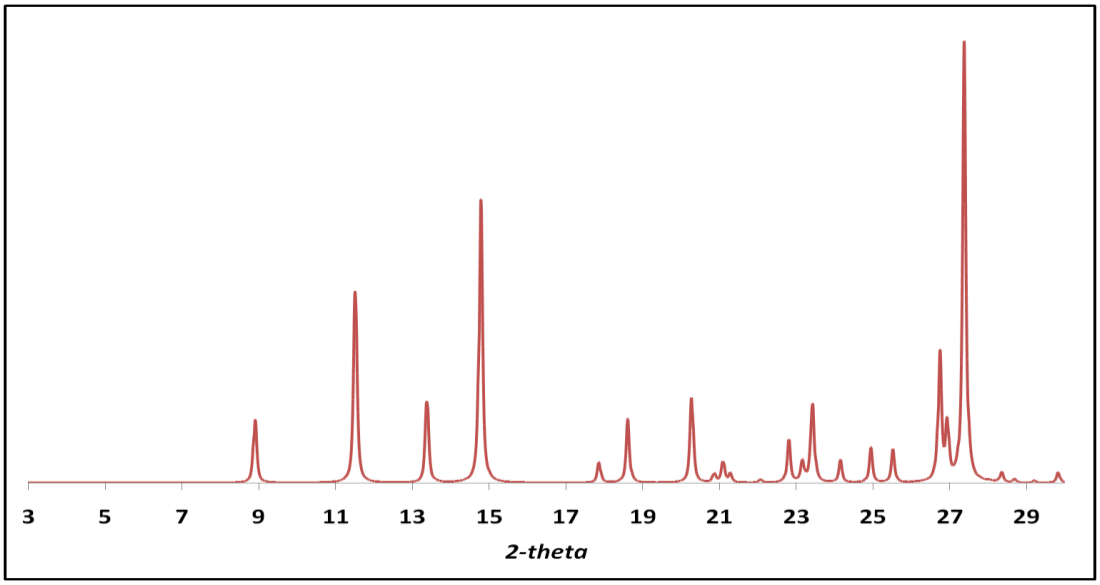

Figure 4.6. *PXRD pattern of THEO monohydrate collected from CSD.*

4.1.3. Theophylline maleic acid 1:1

THEO forms a co-crystal with MAL molecule via $R_2^2(7)$ hydrogen bond motif as observed in case of CAF:MAL 1:1 co-crystal, but no 2:1 structure is reported. The cis geometry of maleic acid is inclined to form an intramolecular hydrogen bond with the second carboxylic acid and the THEO molecules form dimers (Figure 4.8) (Trask, Motherwell and Jones, 2006). The triclinic crystal structure belongs to space

group *P1* with unit cell dimensions: a=7.97 (16) Å, b= 8.61 (17) Å, c= 10.67 (2) Å, α= 69.5^{o}, β= 72.5^{o} and γ= 71.2^{o}. The CSD crystal structure date and PXRD patterns are shown below.

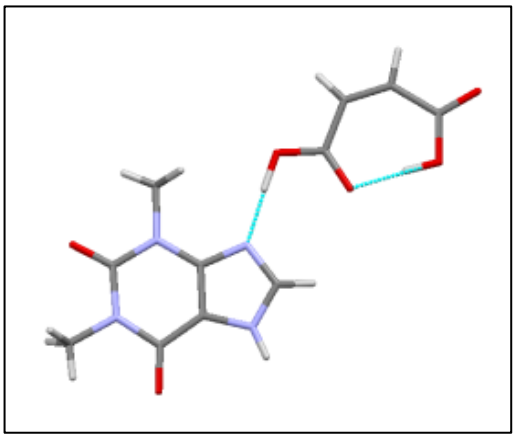

Figure 4.7. *THEO: MAL 1:1 crystal structure (CSD Ref: XEJXEQ).*

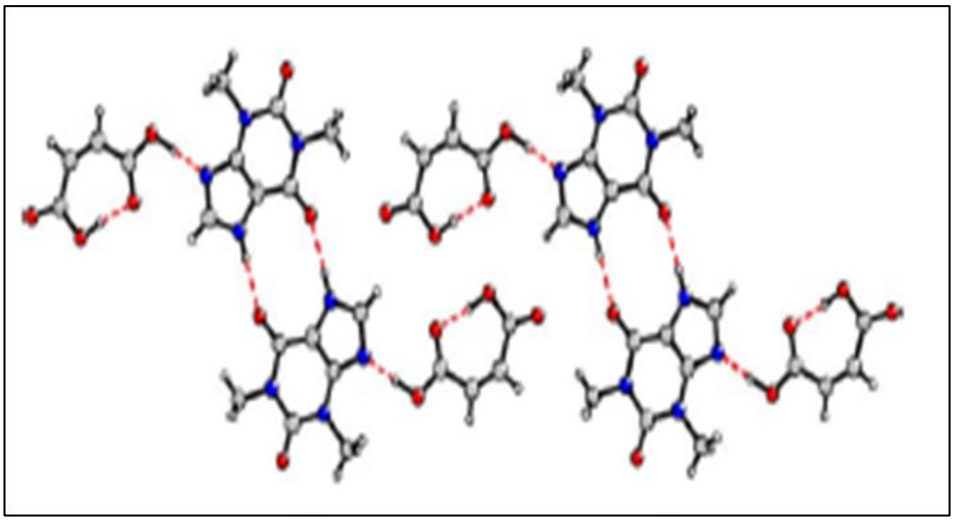

Figure 4.8. *Crystal packing of co-crystal THEO: MAL 1:1 (Trask, Motherwell and Jones, 2006).*

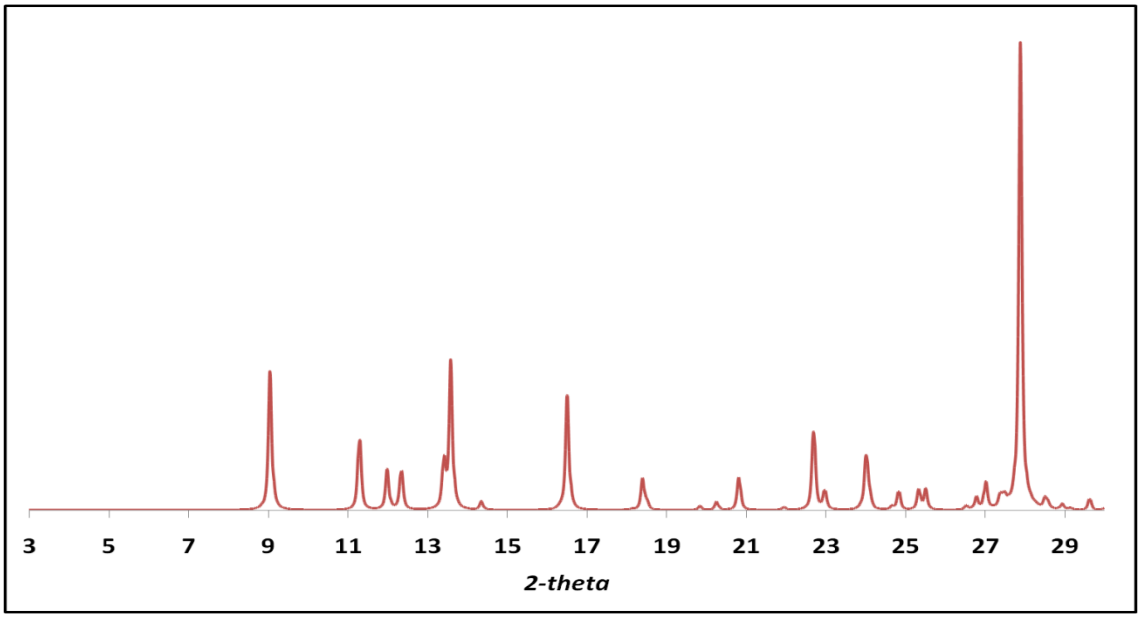

Figure 4.9. *PXRD pattern collected for THEO:MAL 1:1 from CSD.*

4.1.4. Theophylline oxalic acid 2:1

A 2:1 stoichiometry co-crystal is favoured where each oxalic acid binds via O-H...N intermolecular H-bond to THEO as observed in CAF:OX 2:1 co-crystal. However, due to the absence of a methyl group, THEO further binds to another THEO molecule to form homo-dimer of $R_2^2(10)$ motif (N-H...O interaction) creating H-bonded ribbons (Figure 4.11), which is not the case in CAF:OX co-crystal. Due to this molecular arrangement, the molecules form analogous ring and are not co-planar (Trask, Motherwell and Jones, 2006). The crystal structure and calculated PXRD pattern are shown in Figure 4.10 and Figure 4.12, respectively. The dimensions of the monoclinic unit cell are: a= 5.82 (12) Å, b= 16.61 (3) Å; c= 9.81 (2) Å, β= 99.83^o with space group $P2_1/c$.

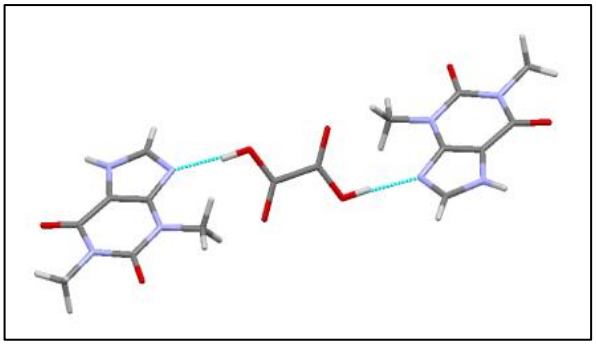

Figure 4.10. *Crystal structure of THEO: OX 2:1 co-crystal (CSD ref: XEJWUF).*

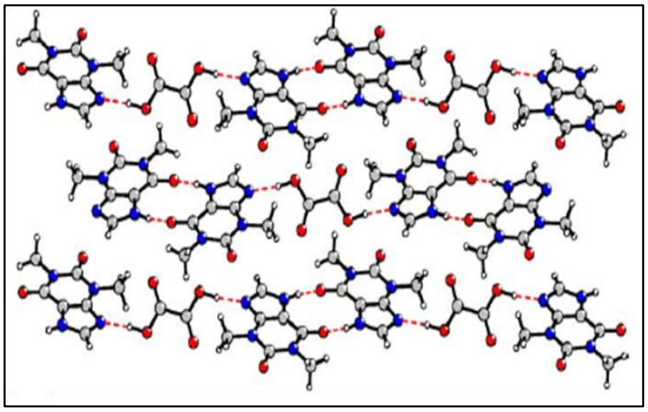

Figure 4.11. *Ribbon like arrangement of THEO:OX 2:1 crystal packing (Trask, Motherwell and Jones, 2006).*

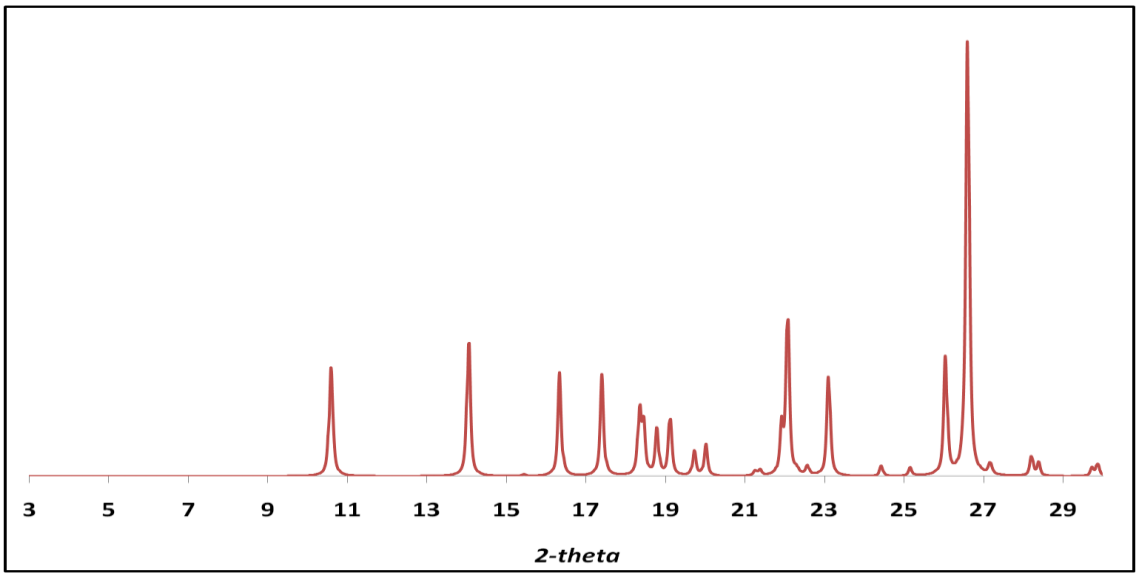

Figure 4.12. *PXRD pattern of THEO:OX 2:1 co-crystal collected from CSD.*

4.1.5. Theophylline malonic acid 1:1

This distinct 1:1 co-crystal has both primary intermolecular O-H...N bond between THEO and MO with additional secondary N-H...O bond forming THF dimer. The carbonyl groups of the neighbouring MO acids forms bisecting H-bonds, emerging as a step away from the plane of THEO dimer as shown in Figure 4.14 (Trask, Motherwell and Jones, 2006). The monoclinic crystal pattern exists with space group C 2/c with unit cell dimensions: a=17.88Å (4), b=8.39Å (2), c=17.63Å (4) and β = 105.7^{o}. The crystal structure and PXRD pattern are shown below.

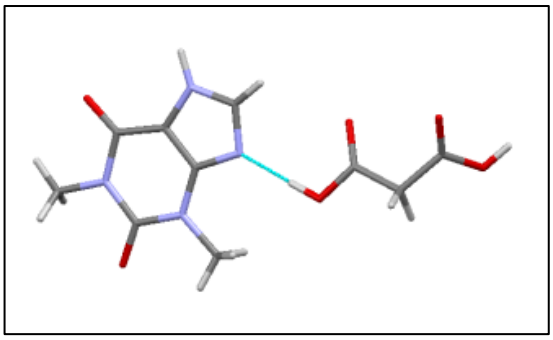

Figure 4.13.*Crystal structure of THEO:MO 1:1 (CSD Ref: XEJXAM).*

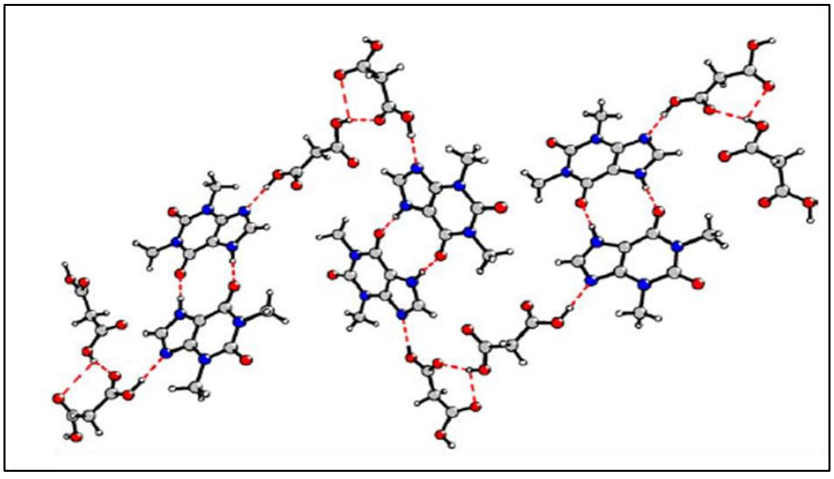

Figure 4.14. *Crystal packing of THEO:MO 1:1 co-crystal (Trask, Motherwell and Jones, 2006).*

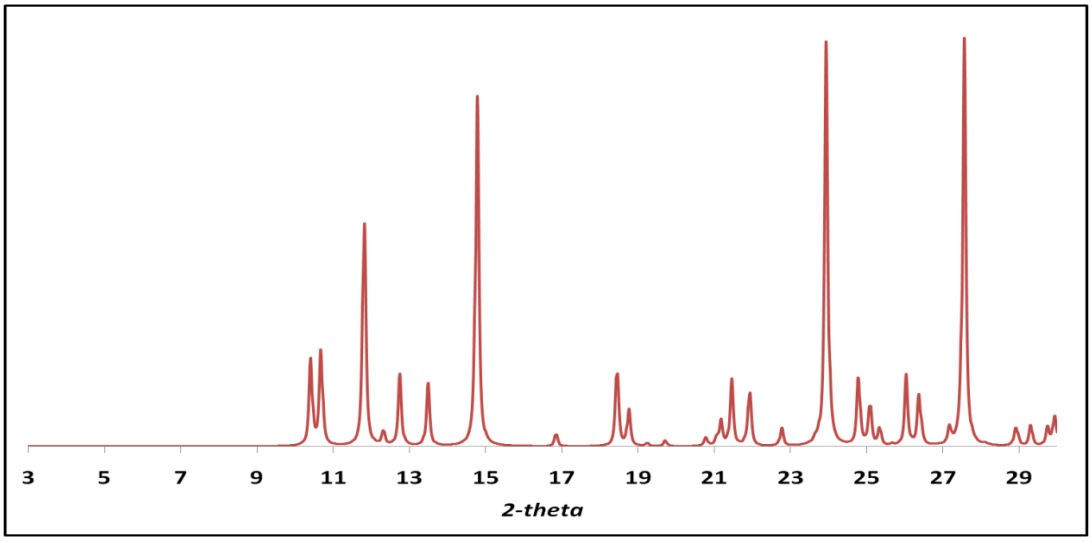

Figure 4.15. *PXRD data for THEO:MO 1:1 gathered from CSD.*

4.1.6. Theophylline glutaric acid 1:1

THEO: GLU 1:1 co-crystal shows similar primary O-H...N bond between THEO and acid along with THEO dimerisation (Figure 4.17). No polymorphic form was observed as in case of CAF: GLU co-crystals. The crystal arrangement is similar to CAF:GLU FI with additional dimer bonds absent in case of CAF (Trask, Motherwell and Jones, 2006).. The monoclinic crystal structure belongs to space group $P2_1/c$ with unit cell dimensions: a=9.60 (2) Å, b= 19.90 (4) Å, c= 15.33(4) Å and β= 107.9^0. The CSD crystal structure date and PXRD patterns are shown below.

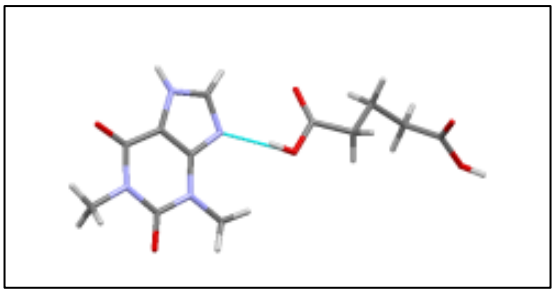

Figure 4.16.*Crystal structure of THEO: GLU 1:1 co-crystal (CSD Ref: XEJXIU).*

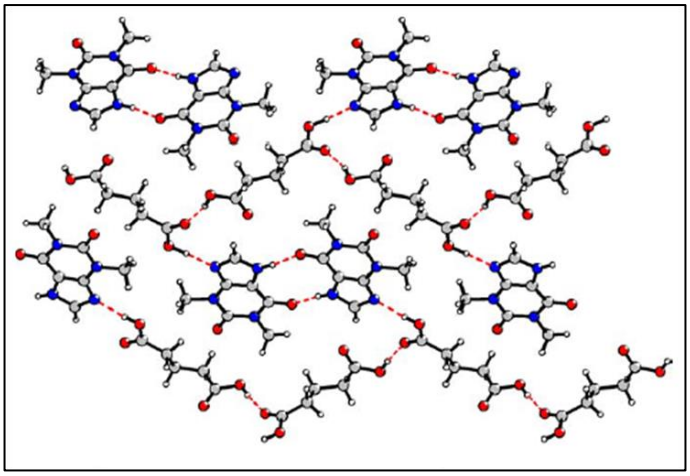

Figure 4.17. *Crystal arrangement of THEO: GLU 1:1 co-crystal (Trask, Motherwell and Jones, 2006).*

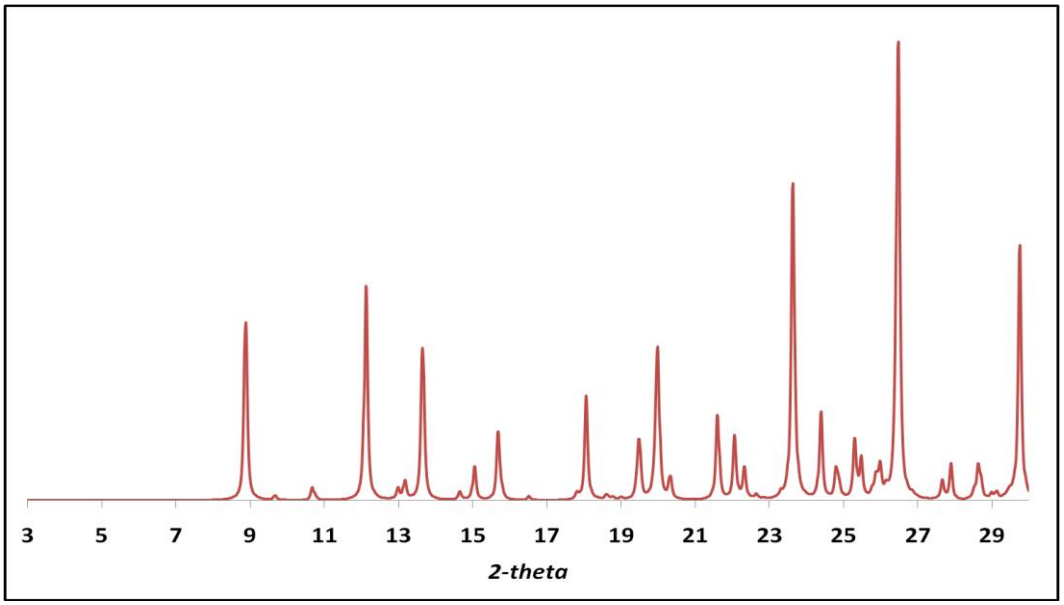

Figure 4.18. *PXRD pattern of THEO: GLU 1:1 co-crystal gathered from CSD.*

4.1.7. Theophylline co-crystal with tartaric and succinic acids

No structural data available.

An earlier attempt for generating THEO co-crystals with succinic acid and L-tartaric acid was a failure via both solid-state grinding and solution growth. Like results were obtained for structural analogue, CAF (Trask, Motherwell and Jones, 2006).

Previous spray drying trials and low solubility data clearly indicates that these molecules will not form co-crystals with THEO.

4.2. Solubility

Solubility of THEO in both aqueous dicarboxylic acid solution and organic solvents were determined to design experiments for successful co-crystallisation using spray drying.

4.2.1. Aqueous solubility

A calibration curve in accordance to Beer-Lambert law was plotted and a linear equation was deduced to calculate solubility results in different solvents (Figure 4.19).

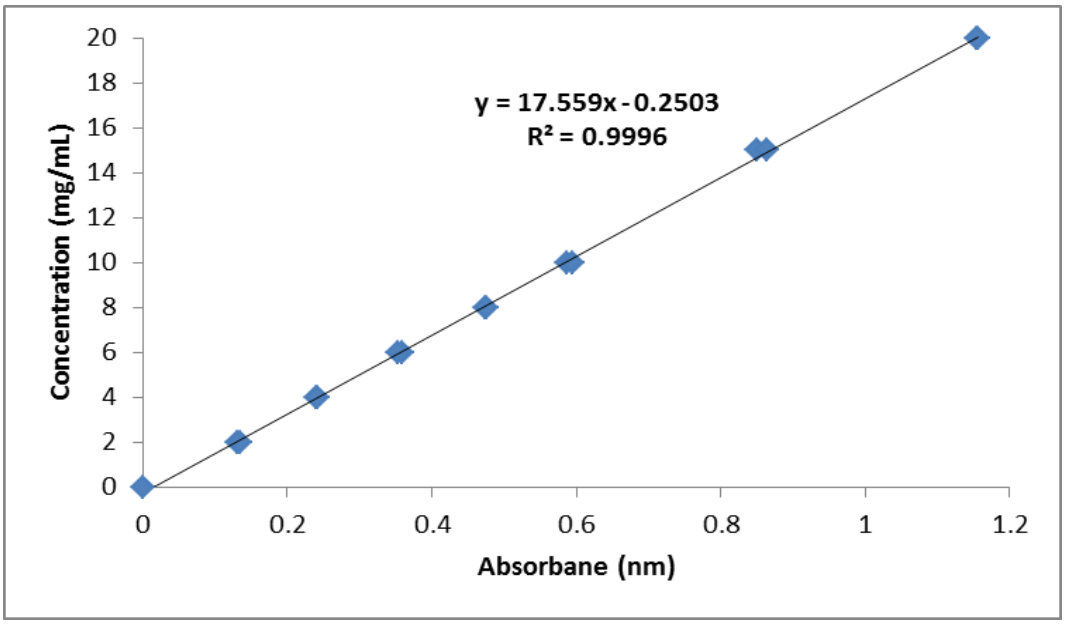

Figure 4.19.*Calibration curve of THEO concentration versus UV absorbance.*

Like CAF, the mole fraction solubility (x) of THEO was measured in water and 0.04M dicarboxylic acid solution at various temperatures as shown in Table 4.1 and Table 4.2, respectively.

Table 4.1. *Mole fraction solubility of theophylline in water at various temperatures.*

T/K	***Theophylline solubility (mg/mL)***	***Mole fraction (10^3x)***
294	6.5	0.38±0.02
313	10.2	0.60±0.08
323	26.1	1.52±0.12
333	33.7	1.97±0.07
343	67.6	3.93±0.06

Table 4.2. *Mole fraction solubility of theophylline in six di-carboxylic acid solutions between 294 and 323 K.*

T/K	***Theophylline (mg/mL)***	***Mole fraction (10^3x)***	***$(x-x^{cal})/x$***
Maleic acid			
294	17.2	1.01±0.02	-0.002
313	28.6	1.67±0.12	0.007
323	40.6	2.37±0.15	-0.005
Malonic acid			
294	11.8	0.68±0.07	-0.002
313	17.5	1.02±0.04	0.007
323	23.6	1.38±0.01	-0.005
Oxalic acid			
294	16.2	0.95±0.01	-0.012
313	21.9	1.28±0.02	0.038
323	45.7	2.67±0.04	-0.029
Glutaric acid			
294	14.2	0.83±0.03	-0.007
313	22.1	1.29±0.01	0.024
323	39.5	2.30±0.01	-0.018
Tartaric acid			
294	3.7	0.21±0.01	-0.005
313	9.0	0.53±0.01	0.019
323	19.3	1.13±0.0.2	-0.014
Succinic acid			
294	7.8	0.45±0.01	0.002
313	22.6	1.32±0.02	-0.008
323	33.3	1.94±0.01	0.006

The solubility measurements in di-carboxylic acid solutions were associated as a function of temperature from equation 3a and the following plot was created (Figure 4.20).

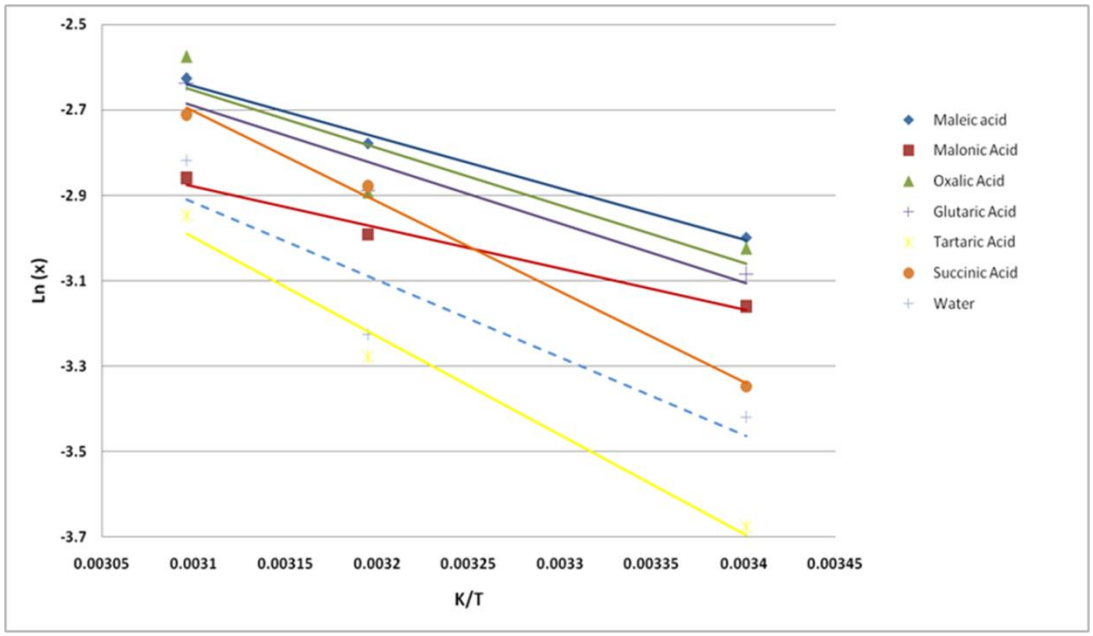

Figure 4.20. *Experimental mole fraction solubilities of theophylline in di-carboxylic acid (markers); calculated solubilities from equation 3a (linear).*

The relative standard deviations (RSD) and parameters A and B for each di-carboxylic acid solution are listed in Table 4.3 and were calculated from equation 3b.

Table 4.3. *A and B values and the root-mean –square deviations of the measured solubilities from the calculated results.*

Acid solution	***A***	***B***	***RSD***
Maleic acid	1.0646	-1196.4	**0.005**
Malonic acid	0.0999	-960.9	**0.005**
Oxalic acid	1.513	-1344.5	**0.029**
Glutaric acid	1.6001	-1383.8	**0.018**
Tartaric acid	4.1826	-2316.6	**0.014**
Succinic acid	3.8314	-2108.2	**0.006**

All dicarboxylic acid solutions enhanced THEO's solubility by almost two folds than in water alone. The solubility increased with rise in temperature in all solutions. In contrary, tartaric acid reduced its solubility. The solubility of THEO decreased in order of MAL > OX >GLU>MO>SUC> water > TAR. OX seems to aid in increased solubility of THEO compared to other acids conflicting with CAF's results. Although, the overall solubility of THEO rose to two folds in dicarboxylic acid solution, its solubility was three to four times lower than CAF's. The factor responsible is the structural difference, where CAF has an extra methylated group which readily participates in H-bonding. In addition to its basic nature, THEO also possesses a weak acidic nature due to the presence of H-bond donor at position 7 (N-H) which has thetendency to form dimers. The perplexing effect of solubilityhas also been explained by electric dipole moments of the molecules, i.e., 3.70 and 3.94 $_{D}$ for CAF and THEO, respectively. Though, the dipole moment are quite similar for the two xanthines, the disparity in solubility can be interpreted possibly by tautomerism, i.e., shifting of hydrogen atom at N(7) and N(9) of THEO (Figure 4.21), which is not viable in CAF due to methylated groups (Weiler-Feilchenfeld and Neiman, 1970).

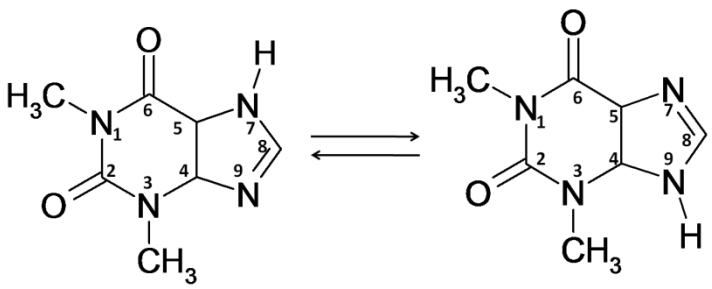

Figure 4.21. *Tautomeric effect at N7 and N9 of theophylline.*

The transition temperature from anhydrous to hydrous form for theophylline is 55-65^{o}C (328-338 K) (Wikstrom, Kakidas and Taylor, 2008).The X-ray diffraction

analysis carried out on excess filtered solid obtained from solubility experiments verifies non-conversion of THEO into its hydrate form at all conditions (Appendix I); even at higher temperature of 343 K in water.

4.2.2. Organic solvents

Due to very low aqueous solubility of THEO, organic solvents were involved for comparison and to establish appropriate methods in developing co-crystals with acids. The results obtained are shown in table below:

Table 4.4. *Thermodynamic solubility of theophylline (mg/mL) in various organic solvents.*

Solvent	***mg/mL***
DMSO (Dimethyl sulfoxide)	13.1±0.05
Methanol	4.8±0.01
Chloroform	3.0±0.03
Ethanol	2.3±0.06
Ethyl acetate	1.1±0.01
Acetonitrile	1.4±0.02
1,2-Dichloroethane	0.3±0.02
Acetone	1.5±0.03

It is noticeable that solubility of THEO in the above solvents is very low compared to water (6.5 mg/mL), except for DMSO. THEO's solubility observed was highest in DMSO with DEC of 46.7, followed by water which is highly polar with DEC of 80. However, due to high boiling point of DMSO (189^{o}C), its evaporation is difficult under rotavap and may decompose components, hence, it was not utilised in this study. The next closest solubility was observed in chloroform and methanol. Previous studies applied binary combination of chloroform ($CHCl_3$) and methanol (MeOH) to generate theophylline co-crystals with acids via solution mediated growth (Trask, Motherwell and Jones, 2006; Zhang, 2010).Therefore, additional solubility tests were performed in different solvent ratios of $CHCl_3$ and MeOH.

Another important consideration is the solvent classification in terms of manufacturing pharmaceutical products to combat toxicity and /or any other destructive environmental effect. $CHCl_3$ is considered as a Class 2 solvent due to its toxicity with a permissible daily exposure (PDE) limit of 0.6 mg/day (ICH, 2012; Chemical-ecology, 2010). Therefore, ethyl acetate (Class 3) was applied as a safe replacement solvent for chloroform (polarity index = 4.1) bearing almost similar polarity index of 4.4 (FPN, n.d.), and a permissible boiling point for the experimental design. The ethylacetate (EtAc) and MeOH binary mixtures at various ratios were compared to mixtures of $CHCl_3$ and MeOH and their DEC values recorded (Table 4.5; Figure 4.22).

Table 4.5. *Theophylline's solubility and DEC values in binary mixture of solvents:- chloroform: methanol and ethyl acetate: methanol.*

Solvent Ratio	***Chloroform/ methanol mixture***		***Ethyl acetate/ methanol mixture***	
	DEC	**mg/mL**	**DEC**	**mg/mL**
1:9	22.85	4.7±0.04	22.44	1.2±0.01
2:8	18.70	6.9±0.04	21.20	2.2±0.01
3:7	17.30	10.3±0.01	20.62	3.0±0.02
4:6	14.84	18.8±0.09	18.13	3.5±0.01
5:5	12.91	24.2±0.01	16.60	3.7±0.02
6:4	11.39	31.0±0.05	14.28	4.3±0.01
7:3	9.89	42.1±0.01	12.58	4.9±0.05
8:2	8.49	43.4±0.02	10.38	5.3±0.05
9:1	6.89	44.8±0.01	8.39	5.45±0.01
DEC values: Chloroform=4.8, Ehtyl acetate=6.02 and Methanol = 32.7				

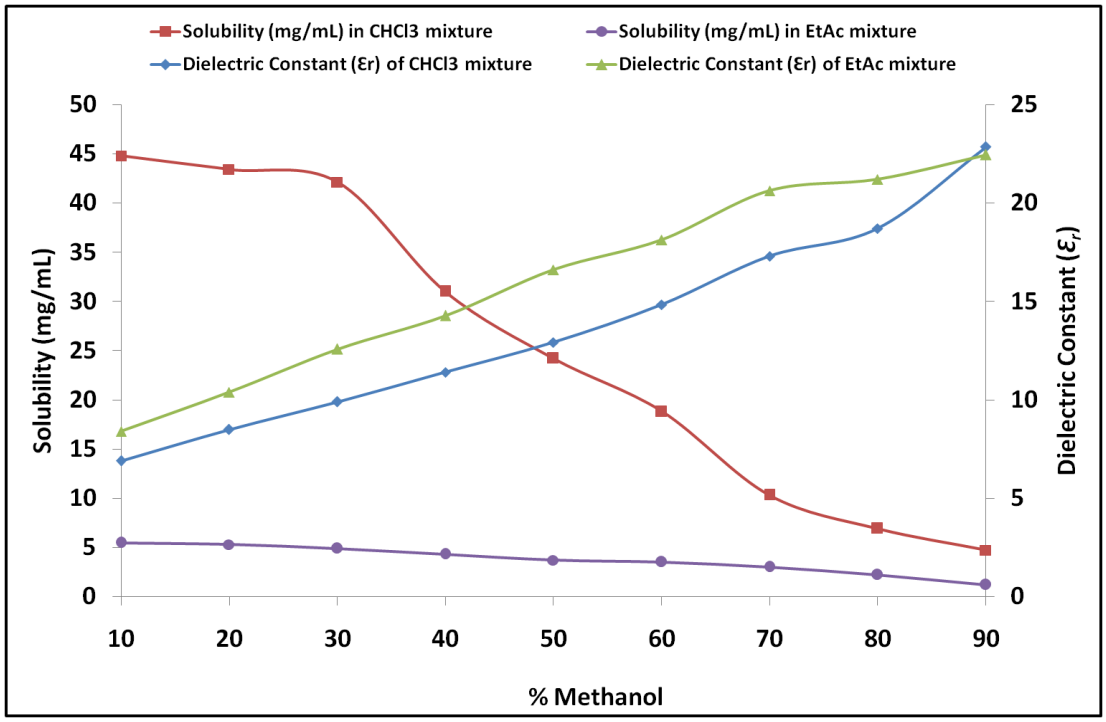

Figure 4.22. *Graphical representation of DEC values and THEO's solubility in binary mixtures of EtAc+ MeOH and $CHCl_3$+ MeOH.*

Hansen solubility parameters

A three dimensional solubility parameter (δ) concept describes solvent properties in terms of hydrogen bonding forces (δ_h), polar bonding forces (δ_p) and dispersion forces (δ_d) (Hansen, 1967). These forces collectively hold a liquid together and explain its solubility. The three parameters for the selected solvents are depicted in table below:

Table 4.6. *Hansen's solubility parameters for three solvents used in binary mixtures: MeOH, EtAc and $CHCl_3$ (Hansen, 1967).*

Solvent	***Solubility Parameters***		
	Dispersion forces (δ_d)	***Polar forces (δ_p)***	***Hydrogen bond forces (δ_h)***
Methanol	7.4	6.2	11.0
Ethyl acetate	7.4	2.6	4.5
Chloroform	8.7	1.8	2.8

$CHCl_3$ and EtAc possess similar polarity index; yet the difference in THEO's solubility observed is explained via factors such as their individual binding parameters (hydrogen and polar forces). The decreasing hydrogen bond and polar bond association capacity is in the order: MeOH<EtAc<$CHCl_3$. London dispersion forces which are weak induced dipole forces were almost similar in case of MeOH and EtAc and slightly higher for $CHCl_3$. When solvents are combined these forces may vary and affect their properties or interaction with the solute. For instance, it may decrease or increase the overall association forces, δ_a (δ_h + δ_p). Hansen also proposed that two bad solvent when mixed lying at the centre of Hansen solubility parameter (HSP) sphere emerge as a good solvent. The variation in these forces of binary solvent mixtures was calculated using HSP solvent blend tool (Table 4.7; Appendix III) (Hansen-solubility, 2015).

Table 4.7. *Three solvent parameters for solvent blends: a) $CHCl_3$+methanol; b) ethyl acetate+ methanol (Hansen-solubility, 2015).*

a)

	Solvent	**δ_d**	**δ_p**	**δ_h**
S1	*Chloroform*	8.7	1.8	2.8
S2	*Methanol*	7.4	6.2	11
% S1	*% S2*			
100	0	8.7	1.8	2.8
90	10	8.57	**2.24**	**3.62**
80	20	8.44	2.68	4.44
70	30	8.31	3.12	5.26
60	40	8.18	3.56	6.08
50	50	8.05	4	6.9
40	60	7.92	4.44	7.72
30	70	7.79	4.88	8.54
20	80	7.66	5.32	9.36
10	90	7.53	5.76	10.18
0	100	7.4	6.2	11

b)

	Solvent	**δ_d**	**δ_p**	**δ_h**
S1	*Ethyl acetate*	7.4	2.6	4.5
S2	*Methanol*	7.4	6.2	11
% S1	*% S2*			
100	0	7.4	2.6	4.5
90	10	7.4	**2.96**	**5.15**
80	20	7.4	3.32	5.8
70	30	7.4	3.68	6.45
60	40	7.4	4.04	7.1
50	50	7.4	4.4	7.75
40	60	7.4	4.76	8.4
30	70	7.4	5.12	9.05
20	80	7.4	5.48	9.7
10	90	7.4	5.84	10.35
0	100	7.4	6.2	11

The results in Table 4.5 indicate an enormous increase in THEO solubility in $CHCl_3$+MeOH mixture compared to EtAc+MeOH mixtures. The solubility was enhanced with high concentrations of $CHCl_3$ and EtAc in the mixtures, the highest being at 9:1 ($CHCl_3$/EtAc:MeOH) ratio. At this ratio, solubility accelerates from 3 to 44.8 mg/mL in $CHCl_3$+MeOH and 1 to 5.5 mg/mL in EtAc+MeOH. MeOH alone exhibits higher solubility and higher association forces [δ_p (6.2) +δ_h (11)] compared to the other two solvents (Table 4.6). Even though, the calculated association forces of 9:1 mixture was slightly higher than that of the two bad solvents ($CHCl_3$ and EtAc), it gave a much better solubility than MeOH. It must also be noted that the dispersion forces in case of EtAc/MeOH remains the same (7.4), whereas, it varies in $CHCl_3$/MeOH mixtures.

DEC

MeOH being a polar solvent possesses higher DEC value of 32.7 than $CHCl_3$ (4.8) and EtAc (6). The DEC values generated for the two solvent mixtures did not show a significant variation. It decreased with decrease in MeOH's concentration as it enhances THEO's solubility by association, thus, reducing the polarity of the solution (explained in chapter 3.2.3). The polarityis further supported by decline in the calculated association forces in the solvent mixtures.

Binary mixture: Type of solvents

Another distinguishing feature to be observed in a binary mixture is the type of polar solvent involved: protic and aprotic solvent. This explains varying polarity denoted by DEC, its tendency to form H –bonding (Son, 2014, p.117), and/or its participation as a nucleophile. Polar protic solvents have high H-bonding tendency as they contain O-H or N-H bonds which can lose protons, example, water and methanol. Water contains both H-donor and acceptor properties indicated by its high DEC value and dipole moment. It also behaves as a nucleophile due to the presence of electron pair on oxygen which has tendency to form bonds with strong electrophile such as acids. Aprotic solvents are polar as they contain strong dipole-dipole interaction, but do not undergo hydrogen bonding due to lack of H atom next to O or N, for example, DMSO. EtAc is a slightly polar aprotic solvent with DEC >5. Whereas, chlorinated solvent such as $CHCl_3$ (DEC <5) transforms into a singlet carbene in the presence of a strong base, acting as both electrophile and nucleophile due to a filled sp2 and an empty p orbital (Figure 4.23) (Hultin, 2002; Master Organic Chemistry, 2015).

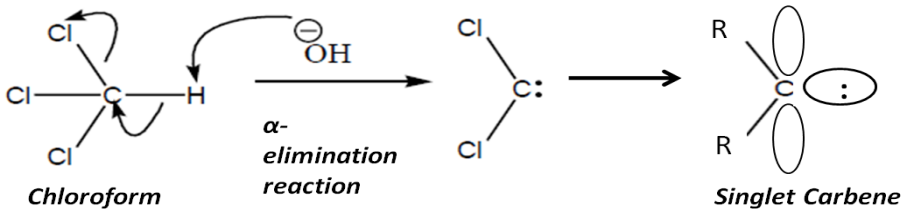

Figure 4.23. *Chloroform undergoes α-elimination reaction in presence of strong base forming a singlet carbene (Hultin, 2002).*

Microscopic solvent properties in binary mixture

Understanding the solute and solvent in a binary mixture is very difficult as the extent to which a solute may react each component of mixture varies. Mancini *et al*., (2000) analysed effect of binary mixtures of aprotic H-bond acceptor (EtAc) with co-solvents: aprotic H-bond donor, $CHCl_3$ and strong protic H-bond donor, MeOH. Further studies examined their association using solvatochromatic indicators such as polarisability (SPP), hydrogen bond donor acidity (SA) and acceptor basicity (SB). The parameters of the binary mixtures components are provided in Table 4.8. The observation of variability in parameters at different co-solvent concentrations were reported (Figure 4.24) (Mancini *et al.*, 2003).

Table 4.8. *The three microscopic solvent properties of EtAc, $CHCl_3$ and MeOH (Mancini et al., 2003).*

Solvent	***SPP***	***SB***	***SA***
EtAc	0.795	0.542	0
MeOH	0.857	0.545	0.605
$CHCl_3$	0.786	0.071	0.047

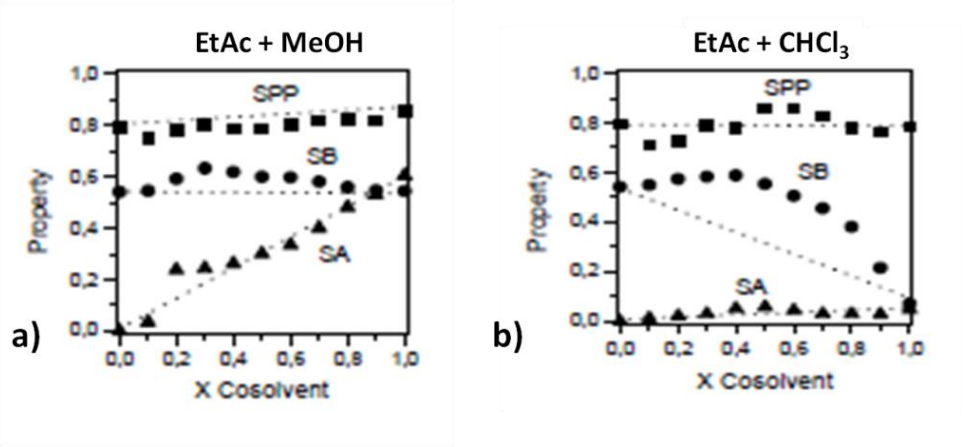

Figure 4.24. *Plots of SPP, SB and SA parameters against mole fraction of co-solvent: a) MeOH; b) $CHCl_3$ (Mancini et al., 2003).*

The SPP values of polarity were same in both the binary mixtures, but varied in their SA and SB values. The SA values increased in MeOH rich region, whereas, value corresponding to $CHCl_3$ was unimportant. In contrary, the SB values produced synergistic effect for all MeOH concentrations and for $CHCl_3$ below 0.50, but decreased rapidly above 0.50 $CHCl_3$ co-solvent concentration (Mancini *et al.,* 2003). Our observations of highest solubility in EtAc+MeOH mixtures were at lowest co-solvent concentrations indicating very low SA property. Similarly, looking at the table values above, we can estimate that $CHCl_3$+MeOH mixtures at high MeOH concentration will obtain a high SA and SB values and vice-versa. Therefore, THEO was preferentially solvated by $CHCl_3$+MeOH mixture at almost negligible SA and SB values slightly above 0.047 and 0.071, respectively.

4.3. Fast evaporating techniques

Solubility measurements of THEO neither produced convincing results in water with dicarboxylic acids nor in organic solvents. However, a drastic increase was observed in binary solvent mixture of $CHCl_3$+ MeOH and hence, further studies were commenced in this suitable media for the production of THEO co-crystals.

4.3.1. Rotavap

Rotavap experiments of THEO and dicarboxylic acid were conducted, but the vapour pressure of the binary mixture could not be obtained. However, the vapour pressure of individual solvent was calculated to get an estimate using the parameters shown in Table 4.9. The ratio of solvents differs for each dicarboxylic acid as MeOH required to dissolve each acid relates to their polarity and solubility collectively along with the varying stoichiometric ratios.

Table 4.9. *Antoine's parameters for MeOH and $CHCl_3$ solvent to determine their vapour pressures (DDBST GmbH, n.d.).*

Solvent	**Antoine's equation parameters**		
	A	**B**	**C**
Chloroform	6.9	1171.0	226.2
Methanol	8.1	1582.3	239.7

All solutions prepared for rotavap experiment were subjected to 45^0C water bath temperature (Table 4.10). The calculated vapour pressure for $CHCl_3$ and MeOH was 434 and 334 mbar, respectively. The pressure was reduced to 250 mbar to enable fast evaporation of the binary mixture. The PXRD pattern collected from the rotavap experiments are shown in Figure 4.25.

Table 4.10. *Experimental set up and XRD results for THEO and dicarboxylic acid solutions.*

Solution Mixture	Solvent ($CHCl_3$:MeOH)	Concentration (%)	XRD
THEO:GLU 1:1	*$CHCl_3$+MeOH; 20+27 mL (~1:1)*	4.4	*1:1+ **T†***
THEO: MAL 1:1	*$CHCl_3$+MeOH; 25+6mL (~4:1)*	4.8	*1:1 + **T†***
THEO: MO 1:1	*$CHCl_3$+MeOH; 30+7 mL (~4:1)*	5.1	*1:1+**T†***
THEO:OX 2:1	*$CHCl_3$+MeOH; 30+15 mL (2:1)*	3.3	*2:1+ **T†***
†----minor impurity; T---theo anhydride			

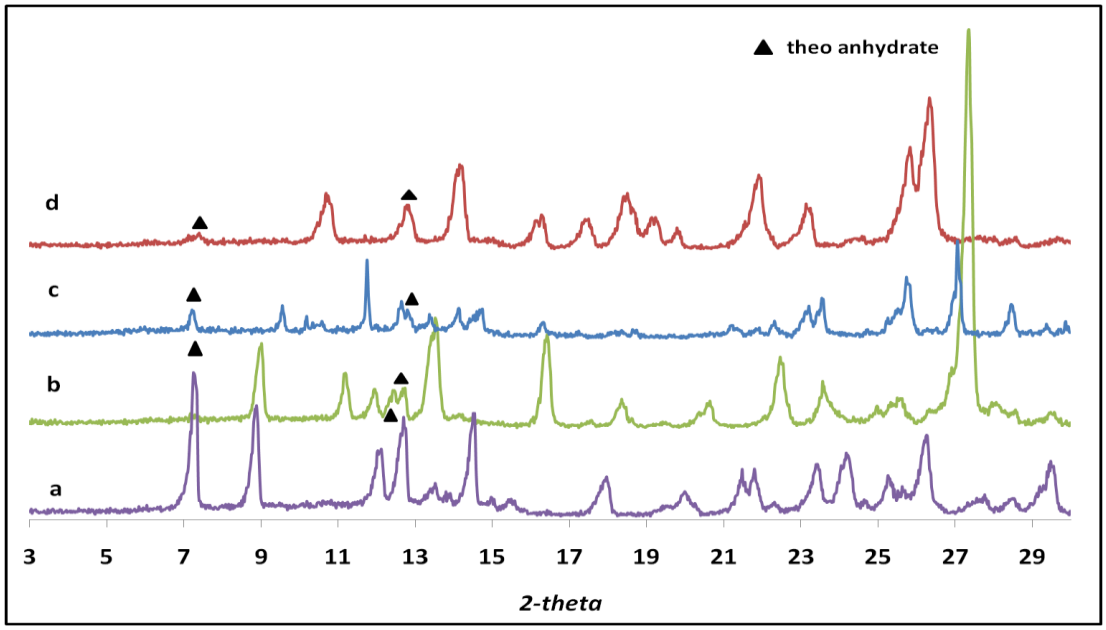

Figure 4.25*: PXRD patterns of theophylline and dicarboxylic acid solutions under rotavap: a) 1:1 glutaric acid; b) 1:1 maleic acid; c) 1:1 malonic acid; d) 2:1 oxalic acid.*

Trask *et. al*., (2006) obtained THEO: MAL 1:1 co-crystal with excess impurity of THEO anhydrate after filtration. However, the precipitate from the filtrate generated phase pure co-crystals. In their second attempt, excess maleic acid was used in acetonitrile to attain single crystal under slow evaporation. Co-crystals of malonic and glutaric acids from solution were assisted by seeding with phase-pure co-crystals formed via grinding followed by slow evaporation of the filtrate. The above results

above depict co-crystals with impurity of THEO anhydride which could be due to variation in evaporation of binary solvents involved.

The existence of azeotrope of methanol (b.p. 64.7^{o}C) and chloroform (61.7^{o}C) mixture is illustrated via plot of vapour and liquid phase composition against the boiling point (Figure 4.26) (PHYWE, n.d.). When the boiling and condensate curve coincide at X_{MeOH} = 0.35, similar composition of solvents is observed in both liquid and vapour phase.

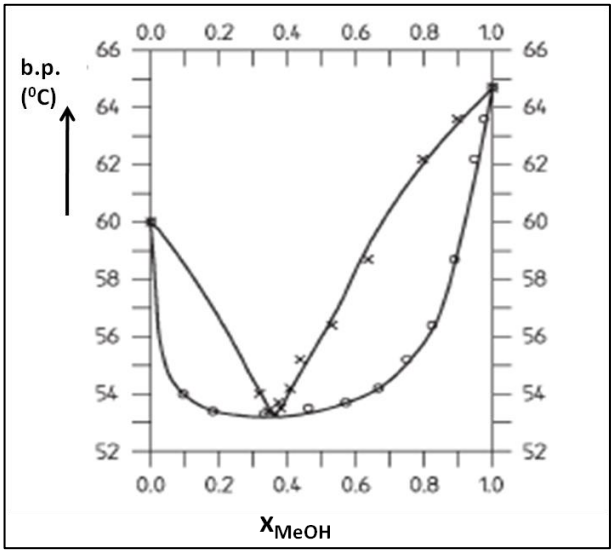

Figure 4.26. *Plot of liquid and vapour curves of MeOH/$CHCl_3$ system against boiling point (PHYWE, n.d.).*

Under rotavap, the composition of these two solvents changes continuously decreasing the proportion of more volatile component in the liquid phase until it attains azeotropic state as an equilibrium or final composition. Hence, the components held in the solution may vary until it reaches the azeotropic point affecting crystallisation.

4.3.2. Spray drying – inert loop

The co-crystal component solutions in binary mixture of $CHCl_3$/MeOH were introduced into the experimental design with a safe, closed, recirculating inert loop (Chapter 2, Fig. 2.3). The solvent evaporated was condensed within this recirculating N_2 loop straight after evaporation and collected in solvent bottle. The inlet temperature was kept higher than the boiling points of the two solvents and the other parameters used were similar as optimised in chapter 3.3.2, i.e. aspirator speed (60 m^3/hr), atomisation (1.5 bar), and feed rate (3 mL/min) (Table 4.11). The outlet temperature stretches from 33-35^oC to which the final product gets exposed. Powder X-ray analysis confirm pure co-crystals in all cases (Figure 4.27).

Velaga *et al*., (2013) used spray dryer to prepare co-crystals of THEO with urea, saccharin and nicotinamide and compared its aerosolisation properties against milled co-crystals. Though the surface energy of spray dried material was lower than the milled product, the aerosol efficiency was better demonstrated by spray dried co-crystals due to their physicochemical properties. Also, co-crystallisation of incongruent mixtures in binary solvent via spray drying surpasses the hindrances incurred by rotavap producing phase pure forms. Though, co-crystals produced via rotavap are not pure, it can still be used as a screening tool to depict the co-crystal formation under spray drying.

Table 4.11. *Experimental set-up for THEO and dicarboxylic acid in an inert loop.*

API + co-former	$CHCl_3$ + MeOH (mL)	Feed Concentration (%)	XRD result
THEO:GLU 1:1	58 +20(~3:1)	5.6	*1:1*
THEO:MAL 1:1	72 + 12 (6:1)	4.7	*1:1*
THEO:MO 1:1	60 + 15 (4:1)	5.1	*1:1*
THEO:OX 2:1	71+ 33 (~2:1)	2.9	*2:1*

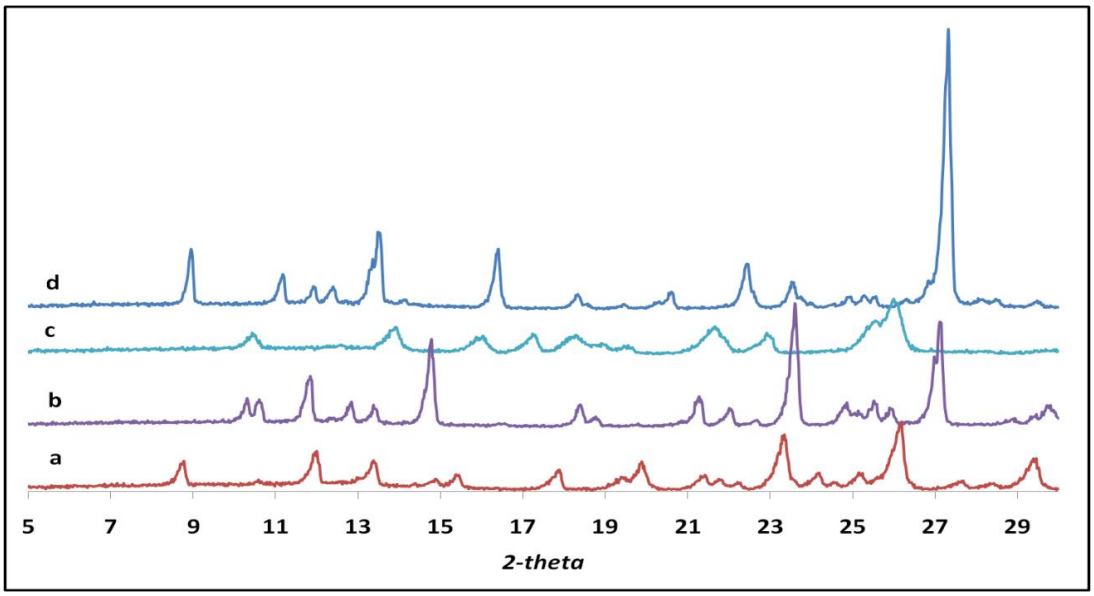

Figure 4.27. *PXRD pattern of a) THEO:GLU 1:1; b) THEO:MO 1:1; c) THEO:OX 2:1 and d) THEO:MAL 1:1.*

DSC

A study investigated thermal stability of THEO: amide co-crystal and suggested that an amino-pseudo-amino synthon was favoured between THEO and primary/secondary amide in a *cis* configuration with $R_2^2(9)$ motif. The thermal stability of co-crystals with this interaction gave a melting point different from the co-formers. It was found out that in an open heated system, these co-crystals dissociate due to loss of amide at lower temperature than their melting point. The amide co-former sublimes while dissociation occurs, followed by residual crystallisation of theophylline (Eddleston *et al*., 2015). Similarly, in case of co-crystals with dicarboxylic acids (OX, MO and MAL), two endotherms were observed (Figure 4.29).

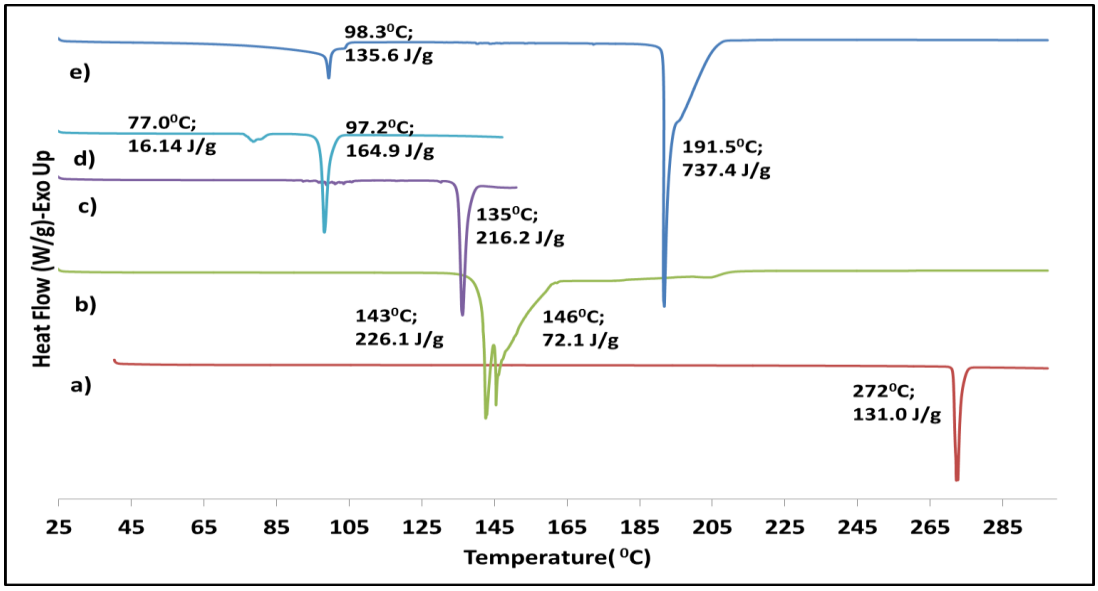

Figure 4.28. *DSC endotherms: a) THEO; b) MAL; c) MO; d) GLU; e) OX.*

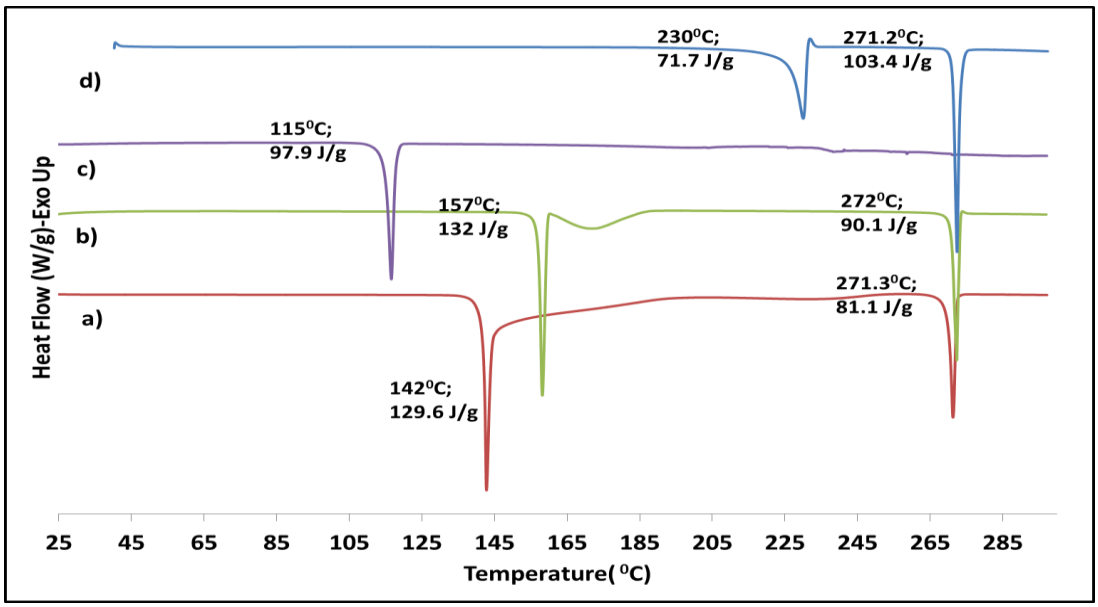

Figure 4.29. *DSC endotherms: a) THEO: MAL; b) THEO:MO; c) THEO:GLU; d) THEO:OX.*

THEO: OX DSC thermogram shows an endothermic peak around 230°C and second at 271.2°C. The first endotherm differs from anhydrous OX's, which undergoes sublimation at 98.3°C and melts at 191.5°C. Oxalic acid disintegrates into carbon dioxide and formic acid (Zhang, 2010). Therefore, the first endothermic peak represents the co-crystal and OX sublimes as a gas leaving the co-crystal and the

remaining THEO generates the second endothermic peak. Glutaric acid has two endothermic peaks at 77.0^{o}C and 97.2^{o}C, and THEO: GLU co-crystal peak melts over the temperature range of 115^{o}C till 116^{0}C. None of these peaks overlaps with the known THEO and GLU values. The two endothermic peaks for MAL are at 143^{o}C and 146^{o}C corresponding to its melting temperature and an unknown endothermic process. The two melts of THEO: MAL co-crystal was observed at 142^{o}C and 271^{o}C corresponding to THEO. Malonic acid has a melt onset at 135^{o}C which is absent in the co-crystal DSC thermogram of THEO: MO 1:1. Two endothermic peaks obtained at 157^{o}C and 272^{o}C relate to co-crystal and THEO melt, respectively.

Particle size

The particle distribution for THEO co-crystal with GLU, MO and MAL was irregular and skewed (Appendix IV) which can be attributed to its morphology and inability of the primary particles to break under dispersive pressure of laser diffraction as explained in Chapter 3. Hence why, the particle size illustrated in the table below is not a true result.

Table 4.12. *Particle size distribution for THEO co-crystals.*

Conc. (%)	**Particle size distribution (µm) Method: Lens- R_1 (0.1-35µm) Dispersive pressure: 4bar 40mm/s**			**Particle volume over particle size**
	X_{10}	X_{50}	X_{90}	*VMD (Volume mean diameter in µm)*
THEO:GLU	3.8±0.08	15.1±0.56	28.1±0.30	15.61
THEO:MO	1.19±0.03	9.7±0.04	27.6±0.17	12.43
THEO:OX	0.72±0.00	2.6±0.18	4.03±0.11	2.56
THEO:MAL	2.8±0.19	15.1±0.46	28.5±0.31	15.47

Also, the microscopic images (Figure 4.30 and Figure 4.31) display big clusters of co-crystals with GLU and MAL corresponding to their high median particle dimension (X_{50} = 15.1 μm). Whereas, co-crystal with OX show a symmetrical gaussian curve (Appendix IV) with X_{50} = 2.6 μm where small primary particles can be visualised under microscope (Figure 4.31; c).

SEM image in Figure 4.32a illustrate huge clusters of partially spherical primary particles clumped together in case of THEO:GLU co-crystals. The primary particles in case of THEO:MO (Figure 4.32b) are not as distinguishable and adhere to each other forming big irregular rod-like structures. THEO:OX 2:1 (Figure 4.33a) exhibits tiny spherical primary particles which seem to be readily separated and detected via laser diffraction. On the other hand, THEO:MAL (Figure 4.33b) 1:1 appears like layers of flat structures joined together, corresponding to a larger particle size detection or perhaps, an invalid result via laser diffraction.

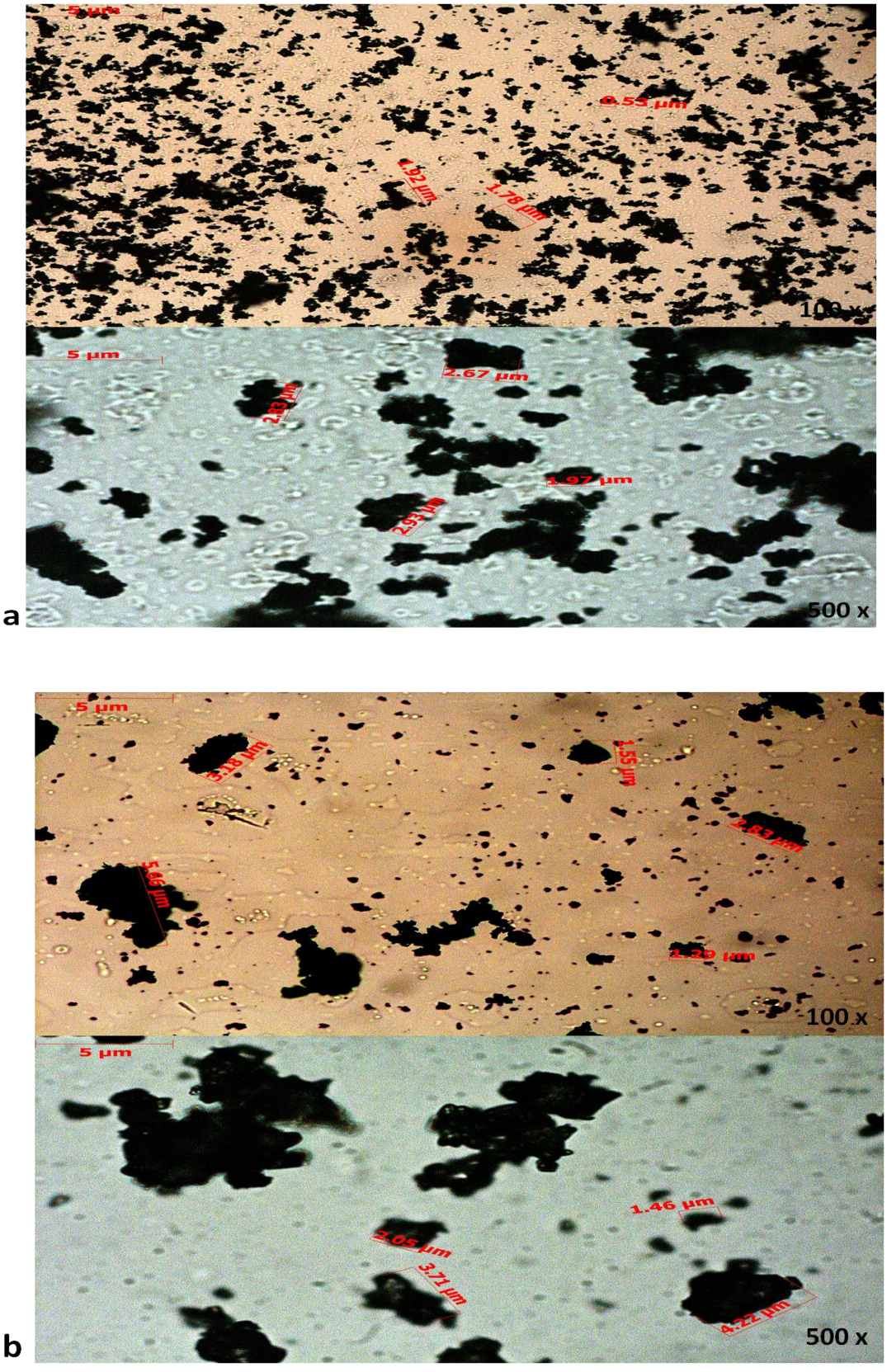

Figure 4.30. *Microscope images of co-crystals: a) THEO:GLU; b) THEO:MO.*

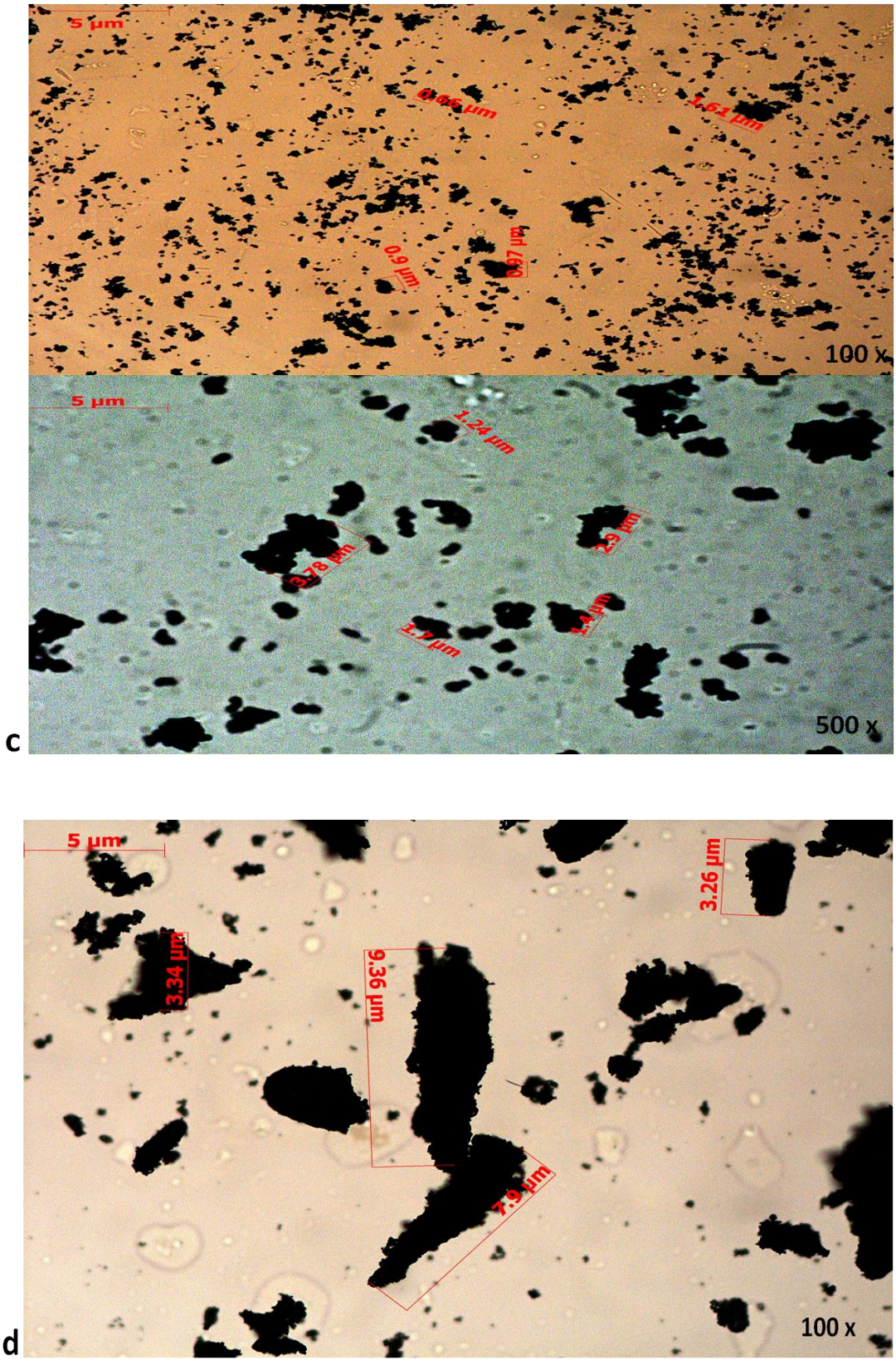

Figure 4.31. *Microscope images of co-crystals: c) THEO:OX and d) THEO:MAL.*

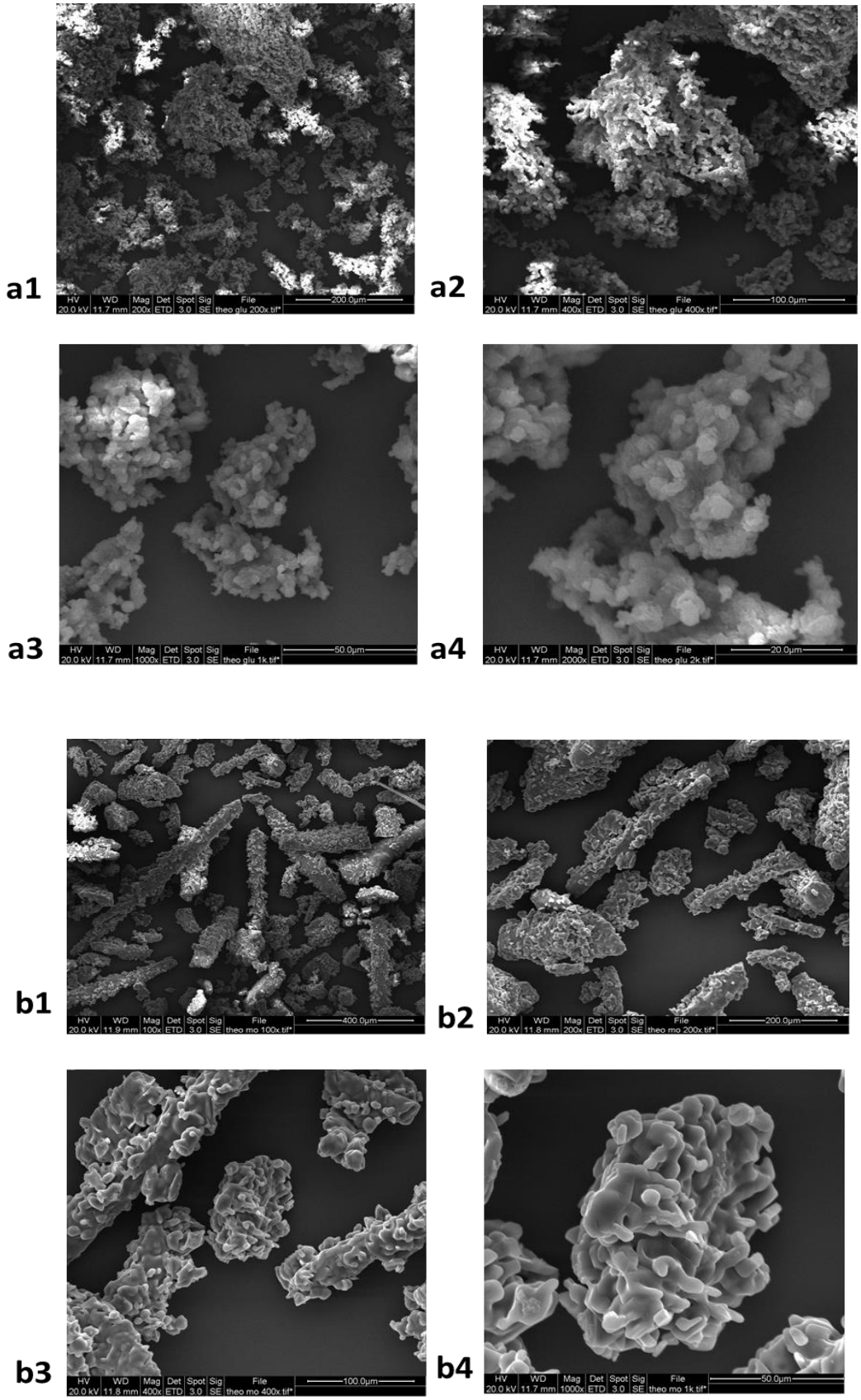

Figure 4.32. *SEM images of THEO: GLU 1:1 a1) 200x, a2) 400x, a3) 1000x, a4) 2000x; THEO: MO 1:1 b1) 100x; b2) 200x; b3) 400x; b4) 1000x*

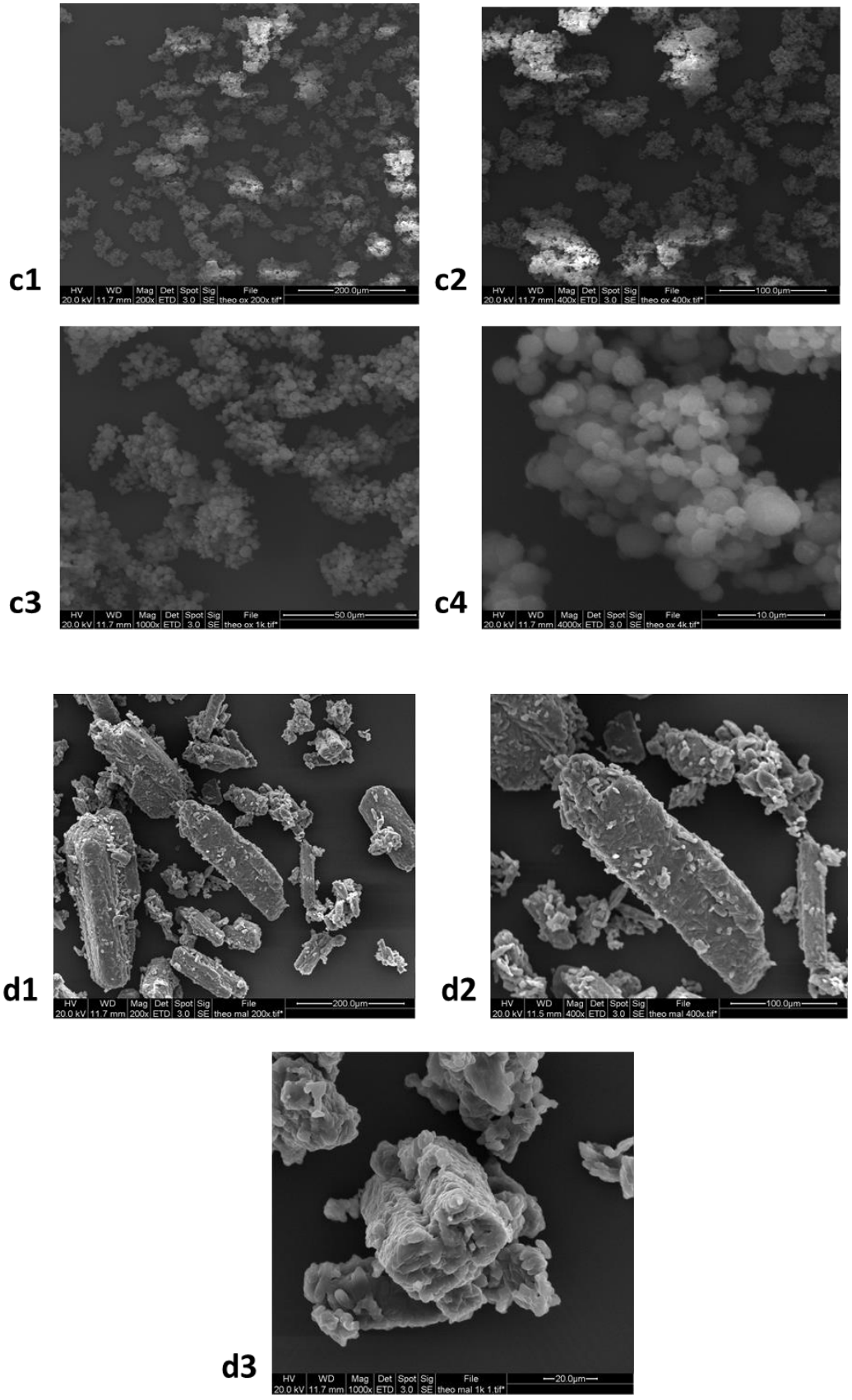

Figure 4.33 *SEM images of THEO:OX 2:1 c1) 200x, c2) 400x, c3) 1000x, c4) 4000x; THEO:MAL 1:1 d1) 200x, d2) 400x, d3) 1000x.*

Summary:

Unlike CAF, THEO being an analogue did not show a significant improvement in its solubility in the presence of dicarboxylic acids. In addition, its solubility in organic solvents was poor, apart from DMSO. DMSO could not be involved in this study due to its high boiling point which would have been difficult to process in the two evaporating techniques. Surprisingly, a 15 fold increase and 5 fold increase was observed in binary mixtures of 9:1 $CHCl_3$:MeOH and EtAc:MeOH, respectively. This increase in solubility was supported by Hansen's solubility parameters, namely, hydrogen bonding forces, polar bonding forces and dispersion forces present in a solvent blend. $CHCl_3$:MeOH solvent mixtures were utilised to form co-crystals of THEO and dicarboxylic acids. The rotavap successfully formed co-crystals with minor impurity of THEO anhydrate. Spray drying resulted into pure co-crystals overcoming the issue of starting component impurity.

CHAPTER 5

CARBAMAZEPINE AND SACCHARIN COCRYSTAL RESULTS

This chapter encompasses formation of co-crystals of carbamazepine (CBZ) and saccharin (SAC) via fast evaporating techniques. CBZ attains low solubility and high permeability belonging to BCS Class II category. It has been used as an analgesic and antiepileptic and is a very challenging API as it exists in four different polymorphic forms and readily converts into its dihydrate and solvate when exposed to water and other organic solvents, respectively (Tomaszewska et al., 2013). Its complex with saccharin as a co-crystal has been extensively studied to overcome the problems of solubility, polymorphism, scale-up and solvate formation. A solvent-free approach using twin-screw extruder for scale-up of CBZ: SAC 1:1 co-crystal, lead to its degradation and polymorphic transformation under high temperature conditions (Joshi, 2012). Therefore, this compound is also susceptible to degradation and requires controlled procedures. In this study, we investigate co-crystal formation via spray drying and obtain metastable FII of CBZ:SAC 1:1. Further tests were performed to analyse degradation upon storage which is supported by a hypothesis suggested in this study.

5.1. Introduction

Previous attempts of attaining CBZ: SAC 1:1 co-crystal have adopted various solution based strategies avoiding solvate mediated phase transformation (SPMT) such as solvent mixtures, anti-solvent, spherical co-crystallisation, sonic slurry and introduction of polymers. Hickey *et al*., (2007) examined CBZ's solubility in mixture of ethanol and methanol, and deduced a scale-up method without employing seeding. This was achieved in 62.5:37.5% v/v EtOH: MeOH mixture under reflux and then cooled; nucleating 1:1 co-crystal. Interestingly, application of polymorphs while evaporating equimolar solution of CBZ and SAC in ethanol resulted in crystal growth of new polymorphic form II of CBZ: SAC 1:1 co-crystal. Form II was favoured by evaporation of methanolic solution containing beads of poly(4-methyl-1-pentene) (Porter, Elie and Matzger, 2008).

Mixed solvents were also used to enhance the transformation kinetics, that is, trigger nucleation rate higher than in pure solvents. It was observed that solubility was enhanced in solvent mixtures compared to individual bad solvent and reduced incongruent solubility of the components. In addition, excess of CBZ in saturated solutions of SAC was subjected to ultrasound in order to overcome solvate formation. Solvent mixture of acetone and dioxane generated FII co-crystal and, ethylene glycol and DMSO led to FI co-crystal (Rager and Hilfiker, 2010). Also, sonic slurry method using equimolar ratio of CBZ and SAC in ethylacetate formed CBZ: SAC co-crystals (Tomaszewska *et al*., 2013). Another study utilised anti-solvent approach to achieve highly pure co-crystals and found methanol as a suitable solvent for dissolving CBZ and SAC, followed by co-crystal nucleation with addition of water as anti-solvent (Wang *et al*., 2013).

Spherical co-crystallisation (Chapter 1.3.2) investigated factors affecting supersaturation such as, proportions of good and bad solvents, introduction of bridging solvent and ratio of components used. DMSO, ethanol and methanol were selected as good solvents; where methanol depicts more congruent solubility for the pair (Table 5.1). Whereas, form II was generated at high co-former concentration, high proportion of bad solvent and delayed addition of bridging solvent; inducing high supersaturation levels (Pagire *et al*., 2013).

Table 5.1. *Solubility of CBZ and SAC in good solvents: DMSO, methanol and ethanol (Pagire et al., 2013).*

Solvent	**Solubility (M/L)**	
	CBZ	**SAC**
DMSO	0.345	5.397
Methanol	0.264	0.389
Ethanol	0.0804	0.268

Recently, solvent-free HME generated CBZ: SAC co-crystals using PAT tool to monitor temperature conditions and demonstrated increase in its dissolution rate which was dependant on temperature utilised (Moradiya *et al*., 2013). However, another HME study observed degradation under temperature and induced sheer conditions (Joshi, 2012). Hickey *et al*., (2007) earlier found equivalent chemical instability of CBZ: SAC to the marketed carbamazepine product (Tegretol) where both co-crystal and CBZ FIII in Tegretol depict slow degradation pattern at higher humidity conditions. Recently, CBZ: SAC conversion into its dihydrate form was inhibited using HPMC (hydroxypropyl methylcellulose) based tablets (Qiu and Li, 2015). In addition, the metastable co-crystal FII was kinetically favoured via roatavap with traces of FI (Bag, Patni and Reddy, 2011). This study investigates co-

crystallisation and chemical stability of CBZ: SAC using rotavap and spray dryer with range of solvents showing both congruent and incongruent solubility of the pair.

5.2. Crystal data

5.2.1. Carbamazepine, anhydrous Form III (CSD Ref: CBMZPN10)

Carbamazepine (CBZ) exists in four different polymorphic forms: two monoclinic, one trigonal and one triclinic. Out of these, P- monoclinic form (Form III) is the most thermodynamically stable polymorph. Polymorph Form IV is a C-lattice monoclinic form which is an enantiotropic pair to P-monoclinic form. Form I (triclinic) was observed during high temperature modification. Trigonal Form II is the least stable form and undergoes fast transformation. For all the forms, molecular conformation and hydrogen bonding pattern were similar and the difference only lies in the pattern of R_2^2 (8) carboxamide dimer units (formed via hydrogen bond between carboxamide donor and carbonyl acceptor). The unit cell of Form III is in $P2_1/n$ space group with cell length: a=7.53(1), b=11.15(2), c=15.47(2) and angle β= 116.2(1)^o (Harris *et al*., 2005; Grzesiak *et al*., 2003). The calculated PXRD pattern and crystal structure is shown in Figure 5.1and Figure 5.2, respectively.

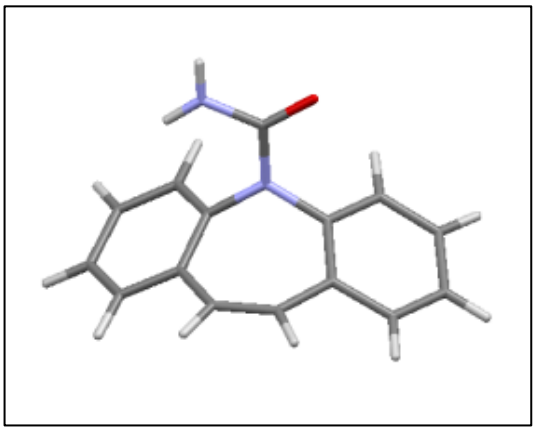

Figure 5.1. *Crystal structure of CBZ Form III (obtained from CSD).*

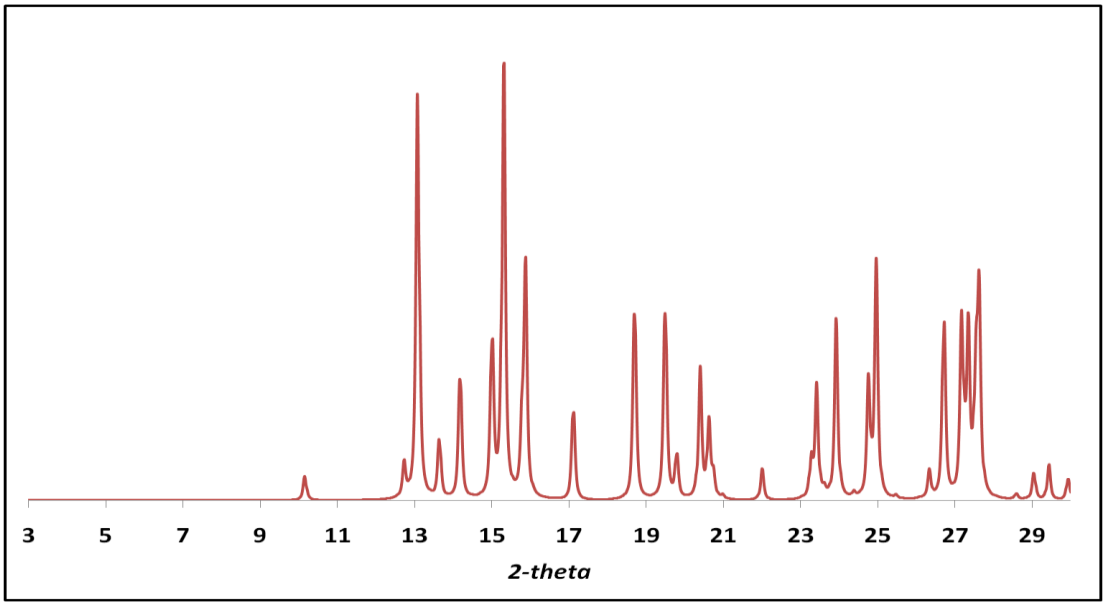

Figure 5.2. *PXRD pattern of CBZ Form III (CSD ref: CBMZPN10).*

5.2.2. Carbamazepine dihydrate (CSD Ref: FEFNOT02)

The dihydrate form is monoclinic with space group *P* $2_1/c$ and unit cell dimensions: a = 10.07(2) Å, b = 28.72(5) Å, c = 4.83(1) Å and β = 103.45^{o}. The asymmetric unit contains one CBZ molecule and two water molecule (Figure 5.3). The dimers of CBZ are linked via pair of hydrogen bond at N-H...O alongside hydrogen bond network between amino group and water molecules forming double layers. The hydrophilic water molecules are present at the core of the layer forming channels and the hydrophobic CBZ present outside (Figure 5.4) (Harris *et al*., 2005). The PXRD pattern for CBZ dihydrate is shown in Figure 5.5.

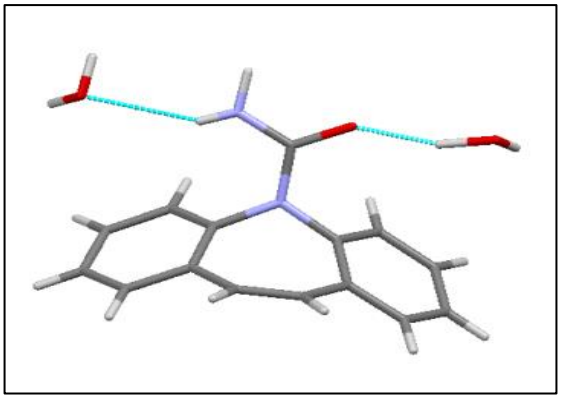

Figure 5.3. *Crystal structure of CBZ dihydrate (CSD Ref: FEFNOT02).*

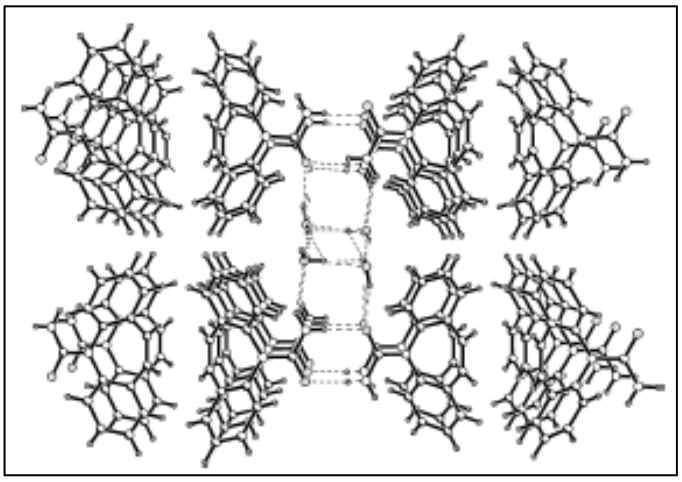

Figure 5.4. *CBZ dihydrate hydrogen- bonded network arrangement with stacks of CBZ molecules (Harris et al., 2005).*

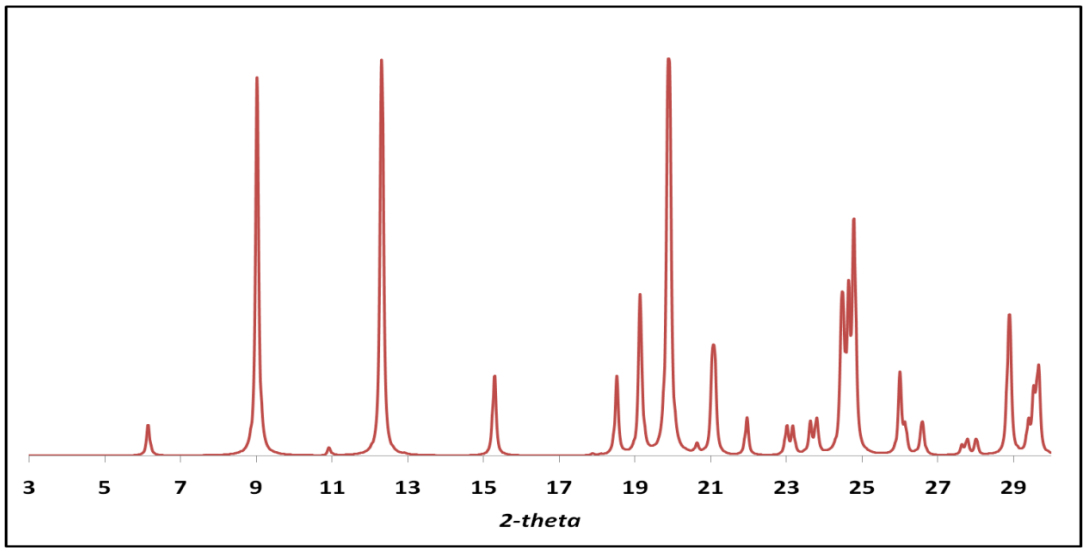

Figure 5.5. *PXRD pattern for CBZ dihydrate (CSD Ref: FEFNOT02).*

5.2.3. Saccharin (CSD Ref: SCCHRN)

The saccharin (SAC) crystal structure (Figure 5.6) is monoclinic and lies in P 2_1/c space group with a = 9.56(4) Å, b=6.91(3) Å, c=11.82(4) Å and β = 103.85(17)^o. The crystal structure forms centrosymmetric dimer molecules via N-H----O H-bond between keto oxygen and imide nitrogen of the five-membered rings. The hydrogen bond around the centre of symmetry forming the six-sided ring and narrow angle at C-S-N alleviate the strain from the molecule making it a planar structure (Okaya, 1969). Figure 5.7 illustrates the PXRD pattern for SAC.

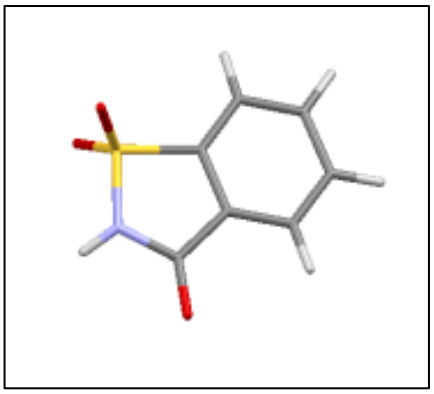

Figure 5.6. *Crystal Structure of SAC attained from CSD Ref: SCCHRN.*

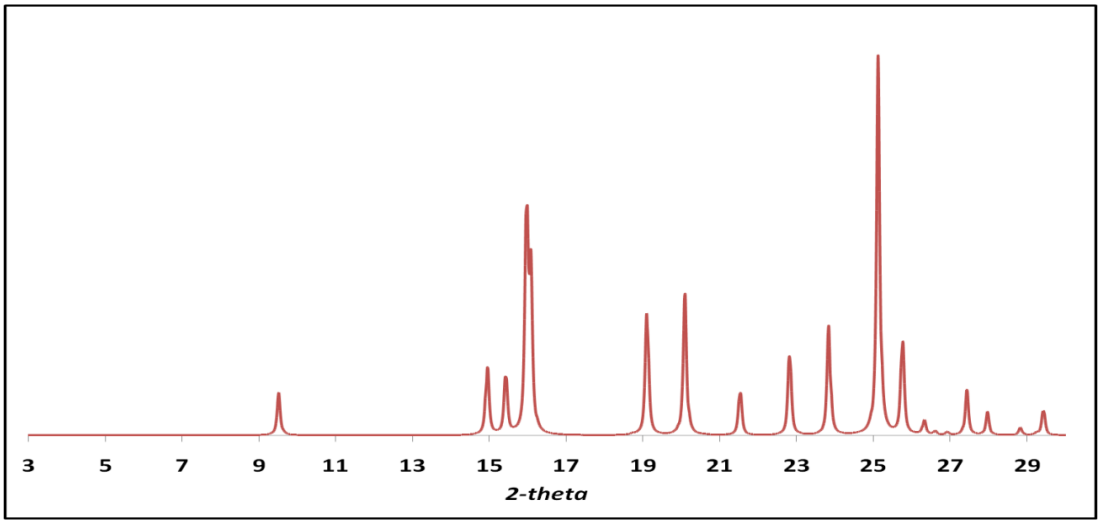

Figure 5.7. *Calculated PXRD pattern for SAC obtained from CSD Ref: SCCHRN.*

5.2.4. CBZ:SAC 1:1

5.2.4.1. CBZ: SAC 1:1 Form I

This triclinic form of CBZ: SAC 1:1 relates to space group *P-1* with unit cell dimensions: a 7.52(11) Å, b 10.45(15) Å, c 12.68(18) Å, and angles: α= 83.64(2)^{o}, β= 85.70(2)^{o}, and γ= 75.41(2)^{o} (CSD Ref: UNEZAO). The crystal packing consists of homosynthons between two CBZ carboxamide groups. Ana additional hydrogen bonded homodimer is present between SAC N-H and CBZ carboxyl group, and anti-NH of CBZ urea with S=O of SAC (Porter, Elie and Matzger, 2008). The crystal structure and PXRD data is shown in Figure 5.8 and Figure 5.9, respectively.

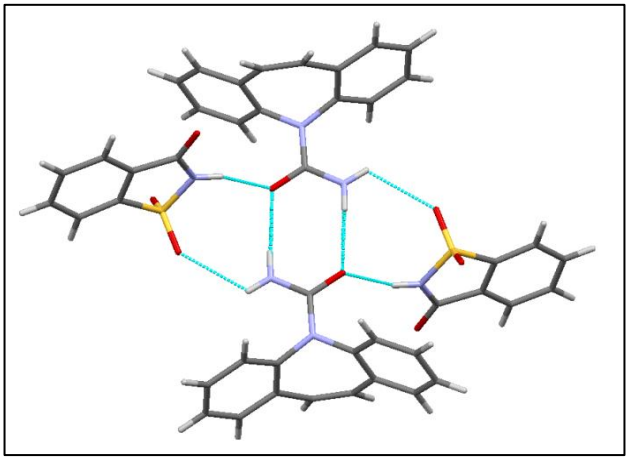

Figure 5.8. *Crystal structure of CBZ:SAC 1:1 Form I (CSD Ref: UNEZAO)*

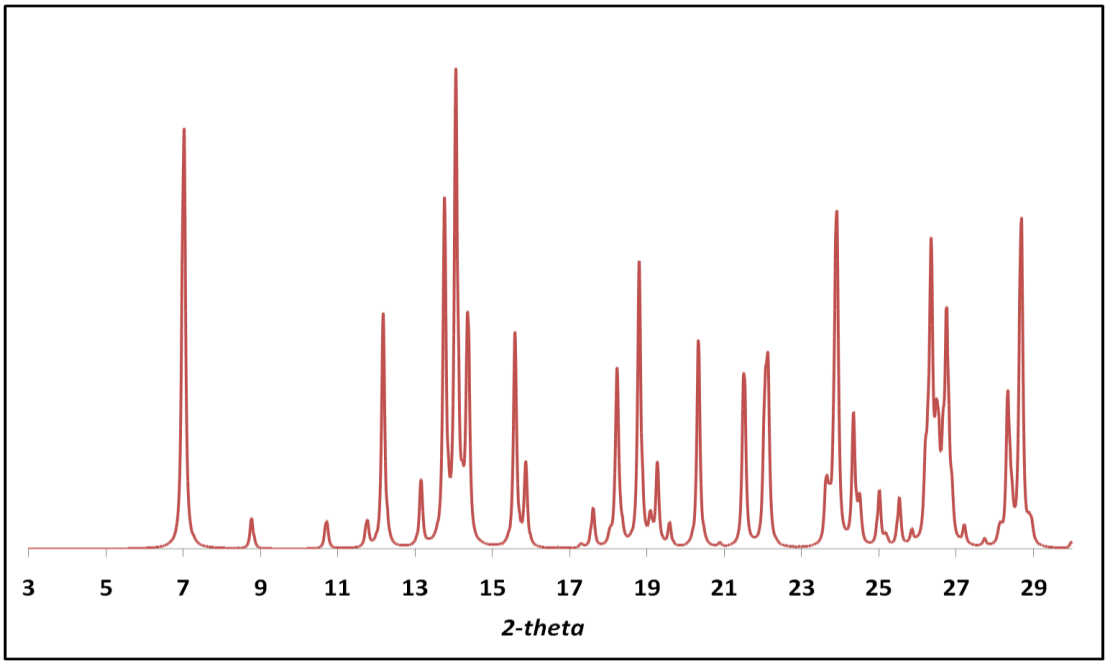

Figure 5.9. *PXRD pattern obtained from CSD for CBZ: SAC 1:1 Form I with characteristic peak at 2θ = 6.88°.*

5.2.4.2. CBZ: SAC 1:1 Form II

This monoclinic form lies in the space group C 2/c with unit cell dimensions: a= 35.72(10) Å, b= 6.84(2) Å, c=16.11(5) Å and β = 98.03(2)° (CSD Ref: UNEZAO01). The molecules form heterosynthon via H-bonding of CBZ (C=O) with SAC (N-H) and SAC (N-H) with CBZ (C=O). It further links anti N-H of CBZ urea with S=O of SAC (Porter, Elie and Matzger, 2008). The crystal structure and PXRD pattern collected are shown in Figure 5.10 and Figure 5.11, respectively.

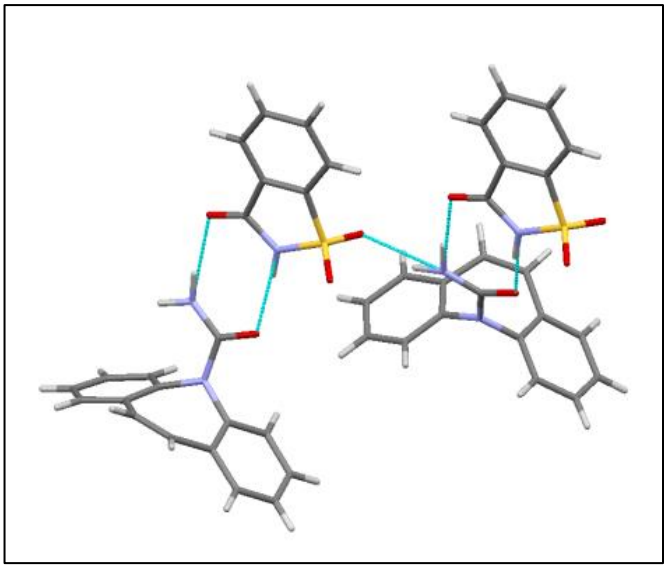

Figure 5.10. *Crystal structure of CBZ:SAC Form II (CSD Ref: UNEZAO01).*

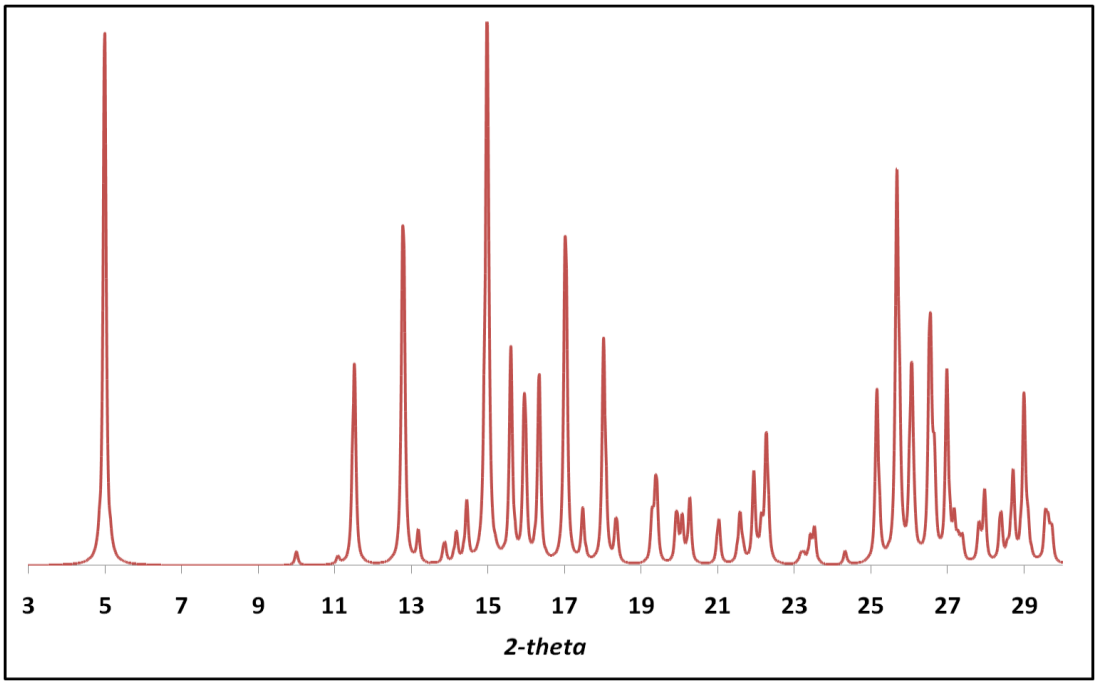

Figure 5.11. *PXRD data collected from CSD for CBZ: SAC Form II with characteristic peak at* $2\theta = 4.80^{o}$.

5.3. Fast evaporating techniques

Co-crystals of CBZ: SAC 1:1 were examined in three organic solvents: ethanol, methanol and acetone, and solvent mixture of ethanol and methanol (Hickey *et al*., 2007). A reverse proportion of this solvent mixture was also investigated, i.e. MeOH: EtOH 62.5:37.5% v/v.

5.3.1. Rotavap

Equimolar concentration of CBZ and SAC were dissolved in solvents and subjected to evaporation under rotavap. The vapour pressure of the three solvents was obtained using the Antoine's equation parameters as shown in Table 5.2. Unfortunately, the vapour pressure of the solvent mixtures could not be generated and was believed to lie between the individual solvent values.

Table 5.2. *Antoine's parameters obtained for each solvent to determine their vapour pressure (DDBST GmbH, n.d.).*

Solvent	**Antoine's equation parameters**		
	A	**B**	**C**
Methanol	8.1	1582.3	239.7
Acetone	7.1	1220.0	230.7
Ethanol	8.2	1642.9	230.3

The temperature and reduced vapour pressure applied to each solution are shown in Table 5.3. The calculated vapour pressure of EtOH and MeOH was 294 and 554 mbar at 50^{o}C, respectively. Therefore, pressure applied for solvent mixture was below the pressure values of the two solvents, i.e. 150 mbar to initiate rapid evaporation. PXRD results are illustrated in Figure 5.12.

Table 5.3. *Experiments conducted for the production of CBZ and SAC co-crystals via rotavap.*

Solvent	CBZ: SAC 1:1 Concentra-tion (%)	Bath Temp (^{o}C)	Vapour pressure of solvent (mbar)	Reduced Pressure Applied (mbar)	XRD
Acetone	2.6	50	814	150	***FI***
Methanol	4.2	50	554	200	***FI***
Ethanol	2.8	50	294	150	***FII + FI***
EtOH:MeOH (62.5:37.5)	5.6	50	--	150	***FI***
MeOH:EtOH (62.5:37.5)	5.6	50	--	150	***FI***
Form I-----FI; Form II------FII					

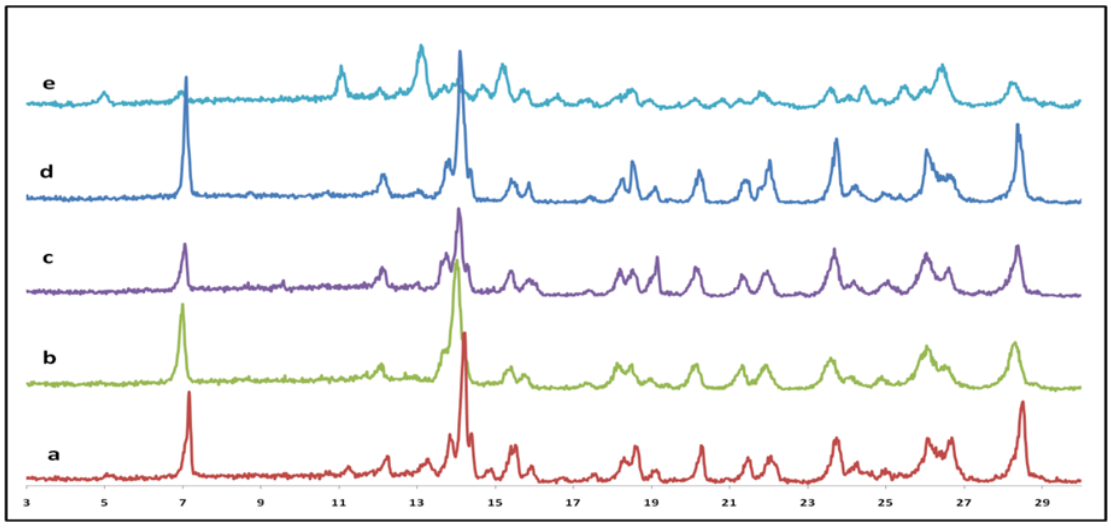

Figure 5.12. *Calculated PXRD pattern of CBZ:SAC 1:1 spray dried in a) acetone; b) MeOH; c) EtOH:MeOH; d) MeOH: EtOH; e) EtOH.*

All the solvents except ethanol, produced CBZ: SAC co-crystal FI. This result is in agreement with earlier rotavap attempt with dimorphic CBZ: SAC 1:1 in ethanol which generated metastable FII and traces of FI (Bag, Patni and Reddy, 2011). Although, fast evaporation under rotavap should favour metastable form and eradicate any solvent mediated transformation, solvent selection seems to be closely associated in generating kinetically-favoured metastable FII.

5.3.2. Preparation of phase pure co-crystals via spray drying

Solutions containing equimolar CBZ and SAC were spray dried using an inert loop at feed rate of 3mL/min, atomisation of 1.5 atm and aspiration rate of 60 m^3/hr. The inlet temperature conditions were varied with solvents used and their boiling points, accordingly. The outlet temperature varied between 35-45^oC. The co-crystals formed were characterised and compared using four different techniques: XRD, DSC, Raman and FTIR (Table 5.4). The observations from XRD, Raman and FTIR show a unanimous result, i.e. formation of metastable CBZ: SAC 1:1 FII. Whereas, DSC scan rate of 10^oC/min generated one endothermic peak in agreement with FI.

Table 5.4. *Spray dried results for CBZ: SAC co-crystals.*

Solvent	Feed (%)	Inlet Temperature (^oC)	XRD result	DSC slow 10^oC/min	DSC rapid 40^oC/min	Raman	FTIR
Ethanol	2.8	80	*FII*	*FI*	*FI+FII*	*FII*	*FII*
Methanol	3.3	70	*FII*	*FI*	*FI+FII*	*FII*	*FII*
		80	*FII*	*FI*	*FI+FII*	*FII*	*FII*
EtOH: MeOH	2.6	85	*FII*	*FI*	*FI+FII*	*FII*	*FII*
MeOH: EtOH	1.8	85	*FII*	*FI*	*FI+FII*	*FII*	*FII*
Acetone	2.8	65	*FII*	*FI*	*FI+FII*	*FII*	*FII*
	2.8	75	*FII*	*FI*	*FI+FII*	*FII*	*FII*
Form I -----FI; Form II------FII							

The XRD results in Figure 5.13 displays a characteristic peak at $2\theta = 4.80^o$ for FII in all solvents which do not comply with rotavap results. DSC results were somewhat misleading with an endothermic peak at 174^oC for CBZ: SAC FI (Good and Rodrigeuz-Hornedo, 2009) in all solvents at heating rate of 10^oC/min (Figure 5.14). The results did not coincide with DSC of CBZ which produces two endotherms. The first endotherm for CBZ form III (stable) lies between 162 and 175^oC, which transforms into Form I subsequently melting between 189 and 193^oC (Grzesiak *et*

al., 2003). A single endotherm for SAC at 224^{o}C (Wang *et al*., 2013) was also absent.

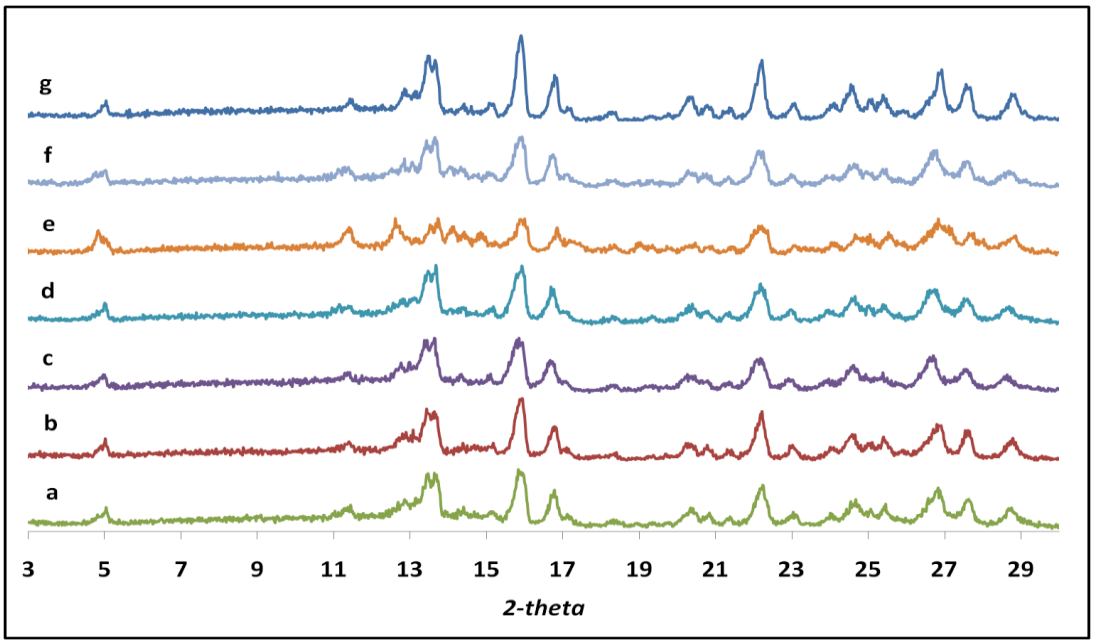

Figure 5.13. *PXRD pattern of CBZ:SAC 1:1 co-crystals spray dried using a) MeOH @ 70^{o}C; b) MeOH @ 80^{o}C; c) acetone @65^{o}C; d) acetone @ 75^{o}C; e) EtOh:MEOH @ 85^{o}C; f) MeOH:EtOH @85^{o}C; g) EtOH @ 80^{o}C.*

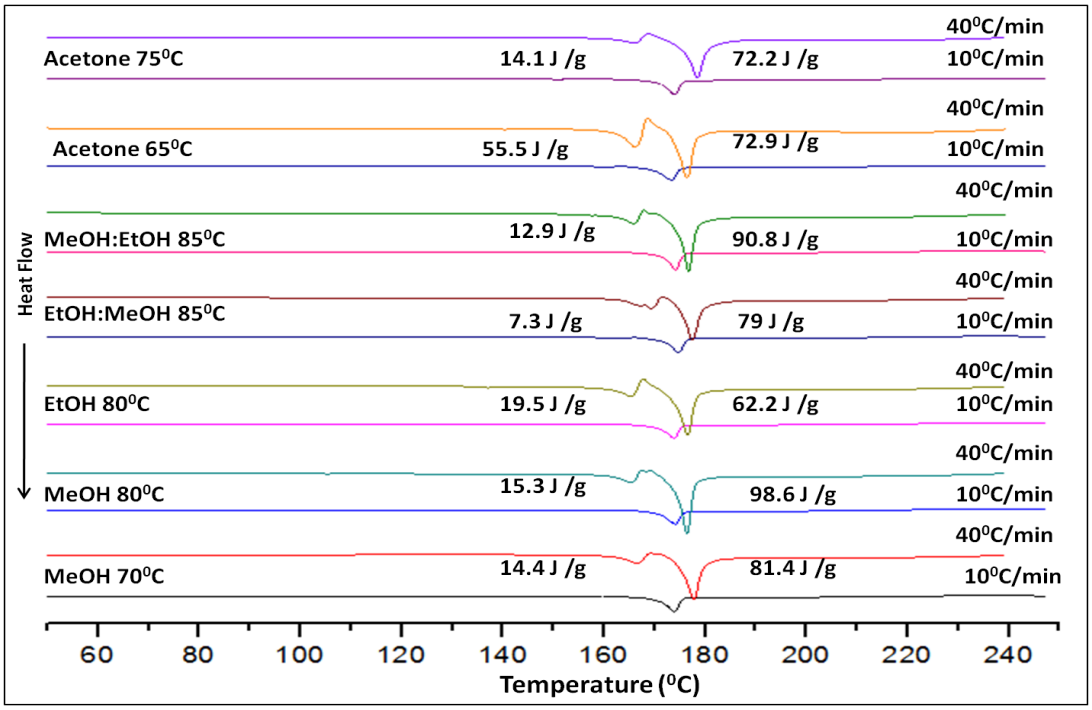

Figure 5.14. *DSC endotherms obtained for CBZ and SAC 1:1 spray dried solutions at slow and fast heating rates, i.e., 10^{o}C/min and 40^{o}C/min, respectively.*

Due to disparity in results, a fast DSC scan at 40^{o}C/min was also investigated which liberated two endothermic peaks at around 166^{o}C and 176^{o}C as shown in Figure 5.14. These results correspond to DSC trace for FII followed by FI. Similar transition was observed for DSC scan of CBZ: SAC FII discovered by polymer induced heteronucleation from a single solvent (Porter, Elie and Matzger, 2008).

Prototype of CBZ: SAC FI for comparison

A prototype of CBZ: SAC 1:1 FI was prepared using solvent method by Hickey *et al*., (2007) (Chapter 2.4.6) for comparison with the predicted FII results above. The PXRD and DSC results for FI are shown in Figure 5.16 and Figure 5.15, respectively. The PXRD pattern displays a distinct characteristic peak at 2θ= 6.88^{o} confirming formation of FI. In addition, the DSC results at 10^{o}C/min and 40^{0}C/min produced only one endothermic peak of 174^{o}C and 177^{o}C, respectively. Due to very fast scan rate of 40^{o}C/min, a slight forward shift in the melting peak was observed. In contrary, the spray dried results gave two endothermic peaks: FII melt followed by FI endotherm. This could be due to thermally induced polymorphic transformation of compounds into their stable form when subjected to DSC. Hence, DSC results were not a true indication of the product obtained.

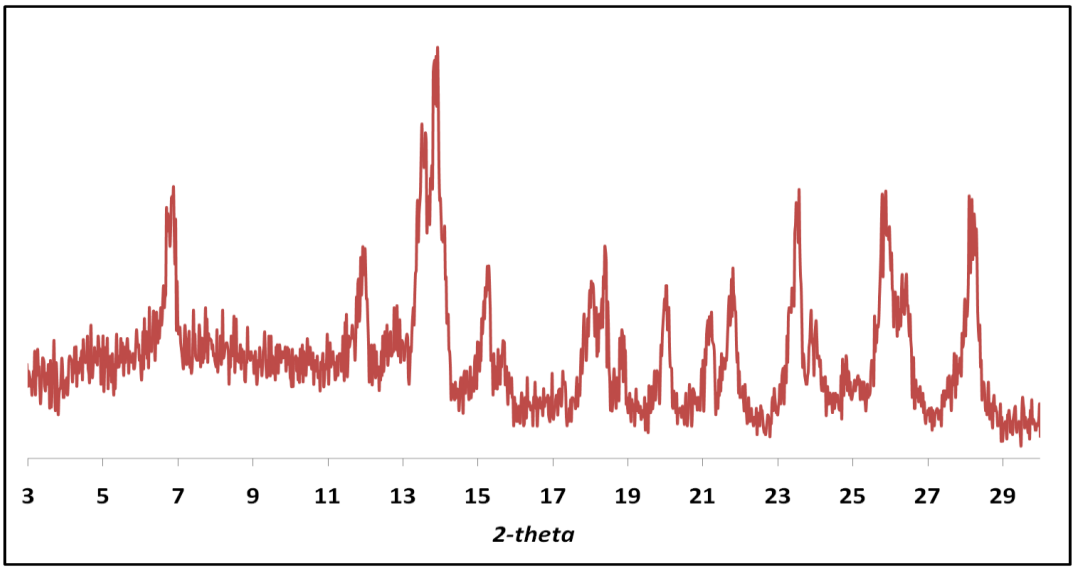

Figure 5.15. *PXRD for the prototype, CBZ: SAC 1:1 FI formed via solvent mixture.*

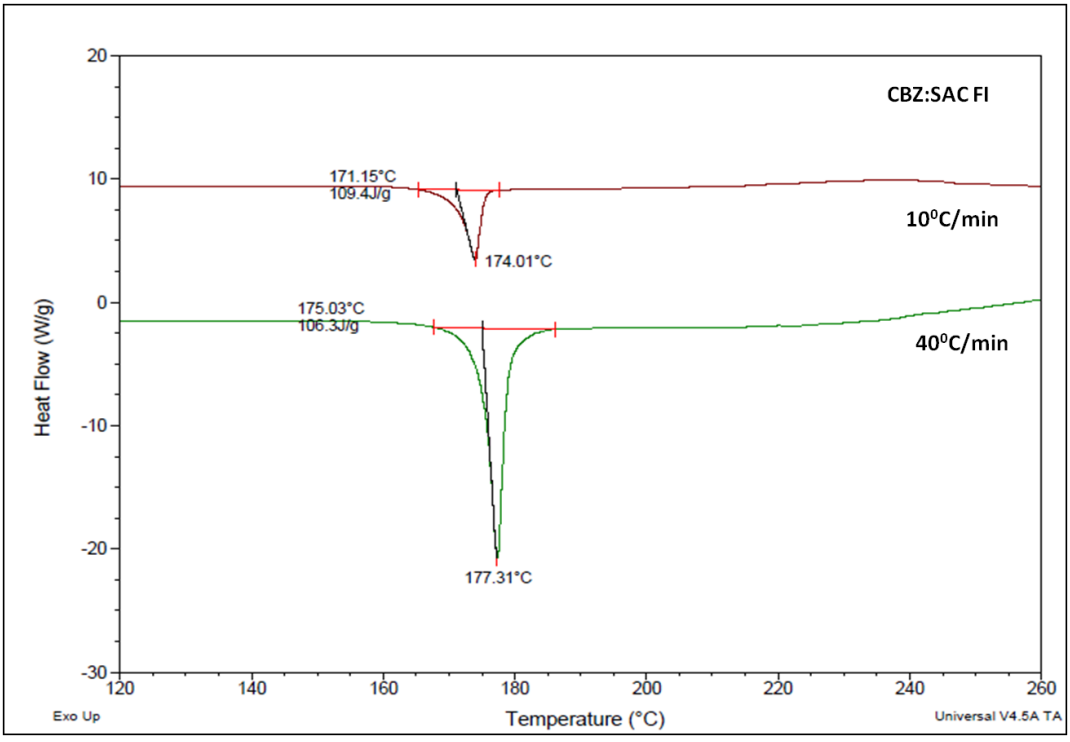

Figure 5.16. *DSC thermogram for CBZ: SAC FI prototype at slow and fast scan rate for comparison with spray dried results.*

FTIR

FTIR was used to examine the interaction between molecular components of CBZ, SAC and the co-crystal formed. The structural packing of CBZ, SAC and CBZ: SAC 1:1 FI form homomeric H-bonding between two dimers where N-H donor binds to C=O acceptor (Figure 5.17). Additional bonding with SAC is observed in co-crystal FI, where the homomeric bonding of SAC (SAC N-H---C=O SAC) gets replaced by heteromeric bonding (SAC N-H---C=O CBZ), leaving SAC's carbonyl group free. In addition, SAC's S=O forms weak hydrogen bonds with CBZ's N-H and SAC's C-H (Jayasankar *et al*., 2006).

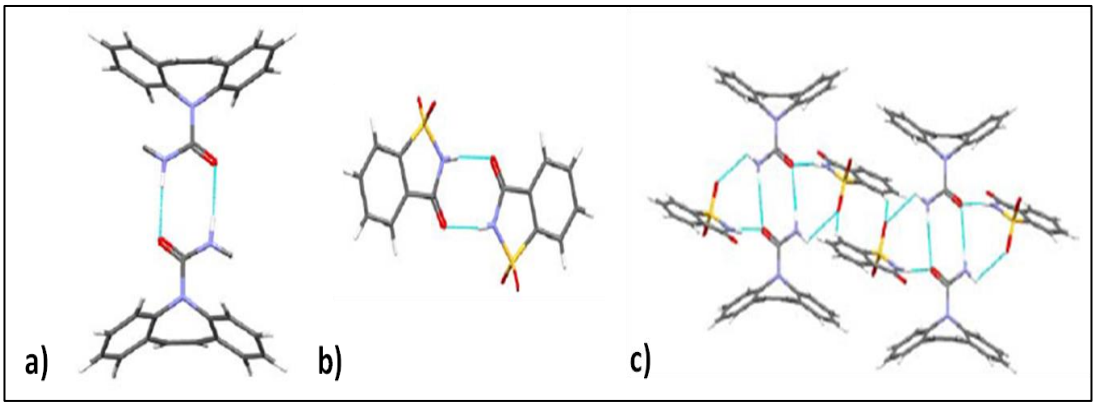

Figure 5.17. *Molecular interaction in crystal structures of a) CBZ; b) SAC and c) CBZ: SAC FI (Jayasankar et al., 2006).*

On the other hand, FII CBZ: SAC co-crystal forms heteromeric dimer of CBZ and SAC (explained in crystal data) with additional H-bond between anti N-H of CBZ and S=O of SAC (Porter, Elie and Matzger, 2008). Due to heterosynthon formation, carbonyl group of SAC is not free and SAC's S=O forms only one weak H- bond with N-H of CBZ. The FTIR spectra observed shows difference in various bond stretches (Figure 5.18).

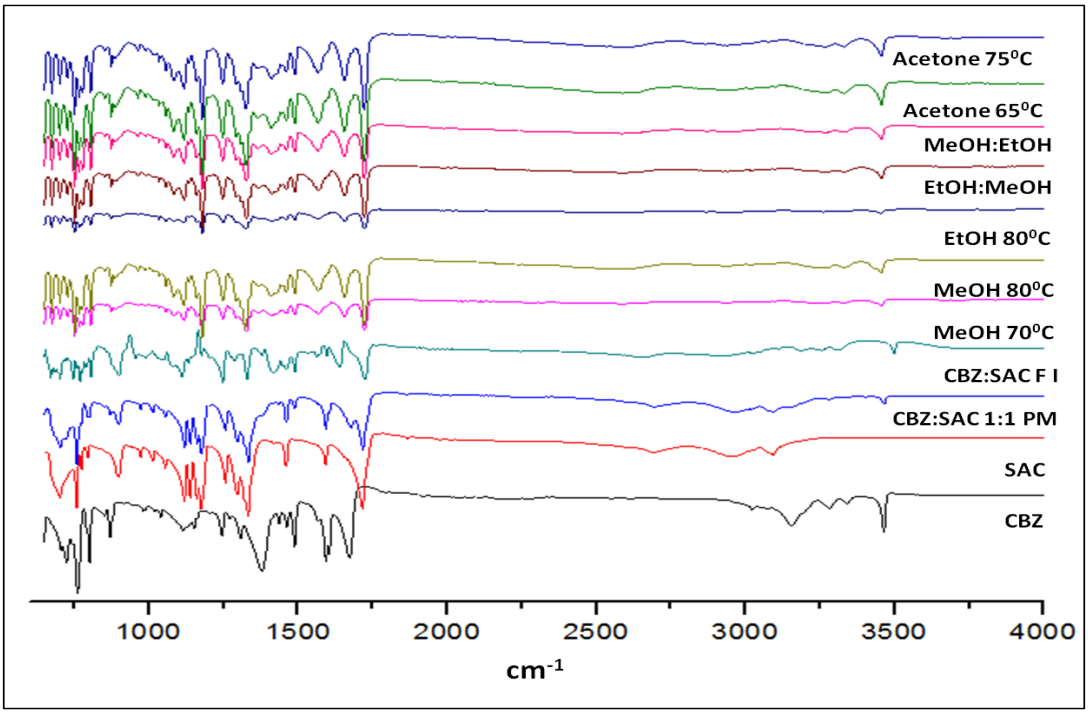

Figure 5.18. *FTIR spectra of CBZ: SAC spray dried co-crystals compared to pure CBZ, SAC, CBZ:SAC 1:1 physical mixture (PM) and CBZ:SAC 1:1 FI.*

FTIR spectra of SAC at 3098 and 1716 cm^{-1} relates to NH and C=O stretch of secondary amide. The SO_2 symmetric and asymmetric stretches were observed at 1333 and 1775 cm^{-1}. In contrary, peak shift of free C=O of SAC and H-bonded C=O of CBZ was observed at 1726 and 1639 cm^{-1} for co-crystal FI. Whereas, the spray dried FII co-crystals gave carbonyl stretches for SAC and CBZ at 1721 and 1655 cm^{-1}. The peak shift of NH stretch from 3464 cm^{-1} (CBZ) to 3498 cm^{-1} (CBZ: SAC FI) is in agreement with the previous study (Jayasankar *et al*., 2006).

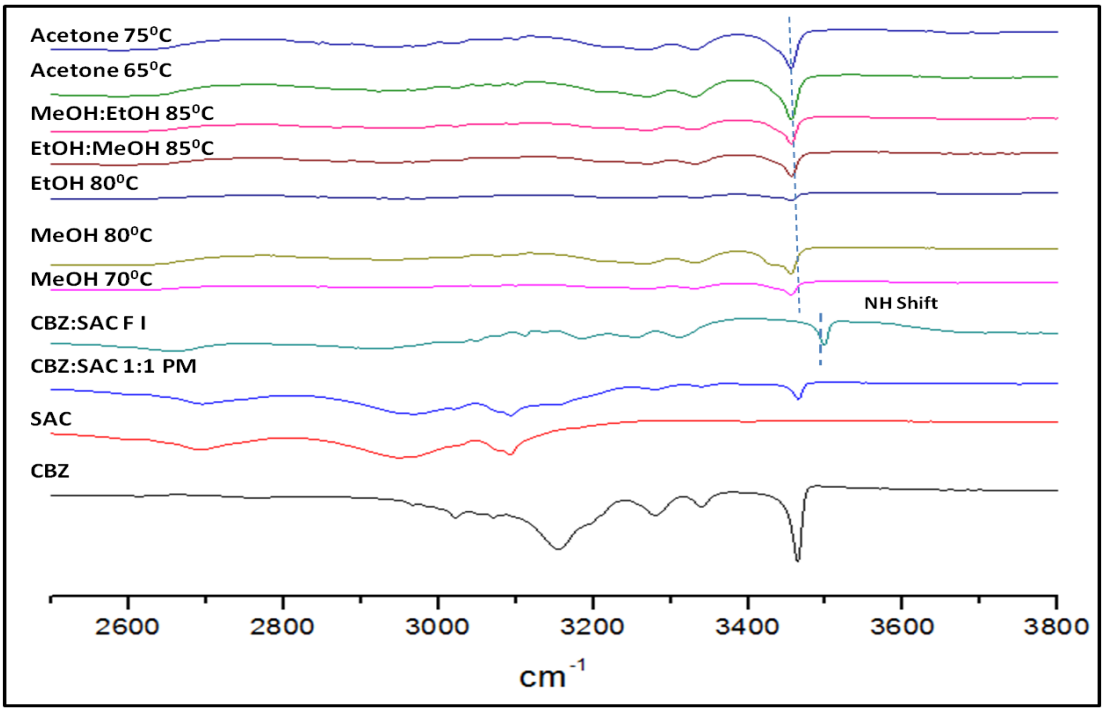

Figure 5.19. *FTIR N-H band spectra for spray dried co-crystals.*

Table 5.5. *FTIR N-H band stretches from 3400 to 3250 cm^{-1}.*

Sample	**N-H Bands (cm^{-1})**		
CBZ	3464	3354	3280
SAC			3098
PM	3464	3350	3282
CBZ:SAC FI	3498	3313	3184
MeOH @70°C	**3456**	**3330**	**3264**
MeOH @80°C	**3455**	**3330**	**3263**
EtOH	**3456**	**3330**	**3268**
EtOH: MeOH	**3456**	**3330**	**3268**
MeOH: EtOH	**3456**	**3331**	**3268**
Acetone @65°C	**3456**	**3331**	**3269**
Acetone @75°C	**3455**	**3331**	**3268**

A drastic change in N-H vibrational bands of CBZ: SAC FI (3498 and 3313 cm^{-1}) and spray dried co-crystals (3455 and 3330 cm^{-1}) was observed (Table 5.5 and Figure 5.19), depicting the formation of co-crystal FII. Similar decrease in N-H vibrational band energy of co-crystal FII was noticed in comparison to FI, as a result of shorter H-bond distances in FII (Porter, Elie and Matzger, 2008). None of the N-H

vibrational stretches for spray dried co-crystals coincided with the starting components. The N-H stretches of CBZ: SAC 1:1 physical mixture was similar to CBZ: SAC 1:1 FI co-crystal.

Raman

Analysis of CBZ, SAC, CBZ: SAC 1:1 FI and FII co-crystals by Raman spectroscopy produced spectra with difference in their peak positions and intensities. Therefore, spectral region between 1500 and 1700 cm^{-1} was evaluated for any polymorphic variation (Figure 5.20). The vibrational bands of the two co-crystal polymorphs were quite closely related and compared to CBZ as shown in the table below.

Table 5.6. *Raman bands to molecular vibrations for CBZ, CBZ: SAC FI and CBZ: SAC FII (O'Brien et al., 2004).*

Vibrational mode	**CBZ**	**CBZ:SAC 1:1 FI**	**CBZ:SAC 1:1 FII**
(C=O) stretch	absent	1724**w**	1718**w**
non aromatic (C=C) stretch	1624**s**	1624**s**	1620**s**
Secondary amide (N-H) bend	1600**w sh**	1598**s**	1599**m sh**
aromatic (C=C) stretch	1566**s**	1566**s**	1566**s**
aromatic (C-H) bend, in-plane	1022 and 1024**m sh**	1028**m sh**	1028**m sh**
Tertiary amide (C-N-C) stretch	723**m**	697 and 705**w sh**,721**m**	730**m,** 703**m**
s: strong; **m**: medium; **w**: weak; **sh**: shoulder			

The carbonyl (C=O) vibrational stretch was a good indicator of CBZ: SAC co-crystal formation. This stretch was higher for CBZ: SAC 1:1 FI (1724 cm^{-1}) compared to spray dried CBZ: SAC 1:1 FII (1718cm^{-1}), as observed earlier in co-crystals from solvent mixtures (Rager and Hilfiker, 2010). The secondary amide bend intensity at 1600 cm^{-1} increases in co-crystals as opposed to weak shoulder

observed in CBZ. The amide bend of the two co-crystal forms are distinguishable as FII bend forms a medium frequency shoulder on C=C non- aromatic stretch and FI produces a strong N-H bend.

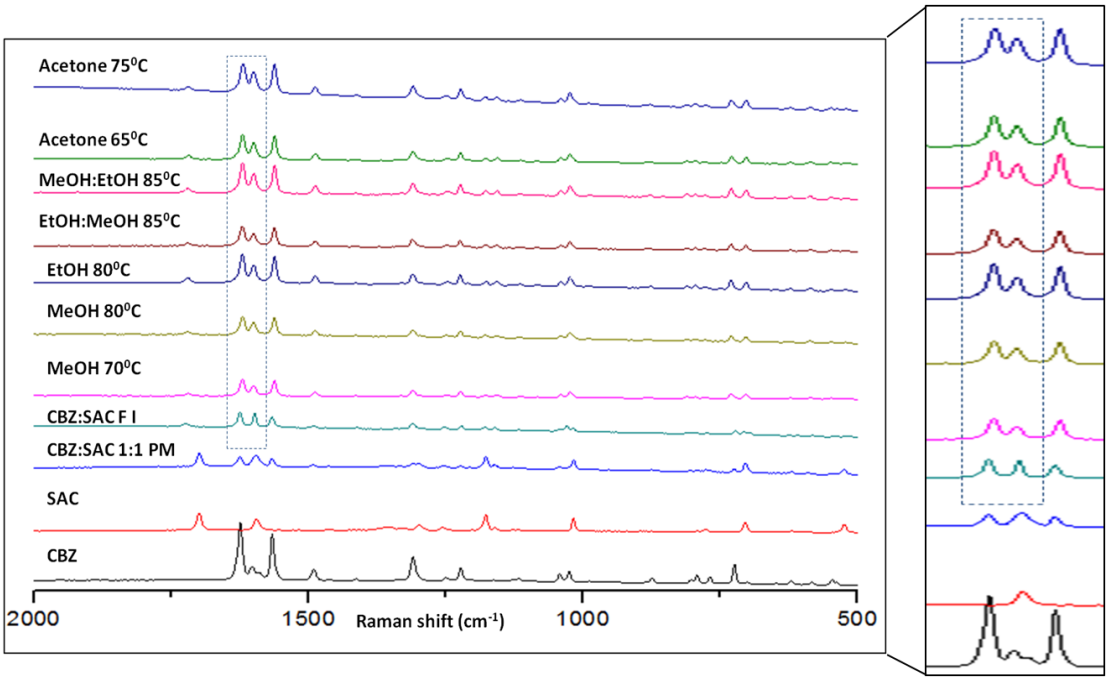

Figure 5.20. *Raman spectra comparison of the spray dried co-crystal and CBZ:SAC 1:1 FI.*

The above results obtained from XRD, Raman and FTIR are in good agreement with the formation of CBZ: SAC 1:1 FII via spray drying. DSC results were ambiguous due to thermally induced polymorphic transition. The CBZ: SAC co-crystal forms generated via two closely related fast –evaporation techniques varied and therefore, suggests that spray dryer is a better technique for production of co-crystals that require polymorphic control and always favours the metastable form.

5.3.3. Chemical stability

According to the United States Pharmacopoeia (USP) standards for chemical substances and drug preparations, the limit set for CBZ related impurities is not more than 0.2% (USP Convention, 2015). The impurity examined in this study is a CBZ

degradation product, iminostilbene. The degradation into iminostilbene of the spray dried product was examined using HPLC over a period of 5 months. A calibration curve was constructed to determine the amount of degraded product as shown in Figure 5.21.

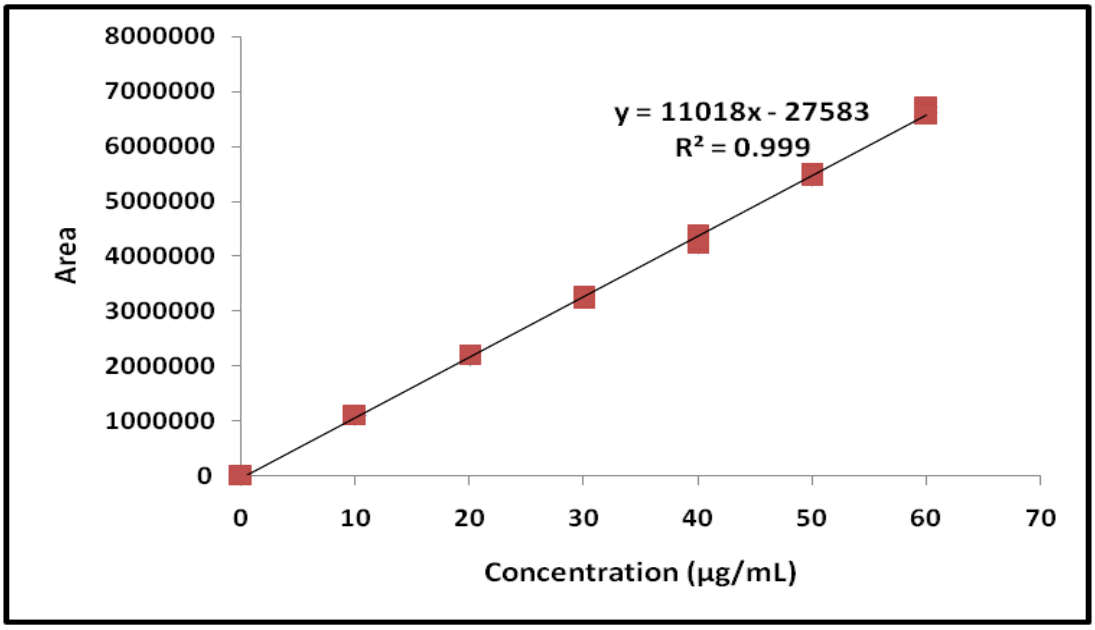

Figure 5.21. *Calibration curve for iminostilbene concentration against the peak area obtained from HPLC analysis.*

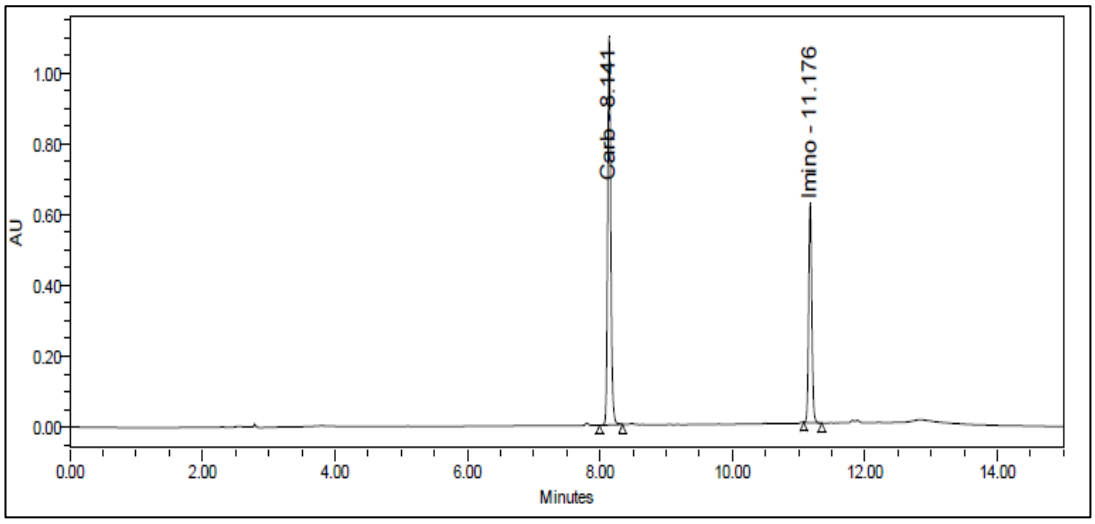

Figure 5.22. *Chromatogram for CBZ and iminostilbene showing peak elution at 8 and 11.2 minutes, respectively.*

Figure 5.22 shows two well separated peaks obtained from the developed HPLC method for CBZ and its degradate at retention times of 8 and 11.2 mins, respectively. The % iminostilbene impurity in each sample was calculated after obtaining their peak area values at three time intervals: 1st month, 3rd month and 5th month (Table 5.7).

Table 5.7. *Degradation results: Percentage iminostilbene in spray dried sample.*

Spray dried CBZ:SAC	**Iminostilbene (%)**		
	Month 1	**Month 3**	**Month 5**
MeOH @70^oC	**0.049**±1.6E-03	**0.064**±2.3E-03	**0.132**±3.2E-05
MeOH @80^oC	**0.072**±3.8E-03	**0.090**±1.5E-03	**0.111**±5.8E-04
EtOH@80^0C	**0.019**±1.4E-04	**0.074**±6E-04	**0.111**±9.9E-04
EtOH: MeOH@85^oC	**0.004**±6.1E-05	**0.079**±1.5E-03	**0.169**±3.3E-05
MeOH: EtOH@85^oC	**0.013**±3.4E-04	**0.073**±9.4E-04	**0.132**±1.9E-04
Acetone 65^oC	**0.024**±1.8E-04	**0.085**±5.2E-04	**0.117**±1.2E-03
Acetone 75^oC	**0.102**±2.6E-03	**0.125**±1.0E-03	**0.142**±9.8E-03

The HPLC results show the presence of iminostilbene in all the samples which gradually increases over time. The amount of degradate observed after one month was lowest in case of sample obtained from solvent mixture, EtOH: MeOH. However, the impurity levels rose to same amounts as others on the 3rd and 5th month. For the first three months, the % impurity observed was highest in co-crystal obtained from acetone at high temperature of 75^{o}C. But, over 5 month period, the results were quite identical for all the samples ranging from 0.11 to 0.17%. In earlier studies, process parameters were observed to play a significant role in CBZ's degradation. In case of twin screw extruder, high temperature conditions and heat imparted due to shear at the screw surface led to impurity formation (Joshi, 2012). Likewise, parameters such as high temperature, microwave irradiation power, and high exposure time elevated degradation levels in microwave-assisted co-

crystallisation of CBZ: SAC (Pagire *et al*., 2013). In addition, ultrasound-assisted slurry co-crystallisation also attributed to CBZ degradation below the USP levels (Apshingekar, 2014). However, these studies did not examine the increase in impurity levels over prolonged time period. Conversely, comparable and gradual increase in iminostilbene levels obtained in spray dried co-crystals dictates its non-dependency on process parameters alone, but rather an additional influence due to external factors or inherent property of the compound.

This gradual increase in iminostilbene content during storage is supported by the hypothesis that CBZ undergoes a two-step conversion into iminostilbene under atmospheric humid conditions and sunlight. The first step conversion involves hydrolysis of CBZ, splitting the primary amide and forming carboxylic acid (Figure 5.23) (Avagadro, 2000-2007). The second step is followed by simultaneous decarboxylative reduction induced by factors such as sunlight and temperature. The latter was implicated in a study where photoredox catalysis was induced by visible light causing excitation (single electron transfer) in α-amino acids leading to its decarboxylation (Cassani, Bergonzini and Wallentin, 2014).

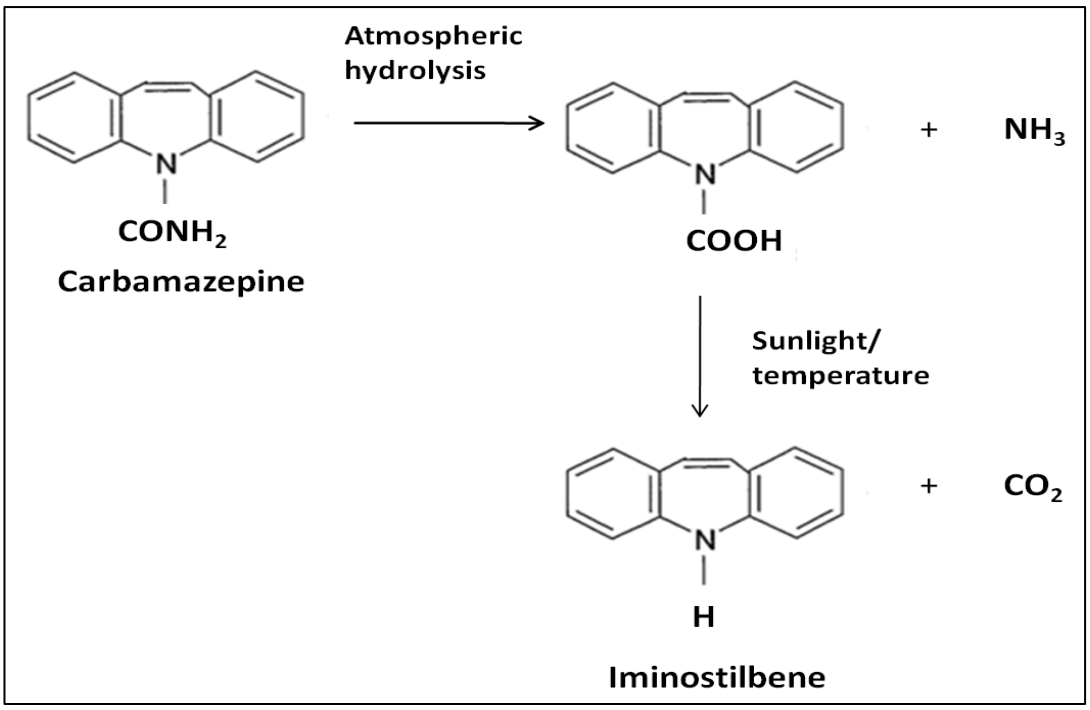

Figure 5.23. *Proposed two-step degradation of CBZ due to atmospheric conditions.*

3.3.4 Physical property – dispersive surface energy

Inverse gas chromatography (iGC) was utilised to investigate the impact of feed rate on the measured dispersive surface energy of CBZ: SAC co-crystals generated via spray drying. The experimental set-up targets a range of surface coverages to obtain comparable results between samples, overcoming any differences in probe coverage due to variation in particle properties such as surface area. The dispersive component of surface energy depicts the apolar interactions due to the forces between two dipoles calculated from the retention time of n-alkane probes. The impact of various feed rates on the surface property of CBZ: SAC co-crystals are shown in Figure 5.24. A reduction in dispersive surface energy was observed with the increase in feed rate of the spray dryer. This shift is attributed to change in surface area due to variation in particle size distribution, altering the probe interaction. For instance, large particles with low surface area will have less energetic sites available for interaction.

Moreover, low probe interaction also signifies low exposure to crystalline sites with higher energy. The shape of heterogeneity distribution determines the availability of range of energetic sites, suggesting the increase in higher energy sites at 0% coverage. It has been proposed that increase in surface area leads to probe interaction with narrow range of high energy sites, thereby increasing its mean dispersive surface energy value (Gamble *et al*., 2012). The lowest feed rate of 1ml/min would further narrow down probe interaction and result in large number of sites available for interaction.

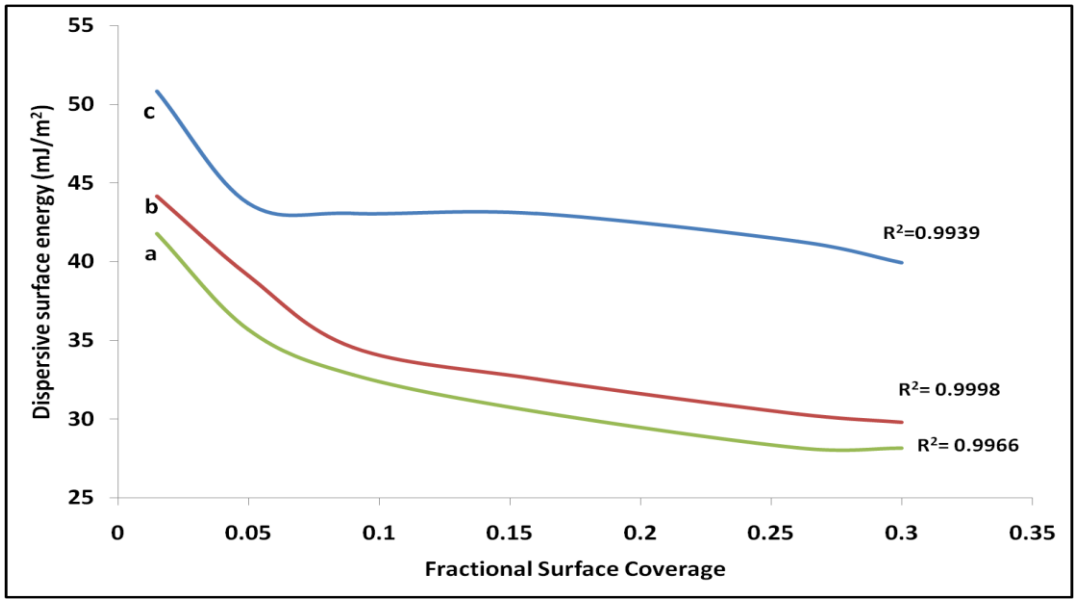

Figure 5.24. *Surface energy heterogeneity graph showing dispersive surface energy over fractional surface coverage of spray dried CBZ: SAC 1:1 sample processed at feed rates: a) 3 mL/min; b) 2 mL/min and c) 1 mL/min.*

The particle size distribution (PSD) for CBZ:SAC co-crystal are presented in Table 5.8. The results obtained for all samples were quite similar with X_{50} values lying between 4 and 6 µm. However, the particle dimension corresponding to 90% undersize distribution (X_{90}) was high for EtOH: MeOH, resulting in an overall high VMD value. The distribution graph in this case was distorted (Appendix V), and

SEM image (Figure 5.27, b) illustrate a unique morphology where small circular particles are embedded on a big irregular shaped particle. The particles obtain more or less of a spherical geometry for other samples as seen via SEM images (Figure 5.28). Therefore, the PSD results for CBZ: SAC sample is valid except for co-crystals via EtOH:MeOH. The microscopic images further supporting PSD has been demonstrated in Figure 5.25 and Figure 5.26.

Table 5.8. *Particle size distribution of CBZ: SAC spray dried samples.*

Conc. (%)	**Particle size distribution (µm) Method: Lens- R_1 (0.1-35µm) Dispersive pressure: 4bar 40mm/s**			**Particle volume over particle size**
	X_{10}	X_{50}	X_{90}	*VMD (Volume mean diameter in µm)*
MeOH 3 mL/min@70^{0}C	0.80±0.04	4.29±0.20	12.53±1.43	5.85
MeOH 3 mL/min@80^{0}C	0.81±0.04	4.27±0.24	12.59±2.19	5.81
MeOH 1mL/min	1.30±0.07	5.65±0.47	15.57±1.05	7.23
EtOH	0.81±0.00	4.35±0.28	12.29±2.59	5.73
EtOH: MeOH	0.89±0.02	4.51±0.16	26.59±0.96	9.62
MeOH: EtOH	0.85±0.01	4.43±0.00	12.72±1.06	5.95
Acetone @65^{0}C	1.25±0.05	3.88±0.21	7.47±0.87	4.24
Acetone @75^{0}C	1.13±0.08	4.22±0.02	9.64±0.34	5.38

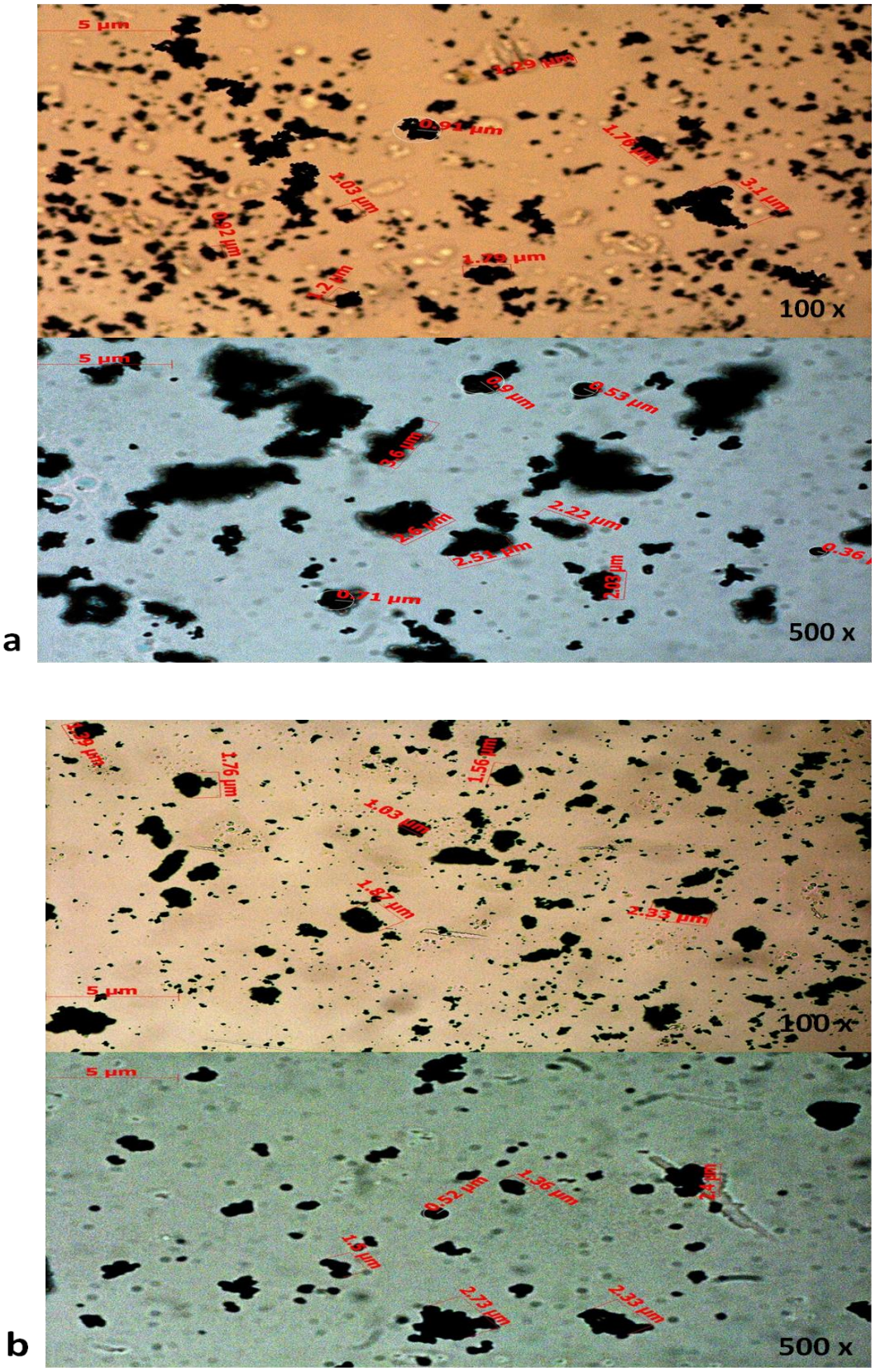

Figure 5.25. *Microscopic images of CBZ:SAC co-crystals: a) MeOH; b) EtOH:MeOH*

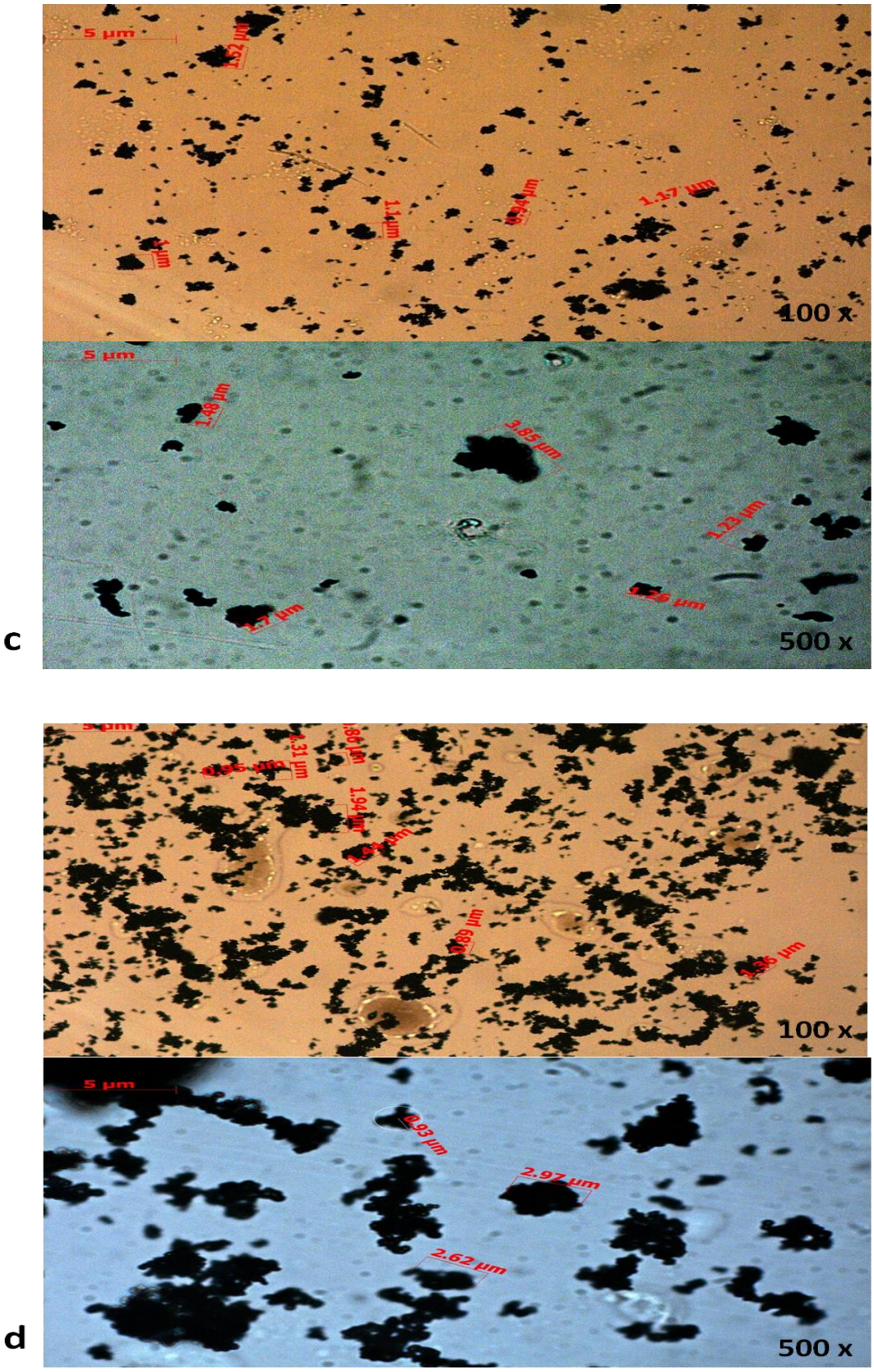

Figure 5.26. *Microscopic images of CBZ:SAC co-crystals: c) MeOH:EtOH; d) acetone @65°C.*

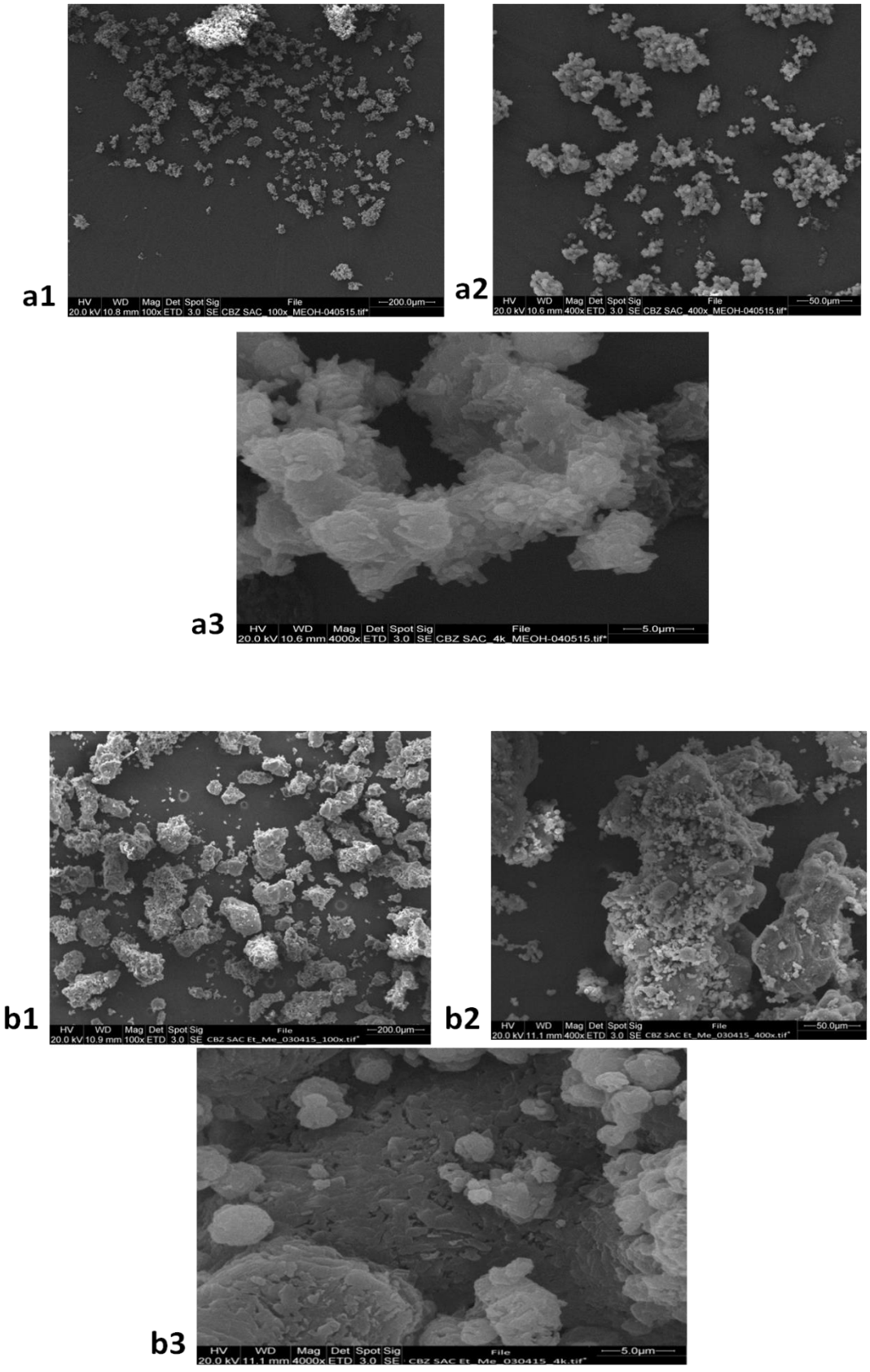

Figure 5.27. *SEM images for CBZ: SAC co-crystals: a) MeOH: a1- 100x, a2- 400x, a3- 4000x; b) EtOH:MeOH: b1-100x, b2-400x, b3-4000x.*

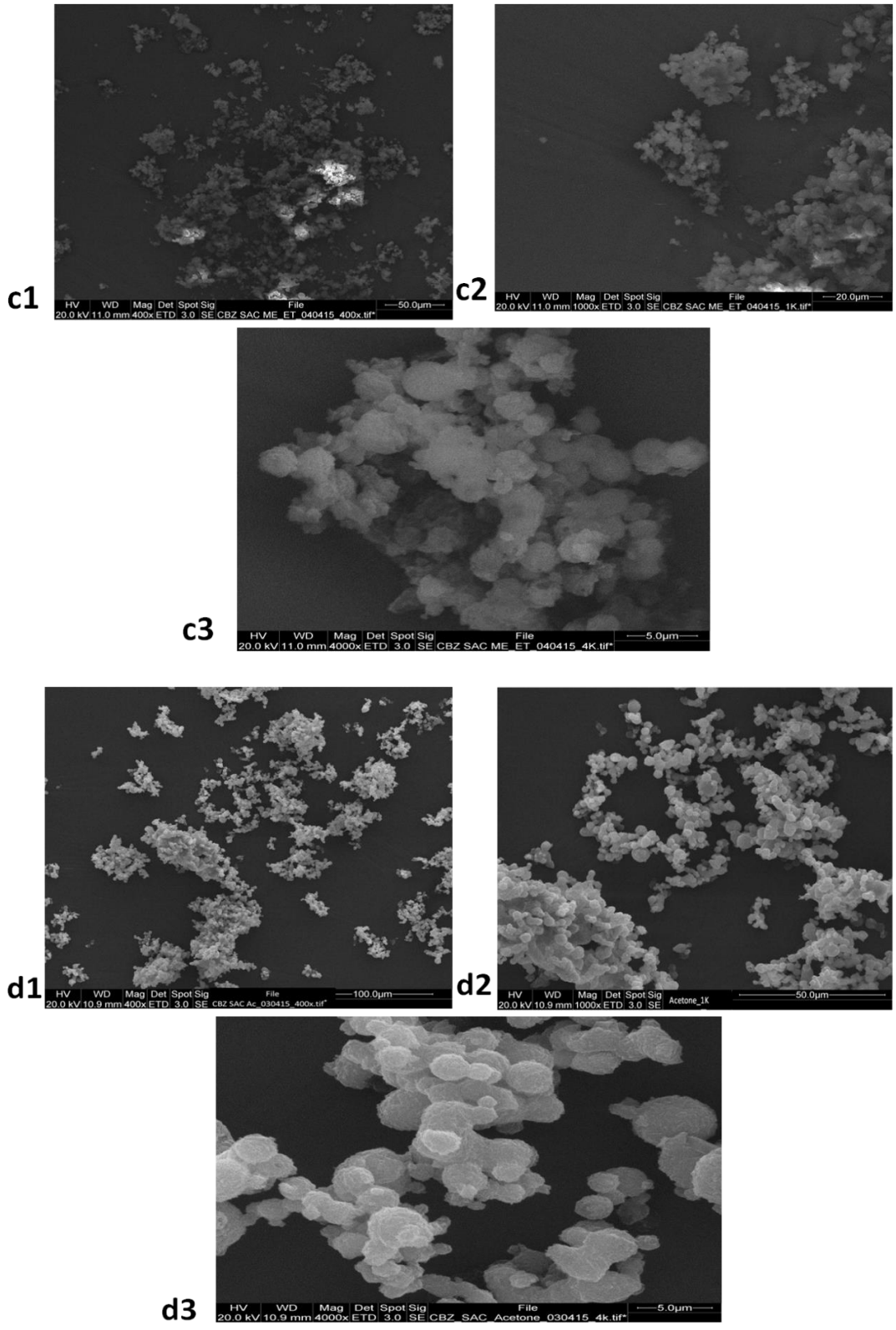

Figure 5.28. *SEM images for CBZ: SAC co-crystals: c) MeOH:EtOH: c1-400x, c2-1000x, c3-4000x; d) acetone: d1-400x, d2-1000x, d3-4000x.*

Summary:

CBZ and SAC exhibit two co-crystal polymorphs of CBZ:SAC 1:1: the most stable FI and metastable FII which has been hard to achieve. CBZ itself has four polymorphic forms and is susceptible to solvate formation and degradation. Its solubility in water is poor, therefore, good solvents such as methanol, ethanol and acetone known from previous studies were utilised. Rotavap resulted in FI co-crystals in acetone, methanol and ethanol:methanol mixtures. However, evaporation under ethanol gave mixtures of the two polymorphic forms, depicting the importance of solvent selection. In contrast, spray drying resulted in FII as illustrated by PXRD results. However, DSC results proclaimed formation of CBZ:SAC FI. Therefore, characterisation tools such as Raman and FTIR were involved to clarify these ambiguous results. Raman and FTIR indicated the formation of metastable FII. In addition, a protoype of FI was formed using previously reported method of solvent co-crystallisation for comparison. Furthermore, DSC scan at a fast rate had demonstrated two peaks for CBZ:SAC FI and FII in all spray dried products. Whereas, the protoype had only shown one characteristic peak for FI at a fast DSC scan rate, suggesting, thermal transformation of FII into FI for spray dried co-crystals. Degradation studies were also carried out for all the samples at 1 month, 3 month and 5 month period. The degradant slowly increased over time at ambient conditions for all samples and was just under FDA limit of 0.2%. A two-step degradation reaction due to atmospheric humid conditions and sunlight was proposed. Physical properties such as dispersive surface energy of the co-crystals reduced with an increase in the feed rate of the spray dryer.

CHAPTER 6

CONCLUSION AND FUTURE WORK

Utility of spray dryer as a scale-up technique for co-crystals from solutions was illustrated using series of co-crystals of CAF and THEO with dicarboxylic acids, and CBZ with SAC. Co-crystals of CAF and THEO with succinic and tartaric acids were not formed by this technique. Attempts were made to enhance solubility of the incongruent pairs of CAF and THEO for scale-up purpose and to attain pure crystal forms. Interestingly, the hydrotropic nature of dicarboxylic acids enhanced solubility of CAF and THEO. However, THEO's solubility was best attained in binary mixture of $CHCl_3$ and MeOH.

Rotavap was applied as a pre-screening tool by simulating fast evaporation under reduced pressure. Though pre-screening via rotavap resulted in impurities, it gave a good indication of co-crystal form that can be expected from spray drying. However, this wasn't achieved in case of CAF: GLU 1:1 and CBZ: SAC 1:1 co-crystals, where polymorphs exist within the same stoichiometry, leading to limitation of its efficacy. CAF co-crystals were successfully accomplished from aqueous solutions, fabricating spray dryer as a green technique. CAF: MAL 2:1 co-crystals were always favoured over 1:1 independent of the starting component stoichiometry in solution. The foremost process parameters that seem to generate almost phase pure CAF: MAL 2:1 reducing CAF impurity were: optimum inlet temperature, feed concentration and feed rate. Introduction of surfactant (SLS) resulted in almost phase pure CAF: MAL 2:1 at higher concentrations, but, the product was susceptible to moisture uptake due

to surfactant's hygroscopic nature. In contrast, organic solvents produced mixtures of co-crystals with starting component impurity; therefore, solvent selection is crucial.

Solubility of CAF analogue, THEO with dicarboxylic acids was best achieved in binary mixture of organic solvents ($CHCl_3$+MeOH) than in water. Rotavap produced co-crystals with minor impurity of THEO which was attributed to variation in phase composition of the two solvents and longer residence time during evaporation. Spray dryer emerged as a suitable fast evaporating environment for the production of pure THEO co-crystals from solvent mixtures. This kinetically-driven technique always favoured metastable form of co-crystals as observed in case of CAF: MAL, CAF: GLU and CBZ: SAC. The metastable CBZ: SAC FII was only observed in ethanol via rotavap, indicating importance of solvent selection. Whereas, spray dryer surpassed the solvent barrier and produced CBZ: SAC FII for range of solvents and their mixtures regardless of the congruent and incongruent nature of the two starting components. In addition, orthogonal testing performed on CBZ: SAC co-crystals using various characterisation tools illustrate non-reliability of DSC results due to thermal influence on the product. Furthermore, escalation in CBZ co-crystal degradate content over time was considered to be influenced by external factors such as humidity, sunlight and temperature. Although, spray dryer provides a unique environment with high supersaturation levels ideal for achieving pure co-crystals from incongruently soluble components, its usage as scale-up is atrocious due to low feed concentrations, despite achieving enhanced solubility for the above co-crystal pairs.

Future work

To further improve the strategy, other surfactants should be involved to enhance solubility and reduce the high solvent concentration utilised. Solubility enhancement experimentation using other mixture of solvents must be explored. Residual solvent evaluation can also be implemented to comprehend product's quality and degradation. Safety issues in regards to toxic solvents such as chloroform should be considered. Spray dried products obtained are mostly amorphous in nature; therefore, effect of process parameters on crystalline content can be elucidated. To further understand and develop the spray drying process, new models based approaches representing QbD should be introduced to define a process operating space.

REFERENCES

Aakeroey, C. B., Rajbanshi, A., Li, Z. J. and Despel, J. (2010). Mapping out the synthetic landscape for re-crystallization, co-crystallization and salt formation. *CrystEngComm* **12**(12) 4231-4239.

Ainouz, A., Authelin, J., Billot, P. and Lieberman, H. (2009). Modeling and prediction of cocrystal phase diagrams. *International Journal of Pharmaceutics*, **374**(1-2) 82-89.

Aher, S., Dhumal, R., Mahadik, K., Paradkar, A. and York, P. (2010). Ultrasound assisted cocrystallization from solution (USSC) containing a non-congruently soluble cocrystal component pair: Caffeine/maleic acid. *European Journal of Pharmaceutical Sciences* , **41**(5) 597-602.

Alhalaweh, A., George, S., Bostrom, D. and Velaga, S. P. (2010). 1:1 and 2:1 Urea-succinic acid cocrystals: structural diversity, solution chemistry, and thermodynamic stability. *Crystal Growth & Design*, **10**(11) 4847-4855.

Alhalaweh, A. and Velaga, S. P. (2010a). Formation of cocrystals by spray drying. *Journal of Pharmacy and Pharmacology* , **62**(10) 1332-1333.

Alhalaweh, A. and Velaga, S. P. (2010b). Formation of cocrystals from stoichiometric solutions of incongruently saturating systems by spray drying. *Crystal Growth & Design* **10**(8) 3302-3305.

Alhalaweh, A., Sokolowski, A., Rodriguez-Hornedo, N. and Velaga, S. P. (2011). Solubility behavior and solution chemistry of indomethacin cocrystals in organic solvents. *Crystal Growth & Design* **11**(9) 3923-3929.

Alhalaweh, A., Roy, L., Rodriguez-Hornedo, N. And Velaga, S. P. (2012) pH-dependent solubility of indomethacin−saccharin and carbamazepine−saccharin cocrystals in aqueous media. *Molecular Pharmaceutics*, **9**, pp. 2605-12.

Alhalaweh, A., Kaialy, W., Buckton, G., Gill, H., Nokhodchi, A. and Velaga, S.P. (2013). Theophylline cocrystals prepared by spray drying: Physicochemical properties and aerosolization performance. *AAPS PharmSciTech*, **14**(1) 265-276.

Apshingekar, P. (2014) Application of ultrasound in pharmaceutical processing and analytics. PhD Thesis:University of Bradford.

Arpagaus, C. and Schwartzbach, H. (2008) Scale-up from bench-top research to laboratory production [online]. Best at Buchi.[Cited 16th March, 2012]. Available at: <http://www.buchi.com/uploads/media/Best_Buchi_52_Scale-up_B-290_Niro_MOBILE_MINOR_07.pdf>.

Arpagaus, C. and Schafroth, N. (2010) Laboratory Scale Spray Drying of Lactose: A Review. Best at Buchi. [Cited 6th September, 2012]. Available at : <http://www.buchi.com/uploads/media/Best_Buchi_57_Laboratory_Scale_Spray_Drying_of_Lactose_02.pdf>.

Avagadro (2000-2007) Hydrolysis of organic compounds [online]. [Accessed on 15th December, 2015]. Available at: <http://www.avogadro.co.uk/organic/hydrolysis/hydrolysis.htm>

Audet, P., Savote, R. and Simard, M. (1990) Synthesis, crystal structure, and vibrational spectra of the complex maleic acid.2H2O.18-crown-6. *Canadian Journal of Chemistry*, **68,** pp. 2183-2189.

Babu NJ and Nangia A (2011) Solubility advantage of amorphous drugs and pharmaceutical cocrystals. *Crystal Growth & Design* **11**, 2662-2679.

Bag P. P., Patni M. and Reddy C. M. (2011) A kinetically controlled crystallization process for identifying new co-crystal forms: fast evaporation of solvent from solutions to dryness. *CrystEngComm* **13**, 5650-5652.

Basavoju, S., D. Bostrom and S. P. Velaga (2006). Pharmaceutical cocrystal and salts of norfloxacin. *Crystal Growth & Design* **6**(12) 2699-2708.

Basavoju, S., Bostrom, D. and Velaga, S. P. (2008). Indomethacin-saccharin cocrystal: Design, synthesis and preliminary pharmaceutical characterization. *Pharmaceutical Research***, 25**(3) 530-541.

Berry, D. J., Seaton, C. C., Clegg, W., Harrington, R. W., Coles, S. J., Horton, P. N., Hursthouse, M. B., Storey, R., Jones, W., Friscic, T. and Blagden, N. (2008) Applying hot-stage microscopy to co-crystal screening: A study of nicotinamide

with seven active pharmaceutical ingredients. *Crystal Growth & Design*, **8**(5) 1697-1712.

Bis, J. A., Vishweshwar, P., Weyna, D. and Zaworotko, M. J. (2007) Hierarchy of supramolecular synthons: Persistent hydroxyl···pyridine hydrogen bonds in cocrystals that contain a cyano acceptor. *Molecular Pharmaceutics*, **4**(3) 401-416.

Bilancetti, L., Poncelet, D., Loisel, C., Mazzitelli, S. and Nastruzzi, C. (2010). A statistical approach to optimize the spray drying of starch particles: Application to dry powder coating. *AAPS PharmSciTech*, **11**(3) 1257-1267.

Blagden, N., de Matas, M., Gavan, P. T. and York, P. (2007) Crystal engineering of active pharmaceutical ingredients to improve solubility and dissolution rates. *Advanced Drug Delivery Reviews*, **59**(7), 617-630.

Blagden, N., Berry, D. J., Parkin, A., Javed, H., Ibrahim, A., Gavan, P. T., de Matos, L. L. and Seaton, C. C. (2008). Current directions in co-crystal growth. *New Journal of Chemistry*, **32**(10) 1659-1672.

Brittain, H. G. (2012). Cocrystal systems of pharmaceutical interest: 2010. *Crystal Growth & Design*, **12**(2) 1046-1054.

Buchi (1997-2002) Training papers spray drying [online]. Buchi Labortechnik AG: Switzerland.[Cited 3rd October, 2012]. Available at :<http://www.buchi.com/Spray-Drying. 69.0.html?&no_cache¼1&file¼308&uid¼2283>.

Buchkremer, R. and Brinker, U. H. (1990) A convenient and improved technique to reduce substantially the problem of bumping while using a rotary evaporator. *Journal of Chemical Education*, **67** (12), p. 1071.

Cal, K. and K. Sollohub (2010). Spray drying technique. I: Hardware and process parameters. *Journal of Pharmaceutical Sciences*, **99**(2) 575-586

Cassani, C., Bergonzini, G. and Walentin, C. (2014) Photocatalytic decarboxylative reduction of carboxylic acids and its application in asymmetric synthesis. *American Chemical Society*, **16**(16), pp. 4228-31.

Chemicalland21 (2013) Custom search [online]. [Accessed on 17th October 2015]. Available at:<http://www.chemicalland21.com>

ChemWiki (no date) Rotary Evaporation [online]. [Accessed on 8th August, 2015]. Avialable at: <http://chemwiki.ucdavis.edu/Reference/Lab_Techniques/Rotary_Evaporation>.

Chieng, N., Hubert, M., Saville, D., Rades, T. and Aaltonen, J. (2009). Formation kinetics and stability of carbamazepine-nicotinamide cocrystals prepared by mechanical activation. *Crystal Growth & Design*, **9**(5) 2377-2386.

Childs, S. L., Chyall, L. J., Dunlap, J. T., Smolenskaya, V. N., Stahly, B. C. and Stahly, G. P. (2004). Crystal engineering approach to forming cocrystals of amine hydrochlorides with organic acids. Molecular complexes of fluoxetine hydrochloride with benzoic, succinic, and fumaric acids. *Journal of the American Chemical Society*, **126** (41) 13335-13342.

Childs, S. L. and K. I. Hardcastle (2007). Cocrystals of piroxicam with carboxylic acids. *Crystal Growth & Design*, **7**(7) 1291-1304.

Childs, S. L., Rodriguez-Hornedo, N., Reddy, L.S., Jayashankar, A., Maheshwari, C., McCausland, L., Shipplett, R. and Stahly, B.C. (2008). Screening strategies based on solubility and solution composition generate pharmaceutically acceptable cocrystals of carbamazepine. *CrystEngComm*, **10**(7) 856-864.

Childs SL, Kandi P, Lingireddy SR (2013) Formulation of a danazol cocrystal with controlled supersaturation plays an essential role in improving bioavailability. *Molecular Pharmaceutics*. **10**, 3112-3127.

Chiou, D. and Langrish, T. A. G. (2008). A comparison of crystallisation approaches in spray drying. *Journal of Food Engineering*. 88(2) 177-185.

Chow S. F., Chen, M., Shi, L., Chow, A. H. L. and Sun, C. C. (2012) Simultaneously improving the mechanical properties, dissolution performance, and hygroscopicity of ibuprofen and flurbiprofen by cocrystallization with nicotinamide. *Pharmaceutical Research*, **29**, 1854-1865.

Chow, S. F., Shi, L., Ng, W. W., Leung, K. H. Y., Nagapudi, K., Sun, C.C. and Chow, A. H. L. (2014) Kinetic entrapment of a hidden curcumin cocrystal with phloroglucinol. *Crystal Growth & Design* **14**, 5079-5089.

Daggupati, V. N., Naterer, G. F, Gabriel, K.S., Gravelsins, R. J. and Wang, Z. L. (2011). Effects of atomization conditions and flow rates on spray drying for cupric chloride particle formation. *International Journal of Hydrogen Energy*. **36**(17) 11353-11359.

Dafratec (no date) *Application note 5: Co-crystallization studies* [online]. [Accessed on 15th August, 2015]. Available at: <http://www.dafratec.com/pdf/crystal16_Co_Crystals.pdf>

Daurio, D., Medina, C., Saw, R., Nagapudi, K. and Alvarez-Nunez, F. (2011) Application of twin screw extrusion in the manufacture of cocrystals, Part I: Four case studies. *Pharmaceutics*, **3**, 582-600.

DDBST GmbH (no date) Saturated vapour pressure, calculation by antoine equation [online]. [Accessed on 26th November, 2015]. Available at :<http://ddbonline.ddbst.com/AntoineCalculation/AntoineCalculationCGI.exe>

Dhumal, R. S., A. L. Kelly and A. R. Paradkar (2010). Development of solvent free continuous cocrystallisation (SFCC) technique. *Journal of Pharmacy and Pharmacology*, **62**(10) 1418-1419.

Dobry, D. E., Settel, D. M., Baumann, J. M., Ray, R. J., Graham, L. J. and Beyerinck, R. A. (2009). A model-based methodology for spray-drying process development. *Journal of Pharmaceutical Innovation*, **4**(3) 133-142.

Ebisuzaki, Y. and Angel, S.M. (1981) Raman study of hydrogen bonding in α and β-oxalic acid dehydrate. *Journal of Raman Spectroscopy*.**11** (4), pp.306-310.

Eddleston, M.D., Arhangelskis, M., Fabian, L., Tizzard, G.J., Coles, S. J. and Jones, W (2016) Investigation of an amide-pseudo amide hydrogen bonding motif within a series of theophylline:amide cocrystals. *Crystal Growth & Design*, **16** (1), pp. 51-8.

Ende D. J. am, Anderson S. R. and Salan, J. S. (2014) Development and scale-up of cocrystals using resonant acoustic mixing. *Organic Process Research & Development.* **18** (2), 331-341.

Etter, M. C. (1990). Encoding and decoding hydrogen-bond patterns of organic compounds. *Accounts of Chemical Research* ,**23**(4) 120-126.

Etter, M. C. (1991) Hydrogen bonds as design elements in organic chemistry. *Journal of Physical Chemistry*, **95**(12) 4601-4610.

European Medicines Agency (2014) *Reflection paper on the use of cocrystals and other solid state forms of active substances in medicinal products* [online]. [Accessed on 2nd August, 2015]. Available at: <http://www.enantia.com/files/2014%20EMA%20concept%20paper%20on%20use%20of%20cocrystals.pdf>

Fabian, L. (2009). Cambridge structural database analysis of molecular complementarity in cocrystals. *Crystal Growth & Design*. **9**(3), pp. 1436-1443.

Fakhree, M. A. A., Delgado, D. R., Martinez, F. and Jouyban, A. (2010) The importance of dielectric constant for drug solubility prediction in binary solvent mixtures: electrolytes and zwitterions in water + ethanol. *AAPS PharmSciTech*, **11**(4), pp. 1726-9.

FDA (no date) *Drug databases: Dissolution methods* [online]. [Accessed on 18th November, 2015].Avaialble at: <http://www.accessdata.fda.gov/scripts/cder/dissolution/dsp_getallData.cfm>

FDA (1990) *Guideline for the determination of residual moisture in dried biological products* [online]. [Accessed on 18th November, 2015]. Available at :<http://www.fda.gov/ohrms/DOCKETS/dockets/05d0047/05d-0047-bkg0001-Tab-11.pdf>

FDA (1997) *Guidance for industry: Dissolution testing of immediate release solid dosage forms* [online]. [Accessed on 2nd November, 2015]. Available at: <http://www.fda.gov/downloads/drugs/guidancecomplianceregulatoryinformation/guidances/ucm070237.pdf>

FDA, Food and Drug Administration (2013) *Guidance for industry: Regulatory Classification of Pharmaceutical Co-crystals* [online]. [Accessed on 14th July 2015]. Available at: <http://www.fda.gov/downloads/Drugs/.../Guidances/UCM281764.pdf>

FDA (2015) *Food and drugs: Food and drug administration* [online]. [Accessed on 3rd November, 2015]. Available at: <http://www.accessdata.fda.gov/scripts/cdrh/cfdocs/cfcfr/CFRSearch.cfm?fr=172.822>

Flakus, H.T. and Miros, A. (1999) Infrared spectra of the hydrogen bonded Glutaric acid crystals: polarization and temperature effects. *Journal of Molecular Structure*.**484**, pp. 103-15.

FPN (no date) *Testing ink samples on a laboratory* [online].[Accessed on 25th November, 2015]. Available at:<http://www.fountainpennetwork.com/forum/topic/295309-testing-ink-samples-on-a-laboratory/>

Friščić, T., Fábián, L., Burley, J. C. and Jones, W. (2006) Exploring cocrystal–cocrystal reactivity via liquid-assisted grinding: the assembling of racemic and dismantling of enantiomeric cocrystals. *Chemical Communications*, **48**, pp. 5009-11.

Friščić, T., Trask, A. V., Motherwell, W. D. S. and Jones, W. (2008) Guest-directed assembly of caffeine and succinic acid into topologically different heteromolecular host networks upon grinding. *Crystal Growth & Design*, **8** (5), pp. 1605-9.

Friščić, T. and W. Jones (2009). Recent advances in understanding the mechanism of cocrystal formation via grinding. *Crystal Growth & Design*. **9**(3) 1621-1637.

Gac, J. M. and Gradon, L. (2013) A distributed parameter model for the spray drying of multicomponent droplets with a crust formation. *Advanced Powder Technology* **24**(1) 324-330.

Gagniere, E., Mangin, D., Puel, F., Riboire, A., Monnier, O., Garcia, E. and Klein, J. P. (2009). Formation of co-crystals: Kinetic and thermodynamic aspects. *Journal of Crystal Growth* **311**(9) 2689-2695.

Gamble, J. F., Leane, M., Olusanmi, D., Tobyn, M. and Supuk, E. (2012) Surface energy analysis as a tool to probe the surface energy characteristics of micronized materials-A comparison with inverse gas chromatography. *International Journal of Pharmaceutics*, **422,** pp. 238-44.

General chemistry online (1997-2010) *What is the Antoine equation?* [online]. [Accessed on 27th November, 2015]. Available at :<http://antoine.frostburg.edu/chem/senese/101/liquids/faq/antoine-vapor-pressure.shtml>

Good, D. J. and Rodriguez-Hornedo, N. (2009) Solubility advantage of pharmaceutical cocrystals. *Crystal Growth & Design*, **9** (5), pp. 2252-2264.

Good, D. J. and Rodriguez-Hornedo, N. (2010). Cocrystal Eutectic Constants and Prediction of Solubility Behavior. *Crystal Growth & Design* **10**(3) 1028-1032.

Gorman, W. G. and Hall, G. D. (1964) Dielectric constant correlations with solubility and solubility parameters. *Journal of Pharmaceutical Sciences*.**53**, pp. 1017-20

Grifasi, F., Chierotti, M. R., Gaglioti, K., Gobetto, R., Maini, L., Braga, D., Dichiarante, E. and Curzi, M. (2015) Using salt cocrystals to improve the solubility of niclosamide. *Crystal Growth & Design* **15**, 1939-1948.

Grzesiak, A. L., Lang, M., Kim, K. and Matzger, A. J. (2003) Comparison of the four anhydrous polymorphs of carbamazepine and the crystal structure of Form I. *Journal of Pharmaceutical Sciences*, **92** (11). Pp. 2260-70.

Guo, K., Sadiq, G., Seaton, C., Davey, R. and Yin, Q. (2010). Co-Crystallization in the caffeine/maleic acid system: Lessons from phase equilibria. *Crystal Growth & Design* **10**(1) 268-273.

Hansen, C. M. (1967) *The three dimensional solubility parameter and solvent diffusion coefficient* [online]. [Accessed on 1st December, 2015]. Available at: <http://hansen-solubility.com/Contents/HSP1967-OCR.pdf>

Hansen-solubility (2015) *Make your own designer solvents* [online]. [Accessed on 4th December, 2015]. Available at: <http://hansen-solubility.com/SolventBlends.html>

Harris, R. K., Ghi, P. Y., Puschmann, H., Apperley, D. C., Griesser, U. J., Hammond, R. B., Ma, C., Roberts, K. J., Pearce, G. J., Yates, J. R. and Pickard, C. J.

(2005) Structural studies of the polymorphs of carbamazepine, its dehydrate, and two solvates. *Organic Process Research and Development*, **9**, pp. 902-10.

Hickey, M B., Peterson, M. L., Scoppettuolo, L.A., Morrisette, S. L., Vetter, A., Guzman, H., Remenar, J.F., Zhang, Z., Tawa, M.D., Haley, S., Zaworotko, M. J. and Almarsson, O. (2007) Performance comparison of a co-crystal of carbamazepine with marketed product. *European Journal of Pharmaceutics and Biopharmaceutics*, **67**(1), pp. 112-9.

Horiba Scientific (2014) *A guidebook to particle size analysis* [online]. Irvine, CA:USA [Accessed on 18th August, 2015]. Available at: <https://www.horiba.com/fileadmin/uploads/Scientific/eMag/PSA/Guidebook/pdf/PSA_Guidebook.pdf>

Horst, J. H. and Cains, P. W. (2008). Co-crystal polymorphs from a solvent-mediated transformation. *Crystal Growth & Design* **8**(7) 2537-2542.

Hu, F. H., Wang, L. S. and Cai, S. F. (2009). Solubilities of triphenylphosphine oxide in selected solvents. *Journal of Chemical and Engineering Data*, **54**(4) 1382-1384

Hultin, P. G. (2002) *A guide to solvents and reagents in introductory organic chemistry for students in 2.222* [online]. University of Manitoba: Winnipeg. [Accessed on 2nd December, 2015]. Available at: <http://home.cc.umanitoba.ca/~hultin/chem2220/Support/solvents_and_reagents.pdf>

ICH (2012) *Guidance for industry: Q3C – Tables and List* [online]. [Accessed on 24th November, 2015]. Available at: <http://www.fda.gov/downloads/drugs/guidancecomplianceregulatoryinformation/guidances/ucm073395.pdf>

IKA (no date) *Out of the variety of RV 10 evaporation applications we proudly present ten to only name a few* [online]. [Accessed on 4th August, 2015]. Available at:< http://www.ika.com/distilling/applications.html>

Islam, M. I. U. and Langrish, T. A. G. (2010). An investigation into lactose crystallization under high temperature conditions during spray drying. *Food Research International* **43**(1) 46-56.

Islam, M. I. U., Langrish, T. A. G. and Chiou, D. (2010). Particle crystallization during spray drying in humid air. *Journal of Food Engineering* ,**99**(1) 55-62.

Jayasankar, A., Somwangthanaroj, A., Shao, Z. J. and Rodriguez-Hornedo, N. (2006) Cocrystal formation during cogrinding and storage is mediated by amorphous phase. *Pharm Res*., **23**(10), pp. 2381-92.

Joshi, O. D. (2012) *Development of a solvent free continuous co-crystallisation technique for carbamazepine-saccharin* [online]. University of Bradford Thesis. [Accessed on 12th February, 2014]. Available at: <https://bradscholars.brad.ac.uk/handle/10454/5697>

Jung, M. S., Kim, J. S., Kim, M.S., Alhalaweh, A., Cho, W., Hwang, S. J. and Velaga, S. P. (2010). Bioavailability of indomethacin-saccharin cocrystals. *Journal of Pharmacy and Pharmacology*, **62**(11) 1560-1568.

Kelly, A. L., Gough, T., Dhumal, R. S., Halsey, S. A. and Paradkar, A. (2012) Monitoring ibuprofen-nicotinamide cocrystal formation during solvent free continuous cocrystallization (SFCC) using near infrared spectroscopy as a PAT tool. *International Journal of Pharmaceutics*, **426** (1-2) 15-20.

Kent, J. And McLeod, J. (2007) *Spray- dryer optimization* [online]. PowderBulkSolids. [Cited 25th August, 2012]. Available at: <http://www.niroinc.com/html/chemical/cpdfs/spray_dryer_optimization.pdf>.

Khamar, D., Pritchard, R.G., James, Bradshaw, I. J., Hutcheon, G. A. and Seton, L. (2011) Polymorphs of anhydrous theophylline: stable form IV consists of dimer pairs and meatstable form I consists of hydrogen-bonded chains. *International Union of Crystallography*, **C67**, pp. 496-9.

Khan, M., Enkelmann, V. and Brunklaus, G. (2010). Crystal engineering of pharmaceutical co-crystals: Application of methyl paraben as molecular hook. *Journal of the American Chemical Society*, **132**(14), pp. 5254-5263.

Kojima, T., Tsutsumi, S., Yamamoto, K, Ikeda, Y. and Moriwaki, T. (2010). High-throughput cocrystal slurry screening by use of in situ Raman microscopy and multi-well plate. *International Journal of Pharmaceutics* **399**(1-2) 52-59.

Kulkarni,C., Wood, C., Kelly, A. L., Gough, T., Blagden, N. and Paradkar, A. (2015) Stoichimetric control of co-crystal formation by solvent free continuous co-crystallisation (SFCC).*Crystal Growth and Design*. **15** (12), pp. 5648-51.

Kumar, V. S., Raja, C. and Jayakumar, C. (2014) A review on solubility enhancement using hydrotropic phenomena. *International Journal of Pharmacy and Pharmaceutical Sciences*, **6** (6), pp. 1-7.

Leung, D. H., Lohani, S., Ball, R. G., Canfield, N., Wang, Y., Rhodes, T. and Bak, A. (2012) Two novel pharmaceutical cocrystals of a development compound-screening, scale-up, and characterization. *Crystal Growth & Design* **12**(3) 1254-1262.

Leyssens, T., Springuel, G., Montis, R., Candoni, N. and Veesler, S. (2012). Importance of solvent selection for stoichiometrically diverse cocrystal systems: caffeine/maleic acid 1:1 and 2:1 cocrystals. *Crystal Growth & Design* **12**(3) 1520-1530.

Llinas, A. and J. M. Goodman (2008). Polymorph control: past, present and future. *Drug Discovery Today* **13**(5-6) 198-210.

Lu, E., Rodriguez-Hornedo, N. and Suryanarayanan, R. (2008) A rapid thermal method for cocrystal screening. *CrystEngComm* **10**(6) 665-668.

Maltesen, M. J., Bjerregaard, S., Hovgaard, L., Havelund, S., van de Weert, M. and Grohganz, H. (2011) Multivariate analysis of phenol in freeze-dried and spray-dried insulin formulations by NIR and FTIR. *AAPS PharmSciTech* **12**(2) 627-636.

Malvern (2009) *Laser Diffraction: Particle size distributions from nanometers to millimetres* [online]. Accessed on 4th August 2015]. Available at: <http://www.malvern.com/en/products/technology/laser-diffraction/>

Mancini, P., Adam, C., Perez, A. del C. and Vottero, L. R. (2000) Solvatochromic and kinetic response models in (ethyl acetate+ chloroform or methanol) solvent mixtures. *Molecules*, **5** (3), pp. 587-88.

Mancini, P. M., Bock, A., Adam, C., Perez, A.delC. and Vottero, L. R (2003) Binary solvent mixtures: characterization of molecular environments through multiparametric empirical scales.Concerns about relationships between kinetic data and microscopic solvent properties. *Archive for Organic Chemistry*, 10, pp. 373-81.

Mandavi, R., Sar, S. K. and Rathore, N. (2008) Critical micelle concentration of surfactant, mixed–surfactant and polymer by different method at room temperature and its importance. *Oriental Journal of Chemistry*. **24** (2), pp. 559-64.

Master Organic Chemistry (2015) *Polar protic? Polar aprotic? Nonpolar? All about solvents* [online]. [Accessed on 10th December, 2015]. Available at: <http://www.masterorganicchemistry.com/2012/04/27/polar-protic-polar-aprotic-nonpolar-all-about-solvents/>

Maxwell's equations (2012) *Permittivity* [online]. [Accessed on 8th October, 2015]. Available at: <http://maxwells-equations.com/materials/permittivity.php>

McNamara, D. P., Childs, S. L., Giordano, J., Iarriccio, A., Cassidy, J., Shet, M.S., Mannion, R., O'Donnell, E. and Park, A. (2006). Use of a glutaric acid cocrystal to improve oral bioavailability of a low solubility API. *Pharmaceutical Research* **23**(8), pp. 1888-1897.

Miroshnyk, I., Mirza, S. and Sandlert, N. (2009). Pharmaceutical co-crystals-an opportunity for drug product enhancement. *Expert Opinion on Drug Delivery* **6**(4) 333-341.

Mirza, S., Miroshnyk, I., Heinamaki, J. and Yliruusi, J. (2008) Co-crystals: An emerging approach for enhancing properties of pharmaceutical solids. *Dosis*, **24** (2). pp. 90-6.

Mohammad, M. A., Alhalaweh, A. and Velaga, S. P. (2011). Hansen solubility parameter as a tool to predict cocrystal formation. *International Journal of Pharmaceutics*, **407**(1-2), pp.63-71.

Monissette, S. L., Almarsson, S. L., Peterson, M. L., Remenar, J. F., Read, M. J., Lemmo, A. V., Ellis, S., Cima, M. J. and Gardner, C. R. (2004). High-throughput crystallization: polymorphs, salts, co-crystals and solvates of phan-naceutical solids. *Advanced Drug Delivery Reviews,* **56**(3), pp. 275-300.

Monk, P. (2004) *Physical chemistry, understanding our chemical world*. Manchester Metropolitan University:UK,. Published by: John Wiley and Sons Ltd. p. 188.

Moradiya, H., Islam, M. T., Woollam, G. R., Slipper, I. J., Halsey, S., Snowden, M. J. and Douroumis, D. (2013) Continuous cocrystallization for dissolution rate optimization of a poorly water-soluble drug. *Crystal Growth & Design*, **14**, pp. 189-98.

Mutalik, S., Anju, P., Manoj, K. and Usha, A. N. (2008). Enhancement of dissolution rate and bioavailability of aceclofenac: A chitosan-based solvent change approach. *International Journal of Pharmaceutics* **350**(1-2), pp. 279-290.

Nauha, E. (2012) *Crystalline forms of selected agrochemical actives: design and synthesis of cocrystals* [online]. University of Jyvaskyla: Finland. ISBN 978-951-39-4492-6.[Cited 22nd January, 2013]. Available at :<https://jyx.jyu.fi/dspace/handle/123456789/37362>.

Naumov, D. Y., Podberezskaya, N. V., Boldyreva, E. V. and Virovets, A. V. (1996) Crystal-chemical analysis of the structures of oxalic acid and its salts M x(C2O4) y ·nH2O (n=0−3). *Journal of Structural Chemistry*, **37** (3), pp. 480-503.

Nehm, S. J., Rodriguez-Spong, B. and Rodriguez-Hornedo, N. (2006). Phase solubility diagrams of cocrystals are explained by solubility product and solution complexation. *Crystal Growth & Design* **6**(2) 592-600.

O'Brien, L. E., Timmins, P., Williams, A. C. and York, P. (2004) Use of in situ FT-Raman s[ectroscopy to study the kinetics of the transformation of carbamazepine polymorphs. *Journal of Pharmaceutical and Biomedical Analysis*, **36**, pp. 335-40.

Okaya, Y. (1969) The crystal structure of saccharin o-sulfobenzoimide, C6H4CO.NH.SO2, an artificial sweetening. *Acta Crystallographica..*, **B25** (11), p. 2257-63.

Padrela, L., Rodriguez, M. A., Velaga, S. P., Matos, H. A., and Azevedo, E. G. de (2009) Formation of indomethacin-saccharin cocrystals using supercritical fluid technology. *European Journal of Pharmaceutical Sciences*, **38**(1), pp. 9-17.

Pagire, S. K., Korde, S. A., Whiteside, B. R., Kendrick, J. and Paradkar, A. (2013) Spherical crystallization of carbamazepine/saccharin co-crystals: selective agglomeration and purification through surface interactions. *Crystal Growth & Design* **13**, pp. 4162-4167.

Paruta, A. N., Sciarrone, B. J. and Lordi, N. G. (1962) Correlation between solubility parameters and dielectric constants. *Journal of Pharmaceutical Sciences*. **51** (7), p. 704-5.

Paruta, A. N. (1964) Solubility of several solutes as a function of the dielectric constant of sugar solutions. *Journal of Pharmaceutical Sciences*. **53** (10), p. 1252-4.

Paruta, A. N., Sciarrone, B.J. and Lordi, N. G. (1965) Solubility profiles for the xanthenes in dioxane – water mixtures. *Journal of Pharmaceutical Sciences*. **54** (6), p. 838-41.

Patil S. P., Modi, S. R. and Bansal, A. K. (2014) Generation of 1:1 carbamazepine:nicotinamide cocrystals by spray drying. *European Journal of Pharmaceutical Sciences* **62**, 251-257.

PHYWE (no date) *LEC 03.04:Boiling point diagram of a binary mixture* [online]. [Accessed on 8th December, 2015]. Available at :<http://www.phywe.fr/index.php/fuseaction/download/lrn_file/versuchsanleitungen/P3030401/e/LEC03_04_LV.pdf >

Pop, M., Sieger, P. and Cains, P. W. (2009). Tiotropium fumarate: An interesting pharmaceutical co-crystal. *Journal of Pharmaceutical Sciences* **98**(5), pp. 1820-1834.

Porter, W. W., Elie, S. C. and Matzger, A. J. (2008) Polymorphism in carbamazepine cocrystals. *Crysal. Growth & Design*, **8** (1). pp.14-6.

Qiao, N., Mingzhong, L., Schlindwein, W., Malek, N, Davies, A. and Trappitt, G. (2011). Pharmaceutical cocrystals: An overview. *International Journal of Pharmaceutics*, **419** (1-2) 1-11.

Qiu, S. and Li, M. (2015) Effects of coformers on phase transformation and release profiles of carbamazepine cocrystals in hydroxypropyl methylcellulose based matrix tablets. *International Journal of Pharmaceutics*, **479**, pp. 118-128.

Rager, T. and Hilfiker, R. (2009). Stability domains of multi-component crystals in ternary phase diagrams. *International Journal of Research in Physical Chemistry and Chemical Physics*, **223**(7) 793-813.

Rager, T. and Hilfiker, R. (2010) Cocrystal formation from solvent mixtures. *Crystal Growth & Design*, **10**, pp. 3237-41.

Rahman, S. M. H., Telny, T. C., Ravi, T. K. and Kuppusamy, S. (2009) Role of surfactant and pH in dissolution of curcumin. *Indian Journal of Pharmaceutical Sciences*.**71** (2), pp. 139-42.

Reckhard, H (1958) A method for calculating boiling points in distillation under vacuum. *Erdol and Kohle*, **4**. p.234-241.

Reddy, J. P., Delori, A. and Foxman, B. M. (2013) Molecular and crystal structure of a new polymorph of malonic acid with Z'=3. *Journal of Molecular Structure*, **1041**, pp. 122-6.

Remenar, J. F., Morissette, S. L., Peterson, M. L., Moutlon, B., MacPhee, J. M., Guzman, H. R. and Almarsson, O. (2003) Crystal engineering of novel cocrystals of a triazole drug with 1,4-dicarboxylic acids. *Journal of the American Chemical Society*, **125**(28), pp. 8456-8457.

Salem, A., Ahmadlouiedarab, M. and Ghasemzadeh, K. (2011) CFD approach for the moisture prediction in spray chamber for drying of salt solution. *Journal of Industrial and Engineering Chemistry*. **17**(3), pp. 527-532.

Schultheiss, N. and Newman, A. (2009) Pharmaceutical cocrystals and their physicochemical properties. *Crystal Growth & Design*. **9**(6), pp. 2950-2967.

Seaton, C. C., Chadwick, K., Sadiq, G., Guo, K. and Davey, R. J. (2010) Designing acid/acid co-crystals through the application of hammett substituent constants. *Crystal Growth & Design* **10**(2), pp. 726-733.

Sekhon, B. S. (2009) Pharmaceutical co-crystals - a review. *ARS Pharmaceutica*, **50** (3), pp. 99 – 117.

Shan, N. and M. J. Zaworotko (2008). The role of cocrystals in pharmaceutical science. *Drug Discovery Today*, **13**(9-10) 440-446.

Shattock, T. R., Arora, K. K., Vishweshwar, P. and Zaworotko, M. J. (2008) Hierarchy of supramolecular synthons: Persistent carboxylic acid···pyridine hydrogen bonds in cocrystals that also contain a hydroxyl moiety. *Crystal Growth & Design* **8**(12) 4533-4545.

Sigma Aldrich (2015a) *The "Golden Rule" for Solvent Removal* [online]. [Accessed on 7th August, 2015]. Available at: <https://www.sigmaaldrich.com/content/dam/sigma-aldrich/docs/Aldrich/General_Information/1/labwarenotes_v1_7.pdf>

Sigma-Aldrich (2015b) *Buchi rotary evaporator accessories* [online]. [Accessed on 4th October, 2015]. Available at: <http://www.sigmaaldrich.com/labware/labware-products.html?TablePage=18187086>

Shi, B., Wang, Y. and Jia, L. (2011) Comparison of Dorris-Gray and Schultz methods for the calculation of surface dispersive free energy by inverse gas chromatography. *Journal of Chromatography A*, **1218**, pp.860-2.

Smith A. J., Kavuru P., Wojtas L., Zaworotko M. J. and Shytle, R. D. (2011) Cocrystals of quercetin with improved solubility and oral bioavailability. *Molecular Pharmaceutics* **8**, 1867-1876.

Smolinske, S. C. (1992) *CRC Handbook of Food, Drug, and Cosmetic Excipient*. CRC Press: USA, p.359.

Sollohub, K. and Cal, K. (2010). Spray drying technique: II. Current applications in pharmaceutical technology. *Journal of Pharmaceutical Sciences* **99**(2) 587-597.

Son, J. S. (ed.) (2014) *Tetrahertz Biomedical Science and Technology*. CRC Press: Florida. P.117.

Sreekanth, B. R., Vishweshwar, P. and Vyas, K. (2007). Supramolecular synthon polymorphism in 2 : 1 co-crystal of 4-hydroxybenzoic acid and 2,3,5,6-tetramethylpyrazine. *Chemical Communications*, (23) 2375-2377.

Stanton, M. K. and Bak, A. (2008). Physicochemical properties of pharmaceutical co-crystals: A case study of ten AMG 517 co-crystals. *Crystal Growth & Design* **8**(10) 3856-3862.

Stern, F. and Beevers, C.A. (1950) The crystal structure of tartaric acid. *ActaCrystallographica*, **3**, pp. 341-6.

Suresh K, Goud NR, Nangia A (2013) Andrographolide: Solving chemical instability and poor solubility by means of cocrystals. *Chemistry-an Asian Journal* **8**, 3032-3041.

Surface Measurement Systems (2014a) *iGC-SEA* [online]. [Accessed on 28th August, 2015]. Available at: < http://surfacemeasurementsystems.com/products/igc-sea/>

Surface Measurement Systems (2014b) *What is IGC-SEA (Inverse Gas Chromatography-Surface Energy Analyser)?* [online]. [Accessed on 28th August, 2015]. Available at: <http://surfacemeasurementsystems.com/solutions/igc_sea/>

Sympatec GmbH (no date) *Laser Diffraction: Particle size analysis from 0.1 µm to 8.75 mm* [online]. Accessed on 4th August, 2015]. Available at: <https://www.sympatec.com/EN/LaserDiffraction/LaserDiffraction.html>

Szewczyk, J. W., Acton, J., adams, A. D., Chicchi, G., Freeman, S., Howard, A. D., Huang, Y., Li, C., Meinke, P.T., Mosely, R., Murphy, E., Samuel, R., Santini, C., Yang, M., Zhang, Y., Zhao, K. and Wood, H.B. (2011) Design of potent and selective GPR119 agonists for type II diabetes. *Biorganic and Medicinal Chemistry Letters*, **21**, pp. 2665-9.

Thomas, R., Gopalan, R. S., Kulkarni, G. U. and Rao. C. N. R. (2005). Hydrogen bonding patterns in the cocrystals of 5-nitrouracil with several donor and acceptor molecules. *Beilstein Journal of Organic Chemistry*.**1** (15), pp. 1-10

Tomaszewska, I., Karki, S., Shur, J., Price, R. and Fotaki, N.(2013) Pharmaceutical characterisation and evaluation of co-crystals: Importance of in vitro dissolution conditions and type of co-former. *International Journal of Pharmaceutics*, **453**, pp. 380-8.

Tonon, R. V., C. R. F. Grosso and M. D. Hubinger (2011). Influence of emulsion composition and inlet air temperature on the microencapsulation of flaxseed oil by spray drying. *Food Research International* **44**(1) 282-289.

Trask, A. V., W. D. S. Motherwell and W. Jones (2004) Solvent-drop grinding: green polymorph control of cocrystallisation. *Chemical Communications* (7) 890-891.

Trask, A. V., W. D. S. Motherwell and W. Jones (2005). Pharmaceutical cocrystallization: Engineering a remedy for caffeine hydration. *Crystal Growth & Design* **5** (3), pp. 1013-1021.

Trask, A. V., Motherwell, W. D., S. and Jones, W. (2006). Physical stability enhancement of theophylline via cocrystallization. *International Journal of Pharmaceutics* **320** (1-2), pp. 114-123.

Tripathy, S. and Swain, B. B. (1991) Dielectric properties of binary mixtures of some amines in nonpolar solvents-linear correlation factor, excess molar polarisation, and excess Gibbs energy. *Chemical Papers*, **45** (3), pp. 321-329.

Turanyl, T (2014) *Phase transitions* [online]. Institute of Chemistry, ELTE: Hungary [Accessed on 4th August, 2015]. Available at: <http://garfield.chem.elte.hu/turanyi/oktatas/Physical_Chemistry>

UC Davis ChemWiki (no date) *Thermodynamics of Mixing* [online]. [Accessed on 2nd October, 2015]. Available at : <http://chemwiki.ucdavis.edu/Physical_Chemistry/Thermodynamics/Ideal_Systems/Thermodynamics_of_Mixing>

University of Waterloo (no date) *The Clausius-Clapeyron equation* [online]. [Accessed on 5th August, 2015]. Available at: <http://www.science.uwaterloo.ca/~cchieh/cact/c123/clausius.html>

USP Convention (2015) *USP-NF, Revision Bulletins, Carbamazepine Tablets* [online]. [Accessed on 10th December, 2012]. Available at: <http://www.usp.org/usp-nf/official-text/revision-bulletins>.

Vangala V. R., Chow, P. S., Tan, R. B. H. (2011) Characterization, physicochemical and photo-stability of a co-crystal involving an antibiotic drug, nitrofurantoin, and 4-hydroxybenzoic acid. *CrystEngComm* **13**, 759-762.

Vishweshwar, P., McMahon, J. A., Bis, J. a. and Zaworotko, M. J. (2006). Pharmaceutical co-crystal. *Journal of Pharmaceutical Sciences*, **95**(3) 499-516.

Wang, I., Lee, M., Sim, S., Kim, W., Chun, N. and Choi, G. (2013) Anti-solvent co-crystallisation of carbamazepine and saccharin. *International Journal of Pharmacuetics*, **450**, pp. 311-22.

Walsh, R. D. B., Bradner, M. W., Fleischman, S., Morales, L. A., Moulton, B., Rodriguez-Hornedo, N. and Zaworotko, M. J. (2003). Crystal engineering of the composition of pharmaceutical phases. *Chemical Communications* (2) 186-187.

Welch vacuum (no date) *An effective rotary evaporator vacuum system* [online]. Accessed on 7th August, 2015]. Available at: <http://canlabglass.com/index_htm_files/Rotary%20evaporator%20usage.pdf>

Weiler-Feilchenfeld, H. and Neiman, Z. (1970) Dipole moments and electronic structure of some xanthine and xanthine derivatives. *Journal of Chemical Society B*, (0), pp. 596-8.

Weyna, D. R., Shattock, T., Vishweshwar, P. and Zaworotko, M. J. (2009). Synthesis and structural characterization of cocrystals and pharmaceutical cocrystals: Mechanochemistry vs slow evaporation from solution. *Crystal Growth & Design*, **9**(2), pp. 1106-1123.

Wikstroem, H., C. Kakidas and L. S. Taylor (2009). Determination of hydrate transition temperature using transformation kinetics obtained by Raman

spectroscopy. *Journal of Pharmaceutical and Biomedical Analysis*. **49**(2), pp. 247-252.

Yadav, A. V., Shete, A. S., Dabke, A. P., Kulkarni, P. V. and Sakhare, S. S. (2009). Co-Crystals: A Novel Approach to Modify Physicochemical Properties of Active Pharmaceutical Ingredients. *Indian Journal of Pharmaceutical Sciences*, **71**(4), pp. 359-370.

Yeung, M. C., Ling, T. Y. and Chan, C. K. (2010) Effects of the polymorphic transformation of glutaric acid particles on their deliquescence and hygroscopic properties. *Journal of Physical Chemistry*, 114, pp.898-903.

Yu, Q., Dang, L., Black, S. and Wei, H. (2012) Crystallization of the polymorphs of succinic acid via sublimation at different temperatures in the presence or absence of water and isopropanol vapour. *Journal of Crystal Growth*, **340**. pp. 209-15.

Zegarac M. (2007) Pharmaceutically acceptable co crystalline forms of sildenafil. Patent: WO080362 A1.

Zhang, G. G. Z., Henry, R. F., Borchardt, T. B. and Lou, X. (2007). Efficient co-crystal screening using solution-mediated phase transformation. *Journal of Pharmaceutical Sciences*, **96**(5), pp. 990-995.

Zhang, S. (2010) Physical properties and crystallization of theophylline co-crystals. KTH, Royal Institute of Technology: Stockholm, Sweden. ISSN 1654-1081, ISBN 978-91-7415-689-8.

Zhang, T. and Youan, B. B. C. (2010) Analysis of process parameters affecting spray-dried oily core nanocapsules using factorial design. *AAPS PharmSciTech.* **11**(3) 1422-1431.

Zukerman-Schpector, J. and Tiekink, E. R. T. (2008). What is a co-crystal?. *Crystalline Materials*, **223**(3), pp. 233-234.

APPENDIX

I. *PXRD patterns of caffeine and theophylline filtered after solubility tests from di-carboxylic acid solutions. (Caff = Caffeine).*

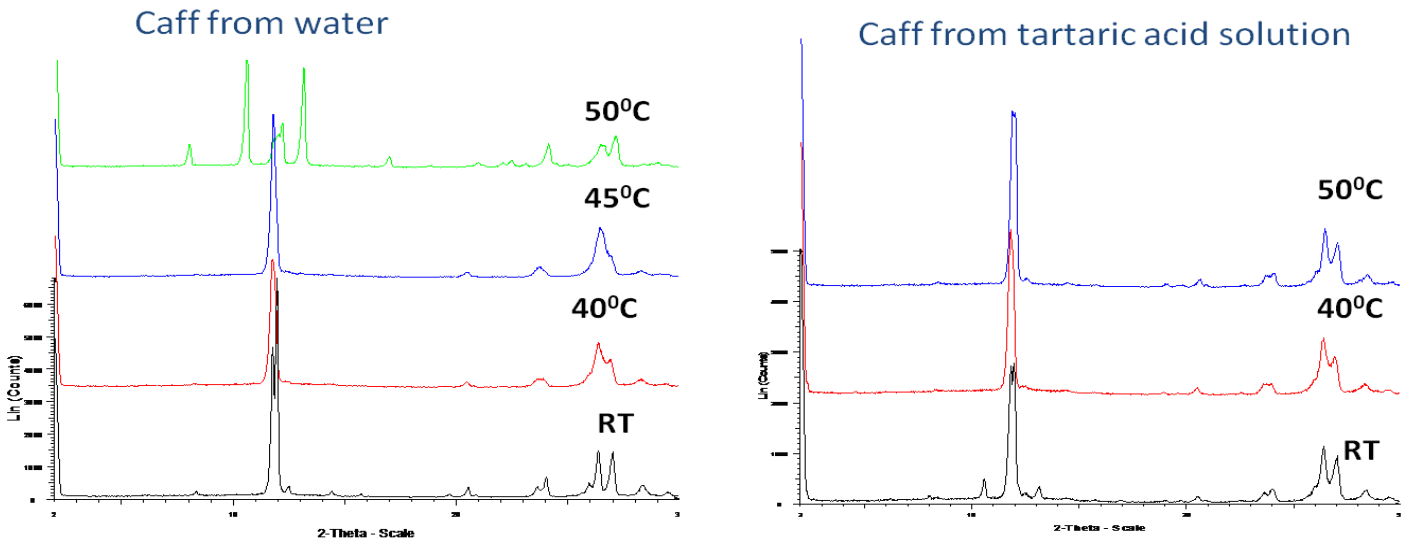

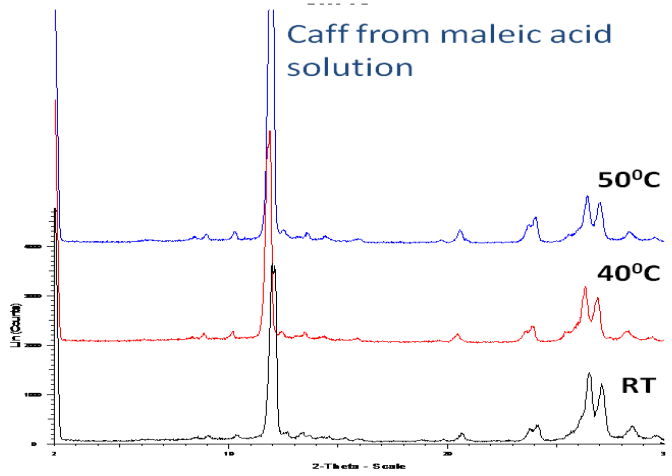
Caff from maleic acid solution
50⁰C
40⁰C
RT
Lin (Counts)
2-Theta - Scale

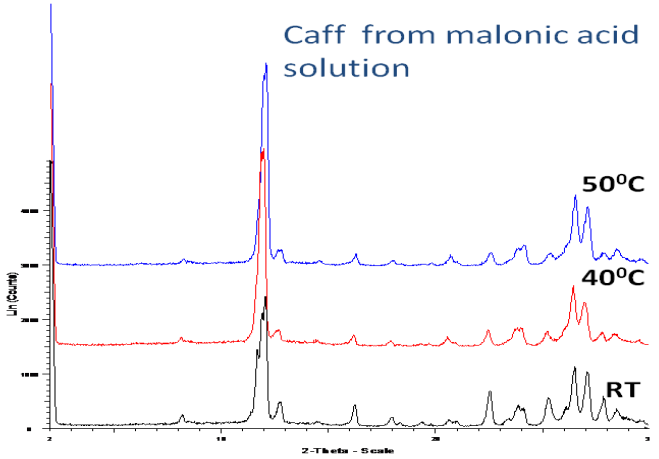
Caff from malonic acid solution
50⁰C
40⁰C
RT
Lin (Counts)
2-Theta - Scale

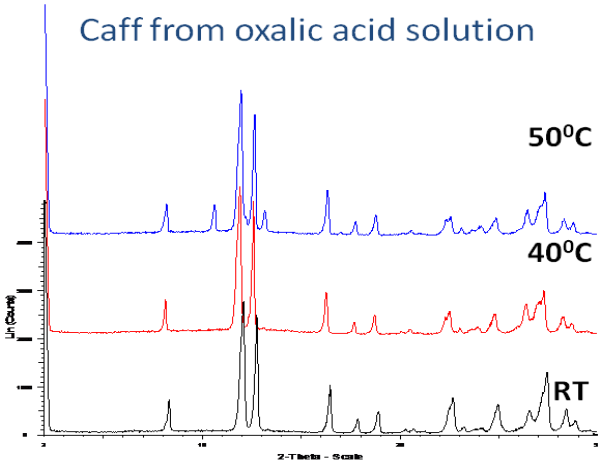
Caff from oxalic acid solution
50⁰C
40⁰C
RT
Lin (Counts)
2-Theta - Scale

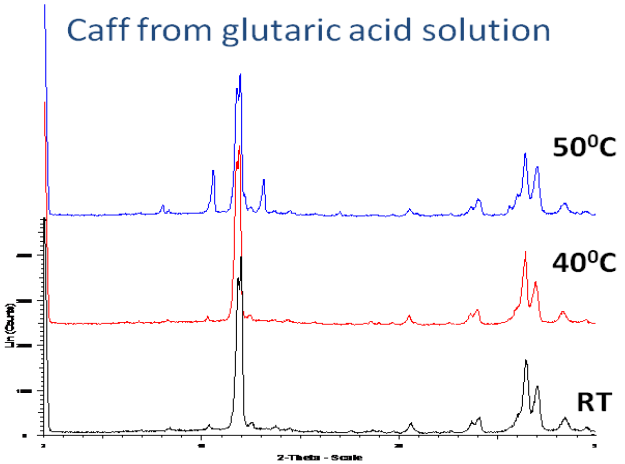
Caff from glutaric acid solution
50⁰C
40⁰C
RT
Lin (Counts)
2-Theta - Scale

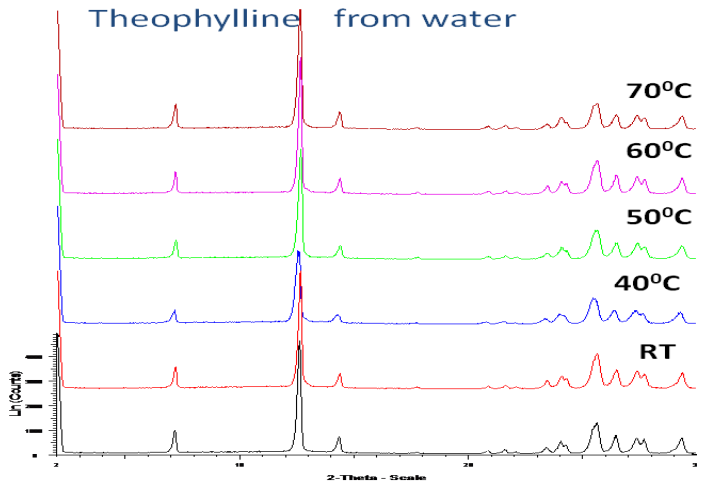
Theophylline from water
70°C
60°C
50°C
40°C
RT
Lin (Counts)
2-Theta - Scale

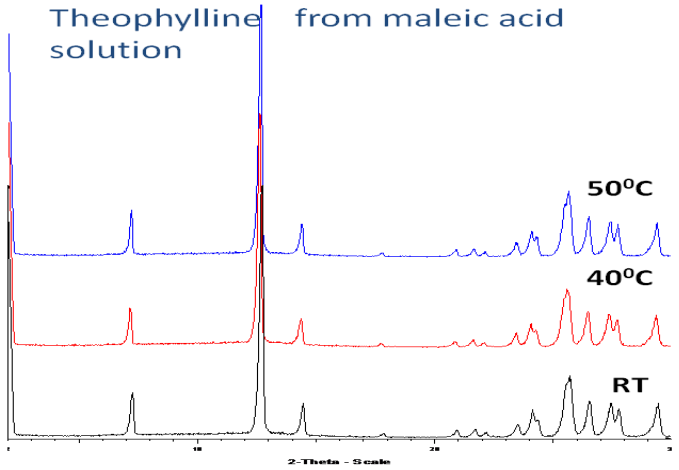
Theophylline from maleic acid solution
50°C
40°C
RT
2-Theta - Scale

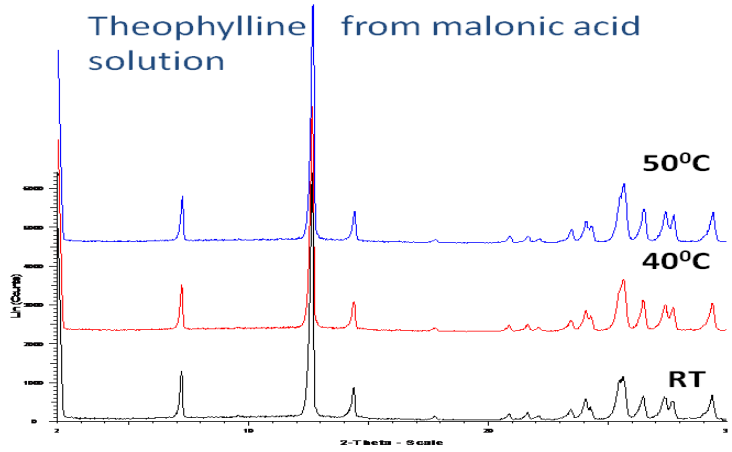
Theophylline from malonic acid solution
50°C
40°C
RT
Lin (Counts)
2-Theta - Scale

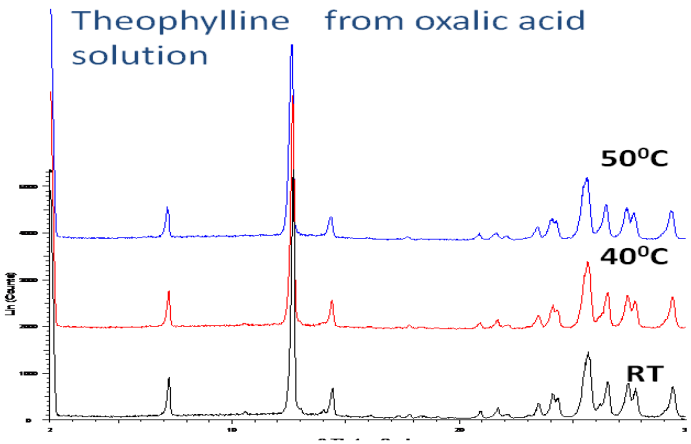
Theophylline from oxalic acid solution
50°C
40°C
RT
Lin (Counts)

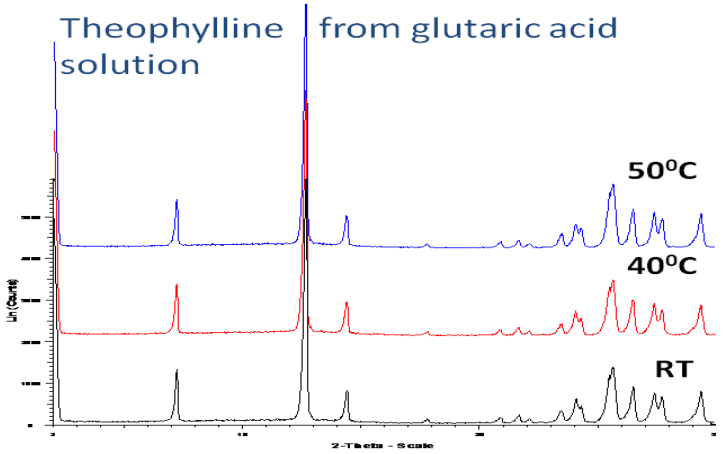
Theophylline solution
from glutaric acid
50°C
40°C
RT

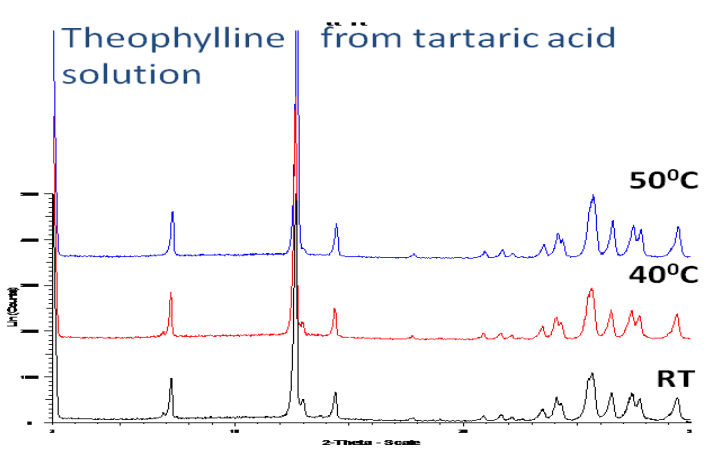
Theophylline solution
from tartaric acid
50°C
40°C
RT

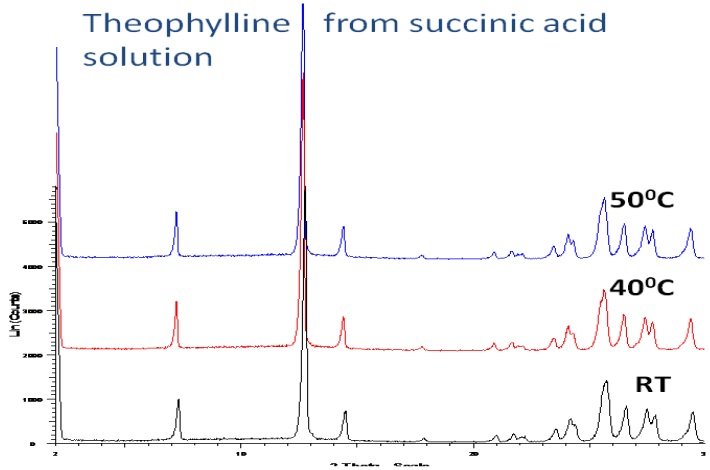
Theophylline solution
from succinic acid
50°C
40°C
RT

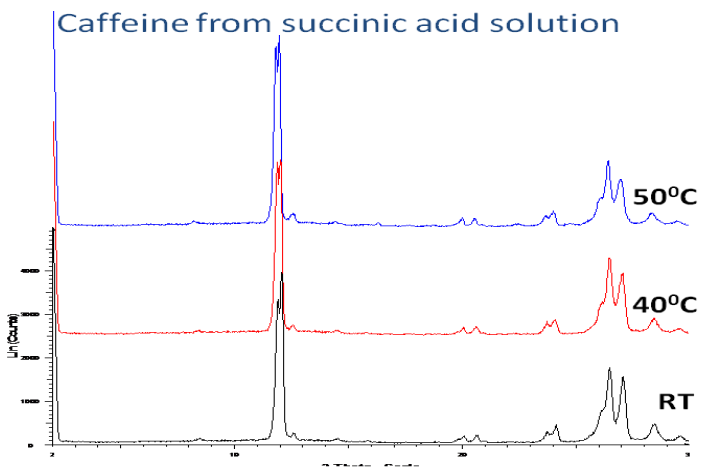
Caffeine from succinic acid solution
50°C
40°C
RT

II. *Particle size distribution of CAF:MAL*

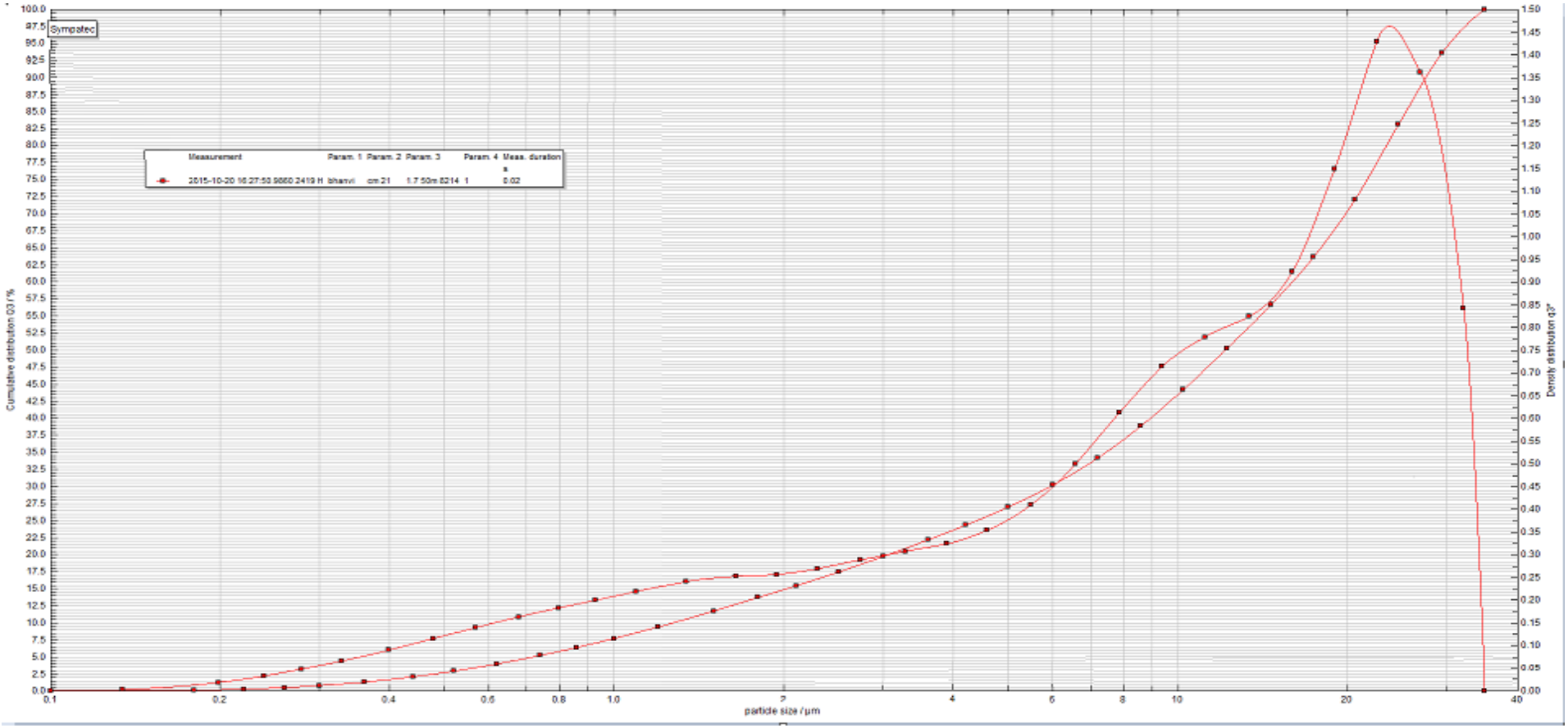

1mL/min

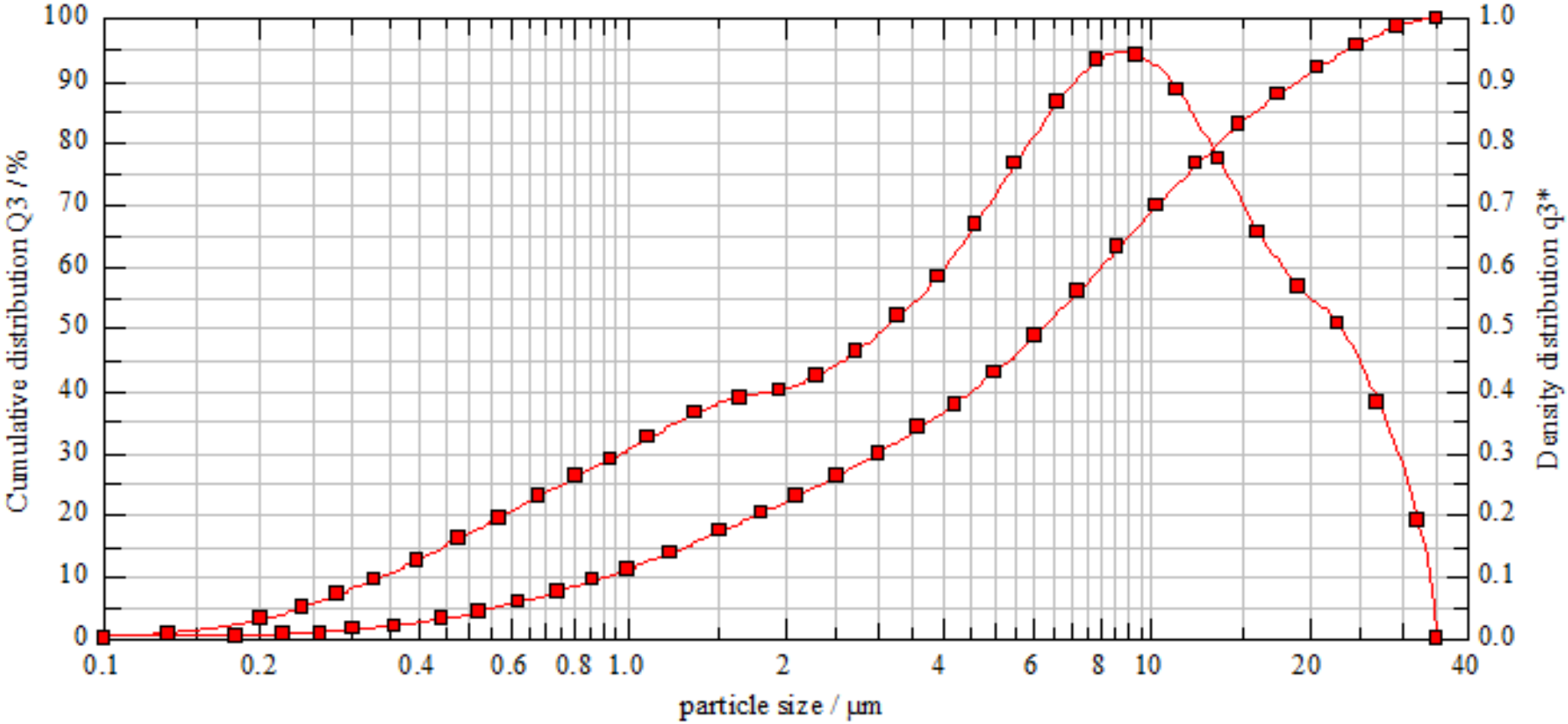
Cumulative distribution Q3 / %
Density distribution q3*
particle size / µm
100
90
80
70
60
50
40
30
20
10
0
1.0
0.9
0.8
0.7
0.6
0.5
0.4
0.3
0.2
0.1
0.0
0.1
0.2
0.4
0.6
0.8
1.0
2
4
6
8
10
20
40

2mL/min

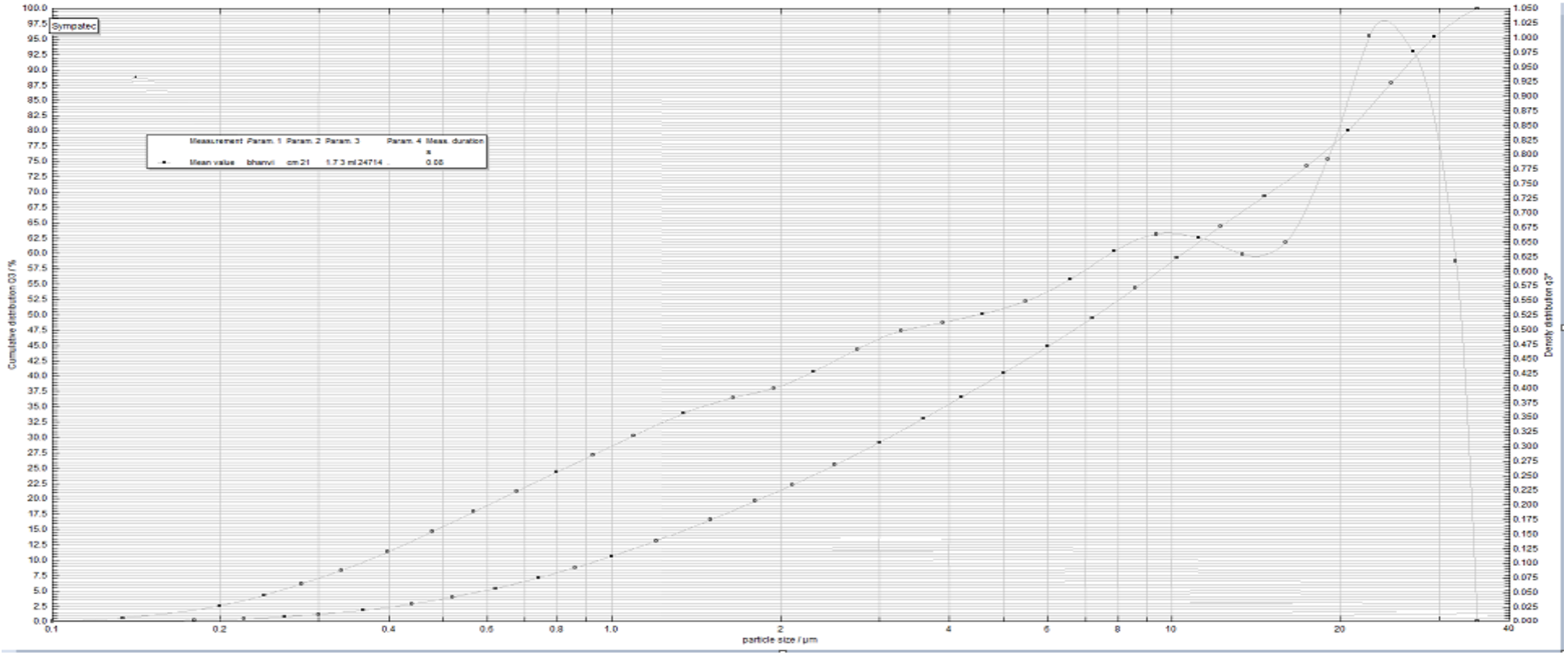
Sympatec
Measurement Param. 1 Param. 2 Param. 3 Param. 4 Meas. duration
Mean value bhanvi cm 21 1.7 3 ml 24714 s 0.00
Cumulative distribution Q3 / %
Density distribution q3*
particle size / µm

3mL/min

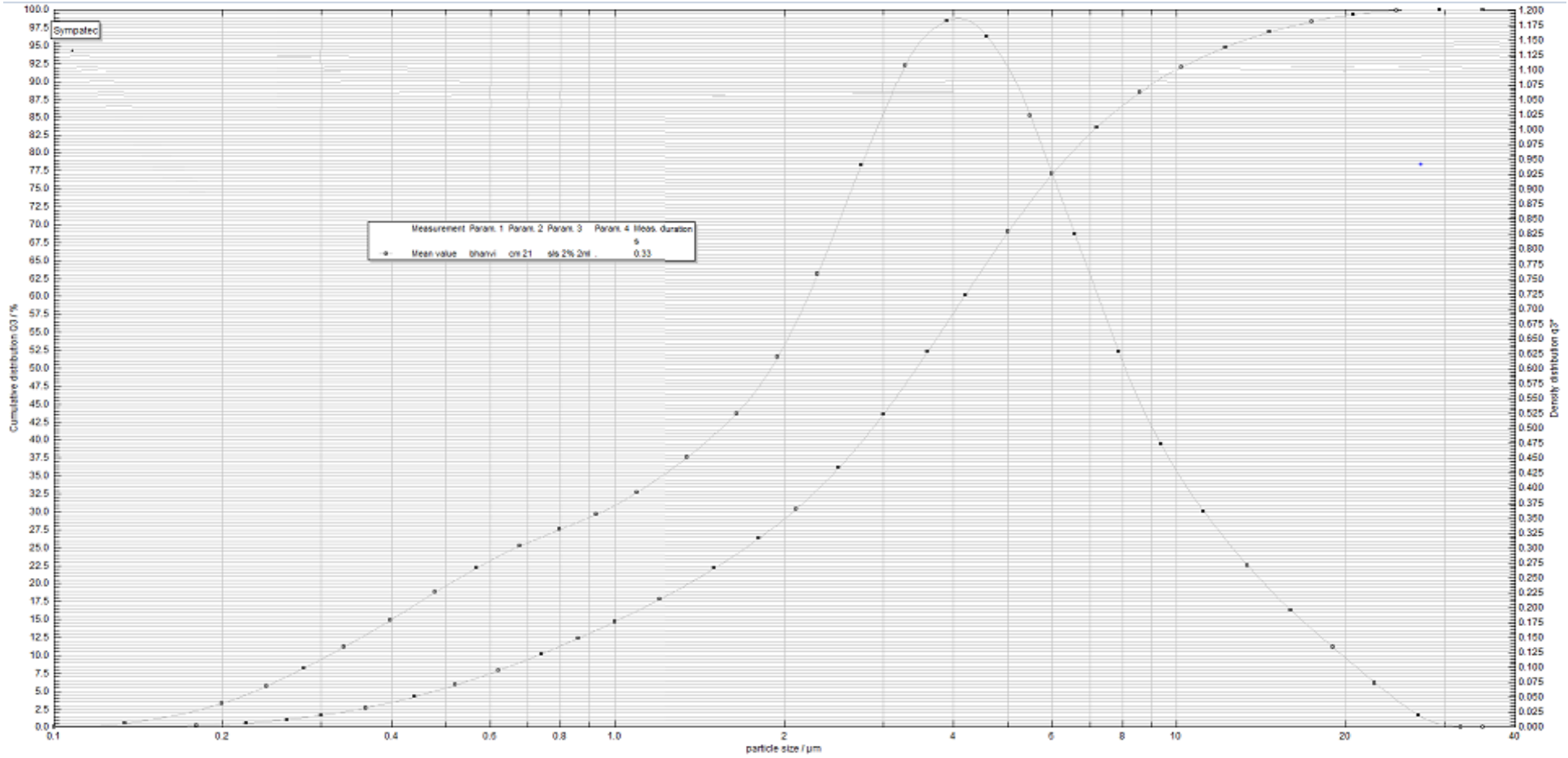
Sympatec
Measurement Param. 1 Param. 2 Param. 3 Param. 4 Meas. duration
s
Mean value bhanvi cm 21 sls 2% 2ml 0.33
Cumulative distribution Q3 / %
Density distribution q3*
particle size / µm

SLS 2mL/min

III. *Screen shot of Hansen Solubility webpage with HSP calculation tool*

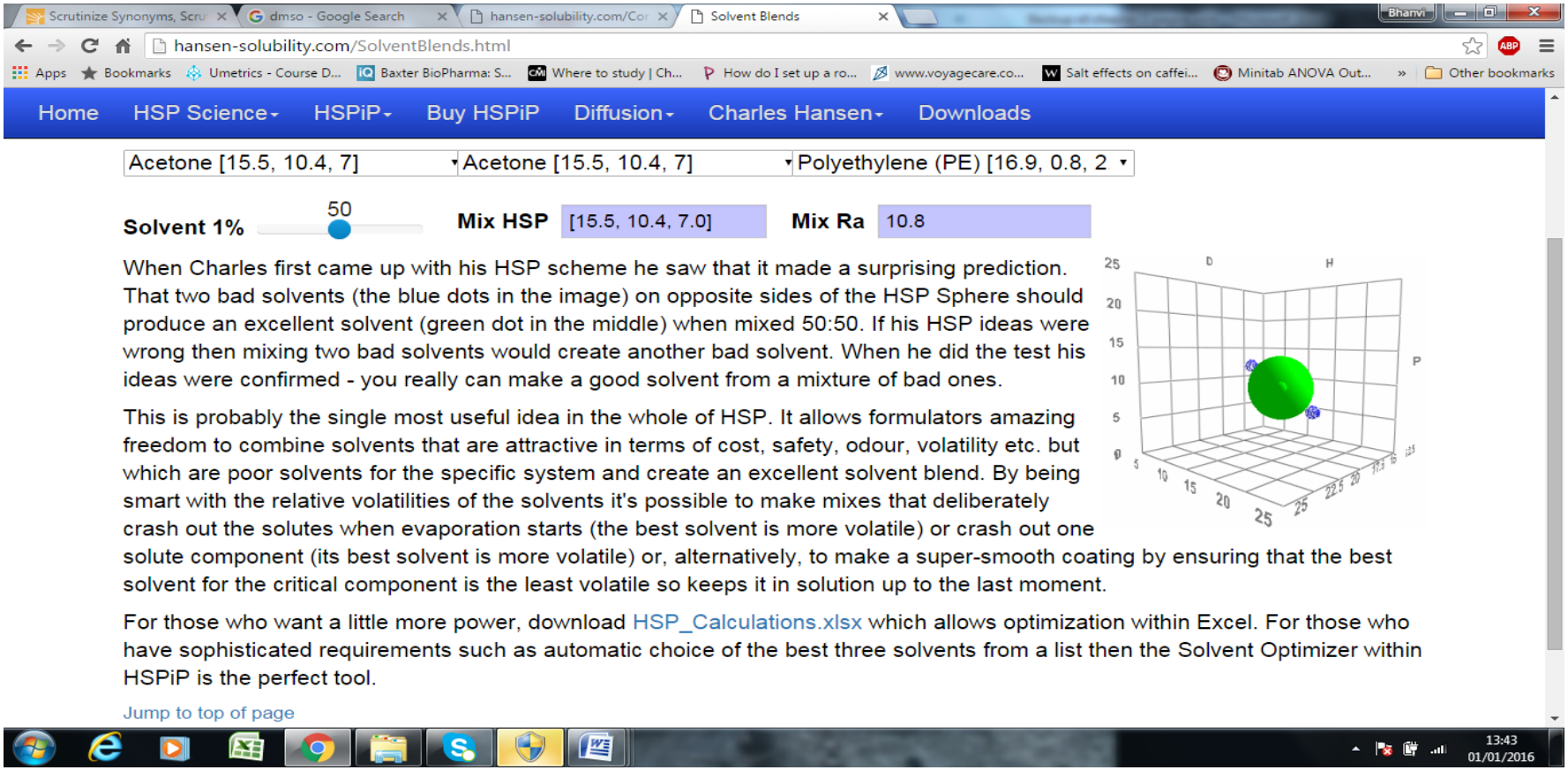

HSP Blend Tool used to determine solubility parameters for: Ethyl acetate and methanol binary mixture at various ratios.

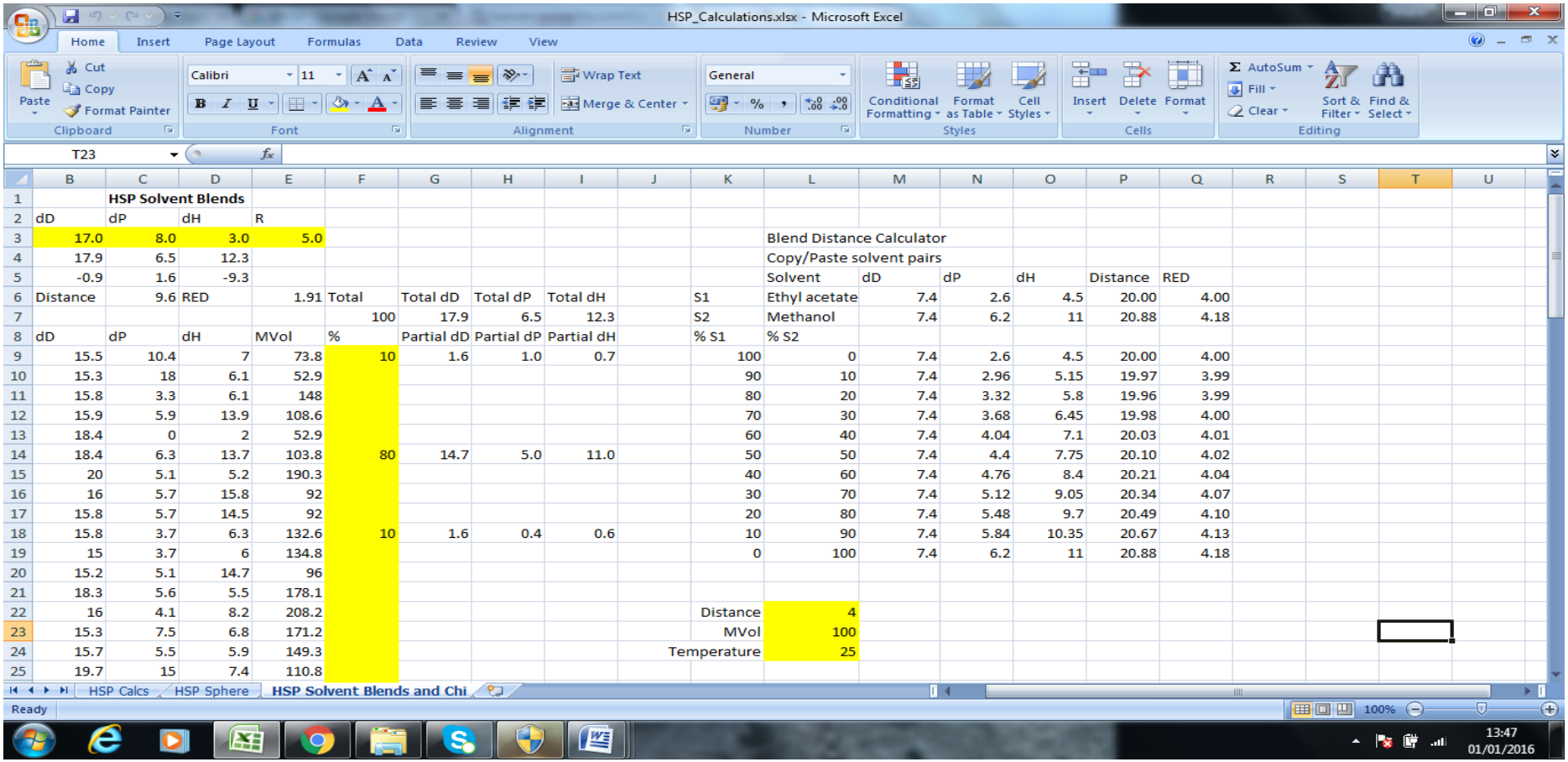

IV. *Particle size distribution of THEO co-crystals*

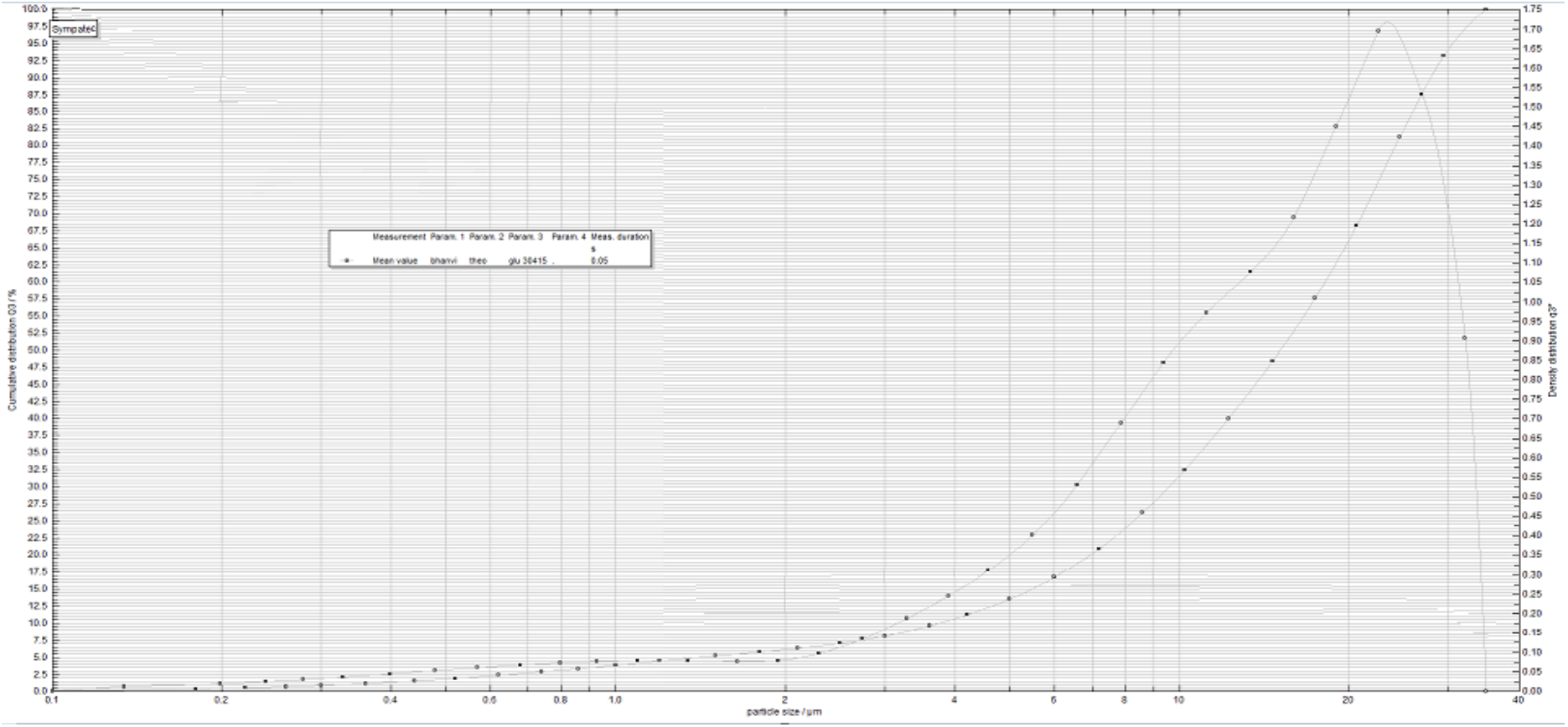

THEO:GLU

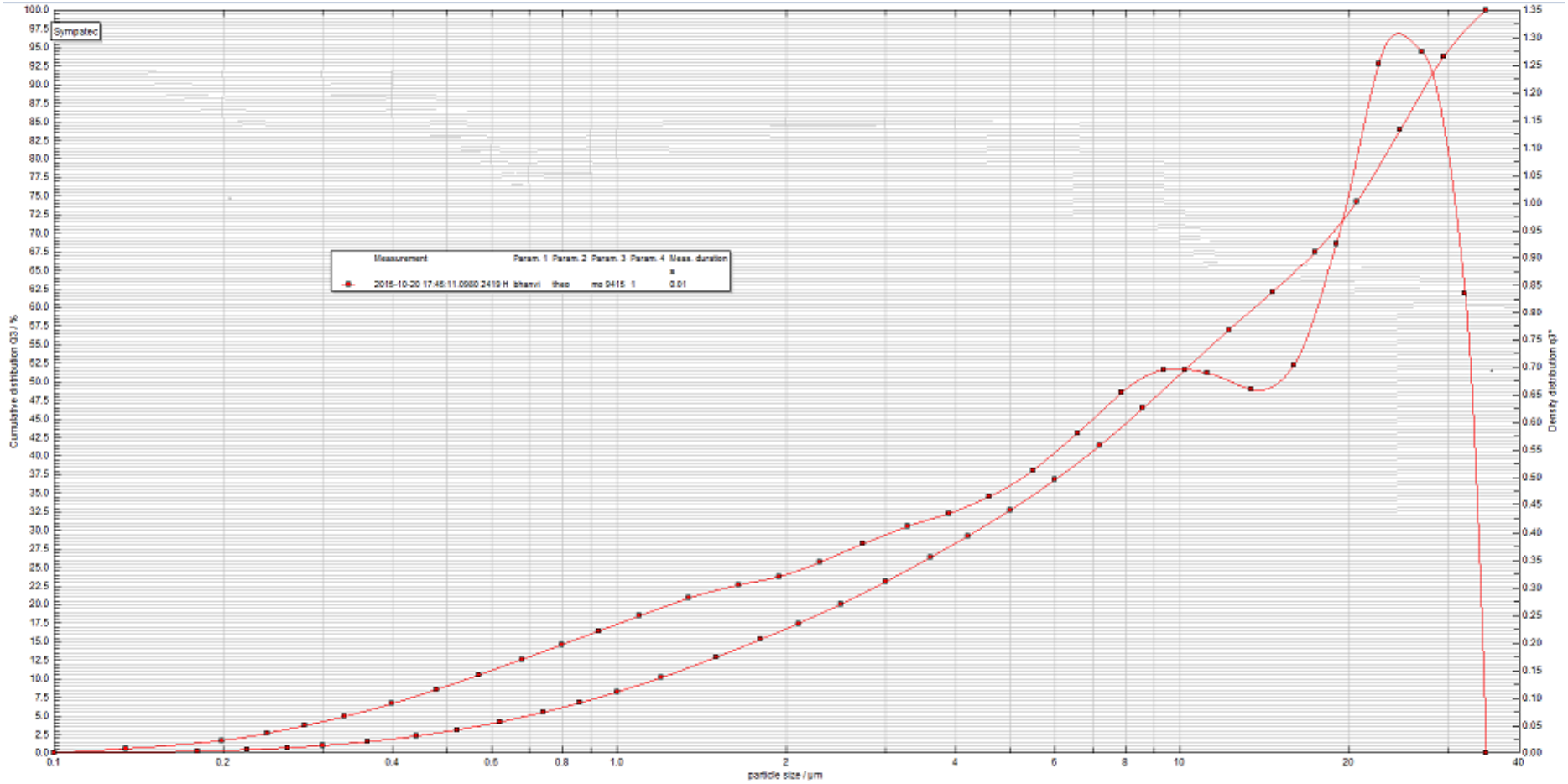
Sympatec
Measurement
Param. 1
Param. 2
Param. 3
Param. 4
Meas. duration
s
2015-10-20 17:45:11.0980 2419 H
bhanvi
theo
mo 9415
1
0.01
Cumulative distribution Q3 / %
Density distribution q3*
particle size / µm

THEO: MO

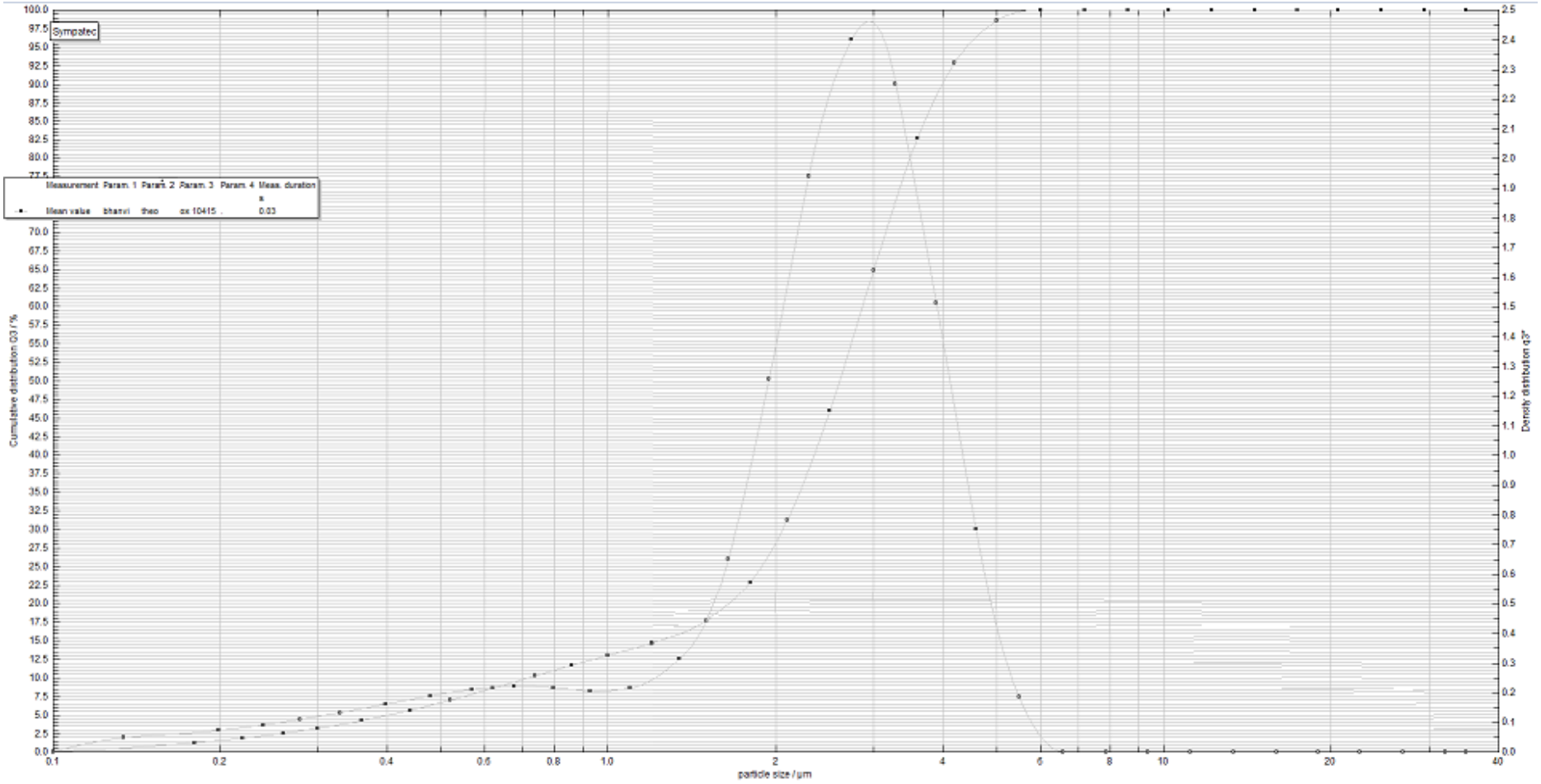
Sympatec
Measurement Param. 1 Param. 2 Param. 3 Param. 4 Meas. duration
s
Mean value bhanvi theo ox 10415 . 0.03
Cumulative distribution Q3 r /%
Density distribution q3*
particle size / µm

THEO:OX

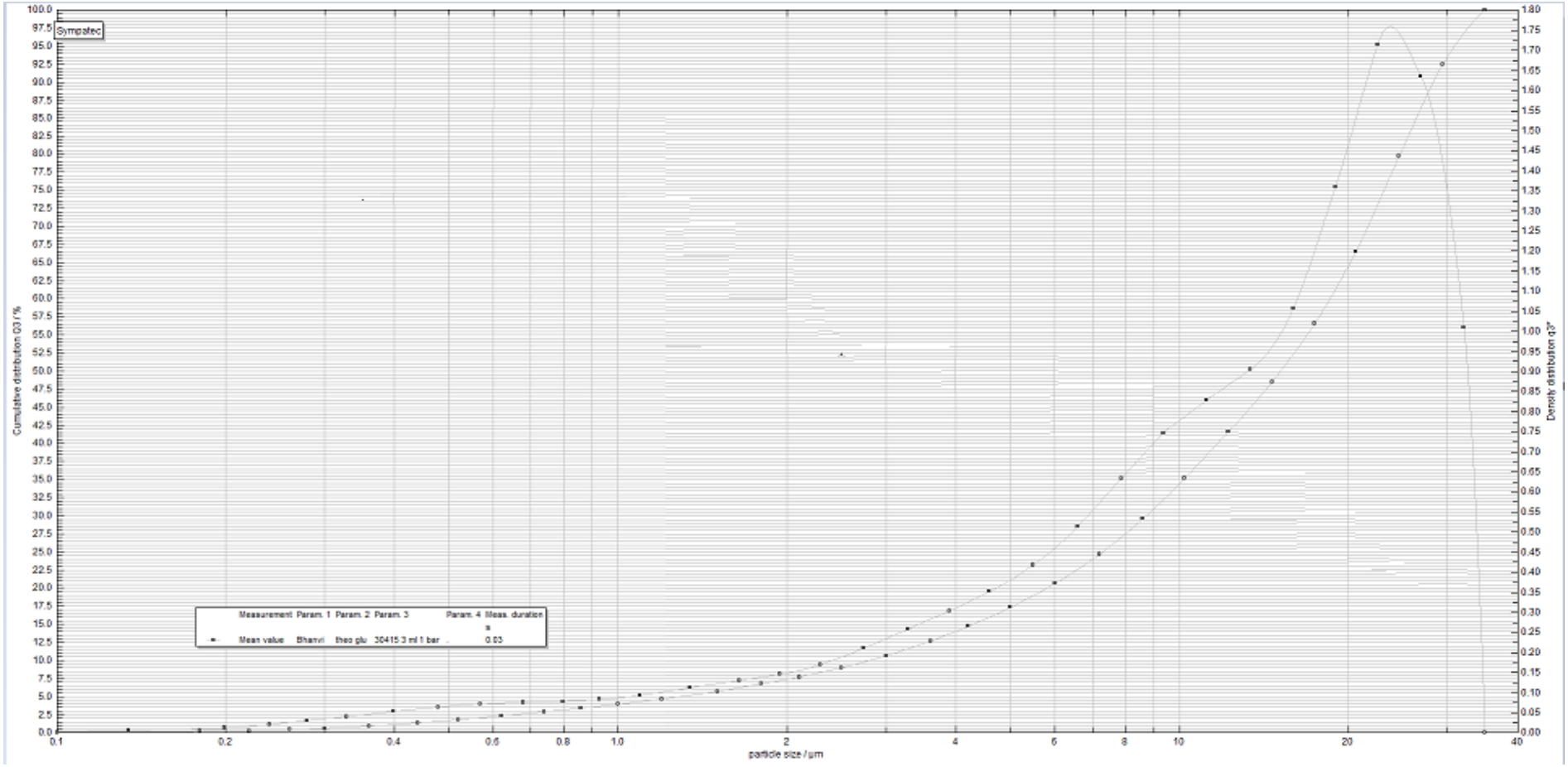
Sympatec
Cumulative distribution Q3 / %
Density distribution q3*
particle size / µm
Measurement Param. 1 Param. 2 Param. 3 Param. 4 Meas. duration
s
Mean value Bhanvi theo glu 30415 3 ml 1 bar 0.03

THEO:MAL

V. *Particle size distribution for CBZ:SAC co-crystals*

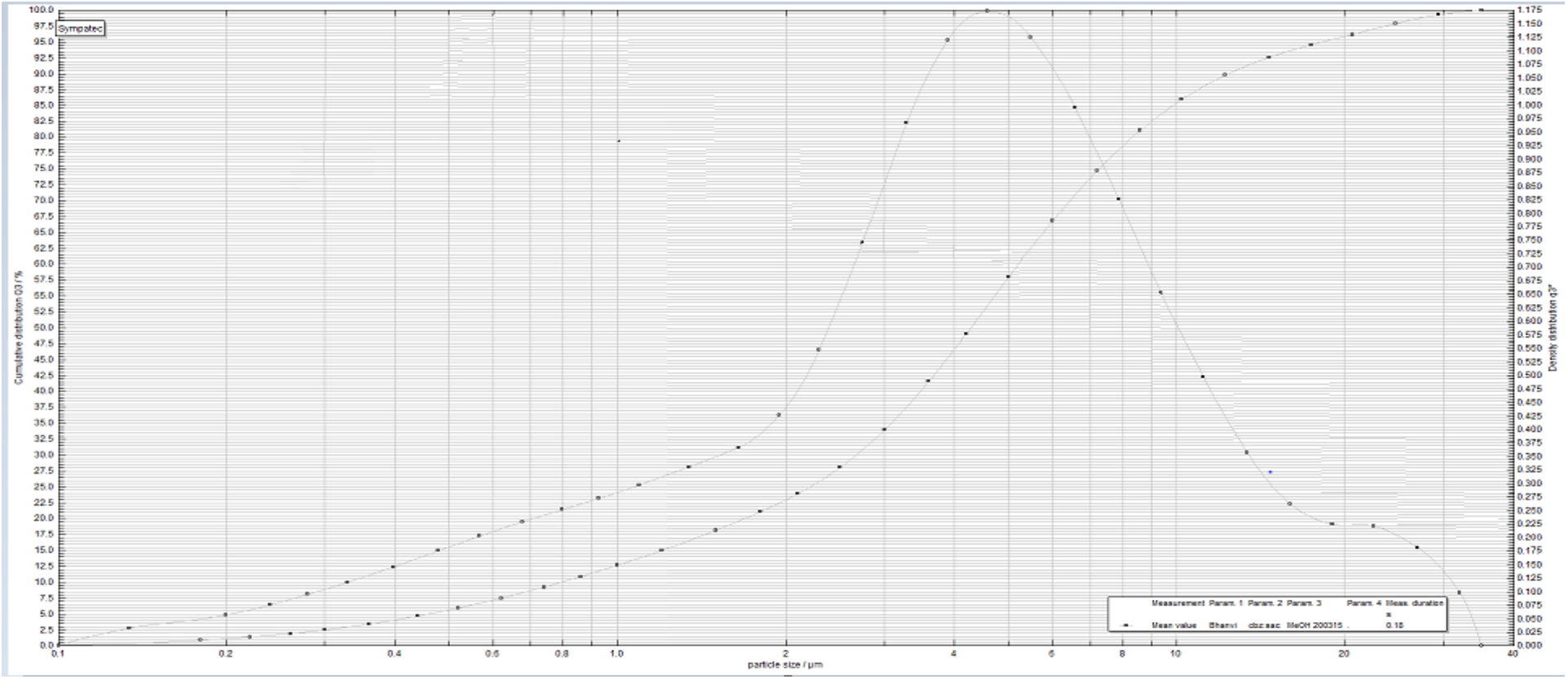

MeOH @70^{0}C

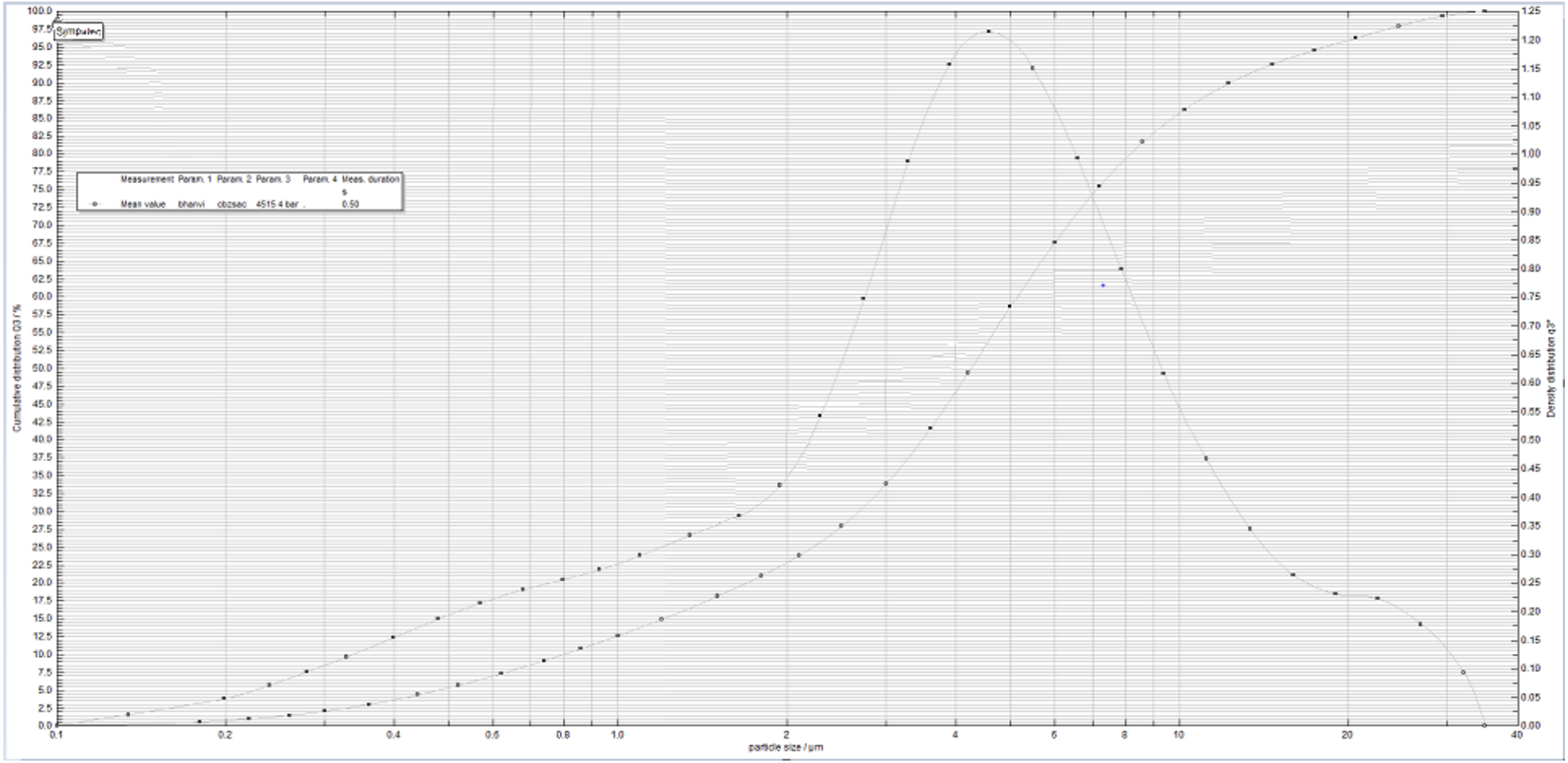
Measurement Param. 1 Param. 2 Param. 3 Param. 4 Meas. duration
s
Mean value bhanvi obzsac 4515.4 bar . 0.50
Cumulative distribution Q3 / %
Density distribution q3*
particle size / µm

MeOH @80^{0}C

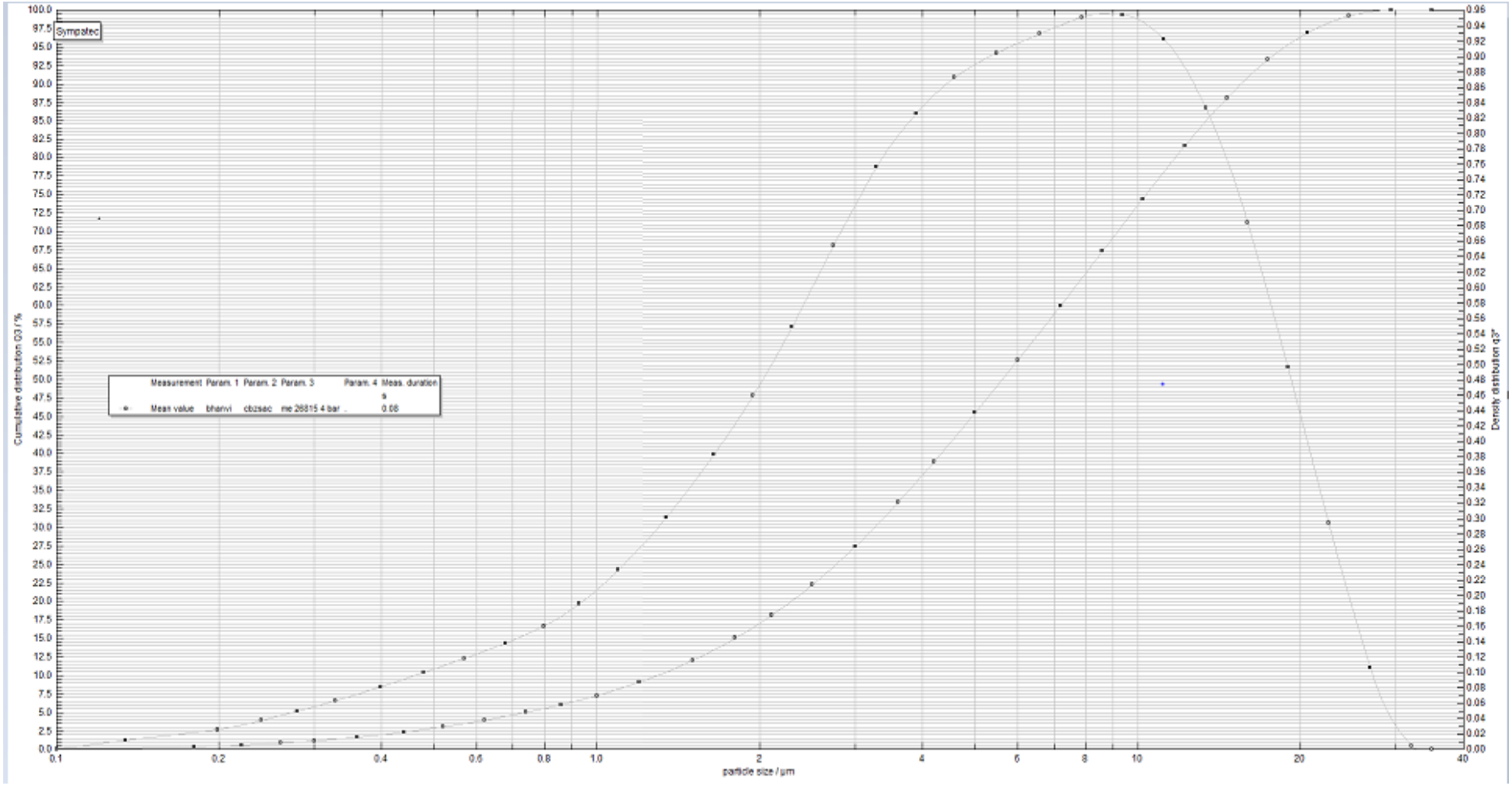
Sympatec
Measurement Param. 1 Param. 2 Param. 3 Param. 4 Meas. duration
s
Mean value bhanvi cbzsec me 26815 4 bar .. 0.66
Cumulative distribution Q3 / %
Density distribution q3*
particle size / µm

MeOH 3mL/min

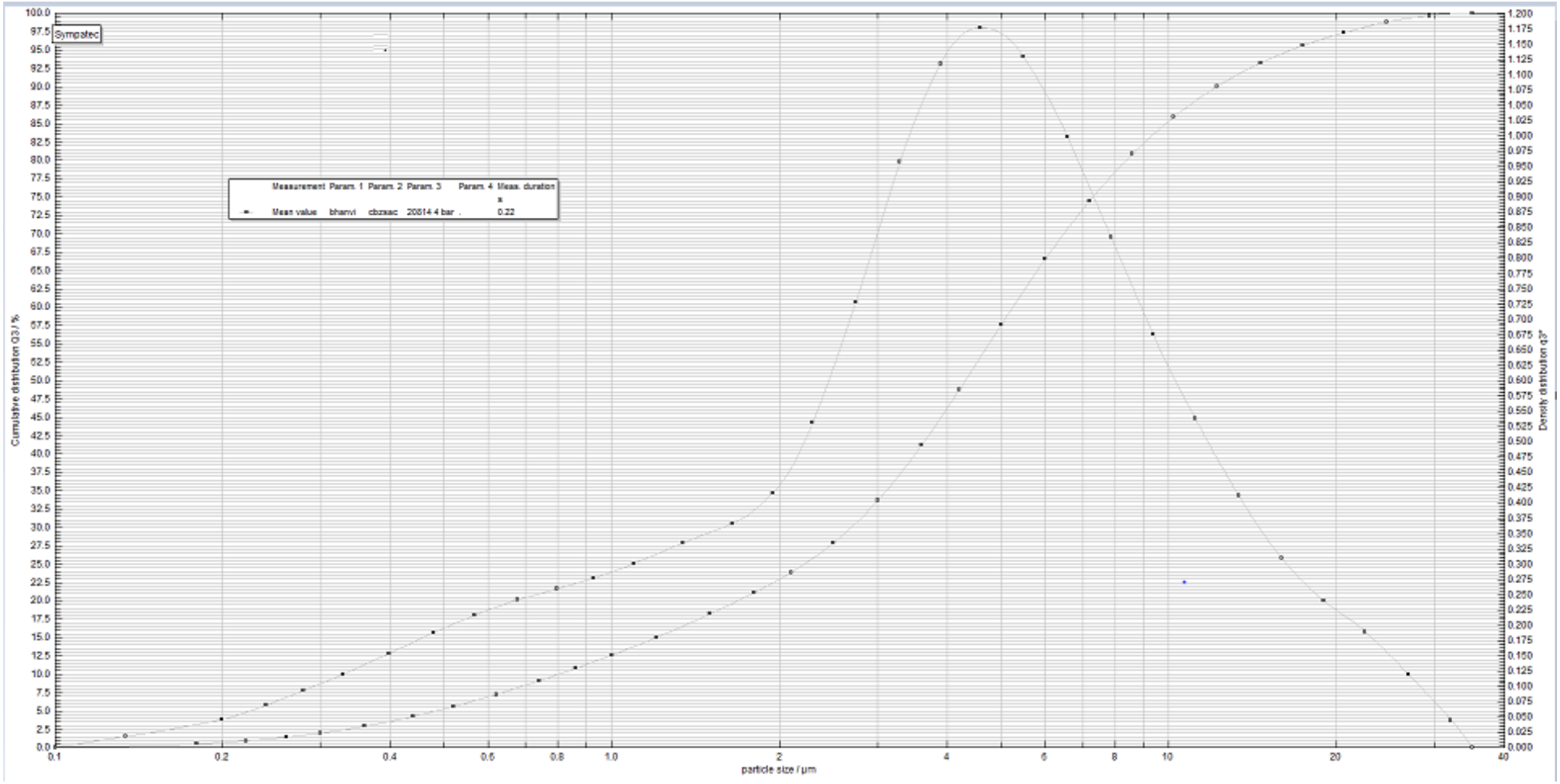
Sympatec
Measurement Param. 1 Param. 2 Param. 3 Param. 4 Meas. duration
s
Mean value bhanvi cbzxac 20814 4 bar . 0.22
Cumulative distribution Q3 / %
Density distribution q3*
particle size / µm

EtOH

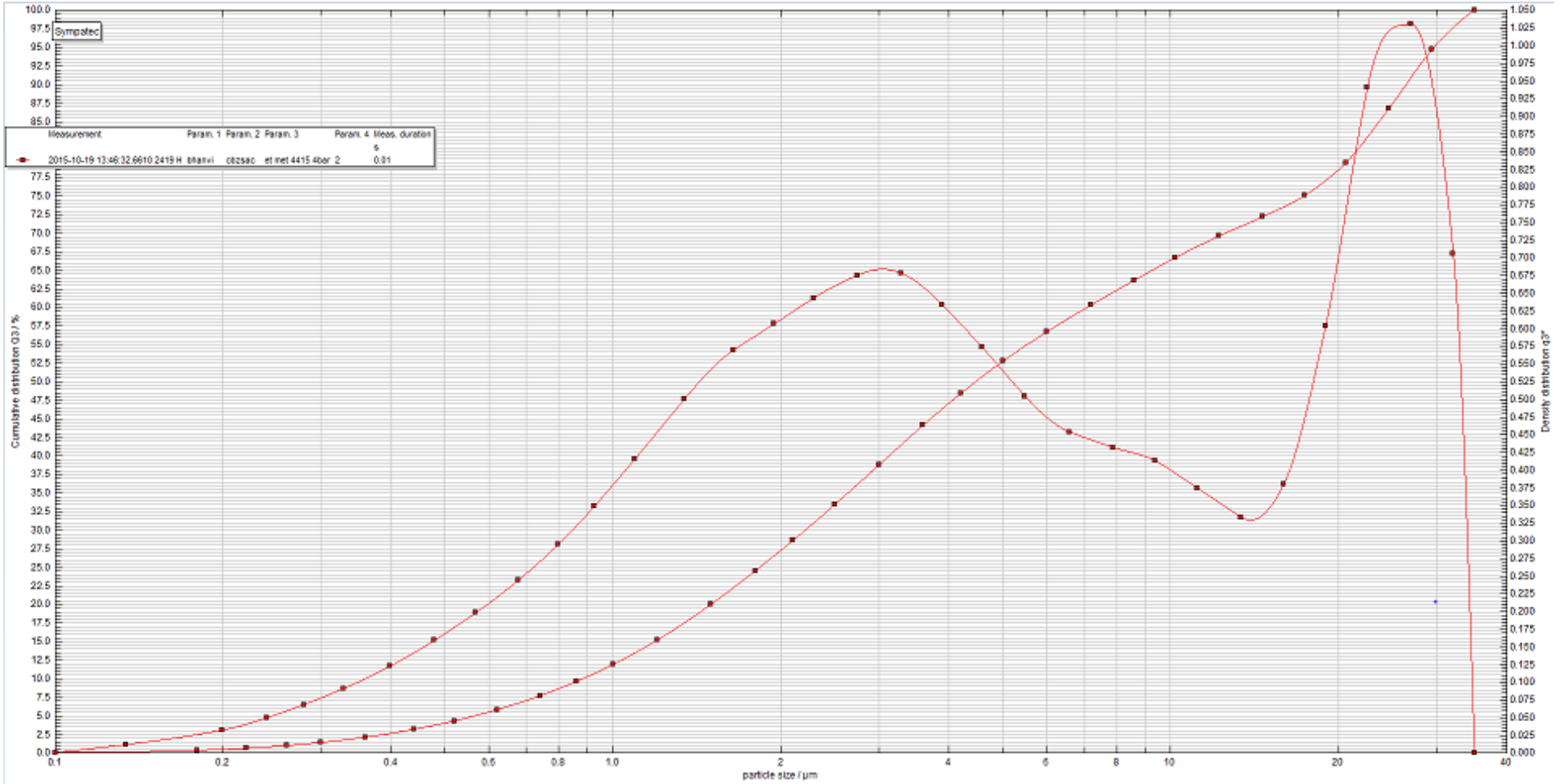
Sympatec
Measurement
Param. 1
Param. 2
Param. 3
Param. 4
Meas. duration
s
2015-10-19 13:46:32.6610 2419 H bhanvi obzsac et inet 4415 4bar 2
0.01
Cumulative distribution Q3 / %
Density distribution q3*
particle size / µm
0.1
0.2
0.4
0.6
0.8
1.0
2
4
6
8
10
20
40

EtOH : MeOH

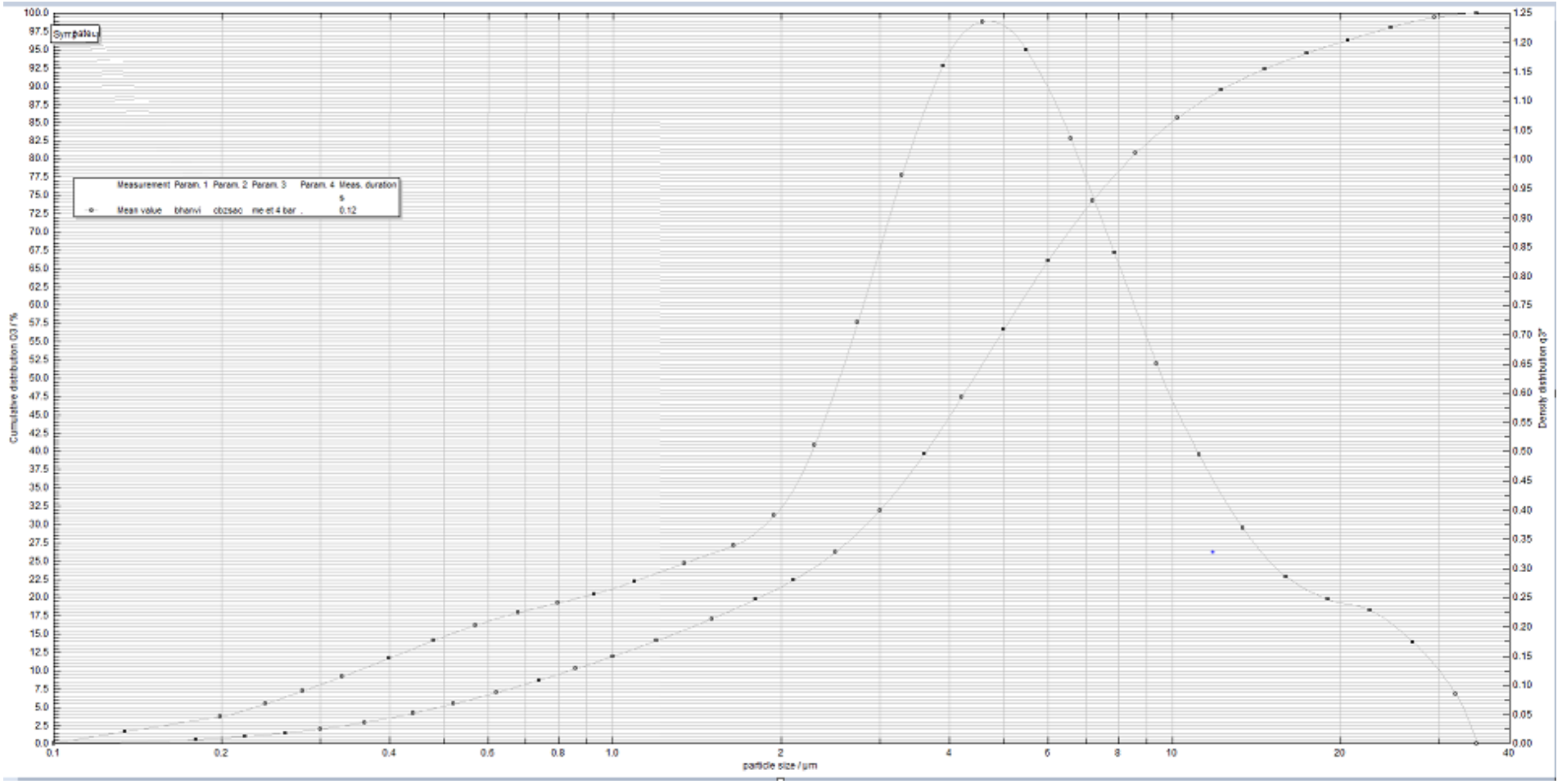
Measurement Param. 1 Param. 2 Param. 3 Param. 4 Meas. duration
s
Mean value bhanvi obzsao me et 4 bar . 0.12
Cumulative distribution Q3 / %
Density distribution q3*
particle size / µm

MeOH: EtOH

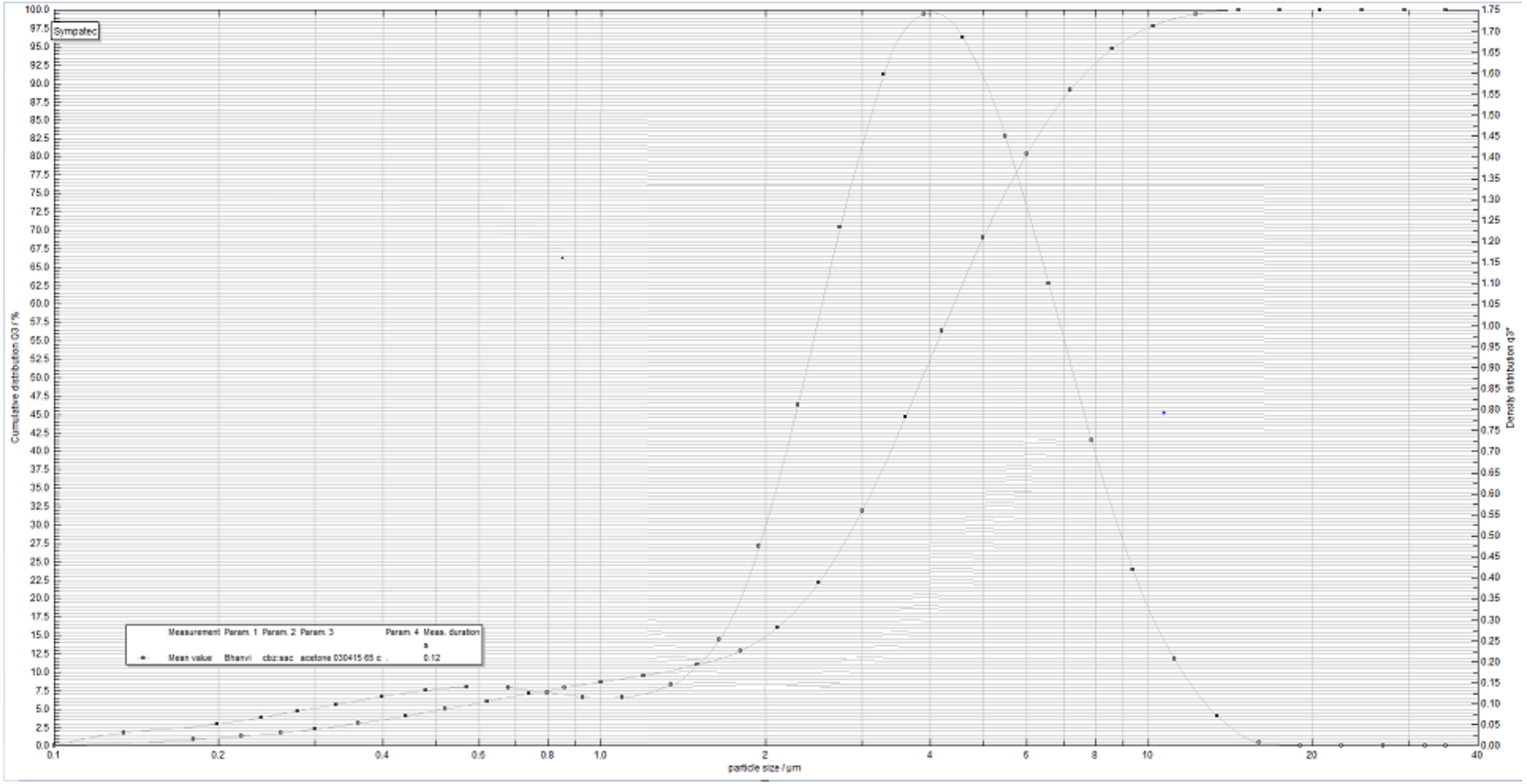

Acetone @65^{0}C

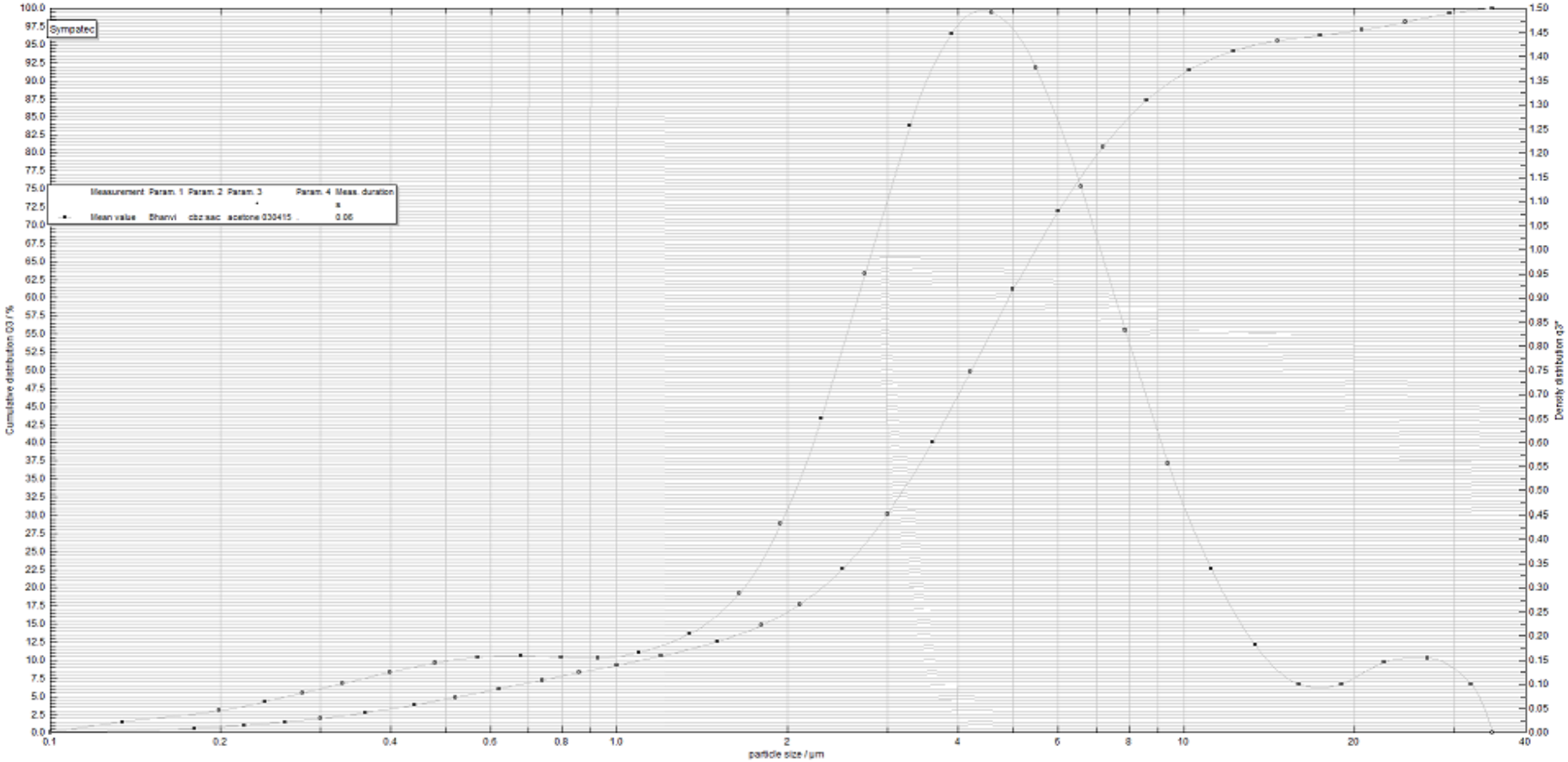

Acetone @75^{0}C